DISSIPATION AND AMPLIFICATION OF WAVES IN SPACE AND LABORATORY PLASMAS

A thesis submitted for examination
for the degree of Doctor of Philosophy

by

ROBERT MATTHEW WINGLEE (B.Sc., Hons.)

Department of Theoretical Physics
University of Sydney

January, 1984

ERRATA

P. 1.3 fifth line: "(b)...plasmas" should read "(b) it allows excitation of waves in the interior of the plasma which damp and heat the plasma without necessarily heating the surface of the plasma".

P. 1.20 seventeenth line: "it is quite possible that" should read "the antennas can be designed so that".

P. 2.1 fourth line: "In this case" should read "When $\omega \simeq \Omega_m$ (where Ω_m is the minority ion-cyclotron frequency)".

P. 2.1 last line: add "Electron heating is inhibited because the damping from the minority ions can be much greater than that from the electrons (Section 2.5). The heating of the plasma surface is also inhibited because (as discussed in Section 1.3) the Alfvén resonance can be well inside the plasma.".

P. 3.32 end of first sentence: add "(Antenna configurations for this current are discussed in Chapter 1.)".

P. 4.12 first line: "H is positive" should read " H is determined by the dispersion equation and is positive".

P. 4.16 third line: "The terms...1978)" should read "the terms azimuthal and axial are used because the instabilities are driven by the wave fields modifying the electron trajectories so that the electrons bunch azimuthally when $k_z^2 c^2 << \omega^2$ and axially when $k_z^2 c^2 >> \omega^2$ (Chu and Hirschfield, 1978; see also Section 4.6)".

P. 4.21 second last line: " = P$\int$" should read " $= -\frac{i}{\sqrt{\pi}}$ P$\int$".

P. R.3 fourth reference:"Lehame" should read "Lehane".

P. R.5 third reference:"Aust. J. Phys. 35, 477" should read "Aust. 4, 221".

P. R.5 fourth reference: "Aust" should read "Aust. J. Phys. 35, 447.".

Amended copy.

21.8.84

TO MY WIFE, MUM AND DAD

AND TO

RAYMOND, JUST AWAY

CONTENTS

SUMMARY

This thesis is concerned with theoretical investigations into the dissipation and amplification of waves in laboratory and space plasmas. Three specific examples of current interest are examined. The first is the dissipation of a magnetosonic wave by resonant mode conversion into a shear Alfvén wave and the subsequent collisionless damping of the shear Alfvén wave by resonant particle interactions. The other two involve the amplification of electromagnetic and whistler waves by electron cyclotron instabilities.

The mode conversion of magnetosonic waves is of interest in radio frequency (rf) heating of tokamak plasmas to fusion temperatures. To produce the heating an external antenna excites a magnetosonic wave which mode converts in a localized region within the plasma (at the Alfvén resonance); the collisionless damping of the excited shear Alfvén wave then produces heating. The mode conversion is important because (a) the collisionless damping of the magnetosonic wave is much weaker than that of the shear Alfvén wave and (b) the shear Alfvén wave cannot be directly excited by an external antenna due to its large spatial decay rate.

Conditions for optimum plasma heating by this method are determined in the first part of this thesis. For simplicity, the heating scheme is divided into three individual processes :

(i) the collisionless damping (and dispersion) of the magnetosonic and shear Alfvén waves in a locally homogeneous plasma;

(ii) the mode conversion of a magnetosonic wave in an inhomogeneous plasma;

(iii) the excitation of a magnetosonic wave by an external antenna.

In the second part of this thesis, electron cyclotron instabilities are investigated. One class of instabilities examined is relevant to the gyrotron, Jupiter's decametric radio emission (DAM), terrestrial kilometric radiation (TKR) and solar spike bursts. The instability producing the emission in the gyrotron is similar but seemingly different from that producing DAM, TKR and solar spike bursts. A theory is presented which interrelates these instabilities. A modified version of this theory is then used in formulating a new theory for the amplification and triggering of discrete VLF emissions in the magnetosphere.

AUTHOR'S CONTRIBUTIONS

Numerical solutions to the plasma dispersion equation were obtained using a complex root finding subroutine supplied by Dr. R. McPhedran.

All other material presented in this thesis is the author's own work except where acknowledged.

ACKNOWLEDGEMENTS

I would like to thank my supervisor, Dr. Neil Cramer, for guidance and assistance during my studies. I particularly wish to thank Prof. Don Melrose, who acted as my co-supervisor, for many enjoyable and valuable discussions during the development of the ideas presented in this thesis. Discussions with Prof. Edward Fackerell on the solution of certain differential equations are gratefully acknowledged.

I am also thankful to Drs. Robert Hewitt and Ian Donnelly for constructive criticism of this manuscript. Equally appreciated has been the friendship and assistance by members of the Department of Theoretical Physics, particularly Dr. Ross McPhedran and Miss Patricia Moroney.

I am deeply indebted to my wife, Jenny, for editing this thesis and, more importantly, for her encouragement and patience throughout my postgraduate studies.

Finally, I acknowledge the support of the Australian Government through a Commonwealth Post-Graduate Scholarship and I am grateful to the Science Foundation for Physics within the University of Sydney and its Director, Prof. H. Messel, for the provision of research facilities.

AUTHOR'S PUBLICATIONS

1. "Finite Frequency Effects on Magnetosonic Wave Mode Conversion"

   R. M. Winglee
   Plasma Physics (1982) 24, 1161.

2. "Alfvén Wave Heating in a Multiple Ion-Component Plasma

   R. M. Winglee
   Plasma Physics (1983) in press.

3. "Interrelation between Azimuthal Bunching and Semirelativistic Maser Cyclotron Instabilities"

   R. M. Winglee
   Plasma Physics (1983) 25, 217.

4. "Amplification of Triggered VLF Emissions by the Phase Bunching of Untrapped Electrons"

   R. M. Winglee
   Planet. Space Science (1984) submitted.

In addition the following papers have been presented at conferences.

(i) "Plasma Heating by Resonant Mode Conversion to the Kinetic Alfvén Wave"

   R. M. Winglee
   13th AINSE Plasma Physics Conference (1981) Lucas Heights, Aust.

(ii) "Dispersion and Damping of Alfvén Waves"

   R. M. Winglee
   14th AINSE Plasma Physics Conference (1983) Lucas Heights, Aust.

(iii) "Amplification of Triggered VLF Emissions: Is It due to Trapping or Phase Bunching?"

   D. B. Melrose, R. M. Winglee and I. H. Cairns
   Chapman Conference on Waves in Magnetospheric Plasmas (1983) Hawaii.

PART I

RF HEATING OF TOKAMAK PLASMAS

CHAPTER 1

INTRODUCTION AND REVIEW

1.1 PLASMA HEATING

A central problem in the achievement of controlled thermonuclear fusion is the heating of the reactor plasma to fusion temperatures. The ignition temperature of a deuterium-tritium (D-T) reaction is 4 keV while the ignition temperatures for D-D and p-^{3}He reactions are 35 keV and 30 keV respectively (Miley, 1976). The simplest plasma heating scheme utilizes ohmic heating generated by a current induced in the plasma by a transformer. However, the plasma resistivity which originates from Coulomb collisions decreases with increasing electron temperature and at a temperature of about 1 keV the plasma is essentially collisionless and ohmic heating is ineffective (Chen, 1974, p. 161).

One possible way to supplement ohmic heating is via the excitation of electromagnetic waves in the plasma by an external antenna. The heating of the plasma arises from the subsequent collisionless damping of these excited waves. To date the proposed heating schemes which utilize collisionless damping include lower hybrid resonance heating (Puri and Tutler, 1973), electron-cyclotron resonance heating (Alikaev et al., 1976) ion-cyclotron resonance heating (Stix and Palladino, 1958), parametric excitation (Hooke and Bernabei, 1972), ion-ion hybrid resonance heating (Stix, 1975; Perkins, 1977) and Alfvén resonance heating (Tataronis and Grossmann, 1973; Chen and Hasegawa, 1974).

However, there are problems with some of these supplementary heating schemes. For example, in the first two, the electrons rather than ions absorb the rf power. In ion-cyclotron resonance heating, the ions absorb the rf power but the plasma tends to shield itself from the

applied field and little energy reaches the plasma interior (Rose and Clarke, 1961, p. 453). In parametric excitation, large wave amplitudes which are hard to produce and may cause plasma disruption are required.

The above problems are not incurred in the ion-ion hybrid and Alfvén resonance heating schemes. Indeed, experimental results for these two schemes are promising. For example, using the ion-ion hybrid resonance heating scheme in a deuterium plasma containing 30% hydrogen, JFT-2 Group (1982) report the heating of ions from 400 to 800 eV and electrons from 600 to 900 eV by 600 kW antenna-power input. The excess in electron temperature is attributed to the direct absorption of rf power by the electrons. Similar results have been reported by Equipe TFR (1982) using a deuterium plasma containing 20% hydrogen. In their experiment ions were heated from 0.8 to 1.6 keV and electrons from 1.0 to 1.5 keV by 1.3 MW antenna-power input.

The most impressive results to date for Alfvén resonance heating are from Heliotron-D in which electrons were heated from about 100 eV to 200 eV and ions from 50 eV to 70 eV by 400 kW antenna-power input (Obiki et al., 1977; Mutoh et al., 1979) and from TCA where electrons were heated from 500 eV to 900 eV and ions from 150 eV to 225 eV by 100 kW antenna-power input (de Chambrier et al., 1982b). The experimental results for Alfvén resonance heating are less impressive than for ion-ion hybrid resonance heating as much of the experimental effort on Alfvén resonance heating has been concentrated on understanding the physical processes involved (e.g. Bengston et al., 1982; de Chambrier et al., 1982a; Cross et al., 1982).

In both the ion-ion hybrid and Alfvén resonance heating schemes a fast magnetosonic wave is excited by an external antenna. The magnetosonic wave then mode converts into an ion-Bernstein wave in

ion-ion hybrid resonance heating and into a shear Alfvén wave in Alfvén resonance heating. The mode conversion is an essential feature of these heating schemes because (a) the damping of the magnetosonic wave is much smaller than the damping of either the ion-Bernstein or shear Alfvén waves and (b) neither the ion-Bernstein wave nor the shear Alfvén wave can be directly excited by an external antenna because of the large spatial decay rate of these waves in low β plasmas.

To date, emphasis in the studies of Alfvén resonance heating has been directed towards the determination of the damping of the magnetosonic wave by mode conversion and the corresponding antenna response. These studies are reviewed in Section 1.2. A comparison between Alfvén resonance and ion-ion hybrid resonance heating is given in Section 1.3. Although ion heating via the ion-ion hybrid resonance has been established both theoretically (e.g. Perkins, 1977) and experimentally (e.g. Equipe TFR, 1982), there has been little corresponding work in determining ion heating via the Alfvén resonance. In Chapters 2 and 3, the conditions for the heating of ions in the plasma interior via the Alfvén resonance are determined and it is shown that this ion heating can occur both efficiently and without the problems of ion-ion hybrid resonance heating.

1.2 ALFVÉN WAVE HEATING

1.2.1 The Wave Equation

The heating of a collisionless plasma via the Alfvén resonance is reviewed in this Section. The wave equation governing the mode

conversion can be derived from either ideal magnetohydrodynamic (MHD) theory or from kinetic theory. In ideal MHD theory the basic equations are (Krall and Trivelpiece, 1973, Ch. 3).

$$\nabla \times \underset{\sim}{B} = \frac{4\pi}{c} \underset{\sim}{J} + \frac{1}{c} \frac{\partial \underset{\sim}{E}}{\partial t} \tag{1.1}$$

$$\nabla \times \underset{\sim}{E} = -\frac{1}{c} \frac{\partial \underset{\sim}{B}}{\partial t} \tag{1.2}$$

$$\frac{d\underset{\sim}{v}}{dt} = \frac{\underset{\sim}{J} \times \underset{\sim}{B}}{\rho_M c} \tag{1.3}$$

$$\underset{\sim}{E} + \frac{\underset{\sim}{v} \times \underset{\sim}{B}}{c} = 0 \tag{1.4}$$

where $\underset{\sim}{E}$ and $\underset{\sim}{B}$ are the electric and magnetic fields respectively and ρ_M is the mass density. In kinetic theory, the fluid equations, (1.3) and (1.4), are replaced by a conductivity tensor relating $\underset{\sim}{J}$ to $\underset{\sim}{E}$ i.e.

$$J_i = \sigma_{ij} E_j . \tag{1.5}$$

The elements of the conductivity tensor are given in standard texts such as Stix (1962, Ch. 8) and Krall and Trivelpiece (1973, Ch. 8). The advantage of kinetic theory over MHD theory is that it allows the inclusion of finite Larmor radius, finite frequency and finite electron mass and temperature corrections.

For simplicity, a planar geometry is assumed in this study. A similar geometry has also been used in many other previous theoretical studies on Alfvén wave heating (e.g. Tataronis and Grossmann, 1973; Chen and Hasegawa, 1974; Hasegawa and Chen, 1975, 1976; Ott et al., 1978;

Karney et al., 1979; Winglee, 1982). The mode coupling has also been previously investigated for cylindrical (Karney et al., 1979; Ross et al., 1982) and toroidal (Appert et al., 1982) geometries. However, in these later studies, no fundamental difference between the planar geometry and the cylindrical and toroidal geometries was found. Thus, the planar geometry is expected to simulate at least qualitatively the more complicated geometry of the tokamak plasma.

In the planar geometry assumed here, a constant magnetic field, $\underset{\sim}{B}_0$, is directed along the z axis and a density gradient along the x axis (Fig. 1.1) so that all perturbations in the field and fluid displacements can be considered to have the form $p(x)\exp(i(k_y y + k_z z - \omega t))$.

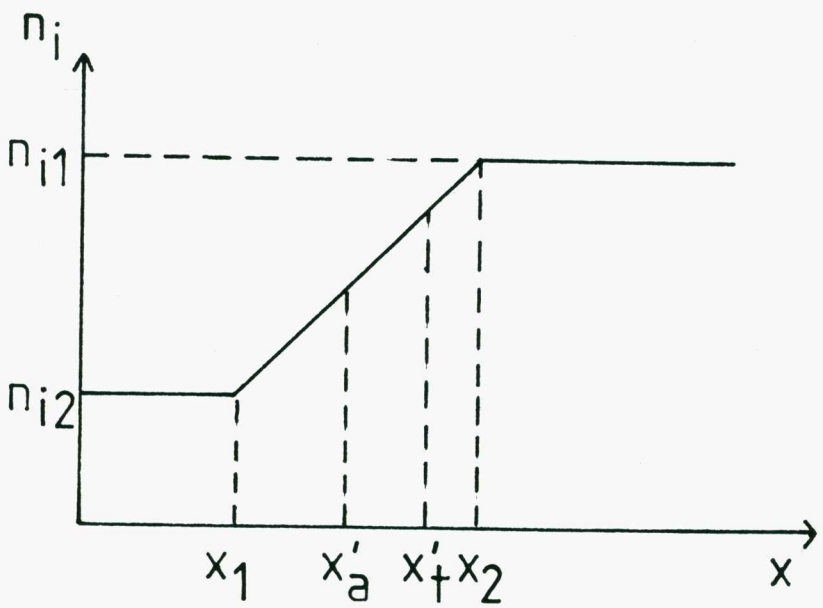

Fig. 1.1 The model density profile. A constant density gradient exists between x_1 and x_2.

Under these assumptions the wave equation in the ideal MHD limit (i.e. (1.1) - (1.4)) has the form (Tataronis and Grossmann, 1973; Chen and Hasegawa, 1974)

$$\frac{d}{dx}\left\{\frac{\varepsilon}{k_y^2 - \varepsilon}\frac{d\xi_x}{dx}\right\} - \varepsilon\xi_x = 0 \qquad (1.6)$$

where $\varepsilon = \omega^2/v_A^2(x) - k_z^2$, $v_A(x)(= (B_0^2/4\pi\rho_i(x))^{\frac{1}{2}})$ is the local Alfvén speed, ρ_i is the ion mass density and ξ_x is fluid displacement in the x direction. In the derivation of (1.1), the parallel electric field is neglected because of the large conductivity in the z direction.

In a homogeneous plasma, (1.6) reduces to

$$\varepsilon(\varepsilon - k_y^2 - k_x^2) = 0 \qquad (1.7)$$

where k_x is the wavenumber in the x direction. From (1.7), the dispersion relation for the shear Alfvén wave (hereafter SAW) is given by

$$\omega^2 = k_z^2 v_A^2 \qquad (\text{i.e. } \varepsilon = 0) \qquad (1.8)$$

and that of the magnetosonic wave (hereafter MW) by

$$\omega^2 = k^2 v_A^2 \qquad (\text{i.e. } \varepsilon - k_y^2 - k_x^2 = 0) \qquad (1.9)$$

where $k^2 = k_z^2 + k_y^2 + k_x^2$.

In an inhomogeneous plasma, the MW propagates on the high density side of the linear turning point x_t', $\varepsilon(x_t') = k_y^2$. (In this thesis, the notation of Ott et al. (1978) is adopted with linear turning points referring to points where $k_x = 0$). However, the SAW root which occurs

at x_a', $\varepsilon(x_a') = 0$, does not represent a wave but rather a resonance in the plasma (Ott et al., 1978). This resonance is called the Alfvén resonance and is where mode conversion of the MW occurs.

In tokamaks like the Princeton Large Torus (PLT) tokamak (Karney et al., 1979) and in the Sydney University TORTUS tokamak (Cross et al., 1982) ideal MHD theory is not valid because the ratio of the wave frequency, ω, to the ion-cyclotron frequency Ω_i is non-negligible. In this case, Karney et al. (1979) have shown (using the cold plasma dielectric tensor and (1.1), (1.2) and (1.5)) that the wave equation has the form

$$\frac{d^2E_y}{du^2} - \frac{M^2}{u(u - M^2)}\frac{dE_y}{du} + \left(\frac{u^2 - S^2}{u} - M^2 + \frac{MS}{u(u - M^2)}\right) E_y = 0 \qquad (1.10)$$

$$M = k_y/(k_z^2K)^{1/3}$$

$$S = (\omega/\Omega_i)(k_z/K)^{2/3}$$

$$u = (x - x_a)(k_z^2K)^{1/3}$$

$$K = \frac{1}{n_i}\frac{dn_i}{dx}\bigg|_{x_a}$$

where x_a is defined by $\omega^2 = k_z^2v_A^2(x_a)(1 - \omega^2/\Omega_i^2)$, n_i is the ion number density and terms of order S^4 and $M^2\omega/\Omega_i$ have been neglected as have finite Larmor radius and parallel electric field corrections.

In the limit $\omega/\Omega_i \to 0$, (1.10) reduces to (1.6) with the y component of the electric field, E_y, being proportional to ξ_x as given by

(1.4). The retention of finite ω/Ω_i terms shifts the Alfvén resonance from the point where $\omega^2 = k_z^2 v_A^2(x_a')$ to the point where $\omega^2 = k_z^2 v_A^2(x_a)(1 - \omega^2/\Omega_i^2)$. This resonance is also sometimes called the perpendicular ion-cyclotron resonance (Stix, 1962, p. 62).

The finite frequency corrections also modify the dispersion of the SAW and MW. In particular, for a homogeneous plasma, (1.10) reduces to

$$A_k(A_k - k_y^2 - k_x^2) - \left(\frac{\omega^2}{v_A^2}\frac{\omega}{\Omega_i}\frac{1}{1 - \omega^2/\Omega_i^2}\right)^2 = 0 \qquad (1.11)$$

where $A_k = \omega^2/v_A^2(1 - \omega^2/\Omega_i^2) - k_z^2$. The dispersion relation for the SAW in this case has the form

$$\omega^2 \simeq k_z^2 v_A^2/(1 + (\omega k/\Omega_i k_z)^2) \qquad (1.12)$$

while that of the MW has the form

$$\omega^2 \simeq k^2 v_A^2/(1 - (\omega k_z/\Omega_i k_\perp)^2) \qquad (1.13)$$

where $k_\perp^2 = k_y^2 + k_x^2$. In the derivation of (1.12) and (1.13) it has been assumed that $\omega/\Omega_i << |k_\perp^2/k^2|$.

It can be seen from either of (1.9) or (1.13) that the magnetosonic wave turning point (i.e. the point where $k_x^2 = 0$) occurs on the high density side of the Alfvén resonance. Thus, depending on the magnitude of k_y, two possible configurations for Alfvén resonance heating are possible. The first is when k_y^2 is sufficiently large so that the magnetosonic wave turning point is not present in the plasma. In this

case, a magnetosonic surface wave (i.e. a cutoff magnetosonic wave) is excited by the antenna. The second is when k_y is sufficiently small so that the magnetosonic wave turning point is present in the plasma and a magnetosonic body wave is excited. The relevant heating scheme (i.e. surface wave or body wave heating) is determined by the antenna configuration.

1.2.2 Surface-Wave Heating

Tataronis and Grossmann (1973), Chen and Hasegawa (1974), Hasegawa and Chen (1976), Stix (1980), Ross et al. (1982) and Cramer and Donnelly (1983) have considered Alfvén wave heating for the case in which k_y is sufficiently large so that the MW turning point is not present in the plasma. Such a configuration can be obtained if an antenna of the form shown in Fig. 1.2 is used. In this case, the antenna excites a surface wave which is damped by mode conversion to the SAW. The subsequent dissipation of the SAW produces plasma heating.

Ionson (1978) and Wentzel (1979a, 1979b) have also used this type of mechanism in a model for the heating of solar coronal loops. However, in their case the surface wave is excited by some plasma disturbance at the feet of the coronal loops.

The properties of the surface-wave eigenmode can be derived from the wave equation, (1.6), which for $k_y^2 >> k_z^2$ and $\omega << \Omega_i$ has the approximate form

$$\frac{d^2\xi_x}{dX^2} + \frac{1}{X}\frac{d\xi_x}{dX} - \xi_x = 0 \qquad (1.14)$$

$$X = \left(\frac{\omega^2}{k_z^2 v_A^2} - 1\right)\frac{|k_y|}{K} .$$

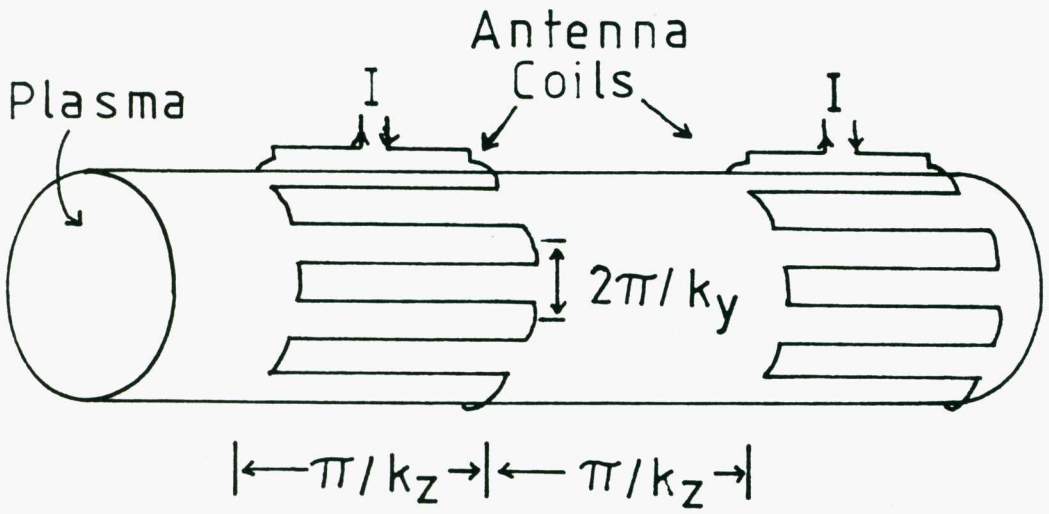

Fig. 1.2 Schematic diagram of an antenna with $k_y^2 >> k_z^2$ for surface wave Alfvén resonance heating. (After Chen and Hasegawa, 1974).

In this case, the two linearly independent solutions, for the density profile shown in Fig. 1.1, are

$$\xi_{x1}(x) = \exp(k_\perp x) \qquad x \leq x_1$$

$$= C_{11} I_0(X) + C_{12} K_0(X) \qquad x_1 \leq x \leq x_2 \qquad (1.15)$$

$$= C_{21} \exp(-k_\perp x) + C_{22} \exp(k_\perp x) \qquad x \geq x_2$$

$$\xi_{x2}(x) = D_{11} \exp(-k_\perp x) + D_{12} \exp(k_\perp x) \qquad x \leq x_1$$

$$= D_{21} I_0(X) + D_{22} K_0(X) \qquad x_1 \leq x \leq x_2 \qquad (1.16)$$

$$= \exp(-k_\perp x) \qquad x \geq x_2$$

where $k_\perp = |k_y|$, I_0 and K_0 are the zeroth-order modified Bessel functions (Olver, 1970) and the constants C_{mn} and D_{mn} are determined by the continuity of ξ_x and its derivative. The logarithm in K_0 is defined by appealing to causality (Chen and Hasegawa, 1974; Ott et al., 1978) i.e. ω is assumed to have a small positive imaginary part so that

$$\begin{aligned} \ell nX &= \ell nX && X > 0 \\ &= \ell n|X| + i\pi && X < 0. \end{aligned} \qquad (1.17)$$

The discontinuity of the imaginary part of ξ_x represents the resonant absorption of energy from the MW.

By applying the boundary condition that ξ_x must be finite as $x \to \pm \infty$ (i.e. $C_{22} = 0$ or $D_{11} = 0$), the dispersion equation for the surface wave is found to have the form

$$(I_0(X_2) + I_1(X_2))(K_0(X_1) + K_1(X_1)) - (I_0(X_1) - I_1(X_1))(K_0(X_2) - K_1(X_2)) = 0 \qquad (1.18a)$$

i.e. $$(I_0(X_2) + I_1(X_2))[K_0(-X_1) - K_1(-X_1) - \pi i(I_0(-X_1) + I_1(-X_1))]$$

$$- (I_0(-X_1) + I_1(-X_1))(K_0(X_2) - K_1(X_2)) = 0 \qquad (1.18b)$$

where $X_i = X(x_i)$, $i = 1,2$ and (1.17) has been used in the derivation of (1.18).

The above dispersion equation has been studied by Ionson (1978), Wentzel (1979a) and Cramer and Donnelly (1983) for the case of a sharp discontinuity i.e. $K^2 >> k_y^2$. In this case, (1.18b) reduces to (Ionson, 1978)

$$\frac{1}{X_1} + \frac{1}{X_2} = i\pi. \qquad (1.19a)$$

The imaginary part of (1.19a) is half that given by Wentzel (1979a) as he assumes that the logarithm for negative arguments has an imaginary part equal to 2π which is incorrect.

In tokamaks, n_{i1} is much less than n_{i2} so that the dispersion relation given by (1.19a) can be approximated by

$$\omega^2 = 2k_z^2 v_A^2(x_2)(1 - i\pi|k_y|/4K). \qquad (1.19b)$$

This dispersion equation implies that the Alfvén resonance (i.e. the point where $\omega^2 = k_z^2 v_A^2(x)$) occurs at approximately half the maximum plasma density. The damping of the surface wave as given by the imaginary part

of (1.19b) arises from energy absorption at the Alfvén resonance. This damping increases with increasing $|k_y|/K$; for a step discontinuity in density (i.e. $K \to \infty$), the surface wave is undamped.

To determine the actual mechanism for the damping of the surface wave, Hasegawa and Chen (1975, 1976) included finite Larmor radius and parallel electric field corrections in the wave equation using kinetic theory. They found that the wave equation (1.14) is replaced by a fourth order differential equation of the form

$$\left(\frac{\omega^2}{k_z^2 v_a^2}\,\frac{3}{4}\,\rho_i^2\,\frac{d^3}{dx^3} + \frac{d^2}{dx^2}\,\frac{1}{g_n}\,\frac{T_e}{T_i}\,\rho_i^2\,\frac{d}{dx}\right)\left(g_n\,\frac{dE_y}{dx}\right)$$

$$+\left[\frac{d}{dx}\left(\frac{\omega^2}{k_z^2 v_a^2}\,g_n - 1\right)\frac{d}{dx} - k_y^2\left(\frac{\omega^2}{k_z^2 v_a^2}\,g_n - 1\right)\right]E_y = 0 \qquad (1.20)$$

where $\rho_i = v_{Ti}/\Omega_i$, v_{Ti} is the ion thermal speed, v_a is the Alfvén speed evaluated at the maximum plasma density, g_n is the normalized plasma density (being equal to unity at the maximum density) and $|k_y| \ll |d/dx|$ is assumed.

The wave fields described by (1.20) differ from those given by ideal MHD theory (i.e. (1.15) and (1.16)) in that the logarithmic singularity at the Alfvén resonance is removed (Rabenstein, 1958). However, Hasegawa and Chen (1976) still found that the MW loses the same amount of energy as given by ideal MHD theory at the Alfvén resonance but this energy appears as a SAW which propagates on the high density side of the Alfvén resonance. Away from the Alfvén resonance where $-id/dx$ in (1.20) can be replaced by $k_\perp$, the dispersion relation of the SAW is found to have the approximate form

$$\omega^2 = k_z^2 v_A^2 [1 + \lambda_i (3/4 + T_e/T_i)] \tag{1.21}$$

where $\lambda_i = k_\perp^2 \rho_i^2$. Because the above corrections to the SAW dispersion equation were originally derived from kinetic theory, the wave described by (1.21) is sometimes called the kinetic Alfvén wave (Hasegawa and Chen, 1976).

It was later pointed out by Stix (1980) and Ross et al. (1982) that the dispersion equation for the SAW as given by (1.21) is only valid for $\beta m_i/m_e > 1$ where β is the ratio of the thermal pressure to the magnetic pressure. In the opposite limit, the SAW propagates on the low density side of the Alfvén resonance. However, they found that even in this case the total absorption rate is still approximately the same as given by MHD. This last point is of particular importance because it allows the neglect of finite electron mass and Larmor radius corrections without producing significant errors in the estimate of the energy lost by the MW at the Alfvén resonance.

Recently, Cramer and Donnelly (1983) investigated the properties of the magnetosonic surface wave with the inclusion of finite ω/Ω_i corrections but with the neglect of finite Larmor radius and electron mass corrections. They found that the finite ω/Ω_i corrections are important in that they split the low frequency surface wave into two modes whose properties depend on the sign of k_y/K and the magnitude of ω/Ω_i; the damping being larger for the mode with k_y/K negative than for the mode with k_y/K positive.

1.2.3 Body Wave Heating

Ott et al. (1978) examined Alfvén resonance heating for the case where $k_y^2 << k_z^2$, $\omega/\Omega_i << 1$ and where the magnetic field also has a small y component (i.e. $0 < B_y/B_z << 1$). In this case, the magnetosonic wave turning point lies close to the Alfvén resonance and the antenna excites a magnetosonic body wave. However, plasma heating still occurs via the mode conversion of the MW into a SAW and the subsequent damping of the SAW. Experimentally, $k_y^2 << k_z^2$ is obtained using an antenna configuration of the form shown in Fig. 1.3. It differs from the antenna used in surface wave heating in that the antenna here consists of a single coil loop without any twists.

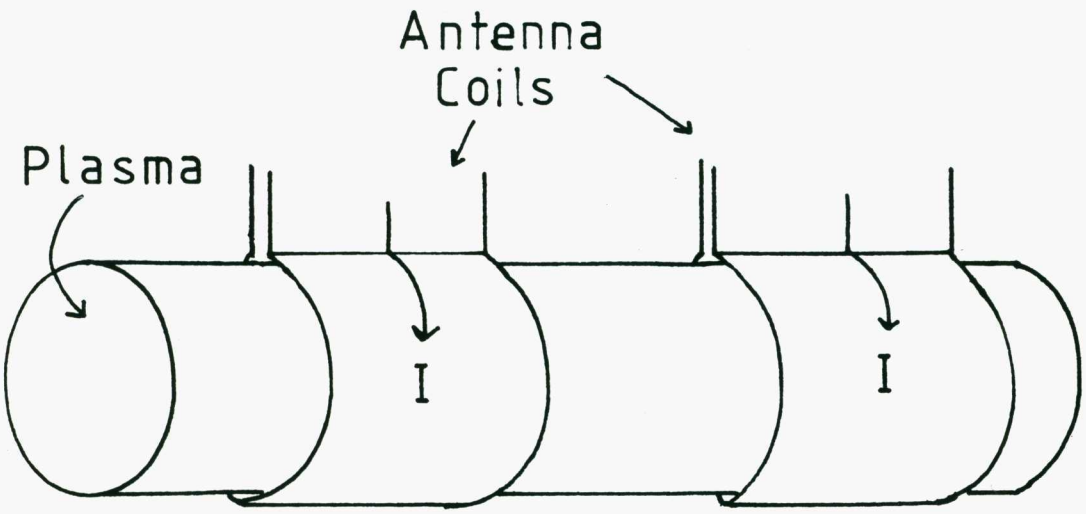

Fig. 1.3 Schematic diagram of an antenna with $k_y^2 << k_z^2$ for body wave Alfvén resonance heating. (After Ott et al., 1978).

Karney et al. (1979) extended the work of Ott et al. (1978) to include finite ω/Ω_i corrections assuming $B_y = 0$. They were motivated by the fact that ω/Ω_i for MW eigenmodes in PLT is non-negligible. Following the method of Karney et al. (1979), the absorption of the MW at the Alfvén resonance is now estimated by considering the reflection of the MW from a constant density gradient using the solution to the wave equation (1.10).

The two linearly independent solutions of (1.10) about x_a are (Karney et al., 1979)

$$E_{y1} = 1 + (S/M + S^2)\, u$$
$$E_{y2} = 1 + MS(1 - MS)\, E_{y1} \ell nu \qquad (1.22)$$

where M^2, $S << 1$ is assumed. The logarithm in (1.22) is again defined by (1.17).

The linearly independent solutions for E_y which are valid away from the Alfvén resonance are the Airy functions Ai(-u) and Bi(-u) (Antosiewicz, 1970).

An analytical solution which is valid throughout the density gradient is obtained by matching the Airy function solutions (and their derivatives) to those given by (1.22) in the region where both types of solutions are valid i.e. in the regions where $M^2 << -u \lesssim u^0 << 1$ and $M^2 << u << 1$ (Karney et al., 1979). By using this procedure the solution which is finite as $u \to -\infty$ is found to have the form

$$
\begin{aligned}
E_y &= Ai(-u) && u \lesssim -u^0 \\
&= a_{11}E_{y1} + a_{12}E_{y2} && -u^0 \lesssim u \lesssim u^0 \qquad (1.23) \\
&= a_{21}Ai(-u) + a_{22}Bi(-u) && u \gtrsim u^0
\end{aligned}
$$

where

$$a_{11} = (M/S)\, c_2 + \ell n(-u^0)(M^2 c_2 - MSc_1)$$

$$a_{12} = c_1 - (M/S)\, c_2$$

$$a_{21} = 1$$

$$a_{22} = i(\pi/2\sqrt{3})\,[M(c_2/c_1)^{1/2} - S(c_1/c_2)^{1/2}]$$

$$c_1 = Ai(0) \simeq 0.355$$

$$c_2 = -Ai'(0) \simeq 0.259.$$

The asymptotic form of (1.23) for $u \gg u^0$ is obtained using (A.3) and (A.4). The incident MW is represented by the $\exp(\frac{2}{3}(-u)^{3/2})$ terms in the asymptotic expansions and the reflected MW by the $\exp(-\frac{2}{3}(-u)^{3/2})$ terms. By comparing the incident wave amplitude to the reflected wave amplitude, the fractional power lost by the magnetosonic wave on reflection from a constant density gradient is found to have the form (Karney et al., 1979)

$$q = (2\pi/\sqrt{3})\,[M(c_2/c_1)^{\frac{1}{2}} - S(c_1/c_2)^{\frac{1}{2}}]^2 . \qquad (1.24)$$

It is seen from (1.24) that for S = 0 i.e. $\omega/\Omega_i = 0$, the fractional power absorbed increases with $|M|$ and is zero for $k_y = 0$. The effect of a finite ω/Ω_i is to increase q for k_y/K negative and to decrease q for k_y/K positive with no energy absorption occurring for $S = Mc_2/c_1$. Note that the above dependence of the energy absorption on k_y/K is similar to that obtained by Cramer and Donnelly (1983) for the damping of the surface wave due to resonant mode conversion. This similarity is to be expected as the mode conversion processes are the same in the two cases and only different boundary conditions applied.

Winglee (1982) extended the work of Karney et al. (1979) to include the effect of terms of order $M^2\omega/\Omega_i$ and M of arbitrary magnitude on the fractional power lost by the MW on reflection from a constant density gradient. This work is discussed in detail in Chapter 3.

1.3 COMPARISON WITH ION-ION HYBRID RESONANCE HEATING

An alternative heating scheme to the above is the resonant mode conversion of a magnetosonic (fast) wave into an ion-Bernstein wave in a two ion-component plasma (Stix, 1975; Perkins, 1977; Jacquinot et al., 1977; Scharer et al., 1977; Colestock et al., 1980; Chiu et al., 1982). The analysis is similar to the above except that k_z is assumed to be small and $\omega/k_z v_{Te} >> 1$ (v_{Te} being the electron thermal speed). In this case the resonance is known as the ion-ion hybrid resonance and occurs for a D-T plasma at those points within the plasma at which

$$\omega = \Omega_T \left[\frac{1.5(1.5\rho_T + \rho_D)}{\rho_T + 1.5\rho_D} \right]^{\frac{1}{2}} \tag{1.25}$$

where Ω_T is the tritium cyclotron frequency and ρ_T and ρ_D are the percentage concentrations of tritium and deuterium respectively.

Using the cold plasma approximation (i.e. $\omega/k_z v_{Te} >> 1$), Perkins (1977) found that in the case of a minority light ion species in a heavy ion plasma roughly equal electron and ion heating is possible. This type of heating was subsequently demonstrated in a D-majority H-minority plasma (e.g. JFT-2 Group, 1982; Equipe TFR, 1982). However, Perkins (1977) found that in the opposite case only electron heating is possible. This feature implies that if ion-ion hybrid heating is to be utilized in the heating of a D-T plasma (this plasma having the lowest ignition temperature) the concentration of tritium must be greater than the concentration of deuterium. Unfortunately, this configuration is expensive as tritium does not occur naturally to any great extent.

On the other hand, in a low β plasma, ion heating using the Alfvén resonance scheme is only possible via the parametric decay of the shear Alfvén wave into an ion-sound wave (Hasegawa and Chen, 1976). The need for parametric decay arises from the fact that in a low β plasma only the ion-sound wave is subject to ion-Landau damping. However, the parametric decay is limited to only a small region about the Alfvén resonance where the wave fields are large so that only a small portion of the energy mode converted into the shear Alfvén wave is available for ion heating. Thus, the effectiveness of the Alfvén resonance heating in heating ions is doubtful. A similar conclusion can be drawn from the experiments using Alfvén resonance heating where there is always a large excess

of electron heating over ion heating (Section 1.1; Obiki et al., 1977; de Chambrier et al., 1982b).

The main disadvantage of the ion-ion hybrid resonance heating scheme is that the resonance occurs on the constant magnetic field surface given by (1.25) so that some surface heating occurs. However, in the Alfvén resonance heating scheme, the resonance lies approximately on a surface of constant density (i.e. $A_k = 0$) which can be well inside the plasma so that surface heating is inhibited.

1.4 OPTIMIZATION OF RF HEATING

In the previously cited references for Alfvén resonance heating, emphasis has been placed on the absorption of the fast magnetosonic wave due to mode coupling. There has been little work in determining how to efficiently heat the ions in the plasma interior. Further, the parameter range investigated in many of the previously cited works may not be representative of the conditions in the tokamak. For example, in a high power heating experiment where there are many heating coils present, it is quite possible that $k_z^2 \simeq k_y^2 \simeq K^2$ and ω/Ω_i may not be non-negligible. This parameter range has not been previously examined.

The purpose of the next two Chapters is to obtain an estimate of the optimum operating conditions for the Alfvén resonance heating scheme for realistic tokamak operating conditions. To make the estimate tractable the heating scheme is divided into three individual processes:

(i) the collisionless damping (and dispersion) of the magnetosonic and shear Alfvén waves in a locally homogeneous plasma (Chapter 2);

(ii) the mode conversion of the magnetosonic wave at the Alfvén resonance in an inhomogeneous plasma (Chapter 3);

(iii) the response of an antenna in the presence of the Alfvén resonance (Chapter 3).

The damping of the SAW determines the deposition of energy amongst the various components of the plasma while the mode conversion processes determine the actual amount of energy coupled into the SAW. Emphasis is placed on the Alfvén resonance heating scheme because, as is shown in the next two Chapters, with the addition of a minority ion species in the Alfvén resonance heating scheme the problems of both ion-ion hybrid and Alfvén resonance heating can be overcome.

CHAPTER 2

ALFVÉN RESONANCE HEATING IN A MULTIPLE ION-COMPONENT PLASMA

2.1 INTRODUCTION

In this Chapter, the dispersion, polarization and damping of the magnetosonic wave (MW) and the shear Alfvén wave (SAW) are determined as functions of density for typical tokamak parameters (a review of tokamak operating conditions is given by Rutherford, 1980). Such a study enables the simulation of the propagation of these waves through the plasma and thereby enables the determination of the wave parameters (ω, k_z and k_y) for which heating of the ions in the plasma interior is possible.

The dispersion and damping of the MW and SAW in a single ion-component plasma have previously been studied by Akhiezer et al. (1967, Ch. 2), Sitenko (1967, Ch. 7), Hasegawa and Chen (1976), Stix (1980) and Ross et al. (1982) under various conditions. However, the ion heating produced by the damping of the SAW (and the MW) in a single ion-component low-β plasma is small (Chapter 1).

As discussed here and in Winglee (1983a) this problem is overcome by using Alfvén resonance heating in a multiple ion-component plasma. This heating scheme, hereafter called minority ion-cyclotron heating, is similar to the ion-ion hybrid resonance heating scheme except that k_z is large rather than small. In this case, the minority ions can gyro-resonantly damp the MW and SAW without significantly modifying the dispersion of the MW and SAW and mode coupling between these two waves still occurs via the Alfvén resonance (Section 2.3).

This heating scheme is thereby able to overcome the problems of both ion-ion hybrid and Alfvén resonance heating i.e. the problems of excess electron heating and heating of the plasma surface.

To determine the properties of the MW and SAW, the local dispersion equation (Section 2.2) is solved analytically with the inclusion of finite Larmor radius, ω/Ω_i, electron mass and minority ion corrections. Expressions for the dispersion, polarization and damping of the MW and SAW are given in Sections 2.3, 2.4 and 2.5 respectively. The dispersion and damping give the regions in the plasma in which the MW and SAW propagate and heat. The polarization vectors allow a physical interpretation of the mode coupling processes which is lacking in the previously cited studies on mode coupling. In Section 2.6, numerical solutions to the dispersion equation are presented. A summary of results is given in Section 2.7.

2.2 THE DISPERSION EQUATION

The wave equation for a locally homogeneous plasma has the form (Melrose, 1980a, p. 49).

$$\Lambda_{ij}(\underset{\sim}{k},\omega)\, E_j(\underset{\sim}{k},\omega) = 0 \qquad (2.1)$$

$$\underset{\approx}{\Lambda} = \begin{pmatrix} \varepsilon_{11} - n^2\cos^2\theta_k & \varepsilon_{12} & \varepsilon_{13} + n^2\cos\theta_k\sin\theta_k \\ -\varepsilon_{12} & \varepsilon_{22} - n^2 & \varepsilon_{23} \\ \varepsilon_{13} + n^2\cos\theta_k\sin\theta_k & -\varepsilon_{23} & \varepsilon_{33} - n^2\sin^2\theta_k \end{pmatrix} \qquad (2.2)$$

where $\underset{\approx}{\varepsilon}$ is the dielectric tensor, the magnetic field is in the 3-direction, $\underset{\sim}{k}$ is in the 1-3 plane and θ_k is the angle between the magnetic field and $\underset{\sim}{k}$. The condition for the existence of a non-trivial solution to (2.1) is that ω and $\underset{\sim}{k}$ satisfy the dispersion equation

$$\det(\underset{\approx}{\Lambda}) = 0. \tag{2.3}$$

The elements of the dielectric tensor are given in standard textbooks such as Stix (1962, Ch. 8), Krall and Trivelpiece (1973, Ch. 8) and Melrose (1980b, Ch. 12). To evaluate the dielectric tensor, the plasma is assumed in the following to consist of electron, majority ion and minority ion components with quantities related to these components being denoted by subscripts e, i and m respectively. It is further assumed that $\omega \lesssim \Omega_m < \Omega_i$, $n_m << n_i$ and that the plasma has a low β with the electron and ion temperatures approximately equal. In this case, the dielectric tensor can be approximated by the form given in Table 2.1.

The dielectric tensor given in Table 2.1 is used in Section 2.6 to evaluate numerical solutions to the dispersion equation (2.3). However, approximate analytic solutions to (2.3) can be obtained by approximating the plasma dispersion function, $\hat{\phi}$, by either its series expansion or by its asymptotic expansion, depending on the magnitude of the arguments of the plasma dispersion function. In particular, for a low β plasma in which $\omega \simeq k_z v_A \lesssim \Omega_m < \Omega_i$, these arguments are such that $|y_{en}| >> 1$, $n = \pm 1$, y_{e0} is of arbitrary magnitude, $|y_{in}| >> 1$ for $n = 0, \pm 1$, and $|y_{mn}| >> 1$, $n = 0, -1$. It is also assumed that the minority ion species is only present if minority ion-cyclotron heating is to be utilized (i.e. $\omega \simeq \Omega_m$) and that the plasma β is sufficiently large so that

TABLE 2.1 DIELECTRIC TENSOR ELEMENTS FOR $\omega \lesssim \Omega_m < \Omega_i$

Element	Expression
ε_{11}	$1 + \sum_\alpha \frac{\omega_{p\alpha}^2}{\Omega_\alpha^2} \frac{e^{-\lambda_\alpha}}{\lambda_\alpha} \left\{ (e^{\lambda_\alpha} - I_0) + I_1 \left[2 + \frac{\Omega_\alpha^2}{\sqrt{2}\, k_z v_{T\alpha} \omega} \left(\frac{\hat{\phi}(y_{\alpha 1})}{y_{\alpha 1}} + \frac{\hat{\phi}(y_{\alpha -1})}{y_{\alpha -1}} \right) \right] + \sum_{\lvert n \rvert > 1} \left(\frac{\omega^2 + 3k_z^2 v_{T\alpha}^2}{\Omega_\alpha^2} \right) \frac{I_n}{n^2} \right\}$
ε_{22}	$\varepsilon_{11} + \sum_\alpha \frac{2\omega_{p\alpha}^2}{\omega^2} \lambda_\alpha e^{-\lambda_\alpha} \left\{ \hat{\phi}(y_{\alpha 0})(I_0' - I_0) + \frac{\omega}{\sqrt{2}\, k_z v_{t\alpha}} (I_1' - I_1) \left(\frac{\hat{\phi}(y_{\alpha 1})}{y_{\alpha 1}} + \frac{\hat{\phi}(y_{\alpha -1})}{y_{\alpha -1}} \right) - \frac{\omega^2}{\Omega_\alpha^2} \sum_{\lvert n \rvert > 1} \frac{I_n' - I_n}{n^2} \right\}$
$\varepsilon_{12} = -\varepsilon_{21}$	$i \sum_\alpha \varepsilon_\alpha \frac{\omega_{p\alpha}^2}{\omega \Omega_\alpha} e^{-\lambda_\alpha} \left\{ (I_0 - I_0') + (I_1 - I_1') \left[2 + \frac{\Omega_\alpha}{\sqrt{2}\, k_z v_{T\alpha}} \left(\frac{\hat{\phi}(y_{\alpha 1})}{y_{\alpha 1}} - \frac{\hat{\phi}(y_{\alpha -1})}{y_{\alpha -1}} \right) \right] + \sum_{\lvert n \rvert > 1} \left(\frac{\omega^2 + k_z^2 v_{T\alpha}^2}{\Omega_\alpha^2} \right) \left(\frac{I_n' - I_n}{n^2} \right) \right\}$
$\varepsilon_{13} = \varepsilon_{31}$	$- \sum_\alpha \frac{2\omega_{p\alpha}^2}{\Omega_\alpha^2} \frac{k_z}{k_\perp} e^{-\lambda_\alpha} \left\{ \frac{\Omega_\alpha}{\omega} \frac{\Omega_\alpha^2}{2k_z^2 v_{T\alpha}^2} I_1 \left(\hat{\phi}(y_{\alpha 1}) - \hat{\phi}(y_{\alpha -1}) \right) + \sum_{\lvert n \rvert > 1} \frac{I_n}{n^2} \right\}$

TABLE 2.1 (CONT.)

Element	Expression
$\varepsilon_{23} = -\varepsilon_{32}$	$\frac{ik_\perp}{k_z} \sum_\alpha \varepsilon_\alpha \frac{\omega_{p\alpha}^2}{\omega\Omega_\alpha} e^{-\lambda_\alpha} \left\{ \left(1-\hat{\phi}(y_{\alpha 0}) \right)(I_0-I_0') + \left(2-\hat{\phi}(y_{\alpha 1}) - \hat{\phi}(y_{\alpha -1})\right)(I_1-I_1') + \sum_{\lvert n\rvert>1} \frac{k_z^2 v_{T\alpha}^2}{\Omega_\alpha^2} \frac{I_n' - I_n}{n^2} \right\}$
ε_{33}	$1 + \sum_\alpha \frac{\omega_{p\alpha}^2}{k_z^2 v_{T\alpha}^2} e^{-\lambda_\alpha} \left\{ \left(1-\hat{\phi}(y_{\alpha 0}) \right) I_0 - \frac{\sqrt{2}\, k_z v_{T\alpha}}{\omega} I_1 \left[y_{\alpha 1}\hat{\phi}(y_{\alpha 1}) + y_{\alpha 1}\hat{\phi}(y_{\alpha -1}) - 2 \right] + \sum_{\lvert n\rvert>1} \frac{k_z^2 v_{T\alpha}^2}{\Omega_\alpha^2} \frac{I_n}{n^2} \right\}$

where $\lambda_\alpha = k_\perp^2 v_{T\alpha}^2/\Omega_\alpha$, $y_{\alpha n} = (\omega - n\Omega_\alpha)/\sqrt{2}\, k_z v_{T\alpha}$, $\hat{\phi}(y_{\alpha n}) = -iy_{\alpha n} F_0(y_{\alpha n})$, F_0 is the plasma dispersion function in the notation of Stix (1962), $I_n (= I_n(\lambda_\alpha))$ is the n order modified Bessel function, ε_α is the sign of species α and $\omega_{p\alpha} (= (4\pi n_\alpha q_\alpha^2/m_\alpha)^{1/2})$ and $\Omega_\alpha (= |q_\alpha| B_0/m_\alpha c)$ are the plasma and cyclotron frequencies of species α respectively.

$$y_{ml} \simeq \frac{\omega - \Omega_m(x_c)}{\Omega_m(x_c)} \frac{v_A(x_c)}{v_{Tm}} \simeq \frac{\Delta B}{2B} \frac{1}{\beta^{1/2}} \lesssim 1$$

i.e. $$\frac{\Delta B}{2B(x_c)} \lesssim \beta^{1/2}$$

where x_c is the position of the centre of the plasma and ΔB is the change in the magnetic field across the Alfvén resonance surface. This requirement is easily fulfilled for tokamaks in which β is greater than a few per cent and the Alfvén resonance is near the centre of the plasma.

Assuming the above inequalities for the arguments of the plasma dispersion function, the dielectric tensor is found to have the form given in Table 2.2. By ordering the elements of this dielectric tensor in terms of the small parameters ω^2/Ω_i^2, v_A^2/c^2, v_{Ti}^2/v_A^2, y_{ml} and λ_i, v_A being the Alfvén speed of the majority ion and retaining only first order corrections the dispersion equation (2.3) can be approximated by

$$(n^2\cos^2\theta_k - \varepsilon_{11})[(n^2-\varepsilon_{22})\,\varepsilon_{33} - \varepsilon_{23}^2]$$

$$\simeq -\{n^4\varepsilon_{11}\sin^2\theta_k + \varepsilon_{33}\varepsilon_{12}^2 - n^2\varepsilon_{12}^2\sin^2\theta_k$$

$$+ n^2(2\varepsilon_{12}\varepsilon_{23}\sin\theta_k\cos\theta_k - \varepsilon_{11}\varepsilon_{22}\sin^2\theta_k)\} \qquad (2.4)$$

The terms on the right hand side of (2.4) are first order corrections as are the contributions from the minority ion species since $n_m \ll n_i$ by assumption.

TABLE 2.2 The approximate form of the dielectric tensor for $\lambda_m \lesssim 1$, $|y_{en}| \gg 1$, $n = \pm 1$, $|y_{in}| \gg 1$, $n = 0, \pm 1$, $|y_{mn}| \gg 1$, $n = 0, -1$ and $|y_{m1}| \ll 1$. In (a) the hermitian part is given and in (b) the antihermitian part.

(a)

Element	Expression
ε^h_{11}	$1 + \frac{\omega_{pe}^2}{\Omega_e^2} + \frac{\omega_{pi}^2}{\Omega_i^2}\left(\frac{\Omega_i^2}{\Omega_i^2-\omega^2} - \frac{3}{4}\lambda_i\right) + \frac{\omega_{pm}^2}{\Omega_m^2}\left(1 - \frac{1}{2}e^{-\lambda_m}(\alpha_m + \frac{5}{2})\right)$
ε^h_{22}	$\varepsilon^h_{11} - \frac{2\omega_{pi}^2}{\omega^2}\lambda_i\left(1 + \frac{\omega^2}{\omega^2-\Omega_i^2}\right)$
ε^h_{12}	$\frac{\omega_{pi}^2}{\omega\Omega_i}e^{-\lambda_i}\left(-\frac{3}{2}\lambda_i + \frac{\omega^2}{\Omega_i^2-\omega^2}\right) + \frac{\omega_{pm}^2}{\omega\Omega_m}e^{-\lambda_m}\left(-\frac{3}{2}\lambda_m - \frac{1}{2}e^{-\lambda_m}(\alpha_m + \frac{3}{2})\right)$
ε^h_{13}	0
ε^h_{23}	$-\frac{i\omega_{pe}^2}{\omega\Omega_e}\frac{k_\perp}{k_z}\sigma_e$
ε^h_{33}	$\frac{\omega_{pe}^2}{k_z^2 v_{Te}^2}\sigma_e - \frac{\omega_{pi}^2}{\omega^2} + 1$

$$\sigma_e = 1 \qquad |y_{e0}| \ll 1$$
$$= -k_z^2 v_{Te}^2/\omega^2 \qquad |y_{e0}| \gg 1$$

TABLE 2.2 (CONT.)

(b)

Element	Expression
ε^a_{11}	$i\frac{\sqrt{\pi}}{2}\frac{\omega^2_{pm}}{\Omega^2_m}\frac{\omega}{\lvert k_z\rvert v_{Tm}}\frac{\Omega^2_m}{\omega^2}\exp\left(-(\lambda_m + y^2_{m1})\right)$
ε^a_{22}	$\varepsilon^a_{11} - i\sqrt{\frac{\pi}{2}}\frac{\omega^2_{pm}}{\omega^2}\frac{\omega}{\lvert k_z\rvert v_{Tm}}\lambda_m\exp\left(-(\lambda_m + y^2_{m1})\right) + i\sqrt{2\pi}\frac{\omega^2_{pe}}{\Omega^2_e}\frac{k^2_\perp v_{Te}}{\lvert k_z\rvert\omega}\exp(-y^2_{e0})$
ε^a_{12}	$\frac{1}{2}\sqrt{\frac{\pi}{2}}\frac{\omega^2_{pm}}{\omega\Omega_m}\frac{\Omega_m}{\lvert k_z\rvert v_{Tm}}\exp\left(-(\lambda_m + y^2_{m1})\right)$
ε^a_{13}	0
ε^a_{23}	$\sqrt{\frac{\pi}{2}}\frac{\omega^2_{pe}}{\Omega^2_e}\frac{k_\perp}{k_z}\frac{1}{\lvert k_z\rvert v_{Te}}\exp(-y^2_{e0})$
ε^a_{33}	$i\sqrt{\frac{\pi}{2}}\frac{\omega^2_{pe}\omega}{\lvert k^3_z\rvert v^3_{Te}}\exp(-y^2_{e0})$

2.3 DISPERSION RELATIONS

It is seen from (2.4), that the zero-order dispersion relations for the SAW and MW are $n^2\cos^2\theta_k = \varepsilon_{11}$ and $n^2 = \varepsilon_{22}$ respectively. The zero-order dispersion relation for a third wave, the ion sound wave, is given by $\varepsilon_{33} = 0$ (e.g. Melrose, 1980a, p. 57). However, the properties of the ion sound wave are not discussed here because this wave can only be excited in a low β plasma by an external antenna via non-linear processes (e.g. Hasegawa and Chen, 1976).

Solving for the real part of (2.4) perturbatively, the dispersion relation for the SAW is found to have the form for $|k_\perp^2/k_z^2| >> \omega/\Omega_i$ and for $\omega^2 << 2k_z^2v_{Te}^2$

$$\omega^2 \simeq k_z^2v_A^2/\left\{1 - \lambda_i(\frac{3}{4} + \frac{z_iT_e}{T_i}) + \frac{\omega^2}{\Omega_i^2}\frac{k^2}{k_\perp^2} + \frac{z_i^2}{z_m^2}\frac{n_m m_m}{n_i m_i}\left[1 - \frac{1}{2}e^{-\lambda_m}(\alpha_m+2.5)\right]\right\} \tag{2.5}$$

and for $\omega^2 >> 2k_z^2v_{Te}^2$

$$\omega^2 \simeq k_z^2v_A^2/\left\{1 - \frac{3}{4}\lambda_i + \frac{\omega^2}{\Omega_i^2}(\frac{z_im_e}{m_i}\frac{k_\perp^2}{k_z^2} + \frac{k^2}{k_\perp^2}) + \frac{z_i^2}{z_m^2}\frac{n_m m_m}{n_i m_i}\left[1 - \frac{1}{2}e^{-\lambda_m}(\alpha_m+2.5)\right]\right\} \tag{2.6}$$

where $\alpha_m = \sqrt{2}\, y_{m1}\Omega_m/k_z v_{Tm}$ and n_α, n_α and z_α are respectively the number density, mass and valence number of species α.

Equation (2.5) implies that for $\omega^2 << 2k_z^2v_{Te}^2$ the SAW only propagates (i.e. $k_\perp^2 > 0$) in regions where the plasma density is greater than the density at the Alfvén resonance i.e. for densities greater than that at the point where

$$\frac{\omega^2}{k_z^2 v_A^2} \simeq \left\{1 - \frac{\omega^2}{\Omega_i^2} + \frac{1}{2}\frac{z_i^2}{z_m^2}\frac{n_m m_m}{n_i m_i}(\alpha_m + 0.5)\right\} . \tag{2.7}$$

On the other hand, for $\omega^2 >> 2k_z^2 v_{Te}^2$ the SAW only propagates in regions where the density is less than the density at the Alfvén resonance (as given by (2.6)). Further, the coefficient of $k_\perp^2$ in (2.5) and (2.6) is small so that, for densities not too close to the density at the Alfvén resonance, $|k_\perp^2| >> k_z^2$.

However, near the Alfvén resonance, $k_\perp^2$ of the SAW becomes small and, depending on the magnitude of ω/Ω_i, the inequality $|k_\perp^2/k_z^2| << \omega/\Omega_i$ may be satisfied. In this case, the SAW dispersion relation becomes (for arbitrary $\omega/\sqrt{2}\, k_z v_{Te}$)

$$\omega^2 \simeq k_z^2 v_A^2 / \left\{1 + \frac{\omega^2}{\Omega_i^2} \pm \frac{\omega}{\Omega_i}\frac{k_z}{k} - \frac{1}{2}\frac{z_i^2}{z_m^2}\frac{n_m m_m}{n_i m_i}(\alpha_m + 0.5)\right\} \tag{2.8}$$

where the sign in (2.8) is chosen so that (2.8) is an analytic continuation of (2.5) and (2.6).

By again using a perturbative expansion of (2.4), the dispersion relation for the MW is found to have the form for $|k_\perp^2/k^2| >> \omega/\Omega_i$ and for $\omega^2 << 2k_z^2 v_{Te}^2$

$$\omega^2 \simeq k^2 v_A^2 / \left\{1 - \frac{3}{4}\lambda_i - \frac{\omega^2}{\Omega_i^2}\frac{k_z^2}{k_\perp^2} - \left(\frac{v_s^2}{v_A^2} + \frac{2v_{Ti}^2}{v_A^2}\right)\frac{k_\perp^2}{k^2} + \frac{z_i^2}{z_m^2}\frac{n_m m_m}{n_i m_i}\left[1 - \frac{1}{2}e^{-\lambda_m}(\alpha_m + 2.5)\right]\right\} \tag{2.9}$$

and for $\omega^2 >> 2k_z^2 v_{Te}^2$

$$\omega^2 \simeq k^2 v_A^2 / \left\{1 - \frac{\omega^2}{\Omega_i^2}\frac{k_z^2}{k_\perp^2} - \frac{1}{2}\frac{z_i^2}{z_m^2}\frac{n_m m_m}{n_i m_i}(\alpha_m + 0.5)\right\} \quad (2.10)$$

where v_s is the majority ion sound speed.

The MW dispersion relation is also modified when $|k_\perp^2/k_z^2| << \omega/\Omega_i$ and has the form

$$\omega^2 \simeq k^2 v_A^2 / \left\{1 + \frac{\omega^2}{\Omega_i^2} \pm \frac{\omega}{\Omega_i} - \frac{1}{2}\frac{z_i^2}{z_m^2}\frac{n_m m_m}{n_i m_i}(\alpha_m + 0.5)\right\} \quad (2.11)$$

where the plus sign is valid on the low density side of the Alfvén resonance and the minus sign on the high density side.

Thus, the MW has two cutoffs (i.e. $k_\perp = 0$), a low density cutoff at

$$\omega^2 \simeq k_z^2 v_A^2 / \left\{1 + \frac{\omega^2}{\Omega_i^2} + \frac{\omega}{\Omega_i} - \frac{1}{2}\frac{z_i^2}{z_m^2}\frac{n_m m_m}{n_i m_i}(\alpha_m + 0.5)\right\} \quad (2.12a)$$

and a high density cutoff at

$$\omega^2 \simeq k_z^2 v_A^2 / \left\{1 + \frac{\omega^2}{\Omega_i^2} - \frac{\omega}{\Omega_i} - \frac{1}{2}\frac{z_i^2}{z_m^2}\frac{n_m m_m}{n_i m_i}(\alpha_m + 0.5)\right\} . \quad (2.12b)$$

These cutoffs can also be derived from the work of Stix (1980).

If ω/Ω_i terms are neglected then the two cutoffs coalesce and the MW can only propagate on the high density side of the Alfvén resonance. However, if ω/Ω_i terms are retained then the cutoffs are distinct and the MW can propagate in two regions of different density. The first region is between the low density cutoff and the Alfvén resonance and in this region the MW is sometimes called an ion-cyclotron wave (Karney et

al., 1979). The second region is the high density side of the high density cutoff and in this region the MW is sometimes called a compressional Alfvén or compressional magnetosonic wave (Puri and Tataronis, 1978).

The finite frequency and ion sound speed corrections given here are the same as Akhiezer et al. (1967) and Sitenko (1967). The finite Larmor radius correction for the SAW is the same as that given by Hasegawa and Chen (1975, 1976). The finite Larmor radius correction is also similar but not the same as that given by Puri and Tataronis (1978) and Puri (1979) as they only considered some and not all of the finite Larmor radius and finite frequency effects.

The importance of the finite frequency, Larmor radius and electron mass corrections is that they allow the SAW to propagate across the field lines. On the other hand, the main effect of the minority ions on the dispersion relations is to shift the Alfvén resonance and the magnetosonic wave cutoffs by a small amount. The effect of the minority ions is small because the thermal velocity spread produces a large spread in the Doppler shifted wave frequency (as represented by $y_{ml}^2 << 1$) which prevents the minority ions from acting collectively even though the wave frequency is close to the minority ion cyclotron frequency.

The minority ion corrections can be neglected if these corrections are much smaller than the finite frequency corrections i.e. if

$$\frac{z_i^2}{z_m^2}\frac{n_m m_m}{n_i m_i}\left|\alpha_m + 0.5\right| \simeq \frac{n_m}{n_i} y_{ml}\beta^{-1/2} << \frac{\omega^2}{\Omega_i^2} . \qquad (2.13)$$

Criterion (2.13) is easily satisfied for β greater than about a few per cent and n_m/n_i less than about a few per cent.

2.4 POLARIZATION VECTORS

In this Section, the polarization vectors of the SAW and the MW are presented. These vectors together with the dispersion relations presented in the previous Section allow a physical interpretation of the features of the mode coupling between the SAW and MW (as reviewed in Chapter 1). For simplicity it is assumed that criterion (2.13) is satisfied so that the effect of the minority ions on the dispersion relations (i.e. on the hermitian part of the dielectric tensor) can be neglected.

The polarization vectors are obtained by substituting the solutions to (2.3) into (2.1). Noting that ω and k_z are constants and $k_\perp$ and v_A are functions of density, the polarization of the SAW is given approximately by

$$E_1 = 1 \tag{2.14}$$

$$E_2 = \begin{cases} -\dfrac{i\omega^2}{k_\perp^2 v_A^2}\dfrac{\omega}{\Omega_i}\left[\left(1-\dfrac{\omega^2}{\Omega_i^2}\right)^{-1} - \dfrac{3}{2}\lambda_i\dfrac{\Omega_i^2}{\omega^2} - \dfrac{k_\perp^2 c^2}{\omega^2}\left(\dfrac{c^2}{v_A^2}\dfrac{\omega^2}{k_z^2 v_s^2} - \dfrac{k_\perp^2 c^2}{\Omega_i^2}\right)^{-1}\right] \\ \qquad\qquad \omega \ll \sqrt{2}\, k_z v_{Te} \qquad (2.15a) \\ -\dfrac{\omega^2}{k_\perp^2 v_A^2}\dfrac{\omega}{\Omega_i}\left[\left(1-\dfrac{\omega^2}{\Omega_i^2}\right)^{-1} - \dfrac{3}{2}\lambda_i\dfrac{\Omega_i^2}{\omega^2} - \left(\dfrac{k_\perp^2 c^2 k_z^2 v_{Te}^2}{\omega^4}\right)\left(\dfrac{c^2}{v_A^2}\dfrac{m_i}{z_i m_e} + \dfrac{k_\perp^2 c^2}{\Omega_i^2}\right)^{-1}\right] \\ \qquad\qquad \omega \gg \sqrt{2}\, k_z v_{Te} \qquad (2.15b) \end{cases}$$

$$E_3 = \begin{cases} -\dfrac{k_\perp k_z v_A^2}{\Omega_i^2}\left(\dfrac{\omega^2}{k_z^2 v_s^2} - \dfrac{k_\perp^2 v_A^2}{\Omega_i^2}\right)^{-1} & \omega << \sqrt{2}\, k_z v_{Te} \qquad (2.16a) \\ \dfrac{k_\perp k_z v_A^2}{\Omega_i^2}\left(\dfrac{m_i}{z_i m_e} + \dfrac{k_\perp^2 v_A^2}{\Omega_i^2}\right)^{-1} & \omega >> \sqrt{2}\, k_z v_{Te} \qquad (2.16b) \end{cases}$$

for $|k_\perp^2| >> k_z^2$.

In the case where $\omega^2/\Omega_i^2 << 1$ and $\omega \simeq k_z v_A$, the polarization vector of the SAW reduces to

$$E_1 = 1$$

$$E_2 = -i\,\frac{\omega}{\Omega_i}\,\frac{k_z^2}{k_\perp^2}$$

$$E_3 = \begin{cases} -\dfrac{\omega^2}{\Omega_i^2}\,\dfrac{v_s^2}{v_A^2}\,\dfrac{k_\perp}{k_z} & \omega << \sqrt{2}\, k_z v_{Te} \\ \dfrac{\omega^2}{\Omega_i^2}\,\dfrac{z_i m_e}{m_i}\,\dfrac{k_\perp}{k_z} & \omega >> \sqrt{2}\, k_z v_{Te}. \end{cases} \qquad (2.17)$$

The polarization given by (2.17) and for $\omega << \sqrt{2}\, k_z v_{Te}$ is equivalent to that given by Sitenko (1967). The case where $\omega >> \sqrt{2}\, k_z v_{Te}$ was not considered by Sitenko (1967).

The polarization of the MW has the approximate form away from the Alfvén resonance (i.e. for $|\Lambda_{11}| >> |\Lambda_{13}^2/\Lambda_{33}|$)

$$E_1 = \frac{\omega}{\Omega_i}\left[1 - \frac{k_z^2 v_A^2}{\omega^2}\left(1 - \frac{\omega^2}{\Omega_i^2}\right)\right] \qquad (2.18)$$

$$E_2 = i \tag{2.19}$$

$$E_3 = \begin{cases} \dfrac{\omega}{\Omega_i}\dfrac{k_\perp}{k_z}\dfrac{k_z^2 v_s^2}{\omega^2}\left[1 - \dfrac{k_z^2 c^2}{\Omega_i^2}\left(\dfrac{c^2}{v_A} - \dfrac{k^2 c^2}{\omega^2}\left(1 - \dfrac{\omega^2}{\Omega_i^2}\right)\right)^{-1}\right] & \\ \qquad\qquad \omega << \sqrt{2}\, k_z v_{Te} & (2.20a) \\ \dfrac{\omega}{\Omega_i}\dfrac{k_\perp}{k_z}\dfrac{z_i m_e}{m_i}\left[\dfrac{k_z^2 v_{Te}^2}{\omega^2} + \dfrac{k_z^2 c^2}{\Omega_i^2}\left(\dfrac{c^2}{v_A^2} - \dfrac{k_z^2 c^2}{\omega^2}\left(1 - \dfrac{\omega^2}{\Omega_i^2}\right)\right)^{-1}\right] & \\ \qquad\qquad \omega >> \sqrt{2}\, k_z v_{Te}. & (2.20b) \end{cases}$$

In the case where $\omega^2 << \Omega_i^2$ and $\omega^2 \simeq k^2 v_A^2$, the polarization vector of the MW reduces to

$$E_1 = \frac{\omega}{\Omega_i}\frac{k^2}{k_\perp^2}$$

$$E_2 = i \tag{2.21}$$

$$E_3 = \frac{\omega}{\Omega_i}\frac{v_s^2}{v_A^2}\frac{k_\perp k_z}{k^2}$$

for arbitrary v_{Te} as given by Sitenko (1967).

The important thing to note about the polarization vectors is that in the ideal MHD limit (i.e. neglecting all first order corrections) the electric field of the SAW is parallel to $\underset{\sim}{k}_\perp$ (i.e. in the 1-direction) and its magnetic field is in the 2-direction. Thus, the Poynting vector of the SAW is directed along the magnetic field lines. The effect of the first order corrections is to produce a difference in the average transverse velocities of the electrons and ions as they

gyrate about the field lines in the presence of the wave fields. This difference then gives rise to the small E_2 and E_3 electric field components of the SAW (e.g. Stefant, 1970). These additional field components allow the SAW to propagate slowly across the field lines.

On the other hand, the MW in the ideal MHD limit has its electric field in the 2-direction and its magnetic field in the 1-3 plane perpendicular to $\underset{\sim}{k}$. Thus, the Poynting vector of the MW is parallel to $\underset{\sim}{k}$ and the magnetosonic wave can propagate across the magnetic field. The first order corrections give the MW finite E_1 and E_3 field components which modify slightly the group velocity of the MW across the magnetic field.

To understand the physical mechanism for the mode coupling note that near the Alfvén resonance the wave frequency and wave number of the MW are close to that of the SAW i.e. the dispersion relations of the SAW and MW have almost the same solution. If the MW has field components in common with the SAW near the Alfvén resonance then mode coupling can occur.

The common field components between the MW and the SAW can be determined by considering $\underset{\sim}{k}_\perp$ and the polarization vectors, (2.14) - (2.21). In the tokamak, $\underset{\sim}{k}_\perp$ has a component perpendicular to the density gradient (hereafter called k_y) determined by the antenna and a component parallel to the density gradient (hereafter called k_x) determined by the plasma dispersion equation. For the SAW, $|k_\perp^2|$ is large so that for tokamak applications $k_y^2 << |k_x^2|$ (Hasegawa and Chen, 1976) and the electric field of the SAW is directed along the density gradient for $\omega << \Omega_i$ (if $k_y^2 >> k_x^2$ then the wave fields have a large spatial decay rate outside the plasma and there is little energy coupled between

the plasma and the antenna (e.g. Chen and Hasegawa, 1974)). Thus, in the ideal MHD limit, the MW must have an electric field component parallel to the density gradient, i.e. k_y must be finite, before mode coupling can occur. This situation is consistent with the results of Ott et al. (1978; their $k_\perp$ is equivalent to k_y here) and Karney et al. (1979).

The retention of first order corrections introduces other field components which modify the mode coupling. The dominant correction is the introduction of an E_1 component in the polarization of the MW; the other corrections to the polarization of the MW and SAW are proportional to second order terms (e.g. (2.17) and (2.21)). Thus, the dominant modification to the mode coupling by the first order corrections is via the coupling between the E_1 fields of the MW and of the SAW. This modification is independent of temperature because the above fields depend only on the finite frequency corrections. This conclusion is consistent with the numerical results of Ross et al. (1982).

2.5 SPATIAL DAMPING RATES

In this Section, the damping of the SAW as it propagates away from the Alfvén resonance is examined for both single and multiple ion-component plasmas. For completeness, the damping of the MW is also given.

The temporal damping rates of the SAW and the MW in a single ion-component plasma have been previously studied by Akhiezer et al. (1967), Sitenko (1967), Fejer and Kan (1969), Stefant (1970), Lashmore-Davies and May (1972) and Hung and Barnes (1973). However, for the tokamak the frequency is fixed by the antenna so that the relevant parameter is the spatial damping rate although the physical mechanism for the damping (i.e. electron and ion Landau damping) is the same in either case.

The spatial damping rates are obtained by solving (2.4) perturbatively for the imaginary part of $k_\perp^2$. For a single ion-component plasma in which $\omega^2 << \Omega_i^2$ and $v_{Ti}^2 << v_A^2$ the imaginary part of (2.4) is significant only if $\omega^2 \lesssim 2k_z^2 v_{Te}^2$. In this case, the damping of the SAW is found to have the form

$$\mathrm{Im}(k_\perp^2)_{eS} \simeq \frac{\sqrt{2\pi}}{3} \frac{z_i T_e}{T_i} \frac{\omega}{k_z v_{Te}} \mathrm{Re}(k_\perp^2) \exp\left[- \left(\frac{\omega}{\sqrt{2}\, k_z v_{Te}} \right)^2 \right] \tag{2.22}$$

and that of the MW by

$$\mathrm{Im}(k_\perp^2)_{eM} \simeq \sqrt{\frac{\pi}{2}} \frac{v_{Te}}{v_A} \frac{\omega}{k_z v_A} \frac{z_i m_e}{m_i} \mathrm{Re}(k_\perp^2) \exp\left[- \left(\frac{\omega}{\sqrt{2}\, k_z v_{Te}} \right)^2 \right]. \tag{2.23}$$

The above damping rates arise from the electron component of ε_{33}^a (with the contributions from ε_{22}^a and ε_{23}^a being negligible for the SAW and cancelling each other for the MW). Physically this situation corresponds to the MW and SAW being electron Landau damped by electrons resonating with the axial electric field of these waves (cf. Stix, 1962, Ch. 7).

The number of ions which can resonate with the axial wave fields is exponentially small as $\omega^2 >> k_z^2 v_{Ti}^2$ so that the contribution from the ions to the above damping rates is negligible. The ions can contribute to the damping through the gyro-resonant interaction with the perpendicular wave fields if ω approaches Ω_i. In this case, the Alfvén resonance (as given by (2.5)) tends towards the plasma surface unless k_z is correspondingly increased. However, increasing k_z increases the spatial decay rate of the wave fields (Ott et al., 1978; see also Section 2.6).

Interior ion heating can be obtained by the addition of a minority ion species whose cyclotron frequency is approximately equal to

the wave frequency (Winglee, 1983a). The minority ions can then cyclotron damp the SAW and the MW with bulk ion heating being produced by Coulomb collisions between the majority and minority ions in a similar fashion as in ion-ion hybrid resonance heating. Further, only a few per cent of the minority ion species need be added before electron and ion heating become approximately equal because the minority ions gyro-resonantly interact with the perpendicular electric wave fields rather than the smaller parallel electric field. Specifically, the damping of the SAW in a multiple ion-component plasma in which criterion (2.13) is satisfied is given by

$$\mathrm{Im}(k_\perp^2) = \mathrm{Im}(k_\perp^2)_{eS} + \frac{1}{3}\sqrt{\frac{\pi}{2}}\frac{\Omega_i^2}{v_{Ti}^2}\left(1 - \lambda_i \frac{z_i T_e}{T_i}\frac{k_z^2 v_A^2}{\omega^2}\right)\frac{\omega}{k_z v_{Tm}}\frac{n_m m_i}{n_i m_m}\exp\left[-(\lambda_m + y_{ml}^2)\right] \tag{2.24}$$

and that of the MW by

$$\mathrm{Im}(k_\perp^2) = \mathrm{Im}(k_\perp^2)_{eM} + \frac{1}{2}\sqrt{\frac{\pi}{2}}\frac{\Omega_i^2}{v_A^2}\frac{\omega}{k_z v_{Tm}}\frac{n_m m_i}{n_i m_m}\exp\left[-(\lambda_m + y_{ml}^2)\right]. \tag{2.25}$$

Note that the damping due to the electrons increases with $k_\perp^2$ while that due to the minority ions decreases with λ_m and $|y_{ml}|$. Because $k_\perp$ of the SAW is smallest at densities close to that at the Alfvén resonance (via (2.6) and (2.7)) minority ion damping tends to dominate electron damping near the Alfvén resonance. However, if the density gradient is large near the Alfvén resonance then the SAW propagates into a region where $k_\perp$ is large, i.e. where electron damping dominates, before significant minority ion damping can occur. Thus the total amount of energy

deposited in the ions depends not only on the concentration of the impurity ions and on the variation of the magnetic field but also on the variation of the density near the Alfvén resonance. These points are discussed further in the next Section.

2.6 NUMERICAL RESULTS

Presented here and in Winglee (1983a) are numerical solutions to the dispersion equation, (2.3), with the dielectric tensor as given in Table 2.1. These solutions were obtained from a complex root-finding subroutine which was developed by Botten et al. (1981) for a problem in diffraction theory. In the following the solutions are shown as functions of density for (a) a single ion-component plasma for various electron temperatures and ω/Ω_i and (b) a multiple ion-component plasma for various ω/Ω_i and impurity concentrations. Such a display of the results simulates the properties of the MW and the SAW as they propagate through a density gradient except possibly near the Alfvén resonance. In the following $T_e = T_i$ unless otherwise stated.

Fig. 2.1 shows $k_\perp^2 c^2/\Omega_i^2$ for the SAW (short perpendicular wavelength branch) and for the MW versus the normalized density, $\omega^2/k_z^2 v_A^2$, for the given electron temperatures. For $\omega < \sqrt{2}\ k_z v_{Te}$ (Fig. 2.1a) the SAW propagates on the high density side of the Alfvén resonance with the $|\mathrm{Re}(k_\perp^2)|$ increasing with decreasing v_{Te} (as given by (2.6)). However, as v_{Te} approaches $\omega/\sqrt{2}\ k_z$ (Fig. 2.1b) the analytic results break down and the $|\mathrm{Re}(k_\perp^2)|$ becomes small so that $k_\perp^2$ is almost purely imaginary. At this point the damping of the SAW is at a maximum. If v_{Te} is further decreased (Fig. 2.1c) then the SAW propagates on the low density side of the Alfvén resonance with $|\mathrm{Re}(k_\perp^2)|$ again increasing with decreasing

Fig. 2.1 $k_\perp^2 c^2/\Omega_i^2$ for the SAW and MW branches versus the normalized density $\omega^2/k_z^2 v_A^2$ for the given electron temperatures ($T_e = T_i$) and $\omega/\Omega_i = 0.25$ and $k_z c/\Omega_i = 9.0$. The real and imaginary parts of $k_\perp^2$ are shown in (i) and (ii) respectively. The SAW propagates ($\mathrm{Re}(k_\perp^2) > 0$) on the high density side of the Alfvén resonance if $\omega < \sqrt{2}\, k_z v_{Te}$ (Fig. a) and on the low density side if $\omega > \sqrt{2}\, k_z v_{Te}$ (Fig. c). For $\omega^2 \simeq \sqrt{2}\, k_z v_{Te}$ (Fig. b) the damping of the SAW is at a maximum and $k_\perp^2$ is almost purely imaginary. For the MW, the $\mathrm{Re}(k_\perp^2)$ away from the Alfvén resonance is approximately independent of electron temperature while its damping increases with electron temperature. Near the Alfvén resonance the MW branch merges into SAW branch and vice versa.

(i) (ii)

(a)

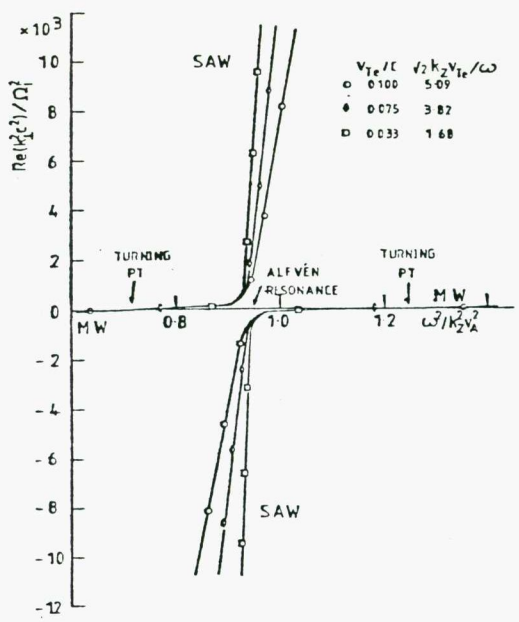
SAW
TURNING PT
ALFVÉN RESONANCE
TURNING PT
MW
SAW
MW
0·8
1·0
1·2

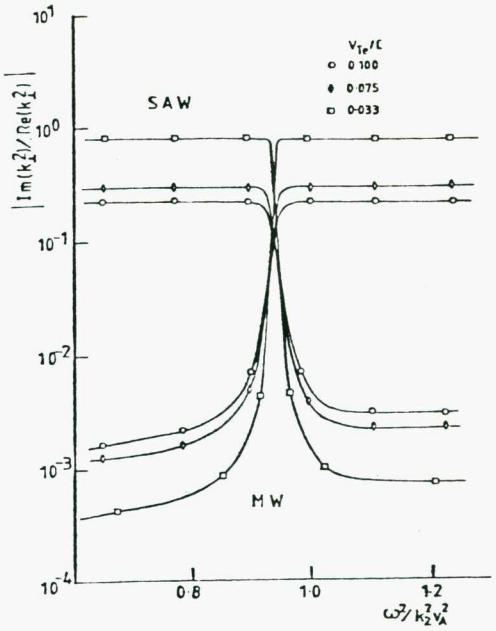
SAW
MW
0·8
1·0
1·2

(b)

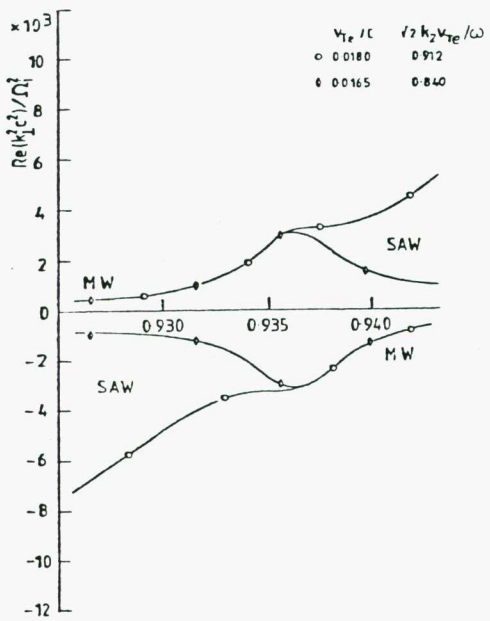
SAW
MW
SAW
MW
0·930
0·935
0·940

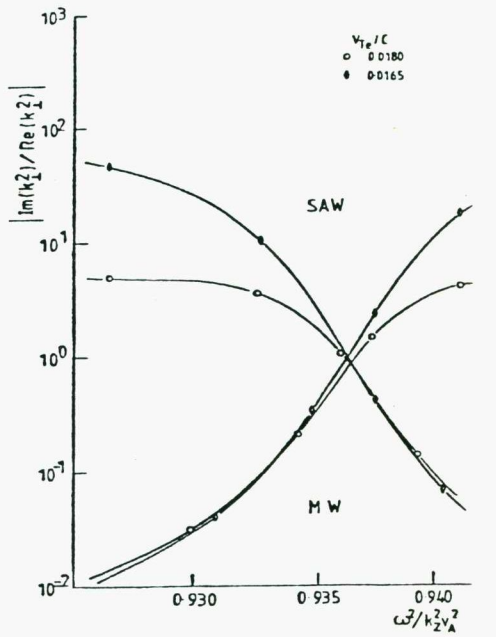
SAW
MW
0·930
0·935
0·940

(c)

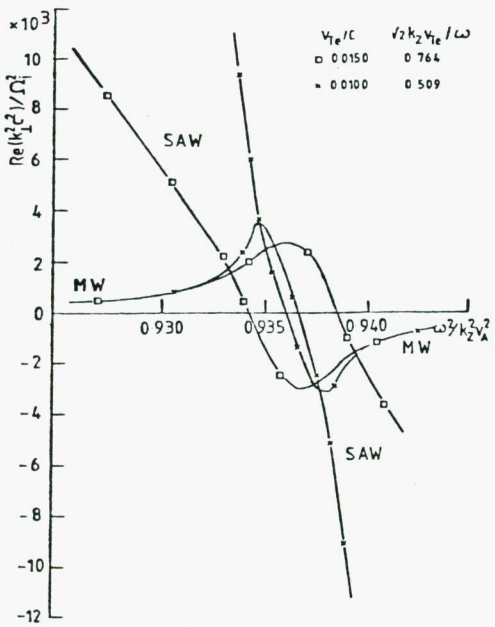
SAW
MW
SAW
MW
SAW
0·930
0·935
0·940

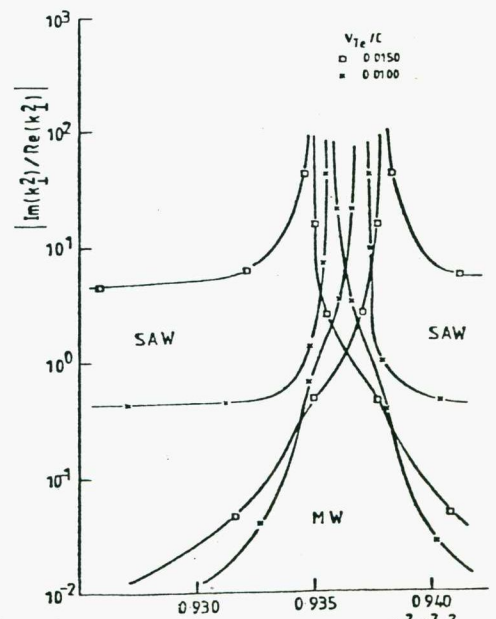
SAW
SAW
MW
0·930
0·935
0·940

v_{Te} as given by (2.5). In contrast, the $Re(k_\perp^2)$ for the MW is approximately independent of the electron temperature and the damping of the MW increases monotonically with electron temperature. The damping of the MW is smaller than that of the SAW because the axial electric field of the MW is smaller as given by (2.16) and (2.20).

To illustrate some of the features of the polarization of the MW and the SAW, the $Re(E_2/iE_1)$ is shown in Fig. 2.2 for $\omega/\Omega_i = 0.495$, (i) $\omega/\sqrt{2}\, k_z v_{Te} = 0.26$ and (ii) $\omega/\sqrt{2}\, k_z v_{Te} = 1.95$. The Im (E_2/iE_1) is not shown because in general $|Im(E_2/iE_1)| << |Re(E_2/iE_1)|$ as given by (2.14) - (2.21). It is seen that $|E_2/iE_1|$ of the SAW is always much less than unity and is temperature dependent. On the other hand E_2/iE_1 of the MW is independent of temperature except near the Alfvén resonance where plasma inhomogeneity effects (i.e. mode coupling) dominate.

Fig. 2.3 shows $k_\perp c/\Omega_i$ for various ω and k_z such that the density at which the Alfvén resonance occurs is fixed. By increasing ω, the low density MW cutoff is shifted towards the plasma surface, as given by (2.12). There is some cyclotron damping present at the higher frequencies given. These advantages are offset by an increase in the spatial rate of decay of the MW and an increase in the k_z required to keep the Alfvén resonance at the same density.

Significant ion heating can be obtained for smaller ω and k_z if a minority ion species is introduced as previously discussed. An example is shown in Fig. 2.4 in which deuterium is the minority ion species in a hydrogen plasma. Only a 1% doping level with $\omega/\Omega_i = 0.495$ and $k_z c/\Omega_i = 18$ is needed before the SAW damping rate exceeds that obtained in a single component plasma with $\omega/\Omega_i = 0.8$ and $k_z c/\Omega_i = 42$.

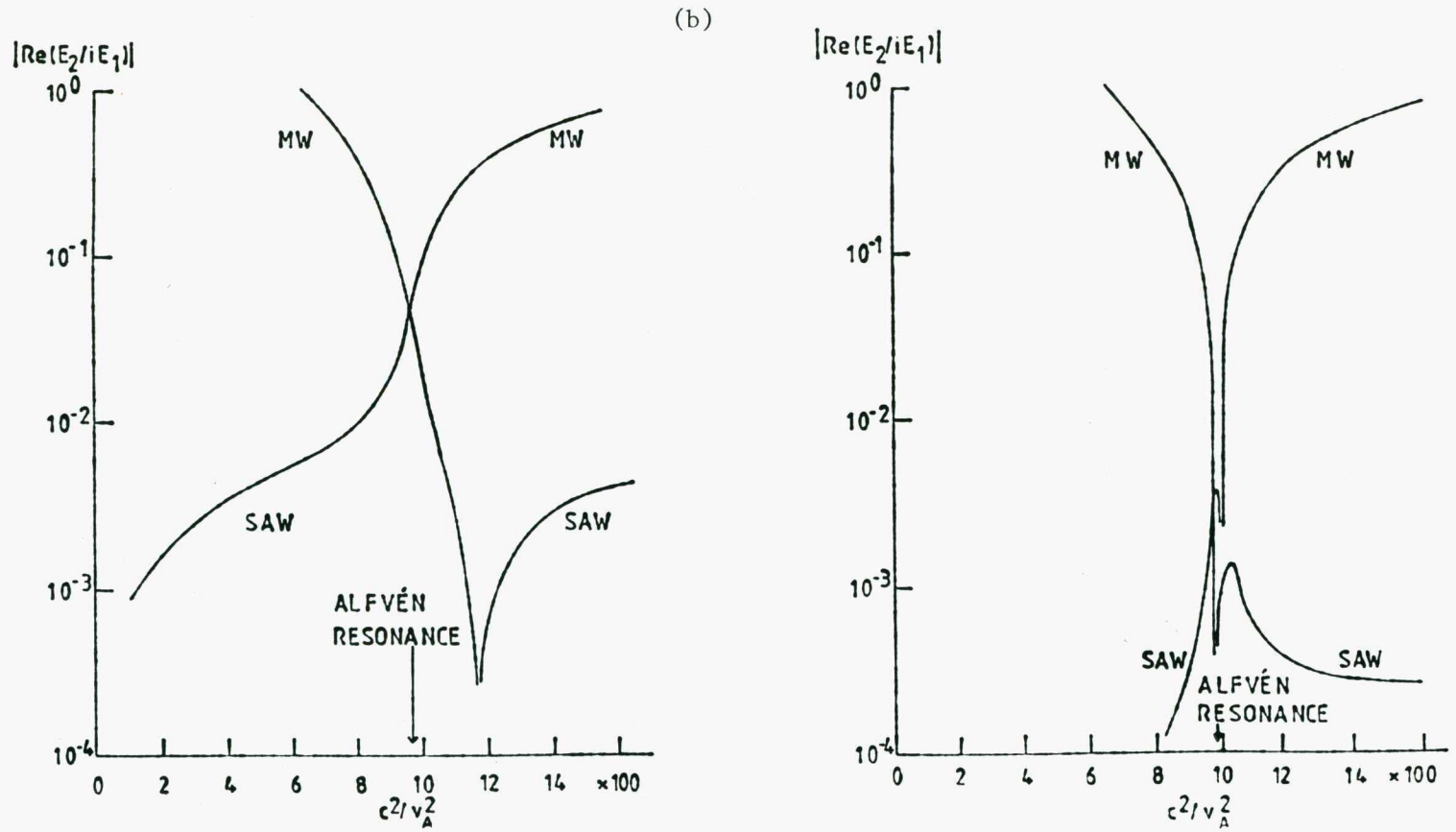

Fig. 2.2 $|\mathrm{Re}(E_2/iE_1)|$ versus the normalized density c^2/v_A^2 for $k_z c/\Omega_i = 18$ and $\omega/\sqrt{2}\, k_z v_{Te}$ equal to (a) 0.26 and (b) 1.95. Away from the Alfvén resonance, $|\mathrm{Re}(E_2/iE_1)|$ for the MW is insensitive to the plasma temperature unlike that for the SAW. $|\mathrm{Re}(E_2/iE_1)|$ is also much greater for the MW than for the SAW. Near the Alfvén resonance, the polarization of the SAW and MW are approximately the same.

(a)

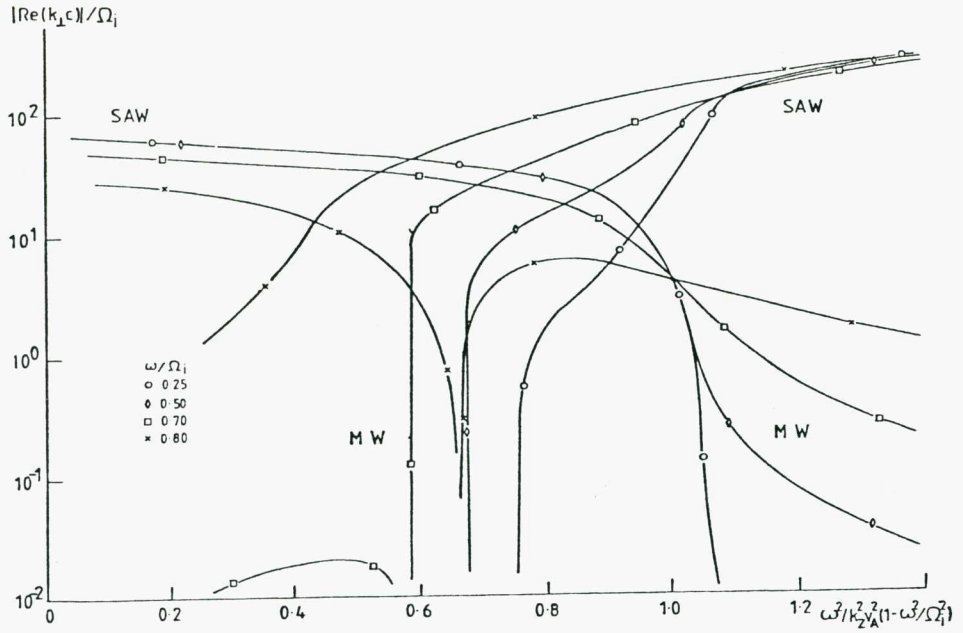

(b)

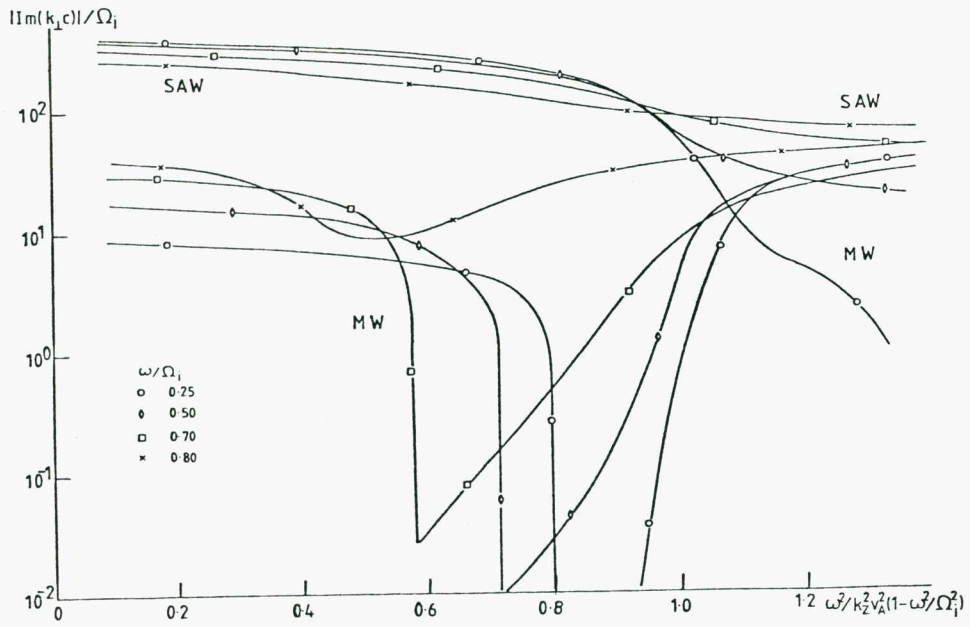

Fig. 2.3 $k_\perp c/\Omega_i$ versus the normalized density $\omega^2/k_z^2 v_A^2(1 - \omega^2/\Omega_i^2)$ for various ω and k_z such that the Alfvén resonance occurs at the point where $c^2/v_A^2 = 10^3$ ($v_{Te}/c = 0.075$, $T_i = T_e$). The real and imaginary parts of $k_\perp$ are shown in (a) and (b) respectively. For a given ω/Ω_i, the portion of the curve with the smaller $|k_\perp|$ represents the MW branch while the portion with the larger $|k_\perp|$ represents the SAW branch. By increasing ω, the region of evanescence of the MW is reduced but the spatial decay rate is increased.

(a)

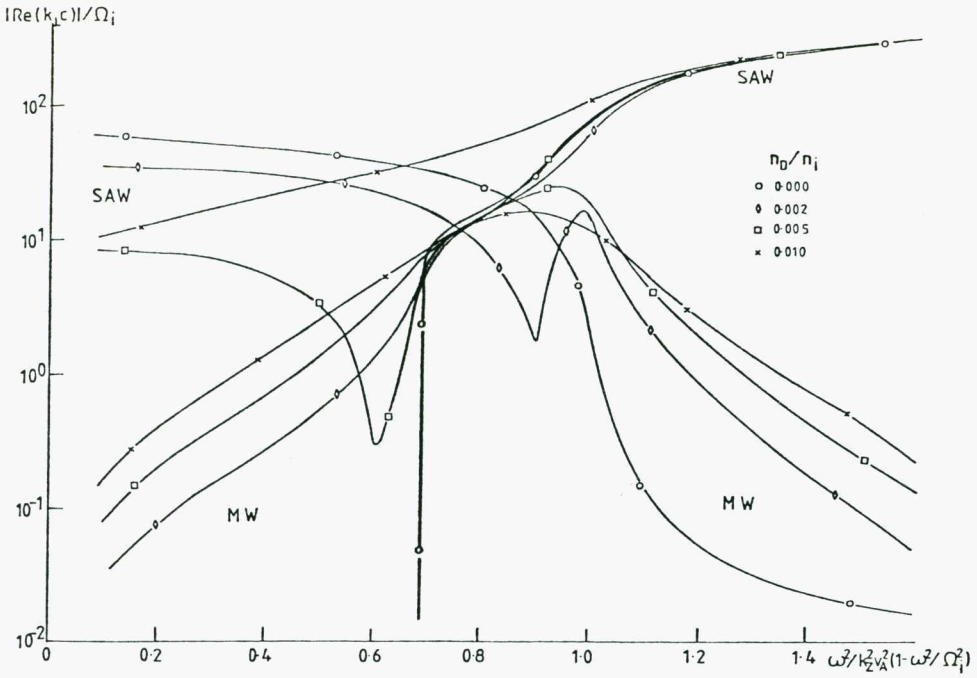

(b)

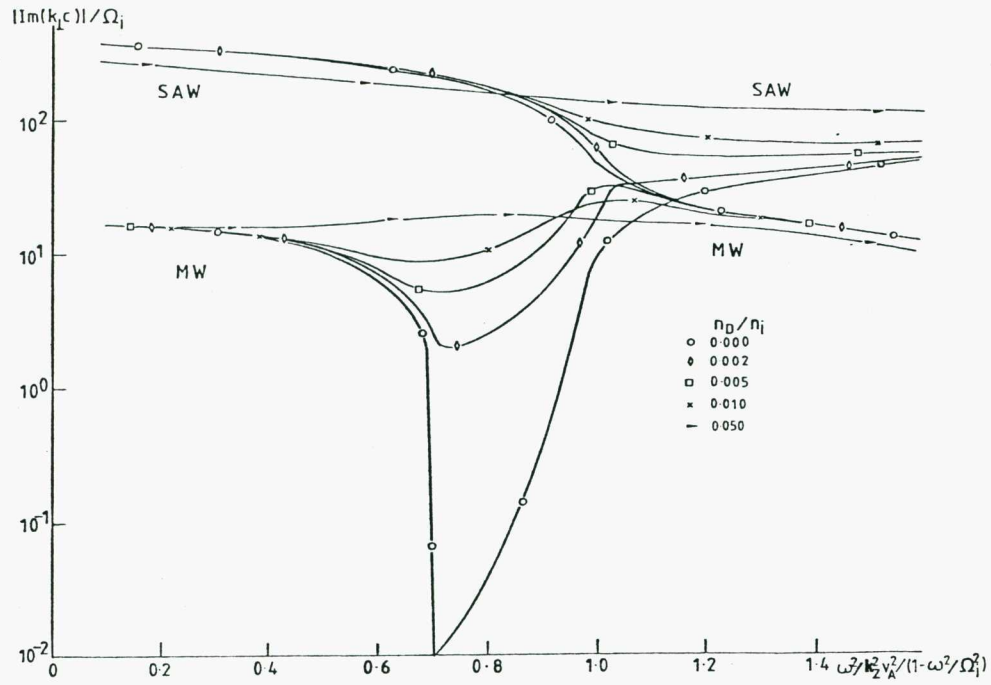

Fig. 2.4 $k_\perp c/\Omega_i$ versus the normalized density $\omega^2/k_z^2 v_A^2(1 - \omega^2/\Omega_i^2)$, for the given levels of deuterium doping with $\omega/\Omega_i = 0.495$ and $k_z c/\Omega_i = 18$, $T_e = T_i$ and $v_{Ti} = v_{TD} = 0.00175$ c. Only a 1% doping level is needed before the SAW damping rate exceeds that of a single component plasma with $\omega/\Omega_i = 0.8$ and $k_z c/\Omega_i = 42$ as given in Fig. 2.3.

The effect of the addition of a minority ion species in a colder plasma is shown in Fig. 2.5. For the same impurity concentration and ω/Ω_i, the resonance occurs at a lower density than in Fig. 2.4. This shift occurs because $k_z v_{Tm}$ is sufficiently small so that $|\omega - \Omega_m|/\sqrt{2}\ k_z v_{Tm} >> 1$ and the minority ion species act collectively to modify the dispersion relation. However, if $k_z v_{Tm}$ is sufficiently large so that $|\omega - \Omega_m|\sqrt{2}\ k_z v_{Tm} << 1$ then the minority ions do not act collectively and only the resonant component interacts with the waves giving rise to the ion cyclotron damping. This effect is illustrated in Fig. 2.6. The modification of the dispersion relation by the minority ion species is at a maximum when $|\omega - \Omega_m|/\sqrt{2}\ k_z v_{Tm} \simeq 1$.

The ratio of the total damping to that due to the electrons is shown in Fig. 2.7 for the given doping levels. The proportion of electron damping increases as the density increases above that at the Alfvén resonance. This increase is due to the dependence of the damping ((2.22)-(2.25)) on $k_\perp^2$ which in turn depends on the density (as discussed in Section 2.5). Ion damping dominates near the Alfvén resonance where $k_\perp$ is small. This damping increases with increasing doping levels and decreasing $|\omega - \Omega_m|$. When the Alfvén resonance is near the plasma centre, the variation of the density and the magnetic field over the region is small so that the ions absorb most of the rf power directly while the electrons are heated by Coulomb collisions with the ions and not directly by the rf power. Thus, the minority ion heating scheme presented here is able to overcome the problem of excess electron heating as observed in Alfvén resonance and ion-ion hybrid resonance heating (Section 1.1).

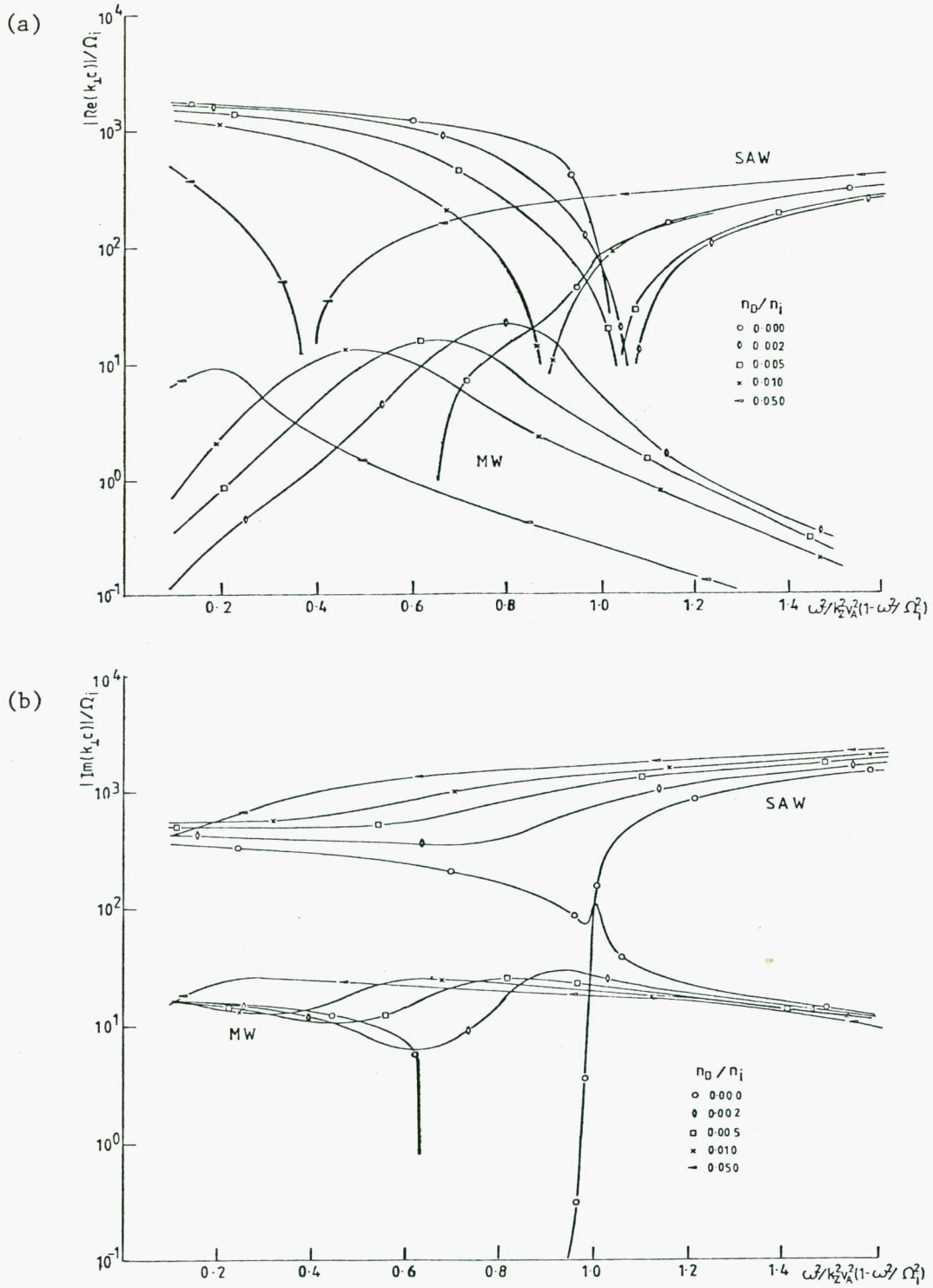

Fig. 2.5 As in Fig.2.4 but with $v_{Ti} = v_{TD} = 2.3 \times 10^{-4}$ c. For the same concentration of impurity ions, the Alfvén resonance is closer to the plasma surface in this colder plasma than in Fig. 2.4.

(a)

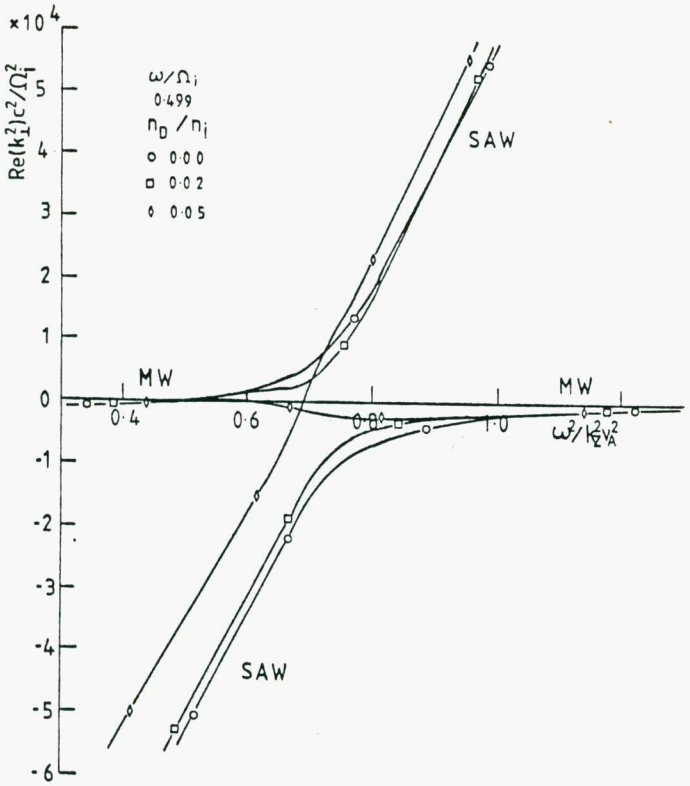

(b)

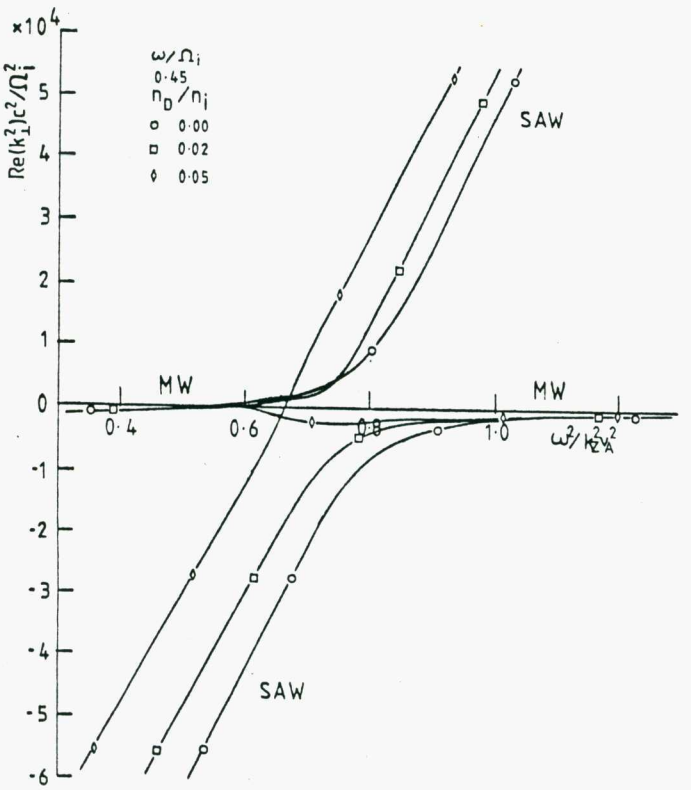

Fig. 2.6 $Re(k^2)$ versus the normalised density $\omega^2/k_z^2v_A^2$ for the same thermal velocities in Fig. 2.4 and for the given levels of deuterium doping with (a) $\omega/\Omega_i = 0.499$ and (b) $\omega/\Omega_i = 0.45$ and $k_zc/\omega = 100$. These parameters correspond to a plasma with a β of 3%.

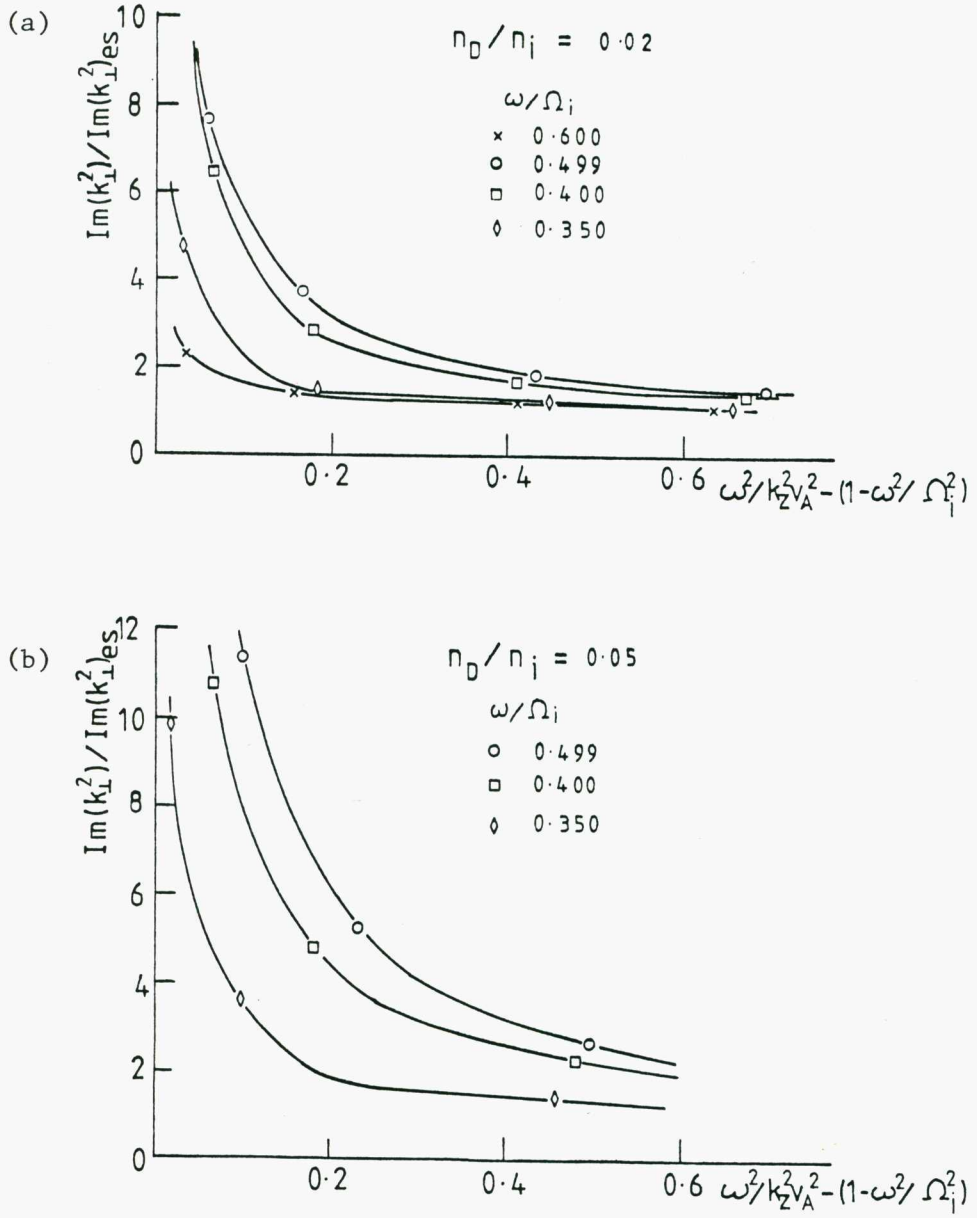

Fig. 2.7 The ratio of the $Im(k_\perp^2)$ of the SAW for the given levels of deuterium doping to the $Im(k_\perp^2)$ with no doping versus the normalized density $\omega^2/k_z^2v_A^2 - (1 - \omega^2/\Omega_i^2)$ for the same thermal velocities in Fig. 2.6.

The dependence of the ion heating on the variation of the magnetic field can be reduced by the introduction of a second minority ion species whose cyclotron frequency lies close to that of the first minority ion species. The SAW can gyro-resonantly interact with one of the ion species on the high field side of the plasma and with the other on the low field side. The enhanced damping due to the presence of deuterium and tritium minority ion species is shown in Fig. 2.8. Note also that the modification to the SAW and MW dispersion relations is smaller than that for the same total doping with one minority ion species.

It can be seen in Figs. 2.1, 2.6 and 2.7 that the WKB solutions predict that the MW branch on the low density side of the Alfvén resonance is connected to the SAW branch on the high density side if the cyclotron damping is small. However, if the cyclotron damping is large then the MW and the SAW branches are unconnected. This change in the dispersive properties of the plasma is due to the presence of finite anti-hermitian parts of ε_{11} and ε_{12}. The actual connection is determined by density gradient effects, in particular mode coupling.

2.7 SUMMARY

In this Chapter, the dispersion, polarization and damping of the MW and SAW were examined in relation to the Alfvén resonance heating of

(a)

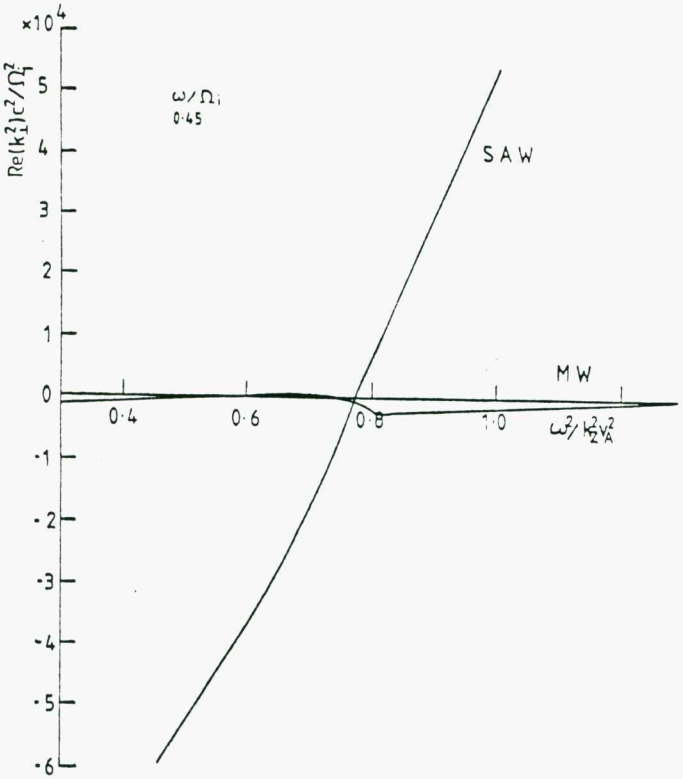

(b)

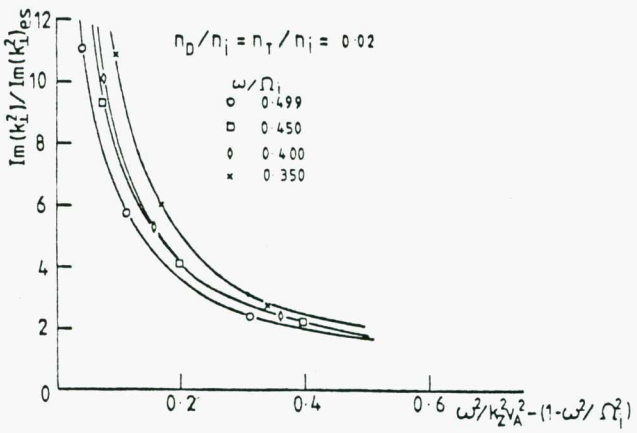

Fig. 2.8 (a) The $Re(k_\perp^2)$ versus the normalised density $\omega^2/k_z^2v_A^2$ for the same thermal velocities in Fig. 2.6 and $v_{TT} = 1.43\times10^{-3}$ c and $n_D = n_T = 0.02\ n_i$.

(b) The ratio of the $Im(k_\perp^2)$ of the SAW for the given D - T doping to the $Im(k_\perp^2)$ with no doping.

tokamak plasmas. Near the Alfvén resonance, the dispersion relations of the MW and the SAW are approximately the same. This feature allows mode coupling between the MW and the SAW if these waves have field components in common. The field components which produce the mode coupling depend only on k_y and ω/Ω_i and not on the plasma temperature (Section 2.4). Further, if ω/Ω_i corrections are neglected and $k_y = 0$ then the wave fields of the SAW and MW are orthogonal and no mode coupling occurs. If ω/Ω_i corrections are retained then mode coupling can then occur even for $k_y = 0$.

The subsequent fate of the energy mode converted into the SAW is dependent on the plasma temperature. In particular, the SAW propagates on the high density side of the Alfven resonance if $\omega << \sqrt{2}\, k_z v_{Te}$ and on the low density side if $\omega >> \sqrt{2}\, k_z v_{Te}$ (Section 2.3). This feature of the SAW assists in the heating of the interior of tokamak plasmas with $\beta > z_i m_e/m_i$ as the SAW in this case propagates towards the centre of the plasma.

Unfortunately, in a single ion-component plasma with a low β and $\omega^2 << \Omega_i^2$, the SAW and MW are principally electron Landau damped and little ion heating occurs (Section 2.5). The damping of the SAW is maximum when $\omega \simeq \sqrt{2}\, k_z v_{Te}$ while that of the MW increases monotonically with electron temperature, the damping rate of both waves increases with increasing $|k_\perp^2|$. This last feature implies that the damping rate of the SAW increases as it propagates away from the Alfvén resonance.

Efficient heating of the ions in the plasma can be obtained if (a) $\omega << \sqrt{2}\, k_z v_{Te}$ and (b) there is present a small percentage of a minority ion which can gyro-resonantly damp the SAW. In particular, if $|y_{ml}| = |\omega - \Omega_m|/\sqrt{2}\, k_z v_{Tm} << 1$ (i.e. $\Delta B/B << \beta^{1/2}$ and $\omega \simeq \Omega_m$) and

$(z_i^2 n_m m_m)/(z_m^2 n_i m_i) << \omega^2/\Omega_i^2$, then the damping of the SAW is significantly enhanced by minority ion-cyclotron damping with little modification to the position of the Alfvén resonance and to the dispersion of the MW and SAW (Section 2.6). Bulk ion heating occurs via Coulomb collisions between the ion species.

Because the resonant ions interact with the perpendicular wave electric fields and the resonant electrons interact with the smaller parallel wave electric field, only a few per cent of minority ions need be added before electron and ion heating become equal. Further, if the Alfvén resonance is near the centre of the plasma then electron heating is minimized and ion-heating maximized because the variation of the density and the magnetic field in the region in which the SAW propagates is small. An alternate way of increasing the ion heating is by the introduction of a second minority ion species such that $\Omega_{m1} \lesssim \omega \lesssim \Omega_{m2} < \Omega_i$ and $|\omega - \Omega_{mj}|/\sqrt{2}\, k_z v_{Tm} \lesssim 1$ for $j = 1,2$. In this case, minority ion species 1 damps the SAW in the low magnetic field region of the plasma and minority ion species 2 damps the SAW in the high magnetic field region.

Although a hydrogen plasma was assumed in the numerical calculations to illustrate the ion heating, there is a wide range of plasma compositions available which allow ion heating and the possibility of fusion. These compositions include:

(i) a p-majority ^{4}He-minority plasma in which ion heating can be demonstrated at low cost but with increased bremsstrahlung radiation due to the presence of ^{4}He;

(ii) a p-majority D-minority plasma which is more expensive but

does not have the problem of increased bremsstrahlung radiation and allows the possibility of fusion reactions in any suprathermal tail of deuterium produced by the rf heating;

(iii) a p-majority D-T-minority plasma in which both D-D reactions in the suprathermal tail of deuterium and D-T reactions in the thermal components of the minority ion species are possible;

(iv) D-majority T-minority plasma or p-majority ^{3}He-minority plasma with the minority ions participating in both rf heating and in fusion reactions.

CHAPTER 3

ALFVÉN RESONANCE DAMPING OF THE MAGNETOSONIC WAVE

3.1 INTRODUCTION

The minority ion-cyclotron heating scheme examined in Chapter 2 utilizes the collisionless damping of the shear Alfvén to produce ion heating. The purpose of this Chapter is to determine whether the shear Alfvén wave can be excited efficiently by the mode conversion of either a magnetosonic body wave or a magnetosonic surface wave.

In order to treat Alfvén resonance heating in the frequency range required for minority ion-cyclotron heating, ω/Ω_i is assumed to be finite but sufficiently small so that $\omega^2/\Omega_i^2 << 1$. This frequency range is also of interest because,in present day tokamaks,ω/Ω_i is non-negligible (e.g. Karney et al., 1979).

A planar geometry is also assumed as it allows the determination of general criteria (in terms of the wave frequency, wavenumber and density profile) for the optimization of Alfvén resonance heating of the plasma interior. These criteria are expected to apply at least qualitatively in the more complicated geometry of the tokamak (Chapter 1). Further, such a study is important because, although numerical results for Alfvén resonance heating have been presented for specific geometries (e.g. Ross et al., 1982; Appert and Vaclavik, 1982; Donnelly and Cramer, 1983) general criteria for the optimization of Alfvén resonance heating have not been given.

The wave equation governing the mode conversion of the magnetosonic wave into the shear Alfvén wave is derived in Section 3.2. This

equation is similar to that of Karney et al. (1979; see also Chapter 1) except that terms of $O(\omega^2/\Omega_i^2)$ are retained. A similar type of wave equation also appears in the study of the mode conversion of an ion-cyclotron wave at the Alfvén resonance (Swanson, 1974, 1975; McKenzie, 1979).

To estimate the mode conversion of the magnetosonic body wave into a shear Alfvén wave, the power lost at the Alfvén resonance by the body wave on reflection from a constant density gradient is determined in Section 3.3. Both the cases where $M^2 = k_y^2(k_z^2K)^{-2/3}$ (K^{-1} being the scale length of the density gradient) is less than and greater than one are examined. This work, which is also presented in Winglee (1982), differs from those reviewed in Chapter 1 in that all terms of $O(\omega/\Omega_i)$ are retained. Ott et al. (1978) and Karney et al. (1979) examined the mode coupling but only for $M^2 < 1$ and neglected terms of $O(\omega/\Omega_i)$ and $O(M^2\omega/\Omega_i)$ respectively. However, these terms are non-negligible if minority ion-cyclotron heating is to be utilized and must be retained.

In Section 3.4, the mode conversion of a magnetosonic surface wave to a shear Alfvén wave is determined. The work differs from those cited in Chapter 1 in that:

(i) a sharp discontinuity (i.e. $k_y^2 << K^2$) is not assumed because, for a finite poloidal mode number, this condition is in general not valid when the Alfvén resonance is away from the plasma edge;

(ii) $k_y^2 >> k_z^2$ is not assumed because in the presence of many heating coils k_z may be of the order of k_y.

The mode conversion of the magnetosonic wave produces a resistive component in the impedance of the antenna which excites these waves. Large resistances correspond to strong absorption of rf power by the plasma (Ott et al., 1978). In Section 3.5, the antenna impedance is evaluated and criteria for a resistive antenna impedance are given. It is shown that, in the parameter range required for minority ion-cyclotron heating, efficient coupling of energy between the antenna and the plasma centre is possible. A summary of results is given in Section 3.6.

3.2 WAVE EQUATION

Using a similar method to that of Karney et al. (1979), the wave equation is derived from Maxwell's equations and the dielectric tensor. A constant magnetic field is assumed to be directed along the z axis. The parallel electric field is neglected as the conductivity in the z direction is large.

Minority ions are assumed to be present only if minority ion-cyclotron heating is to be utilized i.e. if $|y_{m1}| \ll 1$. In this case, the contribution from the minority ions to the dispersion and mode conversion of the magnetosonic wave (i.e. the minority ion contribution to the hermitian part of the dielectric tensor) can be neglected (Sections 2.3 and 2.6). On the other hand, the majority ions and the electrons are assumed to comprise a cold plasma with a density gradient in the x direction. As previously discussed in Chapter 1 and in Section 2.4, neither the assumption of a cold plasma nor of a planar geometry modify qualitatively the mode conversion when the dispersion of the magnetosonic and shear Alfvén waves is determined primarily by the majority ions.

All wave quantities are assumed to have the form $p(x)\exp(i(k_y y + k_z z - \omega t))$. However, in the remainder of this Chapter, the exponential term is omitted for ease of notation.

With these approximations, Maxwell's equations reduce to

$$(A_k - k_y^2)\, E_x + i(D_k - k_y \frac{d}{dx})\, E_y = 0 \qquad (3.1)$$

$$- i(D_k + k_y \frac{d}{dx})\, E_x + (A_k + \frac{d^2}{dx^2})\, E_y = 0 \qquad (3.2)$$

where $A_k = \frac{\omega^2}{w_A^2} - k_z^2$

$D_k = \frac{\omega^2}{w_A^2}\frac{\omega}{\Omega_i}$

$w_A^2 = v_A^2(1 - \omega^2/\Omega_i^2)$.

By eliminating E_x in favour of E_y, the wave equation is found to have the form

$$\frac{d}{dx}\left(\frac{A_k}{A_k - k_y^2}\frac{dE_y}{dx}\right) + \left[A_k - \frac{k_y D_k' + D_k^2}{A_k - k_y^2} + \frac{k_y D_k A_k'}{(A_k - k_y^2)^2}\right] E_y = 0 \qquad (3.3)$$

where $A_k' = \frac{dA_k}{dx} = k_z^2 K$

$D_k' = \frac{dD_k}{dx} = \frac{k_z^2 K\omega}{\Omega_i}$

$K = \frac{1}{n_i}\frac{dn_i}{dx}\Big|_{x_a}$

and a linear density variation is assumed. A similar equation (i.e. (1.10)) was derived by Karney et al. (1979) except that they neglected the terms $k_y D_k'$ and $k_y A_k'$ in the square bracket of (3.3).

In (3.3), singularities occur at the points x_a and x_t where $\omega^2 = k_z^2 v_A^2(x_a)(1 - \omega^2/\Omega_i^2)$ and $\omega^2 = (k_z^2 + k_y^2)\, v_A^2(x_t)(1 - \omega^2/\Omega_i^2)$. The first singularity is the Alfvén resonance where mode coupling occurs. The second is only an apparent singularity (Ince, 1956; Appert et al., 1974; Swanson, 1975) and represents the magnetosonic wave turning point for $\omega/\Omega_i \ll 1$.

An alternative form of (3.3) from which WKB solutions can be deduced (e.g. Mathews and Walker, 1970, Ch. 1) is obtained using the substitution

$$E_y = [(A_k - k_y^2)/A_k]^{1/2}\, E_Y. \tag{3.4}$$

The wave equation then becomes

$$\frac{d^2 E_Y}{dx^2} + \left[A_k - k_y^2 - \frac{D_k^2}{A_k} + \frac{\omega}{\Omega_i}\frac{k_z^2 k_y K(k_y^2 + k_z^2)}{A_k(A_k - k_y^2)} - \frac{1}{4}\frac{(k_z^2 K)^2\, k_y^2(4A_k - k_y^2)}{A_k^2(A_k - k_y^2)^2}\right] E_Y = 0. \tag{3.5}$$

The WKB solutions to (3.5) are

$$E_{Y\pm} = \kappa_x^{-1/2} \exp(\pm i \int \kappa_x dx) \tag{3.6}$$

where

$$\kappa_x^2 = A_k - k_y^2 - \frac{D_k^2}{A_k} + \frac{\omega}{\Omega_i} \frac{k_z^2 k_y K(k_z^2 + k_y^2)}{A_k(A_k - k_y^2)} \tag{3.7}$$

and terms of $O(K^2)$ have been neglected.

If the density gradient in (3.7) is neglected i.e. if terms of $O(K)$ are neglected then linear turning points (where $\kappa_x^2 = 0$) occur at densities where

$$\omega^2/w_A^2 \simeq k_z^2 + k_y^2 + D_k^2/k_y^2 \tag{3.8a}$$

$$\omega^2/w_A^2 \simeq k_z^2 - D_k^2/k_y^2 \tag{3.8b}$$

for $k_y^2/k_z^2 >> \omega/\Omega_i$ and at

$$\omega^2/w_A^2 \simeq k_z^2 + D_k \tag{3.9a}$$

$$\omega^2/w_A^2 \simeq k_z^2 - D_k \tag{3.9b}$$

for $k_y^2/k_z^2 << \omega/\Omega_i$. When $k_y = 0$, the turning points given by (3.9) coincide with the cutoffs (where $k_\perp = 0$) of the magnetosonic wave as derived in Section 2.3. In keeping with the notation of Ott et al. (1978), the high density linear turning point given by (3.8a) or (3.9a) is called the (compressional) magnetosonic wave turning point. The low density linear turning point given by (3.8b) or (3.9b) is called the ion-cyclotron wave turning point.

The effect of including the density gradient on κ_x^2 is shown in Fig. 3.1. It is seen that the spatial decay rate of the magnetosonic

wave (i.e. $(-\kappa_x^2)^{1/2}$, $\kappa_x^2 < 0$) at densities less than that at the Alfvén resonance (i.e. $A_k < 0$) is smaller for $k_y K$ positive than for $k_y K$ negative. However, for densities such that $0 < A_k < k_y^2$, the spatial decay rate is larger for $k_y K$ positive than for $k_y K$ negative. This dependence on $k_y K$ has important consequences on the mode coupling as discussed in the following Sections.

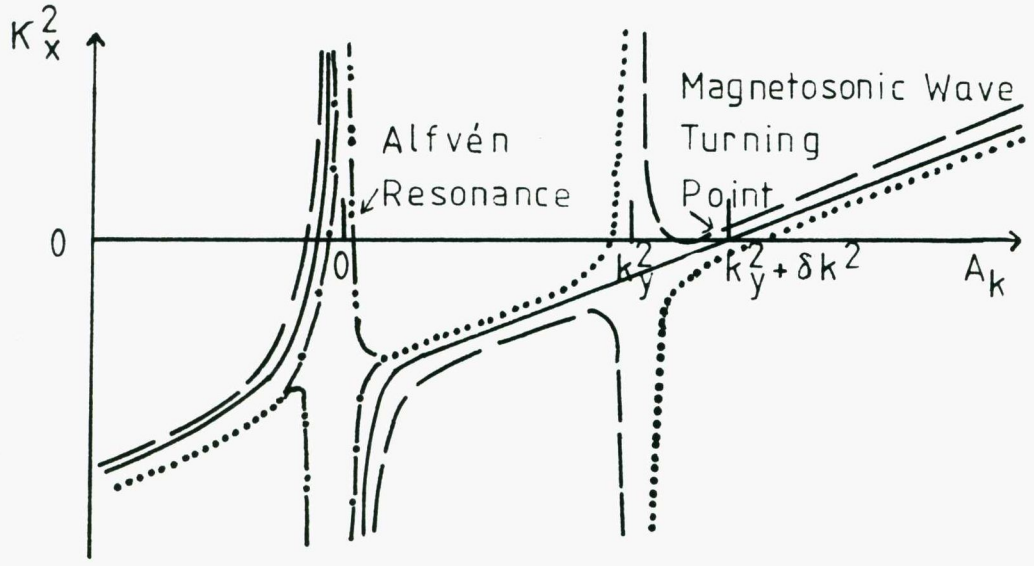

Fig. 3.1 Schematic diagram of κ_x^2. ($\delta k^2 = k_y\{(1+4D_k^2/k_y^4)^{1/2} - 1\}/2$.) The solid curve gives κ_x^2 for $K = 0$ i.e. neglecting the density gradient. The dashed curve gives κ_x^2 for $k_y K$ positive. The dotted curve gives κ_x^2 for $k_y K$ negative with the dash-dot portion applying when $\omega/\Omega_i > |K/k_y|(k_z^2+k_y^2)/k_z^2$ and the dash-double-dot portion when $\omega/\Omega_i < |K/k_y|(k_z^2 + k_y^2)/k_z^2$. Away from the zeros and singularities of κ_x^2 where the WKB solutions are valid, the spatial decay rate (i.e. $(-\kappa_x^2)^{1/2}$, $\kappa_x^2 < 0$) is smaller for $k_y K$ positive than for $k_y K$ negative when $A_k < 0$ and larger when $0 < A_k < k_y^2$.

The WKB solutions are not valid about the zeros and singularities of κ_x. In the following Sections, solutions for E_y which are valid in these regions are found and used with the WKB solutions to estimate the mode conversion of the magnetosonic wave.

3.3 MAGNETOSONIC BODY WAVE HEATING

In this Section, the fractional power lost by a magnetosonic body wave on reflection from a constant density gradient is determined. The incident magnetosonic wave propagates from high density to low density towards the magnetosonic wave turning point. Energy is lost by the incident wave if mode conversion through tunnelling from the turning point to the Alfvén resonance occurs.

The analysis of the reflection of the magnetosonic body wave is facilitated by the use of the dimensionless coordinate

$$\eta = \frac{x - x_a}{x_t - x_a} = \left(\frac{\omega^2}{k_z^2 w_A^2(x)} - 1\right)\left(\frac{k_z}{k_y}\right)^2 \qquad (3.10)$$

($A_k(x_a) = 0$ and $A_k(x_t) = k_y^2$). Using this coordinate, the wave equation (3.3) becomes

$$\frac{d^2E_y}{d\eta} - \frac{1}{\eta(\eta-1)}\frac{dE_y}{d\eta} + \left[M^6((1-F^2)\eta-1) - 2SFM^4 - \frac{M^2S^2}{\eta} + \frac{M(S+M^2F)}{\eta(\eta-1)}\right]E_y = 0 \qquad (3.11)$$

where $M = k_y(k_z^2K)^{-1/3}$

$S = (\omega/\Omega_i)(k_z/K)^{2/3}$

$F = \omega/\Omega_i$.

The method used to solve (3.11) depends on the parameter M^2. For $M^2 \lesssim 1$, an expansion for E_y in M^6 is used (Section 3.3.1). For $M^2 \gtrsim 1$, the method of matched asymptotic solutions (Nayfeh, 1973, Ch. 7) is used (Section 3.3.2).

3.3.1 $M^2 \lesssim 1$

In order to determine an analytic solution to (3.11) for $M^2 \lesssim 1$, terms of order ω^2/Ω_i^2 are neglected so that the wave equation is approximated by

$$\eta(1-\eta)\frac{d^2E_y}{d\eta^2} + \frac{dE_y}{d\eta} - \left[M^6\eta(\eta-1)^2 + \sigma_M\right] E_y = 0 \qquad (3.11')$$

where $\sigma_M = M(S + M^2F)$. The linearly independent solutions to (3.11') for $|\eta| >> 1$ are given approximately by the Airy functions, Ai(- u) and Bi(- u), with $u = M^2\eta$ (Antiosiewiez, 1970).

The power lost by the MW at the Alfvén resonance is obtained by connecting these Airy function solutions across the singularities of the wave equation. The method used by Ott et al. (1978) and Karney et al. (1979) consisted of connecting the series expansion of E_y about $\eta = 0$ directly onto the Airy function solutions (Section 1.2.2). The problem with this method is that the connection depends on an arbitrary point (i.e. u^0 in (1.22)). This problem is overcome here by expanding E_y in terms of functions which can be related to the Airy function independently of any arbitrary point. In particular, let

$$E_y = \sum_{j=0}^{\infty} \delta_M^j e_j(\eta) \qquad (3.12)$$

where $\delta_M = M^6 << 1$. In this case, (3.11') becomes

$$\eta(1 - \eta) \frac{d^2 e_0}{d\eta^2} + \frac{de_0}{d\eta} - \sigma_M e_0 = 0 \tag{3.13}$$

$$\eta(1 - \eta) \frac{d^2 e_j}{d\eta^2} + \frac{de_j}{d\eta} - \sigma_M e_j = \eta(\eta - 1)^2 e_{j-1}. \tag{3.14}$$

The linearly independent solutions for e_0 are obtained by noting that (3.13) is the Gauss hypergeometric equation (Oberhettinger, 1970). Thus, the linearly independent solutions for e_0 about the Alfvén resonance (i.e. $\eta = 0$) are

$$\begin{aligned} e_{01}^{(0)} &= {}_2F_1(a,b;1;\eta) \\ e_{02}^{(0)} &= g(a,b;1;\eta) \end{aligned} \tag{3.15}$$

where $a = (-1 + \sqrt{1 - 4\sigma_M})/2 \simeq -\sigma_M$

$b = (-1 - \sqrt{1 - 4\sigma_M})/2 \simeq -(1 - \sigma_M)$

and ${}_2F_1(a,b;c;\eta)$ and $g(a,b;c;\eta)$ are the Gauss hypergeometric function and the logarithmic solution to the Gauss hypergeometric equation respectively.

Using the change of variable, $\zeta = 1 - \eta$, the linearly independent solutions for e_0 about $\eta = 1$ are found to have the form

$$\begin{aligned} e_{01}^{(1)} &= \zeta^{1-a-b} \, {}_2F_1(1-a,\ 1-b;\ 2-a-b;\ \zeta) \\ e_{02}^{(1)} &= \zeta^{1-a-b} \, g(1-a,\ 1-b;\ 2-a-b;\ \zeta). \end{aligned} \tag{3.16}$$

The second solution in (3.16) has a logarithmic singularity proportional to ω^2/Ω_i^2 arising from the neglect of these order terms in (3.11'). As terms of $O(\omega^2/\Omega_i^2)$ are being neglected here this singularity does not affect the mode coupling. Retention of all ω^2/Ω_i^2 terms removes this singularity.

Similarly the linearly independent solutions of e_0 for $\eta << 1$ are

$$\begin{aligned} e_{01}^{(-)} &= (-\eta)^{-a}\ {}_2F_1(a,\ a;\ 1+a-b;\ 1/\eta) \\ e_{02}^{(-)} &= (-\eta)^{-b}\ {}_2F_1(b,\ b;\ 1+b-a;\ 1/\eta) \end{aligned} \tag{3.17}$$

and for $\eta >> 1$

$$\begin{aligned} e_{01}^{(+)} &= (-\zeta)^{-a}\ {}_2F_1(a,\ 1-b;\ 1+a-b;\ 1/\zeta) \\ e_{02}^{(+)} &= (-\zeta)^{-b}\ {}_2F_1(b,\ 1-a;\ 1+b-a;\ 1/\zeta). \end{aligned} \tag{3.18}$$

Analytic solutions for e_0 which are valid throughout the density gradient are obtained using the connection formulae for the Gauss hypergeometric function given by Luke (1969, p. 86). Using this method, the linearly independent solutions of e_0 for $|\eta| >> 1$ are found to have the form

$$\begin{aligned} e_{01} &\simeq 1 && \eta << -1 \\ &\simeq 1 - i\pi\sigma_M && \eta >> 1 \end{aligned} \tag{3.19}$$

$$e_{02} \simeq -\eta \qquad \eta << -1$$

$$\simeq (1 + i\pi\sigma_M)(-\eta) + M^2(c_0 - i\pi) \qquad \eta >> 1 \tag{3.20}$$

where $c_0 = 1.5 + \Gamma(0) \simeq 0.92$.

Substitution of (3.19) and (3.20) into (3.14) and (3.12), yields the following linearly independent solutions for E_y

$$E_{y1} \simeq f(-u) \qquad \eta << -1$$

$$\simeq (1 - i\pi\sigma_M)\, f(-u) \qquad \eta >> 1 \tag{3.21}$$

$$E_{y2} \simeq g(-u) \qquad \eta << -1$$

$$\simeq (1 + i\pi\sigma_M)\, g(-u) + M^2(c_0 - i\pi)\, f(-u) \qquad \eta >> 1 \tag{3.22}$$

where $f(z) = 1 + \frac{1}{3!} z^3 + \frac{1.4}{6!} z^6 + \ldots$

$g(z) = z + \frac{2}{4!} z^4 + \frac{2.5}{7!} z^7 + \ldots$.

The functions f and g generate the Airy functions with (Antosiewicz, 1970)

$$Ai(-u) = c_1 f(-u) - c_2 g(-u)$$

$$Bi(-u) = \sqrt{3}\,(c_1 f(-u) + c_2 g(-u)) \tag{3.23}$$

where $c_1 = Ai(0) \simeq 0.36$ and $c_2 = -Ai(0) \simeq 0.26$.

Using (3.21) - (3.23) and the asymptotic forms of the Airy functions given in Appendix A, the solution which is finite as $\eta \to -\infty$ is found to have the form

$$
\begin{aligned}
E_y &= Ai(-u) && \eta \ll -1 \\
&= c_A Ai(-u) + c_B Bi(-u) && \eta \gg 1 \\
&\simeq \frac{(-u)^{-1/4}}{2\sqrt{\pi}} \left\{ (c_A + ic_B) \exp(-\tfrac{2}{3}(-u)^{3/2}) \right. \\
&\qquad \left. + (ic_A + c_B) \exp(\tfrac{2}{3}(-u)^{3/2}) \right\}
\end{aligned}
\tag{3.24}
$$

where

$$
\begin{aligned}
c_A &= 1 - 0.5[M^2 c_0 c_2/c_1 - i\pi M^2 c_2/c_1] \\
c_B &= -[M^2 c_0 c_2/c_1 - i\pi(M^2 c_2/c_1 - 2\sigma_M)]/\, 2\sqrt{3}.
\end{aligned}
\tag{3.25}
$$

In (3.24), the term $\exp(\frac{2}{3}(-u)^{3/2})$ represents the incoming magnetosonic wave which propagates from high density to low density towards the magnetosonic wave turning point. The term $\exp(-\frac{2}{3}(-u)^{3/2})$ represents the reflected magnetosonic wave. Thus the ratio of the amplitude of the reflected wave to that of the incident wave (hereafter called the amplitude reflection coefficient) is

$$
R = \left| \frac{c_A + i\, c_B}{c_A - i\, c_B} \right| \tag{3.26a}
$$

$$
\simeq 1 - \frac{\pi}{\sqrt{3}} \left(\frac{c_2}{c_1} M^2 - 2\sigma_M \right) \qquad |\sigma_M| \lesssim M^2 \ll 1. \tag{3.26b}
$$

The corresponding fractional power lost by the magnetosonic wave is given by

$$q = 1 - R^2 \simeq \frac{2\pi}{\sqrt{3}} \left(\frac{c_2}{c_1} M^2 - 2\sigma_M\right) \tag{3.27}$$

for $|\sigma_M| \lesssim M^2 << 1$.

Equation (3.27) implies that:

(i) for $\omega/\Omega_i = 0$ and $k_y = 0$, the plasma does not absorb energy;

(ii) for ω/Ω_i finite, the plasma absorbs little energy when ω and M are chosen such that

$$(S + M^2\omega/\Omega_i)/M \simeq c_2/c_1 \simeq 0.36; \tag{3.28}$$

(iii) the power absorbed is greater for k_y negative than for k_y positive assuming $K > 0$.

A comparison of the square root of the fractional power absorbed as determined by Karney et al. (1979) and by (3.26a) is given in Figs. 3.2 and 3.3. It is seen that if terms of $O(M^2\omega/\Omega_i)$ are neglected then there is good agreement between the numerical integration of the wave equation by Karney et al. (1979) and (3.26a) for $S \lesssim |M|/2$ and for $M^2 \simeq 1$. Note that with the retention of terms of $O(M^2\omega/\Omega_i)$, the power absorbed is determined by $S + M^2\omega/\Omega_i$ rather than by S as given by Karney et al. (1979). This dependence is of importance because, in tokamaks where the poloidial wave number is finite, $M^2\omega/\Omega_i$ is of the order of S or greater except for very large toroidal mode numbers.

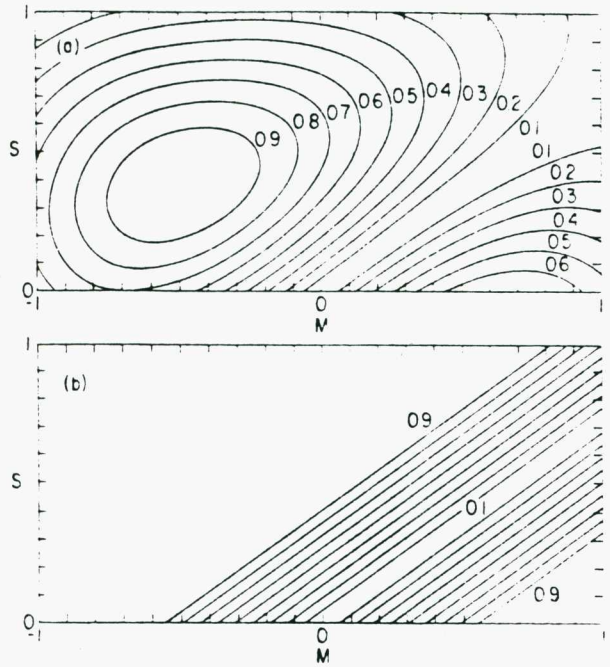

Fig. 3.2 Contour map of $\sqrt{q}$ as determined by Karney et al. (1979). (a) Numerical integration of (3.11) with terms of $O(M^2\omega/\Omega_i)$ neglected. (b) Analytic result (1.23).

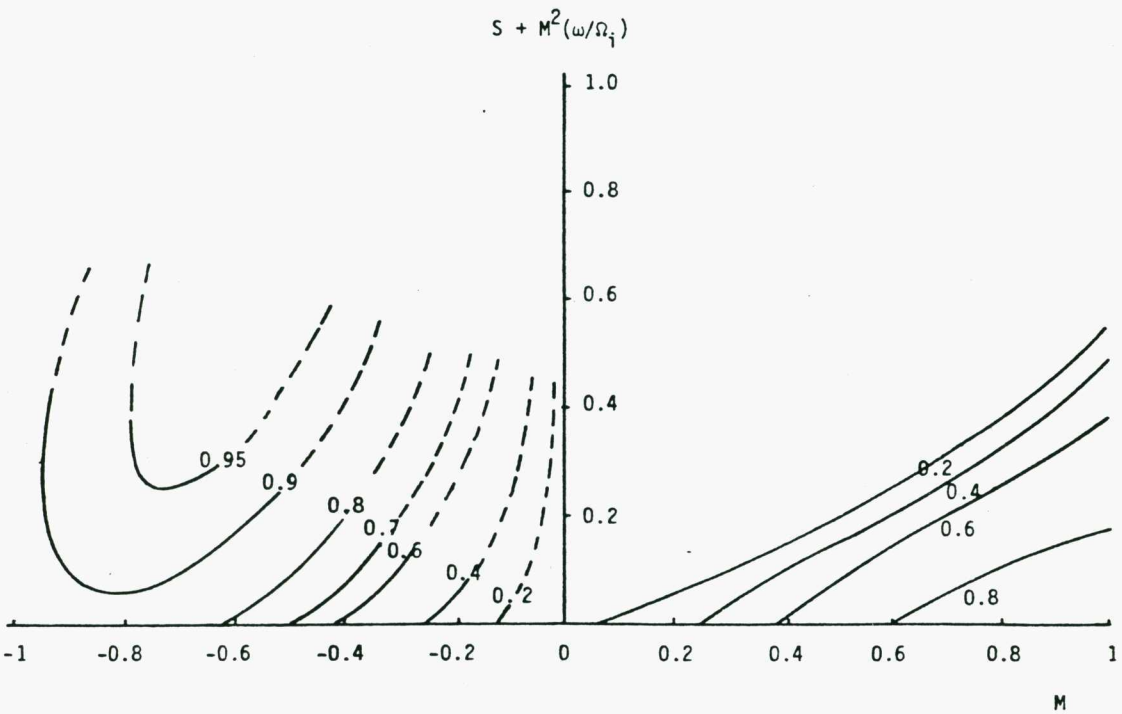

Fig. 3.3 Contour map of $\sqrt{q}$ as determined by (3.26a). Dashed lines represent the region in which (3.26a) is not valid.

3.3.2 $M^2 \gtrsim 1$

For $M^2 \gtrsim 1$, the method of matched asymptotic expansions (Nayfeh, 1973) is used to determine the reflection coefficient of the magnetosonic wave. The method can be best understood by considering the dimensionless form of the wave equation (3.5) which is given by

$$\frac{d^2 E_Y}{d\eta^2} + (\lambda_M^2 \rho(\eta) + r(\eta))\, E_Y = 0 \tag{3.29}$$

$$\rho(\eta) = ((1 - F^2)\eta - 1) - \frac{2SF}{M^2} - \frac{S^2}{M^4 \eta} + \frac{1}{M^5} \frac{S + M^2 F}{\eta(\eta - 1)} \tag{3.30}$$

$$r(\eta) = -\frac{1}{4} \frac{4\eta - 1}{\eta^2 (\eta - 1)^2} \tag{3.31}$$

where $\lambda_M^2 = M^6 >> 1$.

Near the singularities, $\eta = 0$ and $\eta = 1$, approximate solutions to (3.29) can be obtained by retaining in (3.30) and (3.31) only the leading order terms in η about $\eta = 0$ and $\eta - 1$ about $\eta = 1$. Because $\lambda_M^2 >> 1$, $\lambda_M^2 \rho(\eta)$ dominates $r(\eta)$ except very close to the singularities and the asymptotic expansions of these solutions can be matched to the WKB solutions (where the term $r(\eta)$ is neglected; Section 3.2) to give solutions which are valid throughout the density gradient.

In the simplest case i.e. when $\omega/\Omega_i = 0$, $\rho(\eta)$ and $r(\eta)$ reduce to

$$\rho(\eta) \simeq \rho_0 (\eta - \mu)^n [1 + O(\eta - \mu)]$$

$$r(\eta) \simeq r_0 (\eta - \mu)^{-2} [1 + O(\eta - \mu)]$$

about $\mu = 0$ and 1 where $n \geq 0$ and ρ_0, r_0 are constants. Solving (3.29) with the neglect of the above terms of $0(\eta - \mu)$ in $\rho(\eta)$ and $r(\eta)$ and using the transformation (3.4), the linearly independent solutions for E_y are found to have the form

$$\begin{aligned} E_{y1}^{(1)} &= \eta^{-1/2}\, Ai'(\xi_1) \\ E_{y2}^{(1)} &= \eta^{-1/2}\, Bi'(\xi_1) \end{aligned} \tag{3.32}$$

about $\eta = 1$ and the form

$$\begin{aligned} E_{y1}^{(0)} &= \eta^{-1/4}\,(\eta - 1)^{1/4}\left[1 - (1 - \eta)^{3/2}\right]^{1/2} I_0(\xi_0) \\ E_{y2}^{(0)} &= \eta^{-1/2}\,(\eta - 1)^{1/4}\left[1 - (1 - \eta)^{3/2}\right]^{1/2} K_0(\xi_0) \end{aligned} \tag{3.33}$$

about $\eta = 0$ where $\xi_0 = \frac{2}{3}\lambda_M(1 - (1 - \eta)^{3/2})$ and $\xi_1 = \lambda_M^{2/3}(1 - \eta)$. Note that (a) (3.33) reduces to the Bessel function solutions of Chen and Hasegawa (1974) for $|\eta| << 1$ and (b) the logarithm in K_0 is consistent with the definition given by (1.17) if η is assumed to have a small positive imaginary part.

The asymptotic expansions of the functions in (3.32) and (3.33) are (Budden, 1961, p. 311; Luke, 1969, p. 205)

$$Ai'(\xi_1) \simeq -\frac{1}{2}\pi^{-1/2}\xi^{1/4}\exp(-\frac{2}{3}\xi_1^{3/2}) \qquad -\frac{2}{3}\pi \leq \arg\xi_1 \leq \frac{2}{3}\pi$$

$$\simeq \frac{1}{2}\pi^{-1/2}\xi^{1/4}(-\exp(-\frac{2}{3}\xi_1^{3/2}) + i\exp(\frac{2}{3}\xi_1^{3/2})) \qquad \frac{2}{3}\pi \leq \arg\xi_1 \leq \frac{4}{3}\pi$$

$$Bi'(\xi_1) \simeq \frac{1}{2}\pi^{-1/2}\xi^{1/4}(-i\exp(-\frac{2}{3}\xi_1^{3/2}) + 2\exp(\frac{2}{3}\xi_1^{3/2})) \qquad 0 \leq \arg\xi_1 \leq \frac{2}{3}\pi$$

$$\simeq \frac{1}{2}\pi^{-1/2}\xi^{1/4}(-i\exp(-\frac{2}{3}\xi_1^{3/2}) + \exp(\frac{2}{3}\xi_1^{3/2})) \qquad \frac{2}{3}\pi \leq \arg\xi_1 \leq \frac{4}{3}\pi$$

$$I_0(\xi_0) \simeq (2\pi\xi_0)^{-1/2}(\exp(\xi_0) + \exp(-\xi_0 - \frac{1}{2}\pi i) \qquad -\pi < \arg\xi_0 \leq 0$$

$$\simeq (2\pi\xi_0)^{-1/2}(\exp(\xi_0) + \exp(-\xi_0 + \frac{1}{2}\pi i) \qquad 0 \leq \arg\xi_0 < \pi$$

$$K_0(\xi_0) \simeq (\pi/2\xi_0)^{1/2}\exp(-\xi_0) \qquad |\arg z| \leq 3\pi/2.$$

Using the above formulae, the asymptotic expansions of (3.32) are found to be linear combinations of the asymptotic expansions of (3.33) in the region where $1/\lambda_M \lesssim \eta \lesssim 1 - 1/\lambda_M$. By matching these asymptotic expansions, the linearly independent solutions for E_y which are valid throughout the density gradient are obtained. In particular, the solution which is finite as $\lambda_M\eta \to -\infty$ is found to have the form

$$E_y = E_{y2}^{(0)} + i\pi E_{y1}^{(0)} \qquad \eta \lesssim 0$$

$$= c_A^1 E_{y1}^{(1)} + c_B^1 E_{y2}^{(1)} \qquad \eta \gtrsim 1 \qquad (3.34)$$

where $c_A^1 = -i\sqrt{3}\,\pi\lambda_M^{-2/3}\,[\exp(\frac{2}{3}\lambda_M) + \exp(-\frac{2}{3}\lambda_M)]$

$c_B^1 = \sqrt{3}\,\pi\lambda_M^{-2/3}\exp(-\frac{2}{3}\lambda_M)$.

For wave fields described by (3.34), the amplitude reflection coefficients is given by

$$R = \left|\frac{c_A^1 + i\,c_B^1}{c_A^1 - i\,c_B^1}\right| = [1 + 2\exp(-\tfrac{4}{3}\lambda_M)]^{-1}. \tag{3.35}$$

A similar procedure is used when ω/Ω_i is finite except that it is complicated by the fact that $\rho(\eta)$ now has poles at $\eta = 0$ and $\eta = 1$ and zeros at

$$\begin{aligned} \eta_0 &\simeq -(M^2S^2 + \sigma_M)/(M^6 + 2SFM^4) \\ \eta_1 &\simeq 1 + \sigma_M/(M^6F^2 + 2SFM^4 + M^2S^2) \\ \eta_T &\simeq 1 + (F + S/M^2)^2 - \sigma_M/M^6F^2 \end{aligned} \tag{3.36a}$$

where $FM^3 \gg 1$ is assumed. The zeros, η_0 and η_T, correspond to the low and high density turning points given by (3.8) with finite density gradient effects included. For $|MS| \lesssim 1$, the gradient effects dominate with

$$\begin{aligned} \eta_0 &\simeq -\sigma_M/M^6 \\ \eta_1 &\simeq 1 + \sigma_M/M^6F^2 \\ \eta_T &\simeq 1 + F^2 + \sigma_M/M^6F^2. \end{aligned} \tag{3.36b}$$

Assuming $|MS| \lesssim 1$, the linearly independent solutions to (3.29) about these zeros and singularities are (using the transformations (258), (200) and (215) given in Murphy (1960)):

(i) for $\eta \simeq \eta_T$

$$E_{Y1}^{(T)} = (\phi(\eta)/\rho(\eta))^{1/4} \, Ai(-\lambda_M^{2/3}\rho(\eta))$$

$$E_{Y2}^{(T)} = (\phi(\eta)/\rho(\eta))^{1/4} \, Bi(-\lambda_M^{2/3}\rho(\eta)) \qquad (3.37)$$

where $\frac{2}{3}\phi^{3/2} = \int_{\eta_T}^{\eta} \rho(\eta)^{1/2} \, d\eta$;

(ii) for $|\eta - 1| \lesssim \delta^1$, $|\eta_1 - 1| << \delta^1 << 1$

$$E_{Y1}^{(1)} = \xi^{-1/2} \, e^{\xi}$$

$$E_{Y2}^{(1)} = \xi^{3/2} \, e^{\xi} \, {}_1F_1(2;3;-2\xi) \qquad (3.38)$$

where $\xi = \sigma_M(\eta - 1)$ and ${}_1F_1(a;c;z)$ is the confluent hypergeometric function (Slater, 1970);

(iii) for $|\eta| \lesssim \delta^0$, $|\eta_0| << \delta^0 << 1$

$$E_{Y1}^{(0)} = \eta^{1/2} \, e^{-\nu\eta} \, {}_1F_1(a_R;1;2\nu\eta)$$

$$E_{Y2}^{(0)} = \eta^{1/2} \, e^{-\nu\eta} \, g(a_R;1;2\nu\eta) \qquad (3.39)$$

where $a_R = (1 + \alpha/\nu)/2$

$\alpha = M^3F + MS + S^2M^2$

$\nu = |M^3|(1 + 2SF/M^2)^{1/2}$

$|a_R|$, $|MS|$, F, $1/M^2 \lesssim 1$ and $g(a;c;z)$ is the logarithmic solution to the confluent hypergeometric equation.

On the high density side of η_T, the Airy function solutions represent propagating (compressional) magnetosonic body waves. However, no such oscillating solutions occur between the low density cutoff and the Alfvén resonance i.e. in the vicinity of η_0. In this case, the ion-cyclotron wave does not propagate as the magnitude of k_y and the density gradient are such that the region in which it can propagate is less than a wavelength.

In Appendix A, the amplitude reflection coefficient is derived with the inclusion of finite ω/Ω_i corrections. The derivation consists of matching the WKB solution (i.e. (3.8)) which is evanescent in the low density side of the Alfvén resonance to the asymptotic expansions of the solutions about η_0. These solutions are in turn matched to the WKB solutions in the region $0 \lesssim \eta \lesssim 1$ and similarly about η_1 and η_T. From (A.20), the amplitude reflection coefficient is given by

$$R = |(1 + i\theta_M \exp(-2\chi))^{-1}| \qquad (3.40)$$

$$\text{where} \quad \chi = \int_{\delta^0}^{1-\delta^1} (-\lambda_M^2 \rho(\eta))^{1/2} \, d\eta + \int_{1+\delta^1}^{\eta_T} (-\lambda_M^2 \rho(\eta))^{1/2} \, d\eta$$

$$\theta_M = (2\nu)^{-\alpha/\nu} \frac{\Gamma(a_R)}{\Gamma(1-a_R)} [-1 + \exp(-i2\pi a_R)] \exp(i\pi a_R).$$

Note that for $\omega/\Omega_i = 0$, (3.40) reduces to (3.35).

Fig. 3.4 shows $\sqrt{q}$ as determined from (3.26a), (3.35) and from the numerical results of Karney et al. (1979) for $\omega/\Omega_i = 0$. The solid curve gives an upper limit for $\sqrt{q}$ which has a maximum at $|M| \simeq 0.7$. This maximum arises from the dependence of the mode coupling on the magnitude of E_x near the Alfvén resonance (Section 2.4). In particular, the magnitude of E_x relative to E_y increases with k_y^2 but the total amount of energy reaching the Alfvén resonance is limited by the evanescence of the wave fields between the Alfvén resonance and the magnetosonic wave turning point. This evanescence is represented by the exponential terms in (3.35) and (3.40) and increases with M^2.

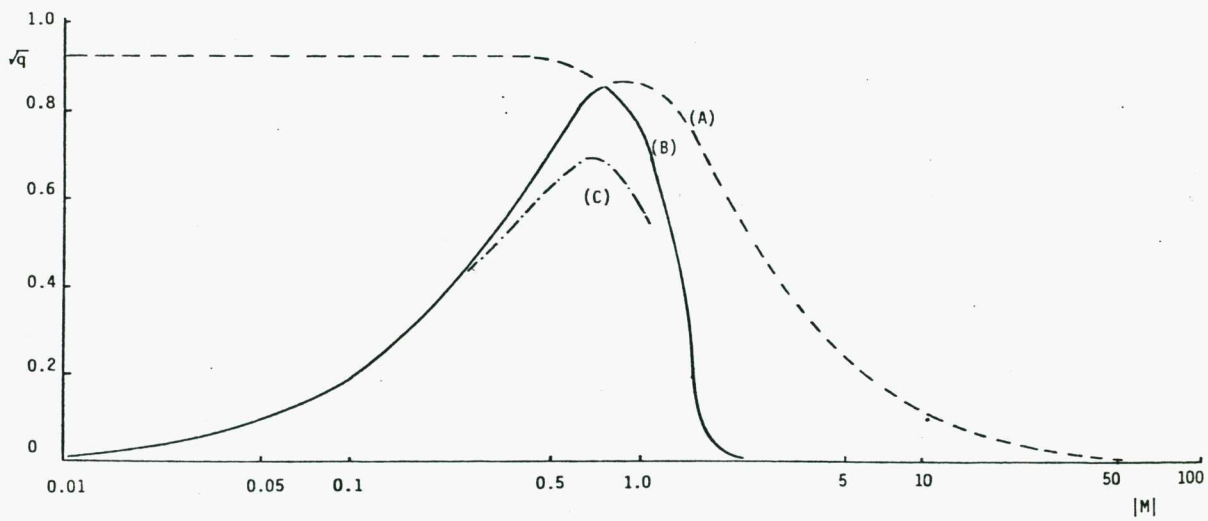

Fig. 3.4 Square root of the fractional power absorbed neglecting finite frequency effect. (A) Analytic result using (3.26a). (B) Using (3.35). (C) Numerical integration by Karney et al. (1979). The power absorbed is limited by the evanescence of the wave fields between the magnetosonic wave turning point and the Alfvén resonance.

Figs 3.5 and 3.6 show the fractional power absorbed as given by (3.40) with ω/Ω_i finite. The finite ω/Ω_i corrections alter the power absorbed in two ways. The first way is by modifying the polarization of the MW and hence the mode coupling (cf. Section 2.4). This effect is represented by the θ_M term in (3.40) which is larger for M negative than for M positive. The second way the finite ω/Ω_i corrections act is by modifying the spatial decay rate and region of evanescence of the magnetosonic wave between its turning point and the Alfvén resonance. This effect is represented by the χ term in (3.40) with the evanescence being smaller for M negative than for M positive as discussed in Section 3.2 and illustrated in Fig. 3.6. These two effects combine to enhance the absorption for $k_y K$ negative and to reduce the absorption for $k_y K$ positive.

3.4 MAGNETOSONIC SURFACE WAVE HEATING

In the previous Section, the wave and plasma parameters were assumed to be such that the magnetosonic wave turning point was present in the plasma. However, if the Alfvén resonance lies near the maximum plasma density and $k_y^2 \gtrsim k_z^2$ then the magnetosonic wave turning point is not present within the plasma. In this case, an external antenna can only excite a magnetosonic surface wave (i.e. a cutoff magnetosonic wave).

The damping of the magnetosonic surface wave due to mode coupling has been previously studied by Ionson (1978), Wentzel (1979a, 1979b) and Cramer and Donnelly (1983) using a density profile of the form shown in Fig. 1.1. In these works a sharp discontinuity, i.e.

(a)

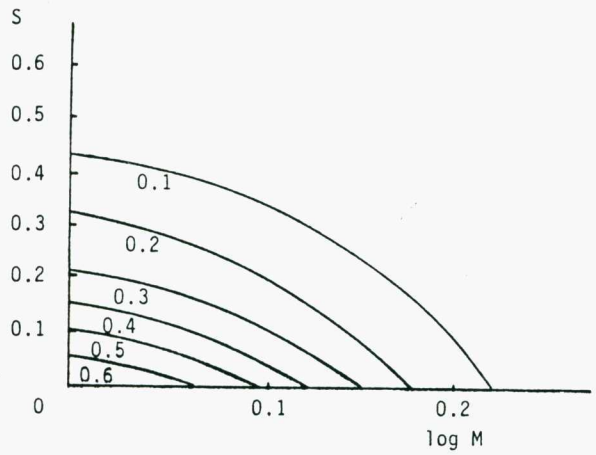

(b)

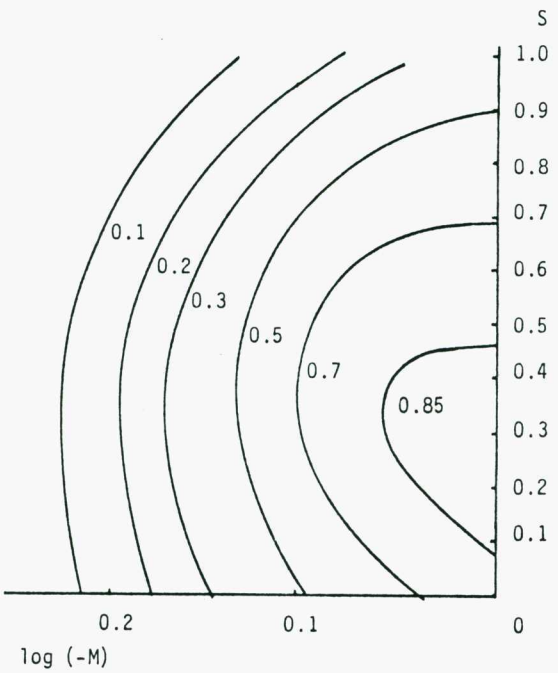

Fig. 3.5 Contour map of $\sqrt{q}$ as given by (3.35) for S finite, $F \ll 1$ and (a) $M > 1$ and (b) $M < -1$. The results about $M^2 \simeq 1$ are consistent with those given in Fig. 3.2.

(a)

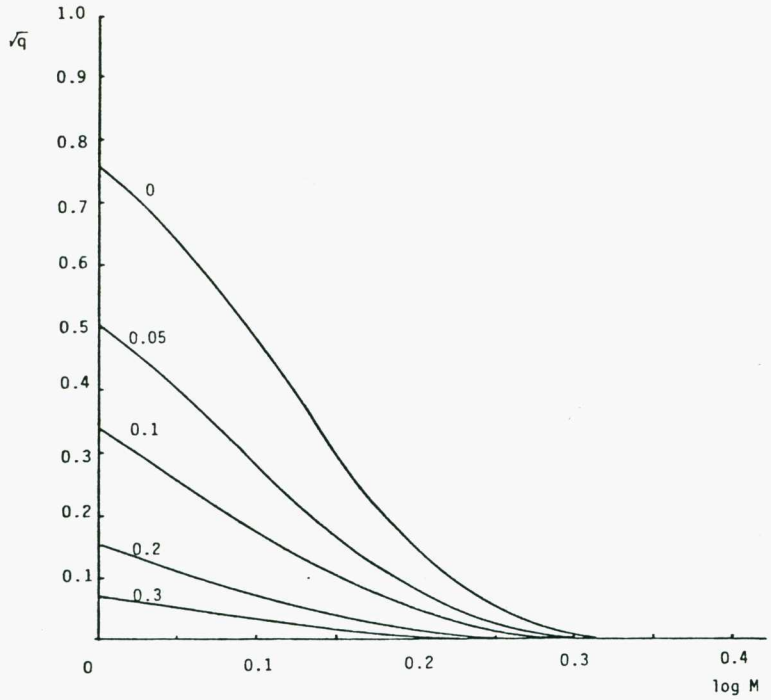

(b)

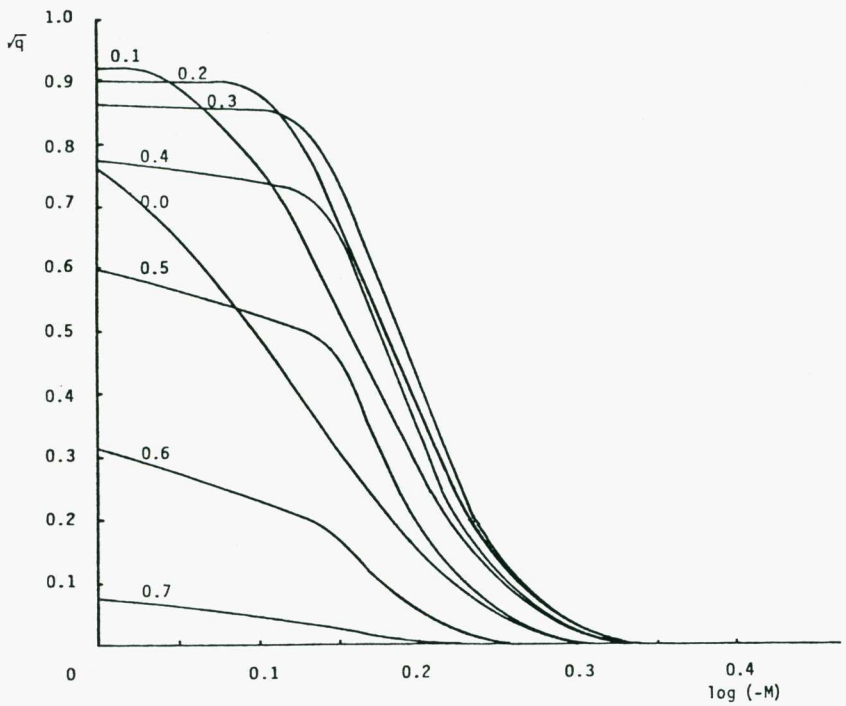

Fig. 3.6 Square root of the fractional power absorbed for the given values of F = S, and (a) M > 0 and (b) M < 0. The finite frequency and density gradient effects enhance the evanescence of the MW for k_y positive and decrease it for k_y negative (assuming K > 0).

$k_y^2/K^2 << 1$, is assumed. However, in the tokamak, away from the plasma edge, k_y/K is of the order of the poloidal mode number so that for a finite poloidal mode number $k_y^2/K^2 \gtrsim 1$ and the assumption of a sharp discontinuity is invalid. Further, for a finite poloidal wave number, $k_y^2 \gtrsim k_z^2$ and hence $M^2 \gtrsim 1$ except for large toroidal mode numbers.

Because of this limitation in the previous works, the properties of the magnetosonic surface wave are now derived for the case where $M^2 \gtrsim 1$ and for a density profile of the form shown in Fig. 1.1. The wave fields in the density gradient are as described in Subsection 3.3.2 and Appendix A except that here the magnetosonic wave turning point is assumed to be absent from the plasma. Thus, assuming $\psi_1 = \nu\eta(x_1) << -1$, the solution for E_y about $x \simeq x_2$ which connects onto the solution which is finite as $x \to -\infty$ is found to have the form

$$
\begin{aligned}
E_y &= \sin(\pi a_R)\, E_{y2}^{(0)} + \pi \exp(-i\pi a_R)\, E_{y1}^{(0)} && x < x_2 \\
&= \{\sin(\pi a_R)\, e_{p2} + \pi \exp(-i\pi a_R)\, e_{p1}\} \exp[k_{x2}(x-x_2)] && (3.41) \\
&\quad + \{\sin(\pi a_R)\, e_{n2} + \pi \exp(-i\pi a_R)\, e_{n1}\} \exp[-k_{x2}(x-x_2)] && x > x_2
\end{aligned}
$$

$$
\begin{aligned}
e_{pi} &= \frac{1}{2}\left[E_{yi}^{(0)} + \frac{dE_{yi}^{(0)}}{d\nu\eta}\right]\Bigg|_{x_2} \\
e_{ni} &= \frac{1}{2}\left[E_{yi}^{(0)} - \frac{dE_{yi}^{(0)}}{d\nu\eta}\right]\Bigg|_{x_2}
\end{aligned}
\qquad (3.42)
$$

where $k_{x2} = (-\kappa_x^2(x_2))^{1/2}\big|_{K=0}$, $E_{yi}^{(0)} = ((\eta-1)/\eta)^{1/2} E_{Yi}$, $i = 1,2$ and $|a_R| < 1$. In the derivation of (3.41) and (3.42), continuity of E_y and its derivative at x_2 has been used.

The dispersion relation for the surface wave is obtained by requiring that E_y remain finite as x goes to positive infinity i.e.

$$\pi e_{p1} \exp(-i\pi a_R) + e_{p2} \sin(\pi a_R) = 0. \tag{3.43}$$

Depending on the position of the Alfvén resonance with respect to x_2 either the asymptotic expansions or the series expansions of $E_{yi}^{(0)}$ are used to evaluate e_{p1} and e_{p2} via (3.42). It is found that a solution to (3.43) only exists if $\psi_2 = \nu\eta(x_2) \lesssim 1$. In this case,

$$\begin{aligned} e_{p1} &\simeq 1 + \alpha/\nu \\ e_{p2} &\simeq (1 + \alpha/\nu + \alpha\psi_2/\nu)\, \ell n(\psi_2) + 1/\psi_2 - (0.12 - 1.35\, \alpha/\nu) \end{aligned} \tag{3.44}$$

where $(\alpha/\nu)^2 << 1$ is assumed.

On substitution of (3.44) into (3.43), the dispersion relation of the surface wave is found to have the form

$$\psi_2 \simeq 0.10 - 0.06\, \alpha/\nu - i(0.19 - 0.22\, \alpha/\nu) \tag{3.45}$$

i.e.

$$\omega^2 \simeq k_z^2 w_A^2(x_2) \left[1 + \left|\frac{K}{k_y}\right|(0.10 - 0.06\, \alpha/\nu) - i\left|\frac{K}{k_y}\right|(0.19 - 0.22\, \alpha/\nu)\right] \tag{3.45'}$$

Using a similar procedure but assuming $|\psi_1| \lesssim 1$ (rather than $|\psi_1| >> 1$) a second type of surface wave is found to exist. (In the limit $\omega/\Omega_i \to 0$, the dispersion relation of this wave is given by $\psi_1 = -0.10 - i\, 0.19$.)

However, this case is not of interest as it corresponds to the heating of the plasma surface rather than the plasma interior.

Neglecting finite ω/Ω_i corrections (i.e. terms of $O(\alpha/\nu)$), the dispersion relation (3.45') is similar to that given by (1.19b) for a sharp discontinuity except that:

(i) the damping increases with $|K/k_y|$ rather than with $|k_y/K|$ as in the case of a sharp discontinuity;

(ii) the Alfvén resonance occurs at $(1 + 0.10\ |K/k_y|)^{-1}$ of the maximum plasma density while for the sharp discontinuity it occurs at half the maximum plasma density.

This behaviour is to be expected because as $K \to 0$ the plasma becomes homogeneous so that no mode coupling can occur and the dispersion equation (3.45) reduces to that of the Alfvén wave.

With the introduction of finite ω/Ω_i corrections, the low frequency surface wave (i.e. the surface wave given by (3.45') for $\omega/\Omega_i = 0$) is found to be split into two modes whose properties depend on the sign of k_y. (A similar result was also obtained by Cramer and Donnelly (1983) for the case of a sharp plasma boundary.) In particular, it is seen from (3.45') that (a) the Alfvén resonance occurs at higher densities for the surface wave with k_y positive than for the wave with k_y negative and (b) the damping of the wave with k_y negative is larger than the damping of the wave with k_y positive. Indeed, when $\alpha/\nu \simeq a_R \simeq 1$ i.e. when

$$\begin{aligned} k_y &> 0 \\ \omega/\Omega_i(1 + k_z^2/k_y^2) &\simeq 1 \end{aligned} \qquad (3.46)$$

the dispersion relation (3.43) reduces to

$$\omega^2 = k_z^2 w_A^2(x_2)\{1 - (K/|k_y|)(\tan(\pi a_R) + i \tan^2(\pi a_R))/\pi\ (1 + \alpha/\nu)\} \quad (3.45")$$

and little damping occurs when $a_R \simeq 1$. Note that for $a_R > 1$ the Alfvén resonance is absent from the plasma and the approximations used in the derivation of the dispersion relation are no longer valid.

3.5 ANTENNA RESPONSE

3.5.1 Introduction

The absorption of energy at the Alfvén resonance gives the antenna impedance a finite resistive component. To determine whether this coupling between the antenna and the plasma is efficient, the antenna response is characterized by $\tilde{Q}$, the ratio of the circulating power to the absorbed power i.e. the ratio of the imaginary (or reactive) part of the impedance to the real (or resistive) part of the impedance. (Alternatively, the antenna response can be characterized by Q, the ratio of the wave frequency at peak resistance to the frequency bandwidth at half height with Q being approximately inversely proportional to $\tilde{Q}$ (Ross et al., 1982).) For efficient coupling of energy between the plasma and the antenna, $\tilde{Q}$ needs to be less than or about unity otherwise most of the input power appears as circulating power in the antenna and very large voltages (and currents) are needed to obtain the desired plasma heating. Further, the resistance of the antenna due to the mode coupling needs to be greater than about the ohmic resistance of the driving circuit (which is unlikely if $\tilde{Q}$ is large and the impedance is small) otherwise little input power actually goes into the heating of the plasma.

In this Section, conditions are determined for when $\tilde{Q}$ of the antenna is small and the antenna resistance large. Attention is restricted to the parameter range in which $\omega/\Omega_i \lesssim 0.5$ so as to simulate conditions in TORTUS (Cross et al., 1982) and to include the parameter range for which minority ion-cyclotron heating is effective.

When ω/Ω_i is non-negligible and the Alfvén resonance is near the centre of the plasma, the magnetosonic wave turning point is unlikely to be present in the plasma and surface wave heating must be utilized. The antenna response for this situation is examined in some detail in the remainder of this Section and only a qualitative discussion is given on the antenna response in the analogous case of body wave heating.

Previously, Donnelly (1982) examined the excitation in TORTUS of waves with zero poloidal mode number. He found that these waves are unlikely to produce efficient Alfvén resonance heating in TORTUS. Because of this result, the poloidal mode number is assumed here to be finite i.e. $M^2 \gtrsim 1$. The parameter range in which $M^2 \gtrsim 1$ and ω/Ω_i is finite is also of interest because it has not been studied previously. For example, Chen and Hasegawa (1974), Hasegawa and Chen (1976) and Cramer and Donnelly (1983) assumed a sharp plasma boundary such that $k_z^2 \lesssim k_y^2 << K^2$ and Ott et al. (1978) and Karney et al. (1979) assumed $M^2 << 1$. In the numerical results of Ross et al. (1982), Appert and Vaclavik (1982) and Donnelly and Cramer (1983) some of the above parameters were examined but the role of finite frequency and density gradient corrections was not studied extensively.

A similar geometry to that used in Section 3.4 is considered here (see Fig. 3.7) except that a perfectly conducting wall is located

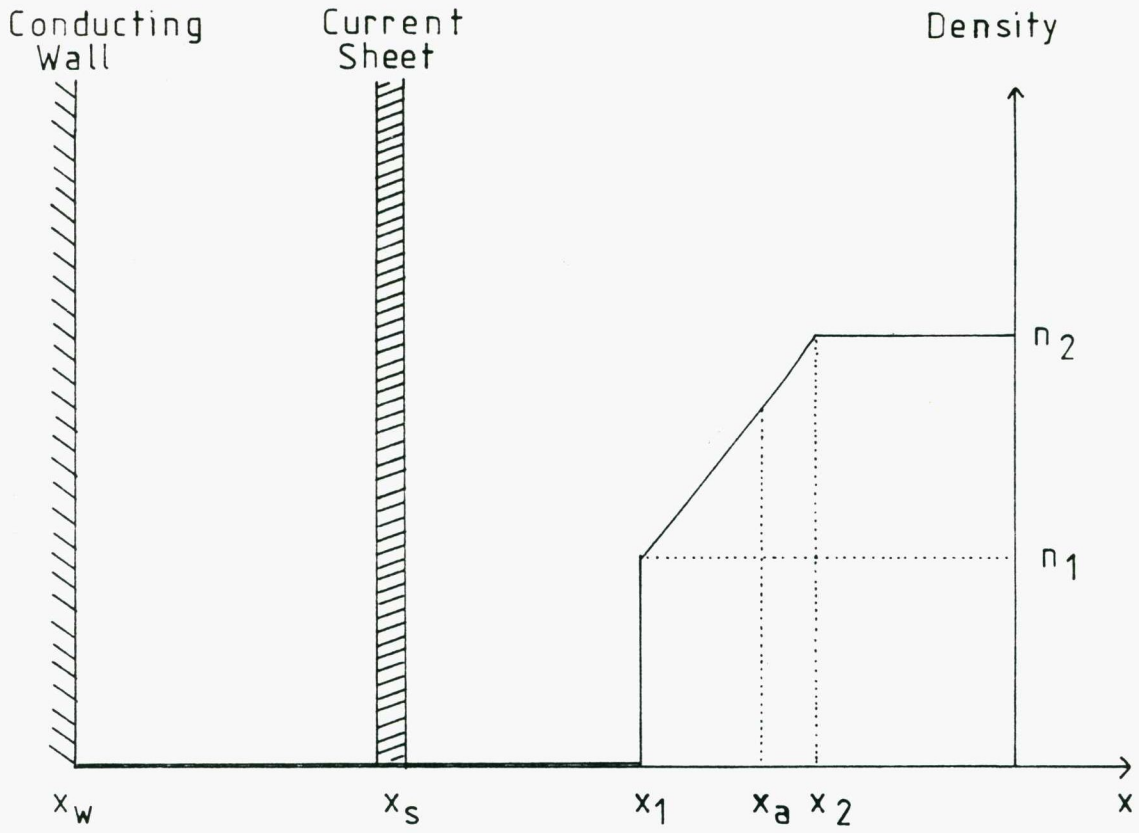

Fig. 3.7 Schematic diagram of the cavity and the density profile.

at $x = x_w$, an antenna at $x = x_s$ and, to simulate conditions at the plasma edge, a step discontinuity in the density occurs at $x = x_1$. The plasma is assumed to be of semi-infinite extent because the magnetosonic wave is, by assumption, everywhere cutoff so that the contribution from the far side of the plasma is exponentially small.

The current density in the antenna is assumed to have the form

$$\underset{\sim}{J} = \underset{\sim s}{J} \delta(x - x_s)\exp(i(k_y y + k_z z - \omega t)) \tag{3.47}$$

$$\underset{\sim s}{J} = J_0(k_z^2 + k_y^2)^{-1/2} (k_z \underset{\sim}{\hat{j}} - k_y \underset{\sim}{\hat{k}})$$

where $\hat{\underset{\sim}{j}}$ and $\hat{\underset{\sim}{k}}$ are the unit vectors in the y and z directions respectively. This form of the current density is chosen so as to satisfy the condition $\underset{\sim}{\nabla}.\underset{\sim}{J} = 0$ i.e. that no free charges accumulate on the current sheet. Transient effects are also neglected i.e. ω, k_y and k_z are assumed to be real.

3.5.2 Boundary Conditions

The boundary conditions for the fields are (Lorrain and Corson, 1970, p. 565; Ott et al., 1978):

(a) the tangential electric field vanish at x_w i.e. $E_y(x_w) = 0$ (E_z is neglected as the plasma conductivity in the z-direction is large);

(b) E_y is continuous as there are no free charges present;

(c) E_y must remain finite as $x \to \infty$;

(d) the magnetic field and hence dE_y/dx is continuous except possibly at the antenna and at the plasma discontinuity. At the antenna, the magnetic field has a step discontinuity due to the antenna current as given by Ampere's circuital law. At the plasma discontinuity, the boundary conditions for the magnetic field or equivalently for dE_y/dx is obtained by integrating the wave equation (3.3) across the plasma discontinuity. Thus, the boundary condition at the plasma discontinuity is that

$$\left[(A_k - k_y^2)^{-1} \left(A_k \frac{d}{dx} - k_y D_k\right) E_y\right]_{x_1^-}^{x_1^+} = 0$$

where $x_1^+(x_1^-)$ is infinitesimally greater (smaller) than x_1. This condition implies that B_z is continuous across the discontinuity (Cramer and Donnelly, 1983).

3.5.3 The Antenna Impedance

3.5.3.1 *Derivation*

The antenna impedance is defined by

$$Z \equiv -\int_{x_s^-}^{x_s^+} dx \; \underset{\sim}{E}.\underset{\sim}{J}^*/\underset{\sim}{J}.\underset{\sim}{J}^* \tag{3.48}$$

where $x_s^-(x_s^+)$ is infinitesimally smaller (greater) than x_s. The product $\underset{\sim}{E}.\underset{\sim}{J}^*$ is determined by applying the above boundary conditions to the solutions of the wave equation (3.3).

Using the first boundary condition the y component of the electric field in the region $x_w \underset{\sim}{<} x \underset{\sim}{<} x_s$ is found to have the form

$$E_y = e_{y0}\sinh[k_{x1}^-(x - x_w)] \tag{3.49}$$

$$k_{x1}^- = (-\kappa_x^2(x_1^-))^{1/2} \simeq (k_y^2 + k_z^2)^{1/2} \tag{3.50}$$

where κ_x is defined by (3.9).

In the region $x_s \underset{-}{<} x \underset{-}{<} x_1$, E_y has the form

$$E_y = e_{y1}\exp(k_{x1}^- x) + e_{y2}\exp(-k_{x1}^- x) \tag{3.51}$$

where from the boundary conditions, (b) and (d),

$$e_{y0}\sinh[\bar{k}_{x1}(x_s - x_w)] = e_{y1}\exp(\bar{k}_{x1}x_s) + e_{y2}\exp(-\bar{k}_{x1}x_s) \tag{3.52}$$

and

$$4\pi J_0 = -i(k_z c/\omega)\Big\{e_{y0}\cosh[\bar{k}_{x1}(x_s - x_w)] - [e_{y1}\exp(\bar{k}_{x1}x_s) - e_{y2}\exp(-\bar{k}_{x1}x_s)]\Big\} . \tag{3.53}$$

In the derivation of (3.53), terms of $0(\omega/kc)$ have been neglected.

By substituting (3.49)-(3.53) into (3.48) the antenna impedance is found to have the form

$$Z = 4\pi(\omega / \bar{k}_{x1}c)Z_N \tag{3.54}$$

$$Z_N = -i\Big\{\coth(\chi_{sw}/2) - (1 - e_R)/(1 + e_R)\Big\}^{-1} \tag{3.55a}$$

$$= -\frac{ie^{\chi_{sw}}(1 - e^{-\chi_{sw}})(1 + e_R)}{2(1 + e^{\chi_{sw}}e_R)} \tag{3.55b}$$

where $\chi_{sw} = 2\bar{k}_{x1}(x_s - x_w)$ and $e_R = (e_{y2}/e_{y1})\exp(-2\bar{k}_{x1}x_s)$. (The term e_R is evaluated in Section 3.5.3.3 by continuing the wave fields described by (3.51) through the density gradient and applying the boundary conditions given in Section 3.5.2).

A similar expression to (3.55a) was obtained by Ott et al. (1978) except that they assumed k_y^2 was much less than k_z^2 so that $(\bar{k}_{x1})^2$ was approximated by k_z^2. Further, Ott et al. (1978) only determined the properties of the impedance numerically and no criteria for the general

response of the antenna were given. In the following Sections, these criteria are derived.

3.5.3.2 *General Characteristics*

Two observations about the antenna impedance can be made from (3.54) and (3.55) without the actual evaluation of e_R. The first observation is that the resistive component of the antenna arises from a finite $Im(e_R)$. The second observation is that $\tilde{Q}$ of the antenna depends not only on $Im(e_R)$ but also on the proximity of the antenna to the wall. In particular if the antenna is brought closer to the wall (i.e. as $x_s \to x_w$) the antenna impedance as given by (3.55) decreases and $\tilde{Q}$ approaches infinity independently of the magnitude of $Im(e_R)$. A similar phenomenon was noted by Ott et al. (1978) and is attributed to oppositely directed image currents in the wall which produce fields which tend to cancel those of the antenna. Thus, a minimum requirement for the efficient coupling of energy between the antenna and the plasma is that

$$\bar{k}_{x1}(x_s - x_w) \gtrsim 1.$$

This condition is assumed in the remainder of this Section.

To see the dependence of the resistance on $Im(e_R)$, first suppose that $|Im(e_R)| \gg 1$. In this case, (3.55) reduces to

$$Z_N = -i\{\coth(\chi_{sw}/2) + 1 - 2/e_R\}^{-1}. \tag{3.56}$$

It is seen from (3.56) that the antenna always has a large $\tilde{Q}$ so that

the coupling of energy between the antenna and the plasma is inefficient. This situation corresponds to "mush" heating (Stix, 1980) where the absorption at the Alfvén resonance is large.

Similarly, suppose $|Re(e_R)| >> |Im(e_R)|$ and $Re(e_R) \neq -1$ or $Re(e_R) \neq -\exp(-\chi_{xs})$ then $\tilde{Q}$ (as derived from (3.55b)) is again large and the coupling between the antenna and the plasma is inefficient. However, more efficient coupling is possible when

$$|Im(e_R)| \lesssim 1 \tag{3.57}$$

$$|Re(e_R) + e^{-\chi_{sw}}| << |Im(e_R)|$$

i.e. when

$$Re(e_R) + e^{-\chi_{sw}} \simeq 0. \tag{3.57'}$$

In this case, (3.55b) reduces to

$$Z_N \simeq -(1 - e^{-\chi_{sw}})(1 - e^{-\chi_{sw}} + iIm(e_R))/2Im(e_R) \tag{3.58}$$

with

$$\tilde{Q} \simeq Im(e_R)/(1 - e^{-\chi_{sw}}). \tag{3.59}$$

Thus, when $|Im(e_R)|$ is small and χ_{sw} is large, the antenna impedance is large and $\tilde{Q}$ is small.

The situation in which the impedance is described by (3.58) corresponds to "eigenmode" heating of Stix (1980) with the resistance being peaked when the antenna excites a weakly damped cavity eigenmode whose dispersion relation is given by (3.57'). Note that very small $\tilde{Q}$ (i.e. very small $|Im(e_R)|$) is undesirable as the frequency bandwidth in which the impedance is resistive (i.e. when (3.57) is satisfied) is small and mode-tracking may be required as the plasma conditions change.

An intermediate type of heating between mush heating and eigenmode heating is obtained when

$$|\mathrm{Im}(e_R)| \lesssim 1$$
$$|\mathrm{Re}(e_R) + 1| \ll |\mathrm{Im}(e_R)|. \tag{3.60}$$

In this case, (3.55b) reduces to

$$Z_N = -\frac{(1 - e^{-\chi_{sw}})\ \mathrm{Im}(e_R)}{2(1 - e^{-\chi_{sw}} - i\mathrm{Im}(e_R))} \tag{3.61}$$

with $\tilde{Q}$ again given by

$$\tilde{Q} = \mathrm{Im}(e_R)/(1 - e^{-\chi_{sw}}). \tag{3.62}$$

Although low $\tilde{Q}$ heating is obtained for $|\mathrm{Im}(e_R)|$ small and χ_{sw} large, small impedances are also obtained which is undesirable.

3.5.3.3 *Specific Characteristics*

It is seen from the above arguments that the most efficient coupling of energy occurs when criterion (3.57) is satisfied. The term e_R is now evaluated and conditions for which (3.57) is satisfied are determined.

Because the emphasis of this Section is on the heating of the plasma interior for a finite poloidal mode number, $M^2 >> 1$ and the Alfvén resonance near the high density edge of the density gradient (i.e. $x_a \simeq x_2$) are assumed. In this case, the antenna fields as given by (3.51) can be continued across the density gradient using the

procedure described in Section 3.4 and applying the boundary conditions given in Section 3.5.2. Using this method, e_R is found to have the form

$$e_R = G_0 \exp(\chi_{xs}) \frac{[\exp(\chi_{ax})\ \Lambda_k - G_1 \theta_a]}{[\theta_a - H_1 \exp(\chi_{ax})\ \Lambda_k]} \tag{3.63}$$

$$\Lambda_k = \frac{\pi \exp(-i\pi a_R)}{\sin(\pi a_R)}\, e_{p1} + e_{p2} \tag{3.64}$$

$$\theta_a = (2\nu)^{\alpha/\nu}\, (\Gamma(1 - a_R))^2\, e_{p1} \tag{3.65}$$

$$G_0 = \frac{1 + G_k}{1 + H_k} \qquad G_1 = \frac{1 - G_k}{1 + G_k} \qquad H_1 = \frac{1 - H_k}{1 - H_k} \tag{3.66}$$

$$G_k = \frac{A_k^+ - k_y^2}{A_k^+ k_{x1}^+} \left\{ \frac{A_k^- k_{x1}^- - k_y D_k^-}{A_k^- - k_y^2} + \frac{k_y D_k^+}{A_k^+ - k_y^2} \right\} \tag{3.67}$$

$$H_k = \frac{A_k^+ - k_y^2}{A_k^+ k_{x1}^+} \left\{ \frac{A_k^- k_{x1}^- + k_y D^-}{A_k^- - k_y^2} - \frac{k_y D_k^+}{A_k^+ - k_y^2} \right\} \tag{3.68}$$

where $k_{x1}^{\pm} = k_x(x_1^{\pm})$, $k_x = (-\kappa_x^2)^{1/2}$, $\chi_{xs} = 2k_{x1}(x_1 - x_s)$

$\chi_{ax} = 2 \int_{\eta(x_1)}^{-\delta 0} (-\lambda_M^2 \rho(\eta))^{1/2}\, d\eta$, $A_k^{\pm} = A_k(x_1^{\pm})$, $D_k^{\pm} = D_k(x_1^{\pm})$ and $a_R(<1)$, α, ν, e_{p1} and e_{p2} are as defined in (3.39) and (3.42).

Note that $G_0 = 0$ corresponds to the dispersion relation of the magnetosonic surface wave propagating in a sharp plasma boundary as derived by Cramer and Donnelly (1983) while $\Lambda_k = 0$ corresponds to the dispersion relation of the magnetosonic surface wave propagating in a diffuse plasma boundary as derived in Section 3.4. However, here, Λ_k can only vanish if there is no mode coupling as ω is real (being determined

by the antenna) rather than being complex as in Section 3.4. Further, conditions are assumed here such that the Alfvén resonance is assumed to be in the plasma interior rather than at the plasma edge so that $A_k^+ < 0$ and $G_0 > 0$ (assuming $\omega^2/\Omega_i^2 \ll 1$).

The terms G_1 and H_1 represent modifications to the wave fields due to reflection at the plasma edge. For a large jump in the density at the plasma edge (i.e. if $n_1 \simeq n_2$) then $G_1 \simeq H_1 \simeq -1$. In this case $e_R (\simeq G_0 \exp(\chi_{xs}))$ is real and positive so that $\tilde{Q} >> 1$ and the coupling of energy between the antenna and the plasma centre is inefficient.

For small jumps in the plasma density at x_1, $|H_1|$ and $|G_1|$ are much less than unity and G_0 is of order unity. In this case, if ω/Ω_i is negligible or ω/Ω_i finite and $k_y < 0$ then low-efficiency high-$\tilde{Q}$ heating is again obtained because either $|\mathrm{Im}(e_R)| \gtrsim 1$ or $\mathrm{Re}(e_R) > |\mathrm{Im}(e_R)| > 0$. However, for $a_R \simeq 1$ i.e. for

$$\begin{aligned} k_y &> 0 \\ (\omega/\Omega_i)(1 + k_z^2/k_y^2) &\simeq 1 \end{aligned} \tag{3.69}$$

more efficient heating is possible (i.e. criterion (3.57) is satisfied) when

$$\frac{\omega^2}{k_z^2 w_A^2(x_2)} - 1 \simeq \frac{K}{k_y} \frac{\sin(\pi a_R)}{\pi(1 + \alpha/\nu)} \times \left\{1 - \pi(2\nu)^{\alpha/\nu} \left[\exp(-\chi_{aw})/G_0 - \exp(-\chi_{ax})G_1\right]/\sin(\pi a_R)\right\}^{-1} \tag{3.70}$$

with

$$\mathrm{Im}(e_R) \simeq - G_0 \frac{(2\nu)^{-\alpha/\nu}}{\pi} \exp(\chi_{as}) \sin^2(\pi a_R) \tag{3.71}$$

$\chi_{aw} = \chi_{ax} + \chi_{xs} + \chi_{sw}$, $\nu\eta(x_2) << 1$ is assumed and terms of $O(H_1 \exp-\chi_{xw}$, $H_1 G_1)$ have been neglected.

Equation (3.70) is the dispersion relation for the surface wave eigenmode with (3.69) being the condition that the damping of this eigenmode be weak. This dispersion relation is similar to that given by (3.45") except that here corrections due to the presence of the conducting wall and the density jump at the plasma edge are included. These modifications are such that the Alfvén resonance occurs at higher densities (and hence is further into the plasma) if the effective separation between the plasma and the conducting wall is increased (i.e. if $k_{x1}(x_1 - x_w)$ is increased) or if the plasma edge is diffuse rather than sharp (i.e. if $|G_1|$, $|H_1| \neq 1$).

If the corrections due to the presence of the conducting wall and the density jump are small then the Alfvén resonance moves towards the plasma centre as a_R approaches unity. In the frequency range required for minority ion heating (i.e. $\omega \simeq \frac{1}{2}\Omega_i$), $a_R \simeq 1$ when $k_z^2 \simeq k_y^2$. For smaller frequencies k_z^2 must be larger than k_y^2.

The antenna resistance is limited by the evanescence of the wave fields between the current sheet and the Alfvén resonance (as represented by the term χ_{as} in (3.71)). Assuming k_y^2 is fixed, this evanescence is minimized if (i) $x_s \simeq x_1$, (ii) k_y is positive rather than negative (Section 3.2) and (iii) $k_z^2 \lesssim k_y^2$. Hence optimum coupling of energy between the antenna and the plasma interior is expected when $\omega \simeq \frac{1}{2}\Omega_i$ and $k_z^2 \simeq k_y^2$.

Note also that the Alfvén resonance is no longer present in the plasma (i.e. $\omega^2/k_z^2 w_A^2(x_2) - 1 < 0$) when

$$\sin(\pi a_R) \lesssim (2\nu)^{\alpha/\nu}\, \pi(\exp(-\chi_{aw})/G_0 - \exp(-\chi_{ax})\, G_1). \quad (3.72)$$

Because of this limitation on $\sin(\pi a_R)$, the $|\mathrm{Im}(e_R)|$ (as given by (3.71)) cannot be made indefinitely small so that at best only moderately small values of $\tilde{Q}$ are expected.

In the analogous case of body wave heating (e.g. Karney et al., 1979), low $\tilde{Q}$ heating is only expected when the absorption of the body wave, as calculated in Section 3.3, is weak and when the evanescence of the wave fields between x_1 and x_a is small. These conditions are equivalent to the requirement that criterion (3.28) is satisfied (i.e. $S + M^2\omega/\Omega_i \simeq 0.36\ M$).

The main disadvantage with body wave heating arises from the fact that the ratio of the density at the magnetosonic wave turning point (as given by (3.8a) or (3.9a) to the density at the Alfvén resonance is of the order of the maximum of $1 + k_y^2/k_z^2$ and $1 + \omega/\Omega_i$. Because body wave heating requires the presence of the magnetosonic wave turning point in the plasma, the Alfvén resonance occurs at a density significantly lower than the maximum plasma density when the antenna frequency is of the order of the ion-cyclotron frequency. If a density profile of the form shown in Fig. 3.7 is also assumed then the Alfvén resonance occurs close to the plasma edge. Thus, in the frequency range required for minority ion-cyclotron heating, coupling of energy between the antenna and the plasma centre is unlikely if body wave heating is utilized.

3.6 SUMMARY

In this Chapter, the Alfvén resonance damping of a magnetosonic wave has been examined in relation to the Alfvén resonance heating of tokamaks. The finite frequency and density gradient effects have been examined in some detail since they modify both the dispersion and mode coupling of the magnetosonic wave and are relevant in tokamaks like TORTUS and PLT. Finite frequency effects are also important if minority ion-cyclotron heating is utilized.

To estimate the strength of the mode conversion of a magnetosonic wave, the fractional power lost by a body wave on reflection from a density gradient has been determined. The fractional power lost in this case depends primarily on the magnitude of E_x of the incident wave near the Alfvén resonance and, for a constant density gradient, is at a maximum when $|M| \simeq 0.7$. This maximum occurs because, although the magnitude of E_x relative to E_y increases with k_y^2, the total amount of energy reaching the Alfvén resonance is limited by the evanescence of the wave fields between the resonance and the magnetosonic wave turning point which increases with k_y^2.

In the absence of finite ω/Ω_i corrections the absorption depends only on the magnitude of M and not on its sign. The introduction of finite ω/Ω_i terms modifies the polarization and the evanescence of the magnetosonic wave so that for $S + M^2F \lesssim |M|/2$ the energy lost by the magnetosonic wave is enhanced for k_y negative and reduced for k_y positive (assuming $K > 0$). Little absorption occurs when

$$S + M^2F \simeq 0.36\ M.$$

The damping of the magnetosonic surface wave due to mode conversion shows a similar dependence on k_y in that when ω/Ω_i is finite the damping is smaller for k_y positive than for k_y negative. Little damping occurs when

$$k_y > 0$$

$$(\omega/\Omega_i)(1 + k_z^2/k_y^2) \simeq 1.$$

Depending on the antenna configuration either the magnetosonic body wave or the magnetosonic surface wave can be used in the heating of the plasma. However, for a finite poloidal mode number and the Alfvén resonance near the plasma centre, the magnetosonic wave turning point is not present within the plasma and surface wave heating must be utilized. In this case, efficient coupling of energy between the antenna and the plasma centre (i.e. $\tilde{Q} \lesssim 1$) is only possible if

(i) the antenna is far from the conducting wall (i.e. $\bar{k}_{x1}(x_s - x_w) \gtrsim 1$);

(ii) the evanescence of the fields between the antenna and the Alfvén resonance is small (i.e. $\bar{k}_{x1}(x_1 - x_s) \ll 1$, $k_y > 0$ and ω/Ω_i finite);

(iii) the absorption at the Alfvén resonance is weak (i.e. $k_y > 0$, $(\omega/\Omega_i)(1 + k_z^2/k_y^2) \simeq 1$ and the surface wave eigenmode is excited (i.e. if dispersion relation (3.65) is satisfied).

Optimum coupling of energy between the antenna and the plasma interior is expected when $\omega/\Omega_i \simeq 0.5$ and $k_z^2 \simeq k_y^2 (k_y > 0)$. This is because, for these parameters, the Alfvén resonance is close to the plasma centre

and the evanescence of the fields between the antenna and the Alfvén resonance is minimized.

The frequency range required for minority ion-cyclotron heating is consistent with the above criteria. Thus, surface wave heating in a multiple ion-component plasma is expected to yield efficient heating of the ions in the plasma interior without the problems of excess electron heating and plasma surface heating.

Similar results are expected when a body wave eigenmode is excited if its absorption at the Alfven resonance is weak i.e. if $S + M^2F \simeq 0.36\ M$. However, in the frequency range required for minority ion-cyclotron heating, body wave heating requires that the Alfvén resonance occur at a much lower plasma density than in surface wave heating so that the coupling of energy into the ions in the plasma interior is less efficient.

Although the above results were obtained using a planar geometry, similar results are expected to apply in the more complicated geometry of the tokamak (e.g. Karney et al., 1979; Donnelly, 1982) if k_y is replaced by $-\ m/r$ and k_z by n/R where m and n are the poloidal and toroidal mode numbers respectively, R is the major radius of the tokamak and r is the radial distance from the plasma centre (k_y corresponds to $-\ m/r$ as the x and y direction of Fig. 3.7 are oppositely directed to the radial and azimuthal directions).

PART II

ELECTRON CYCLOTRON INSTABILITIES

CHAPTER 4

INTERRELATION BETWEEN THE AZIMUTHAL BUNCHING AND WU AND LEE INSTABILITIES

4.1 INTRODUCTION

4.1.1 The Azimuthal Bunching and Wu and Lee Instabilities

In this Chapter, the interrelation between two similar but seemingly different electron cyclotron instabilities, the azimuthal bunching instability (e.g. Chu and Hirshfield, 1978) and the Wu and Lee instability (e.g. Wu and Lee, 1979), is investigated. These instabilities are similar in that both arise from the relativistic dependence of mass on energy but differ in that the azimuthal bunching instability is driven by an essentially monoenergetic beam of electrons while the Wu and Lee instability is driven by an anisotropic electron distribution with a velocity spread.

The main interest in the azimuthal bunching instability is in the development of the gyrotron (for reviews see Hirshfield and Granatstein, 1977; Sprangle and Drobot, 1977; Flyagin et al., 1977; Chu et al., 1979). In this device, a mildly relativistic beam of electrons, travelling along a magnetic field, interacts with a cavity eigenmode via the azimuthal bunching instability to produce radiation at a frequency near the electron-cyclotron frequency and possibly at its harmonics (e.g. Chu, 1978).

Because the wavelength of the emitted radiation is determined primarily by the electron-cyclotron frequency and hence the strength of the magnetic field, the cavity can be large compared to the wavelength

of the emitted radiation. This feature enables the gyrotron to produce millimetre and submillimetre radiation at a power level superior to conventional devices such as the travelling wave tube and the magnetron where the cavity is of the order of the wavelength of the emitted radiation and hence subject to voltage breakdown. Further, the wavelength of the emitted radiation can be tuned by varying the strength of the magnetic field. The fineness of the tuning is however limited by the spacing of the cavity eigenmodes.

Possible applications for high power gyrotrons include electron-cyclotron resonance heating of tokamak plasmas (Alikaev et al., 1976) and in radar and communications (Chu et al., 1980a). A low power tunable gyrotron is being developed at the University of Sydney as a possible source for spectroscopy and for plasma scattering experiments in the study of wave fluctuations (Brand et al., 1982).

The main interest in the Wu and Lee instability is in the interpretation of certain astrophysical phenomena. These phenomena include Jupiter's decametric radio emission, hereafter called DAM, terrestrial kilometric radiation, hereafter called TKR, and solar spike bursts (e.g. Wu and Lee, 1979; Lee et al., 1980; Holman et al., 1980; Hewitt et al., 1981, 1982; Wu et al., 1982; Melrose et al., 1982; Omidi and Gurnett, 1982; Dusenbery and Lyons, 1982; Melrose and Dulk, 1982; Sharma et al., 1982). In these phenomena, an energetic electron component with a velocity spread produces maser-type emission at frequencies near the electron-cyclotron frequency and perhaps also near its harmonics. However, unlike the gyrotron, a denser cold electron component may influence the dispersion of the emitted radiation.

4.1.2 The Maser Instability

The maser-type emission was first discussed by Twiss (1958), Schneider (1959) and Bekefi et al. (1961). Twiss (1958) used detailed balancing and the Einstein coefficients to treat the emission from relativistic electrons. He showed that negative absorption (i.e. maser-type emission) of gyro radiation by electrons with zero axial momentum can occur if

(A) the energy distribution for the ensemble of electrons, $F(E)$, is such that $\partial F/\partial E$ is positive over a finite range of E and

(B) the transition probability has a maximum at some finite value of E.

Maser-type emission is most favoured when the transition probability is sharply peaked at the value of E at which $\partial F/\partial E$ has a positive maximum. Similar conclusions were obtained by Bekefi et al. (1961) in their study of the radiation temperature of non-Maxwellian distributions for emission perpendicular to the ambient magnetic field.

The emission was treated quantum mechanically by Schneider (1959). He considered an initially monoenergetic distribution of electrons with zero axial velocity in state n with energy ε_n in a uniform magnetic field in the presence of photons of frequency ω. Due to the relativistic dependence of mass on energy, the spacing of the quantized energy levels decreases with increasing energy. In this case, stimulated emission $(n \rightarrow n - 1)$ can be more probable than true absorption if $\hbar\omega > \varepsilon_n - \varepsilon_{n-1} (> \varepsilon_{n+1} - \varepsilon_n)$.

Schneider also pointed out that if instead the electrons have a distribution of energies then stimulated emission can still be more probable than true absorption if there is an overpopulation of higher energy states.

4.1.3 The Bunching Instability

The azimuthal bunching instability was first treated by Gaponov (1959). He considered the trajectories (rather than the energy levels) of monoenergetic electrons interacting with an electromagnetic wave in a static uniform magnetic field. During the interaction with the wave, the relativistic cyclotron frequency decreases for those electrons which gain energy while it increases for those electrons which lose energy. This difference in the cyclotron frequencies of the electrons causes them to bunch in the azimuth. The ultimate phase distribution or azimuthal bunching favours emission over absorption if $\omega - k_z v_z > \Omega_e/\gamma$ where γ is the Lorentz factor and Ω_e is the rest mass electron cyclotron frequency (e.g. Sprangle and Drobot, 1977).

The maser and bunching instabilities are similar in that each depends explicitly on the relativistic variation of the electron mass with energy. Because of this common feature, Gaponov's bunching instability is sometimes called the electron cyclotron maser instability (e.g. Sprangle and Drobot, 1977). However, this nomenclature is misleading: the bunching instability described by Gaponov (1959) is

physically different from the maser-type emission described by Twiss (1958), Schneider (1959) and Bekefi et al. (1961). To avoid confusion with the maser-type emission, the alternate nomenclature of Chu and Hirshfield (1978) is adopted with Gaponov's bunching instability being referred to as the azimuthal bunching instability.

4.1.4 Alternate Descriptions of the Maser and Bunching Instabilities

In the theory of Gaponov (1959), the instability is driven by azimuthal bunching of an essentially monoenergetic beam of electrons. Such an instability corresponds to a reactive-medium instability in the notation of Briggs (1964). In this type of instability, the plasma can be considered to be lossless (i.e. the antihermitian part of the dielectric tensor, $\underset{\approx}{\varepsilon}^{(a)}$, is negligible) and the resulting dispersion equation implies the existence of intrinsically growing waves. These waves can also be considered as negative energy waves where, due to the phase bunching of the electrons, the energy associated with the wave becomes more negative and the wave grows (e.g. Bekefi, 1966, p. 289).

On the other hand, the maser-type emission described by Twiss (1958), Schneider (1959) and Bekefi et al. (1961) corresponds to a resistive-medium instability (Briggs, 1964). In this type of instability, the velocity spread in the distribution gives rise to a finite antihermitian part of the dielectric tensor and the resulting dispersion equation implies negative absorption (rather than dissipation by collisionless damping). This instability is sometimes called the semirelativistic maser cyclotron instability; semirelativistic because the instability can still occur for v^2/c^2 finite but much less than unity (Hewitt et al., 1982). It is also called the Wu and Lee instability

(Wong et al., 1982; Winglee, 1983b). This alternate nomenclature arises from the fact that, although Twiss (1958), Schneider (1959) and Bekefi et al. (1961) were the first to discuss this type of maser emission, their theories were restricted to the cases where either the axial velocity of the electrons is zero or where the radiation is emitted perpendicular to the magnetic field. Both cases correspond to neglecting the Doppler shift in the resonance condition. Wu and Lee (1979) included both the Doppler shift and the relativistic effect explicitly.

Another practical difference between the azimuthal bunching and Wu and Lee instabilities is in the plasma conditions under which they occur. The main interest in the Wu and Lee instability at present is in the understanding of DAM, TKR and solar spike bursts as mentioned in Subsection 4.1.1. In these astrophysical applications, the Wu and Lee instability is usually driven by a low density component of energetic electrons with a denser cold component determining the dispersion of the radiation. In contrast, the main interest in the azimuthal bunching instability is in the development of the gyrotron where any cold plasma and any velocity spread are usually neglected.

The purpose of this Chapter is to present a theory (Winglee, 1983b) which interrelates the Wu and Lee and azimuthal bunching instabilities. It is shown that not only can these instabilities exist in the same plasma but that they are just two different cases of the same instability with the Wu and Lee instability passing over into the azimuthal bunching instability when the effective velocity spread of the suprathermal component is decreased.

Previously, Melrose (1973) studied the interrelation between the reactive- and resistive-medium forms of a similar but nonrelativistic

electron-cyclotron instability. However, the treatment of Melrose (1973) was heuristic. Here, physical models of the resistive- and reactive-medium instabilities are developed.

In order to analyse both the Wu and Lee and azimuthal bunching instabilities simultaneously, it is assumed throughout this Chapter that the wave frequency is approximately equal to the electron-cyclotron frequency and that the mean energy of the suprathermal electron component is such that $\langle v^2 \rangle / c^2$ ($\langle v^2 \rangle := \int d^3\underset{\sim}{v}\, v^2 f$) is finite but much less than unity and $k_\perp^2 \langle v_\perp^2 \rangle / \Omega_e^2 \ll 1$. This parameter range is often valid in the astrophysical and laboratory applications mentioned earlier.

The general properties of the Wu and Lee and azimuthal bunching instabilities, as well as their nonrelativistic counterparts are reviewed in Section 4.2. The dielectric tensor is evaluated in Section 4.3 (and also in Winglee, 1983b) for a plasma in which both the Wu and Lee and azimuthal bunching instabilities can be treated together. Specific characteristics of the Wu and Lee and azimuthal bunching instabilities derived from this dielectric tensor are given in Section 4.4 for the case where the cold electron component is absent. The modification to the growth rates due to a cold electron component is discussed in Section 4.5. In Section 4.6, a physical model interrelating these two instabilities is given and its predictions compared with the results given in the previous Sections. A summary of the results is presented in Section 4.7.

4.2 RESISTIVE- AND REACTIVE-MEDIUM ELECTRON-CYCLOTRON INSTABILITIES

4.2.1 A Simplified Form of the Dielectric Tensor for $\omega \simeq \Omega_e$

The properties of the resistive- and reactive-medium instabilities discussed in the previous Section can be illustrated by considering a simplified form of the dielectric tensor for a plasma at wave frequencies near the electron cyclotron frequency. In this frequency range, the contribution to the dielectric tensor from the plasma ions is negligible. As mentioned previously, it is also assumed that the electron distribution is such that $\langle v^2 \rangle / c^2 \ll 1$ and $k_\perp^2 \langle v_\perp^2 \rangle / \Omega_e^2 \ll 1$.

The full relativistic form of the dielectric tensor is given for example in Baldwin et al. (1969). This form is based on standard linear theory and describes the time asymptotic behaviour of the normal modes of oscillation of the plasma (e.g. Stix, 1962, Ch. 8; Krall and Trivelpiece, 1973, Ch. 8). In the present context it can be approximated by

$$\begin{aligned} \underset{\approx}{\varepsilon} = \underset{\approx}{I} &+ 2\pi \sum_\alpha \frac{\omega_{p\alpha}^2}{\omega^2} \int_{-\infty}^{\infty} dv_z \int_0^{\infty} dv_\perp v_z \left(v_\perp \frac{\partial}{\partial v_z} - v_z \frac{\partial}{\partial v_\perp} \right) f \hat{\underset{\sim}{b}} \hat{\underset{\sim}{b}} \\ &+ 2\pi \sum_\alpha \frac{\omega_{p\alpha}^2}{\omega^2} \int_{-\infty}^{\infty} dv_z \int_0^{\infty} dv_\perp \underset{\approx}{T} \left[(\omega - k_z v_z) \frac{\partial}{\partial v_\perp} + k_z v_\perp \frac{\partial}{\partial v_z} \right] f \end{aligned} \qquad (4.1)$$

where $\underset{\approx}{I}$ is the unit tensor, $\hat{\underset{\sim}{b}}$ is the unit vector in the z direction which is chosen to be parallel to $\underset{\sim}{B}$, $\underset{\approx}{T}$ is as given in Table 4.1, the sum over α is the sum over the various electron components and $\underset{\sim}{k}$ is in the x-z plane.

TABLE 4.1 Elements of $\underset{\approx}{T}$

Element	Expression*
T_{xx}	$-\frac{1}{4} v_\perp^2 \left(\frac{1}{\Delta_1} + \frac{1}{\Delta_{-1}}\right)$
T_{yy}	$T_{xx} - \frac{1}{4} v_\perp^2 \left(\frac{k_\perp v_\perp}{\Omega_e}\right)^2 \frac{1}{\Delta_0}$
$T_{xy}, -T_{yx}$	$i \frac{1}{4} v_\perp^2 \left(\frac{1}{\Delta_1} - \frac{1}{\Delta_{-1}}\right)$
T_{xz}, T_{zx}	$-\frac{1}{4} v_\perp^2 \frac{k_\perp v_z}{\Omega_e} \left(\frac{1}{\Delta_1} - \frac{1}{\Delta_{-1}}\right)$
$T_{yz}, -T_{zy}$	$i \frac{1}{2} v_\perp^2 \frac{k_\perp v_z}{\Omega_e} \left[\frac{1}{\Delta_0} - \frac{1}{2}\left(\frac{1}{\Delta_1} + \frac{1}{\Delta_{-1}}\right)\right]$
T_{zz}	$-\frac{v_z^2}{\Delta_0} - \frac{1}{4} v_\perp^2 \frac{k_\perp^2 v_z^2}{\Omega_e} \left(\frac{1}{\Delta_1} + \frac{1}{\Delta_{-1}}\right)$

* $\Delta_n = n\Omega_e + k_z v_z - \omega \qquad n = 0, -1$

$= \Omega_e/\gamma + k_z v_z - \omega \qquad n = 1$

In the derivation of (4.1), only the contributions to the dielectric tensor from the Bessel functions of order $n = 0, \pm 1$ are retained and these Bessel functions are approximated by their series expansions to first order in their arguments $k_\perp v_\perp/\gamma\Omega_e$ because $k_\perp^2 < v_\perp^2>/\Omega_e^2 << 1$ and $\omega \simeq \Omega_e$. Since $<v^2>/c^2 << 1$, the Lorentz factor $\gamma = (1 - v^2/c^2)^{-1/2}$ is set equal to unity everywhere except in the denominator Δ_1. Wu and Lee (1979) and Lee et al. (1980) pointed out that it is important that a relativistic form of γ be used in Δ_1 since the resulting correction to the electron cyclotron frequency can be of the same order as the frequency mismatch between the Doppler shifted wave frequency and Ω_e in situations where Δ_1 is close to zero. The integrals appearing in (4.1) are evaluated in the standard way using the Landau prescription (e.g. Krall and Trivelpiece, 1973, Ch. 8) i.e.

$$\frac{1}{\omega - \omega_0 + i0} = P\frac{1}{\omega - \omega_0} - i\pi\delta(\omega - \omega_0) \tag{4.2}$$

where P denotes the Cauchy principal value.

4.2.2 Resistive-Medium Electron-Cyclotron Instabilities

For $\omega \simeq \Omega_e >> |k_z|<v_z^2>^{1/2}$, the dominant contribution to the antihermitian part of the dielectric tensor and hence to the growth rate of a resistive-medium instability comes from those electrons which can gyro-resonate with the wave i.e. from those electrons which satisfy the resonance condition

$$\omega - k_z v_z - \Omega_e/\gamma = 0. \tag{4.3}$$

In order to determine when the relativistic correction is important, Hewitt et al. (1981) interpreted the resonance condition (4.3) for given values of ω, Ω_e and k_z as an ellipse in $v_z - v_\perp$ space. They found that in the limit $k_z^2c^2 >> \omega^2$, the resonance ellipse is highly eccentric and the physical portion of the curve can be approximated by the straight line $v_z = (\omega - \Omega_e)/k_z$. This result is equivalent to the non-relativistic resonance condition obtained by setting $\gamma = 1$. In the opposite limit $k_z^2c^2 << \omega^2$, the resonance ellipse is approximately a circle with centre

$$v_z = v_c := k_z c^2/\omega, \qquad v_\perp = 0 \tag{4.4}$$

and radius

$$v_r = c[(k_z c/\omega)^2 - 2(\omega - \Omega_e)/\Omega_e]^{1/2}. \tag{4.5}$$

(A similar curve results from approximating the Lorentz factor in (4.3) by $(1 - v^2/2c^2)^{-1}$.) It should be stressed that since $\omega \simeq \Omega_e$ this resonance circle can lie entirely within regions of $v_z - v_\perp$ space where $v^2/c^2 << 1$ and cannot be approximated by the non-relativistic resonance condition.

The corresponding growth rate arising from these resonant electrons is given approximately by

$$\Gamma = \int d^3\underset{\sim}{v}\, H(\underset{\sim}{k},\underset{\sim}{v})\, \delta(\omega - k_z v_z - \Omega_e/\gamma)\hat{D}f \tag{4.6}$$

where

$$\hat{D}f = \left(\frac{\Omega_e}{v_\perp}\frac{\partial}{\partial v_\perp} + k_z \frac{\partial}{\partial v_z}\right) f \tag{4.7}$$

and H is positive; the actual form of H (which is given in Wu and Lee, 1979; Melrose et al., 1982) is unimportant in the following. In all discussions of the resistive-medium electron-cyclotron instabilities, the electron distribution f is taken to have a finite spread in velocity space. Distributions which have been considered include streaming bi-Maxwellian distributions, Dory, Guest and Harris distributions (Dory et al., 1965) and one or two sided loss-cone distributions (e.g. Melrose, 1976; Wu and Lee, 1979; Lee et al., 1980; Melrose et al., 1982; Omidi and Gurnett, 1982). In most cases, the plasma also has a dense cold background component which determines the dispersive properties of the waves.

Resonant electrons give positive contributions to growth in (4.6) if $\hat{D}f$ is positive and negative contributions if $\hat{D}f$ is negative. However, the two limiting forms of the resonance ellipse imply different conditions for the stability of waves. In particular, when $k_z^2c^2 << \omega^2$ the resonance curve is approximately a circle with the maximum $v_\perp$ along the resonance curve, $v_{\perp max}$, being much less than c. In this case, $|k_z v_\perp| << \Omega_e$ and $\hat{D}f \simeq \frac{\Omega_e}{v_\perp}\frac{\partial f}{\partial v_\perp}$ if $\frac{\partial f}{\partial v_\perp}$ and $\frac{\partial f}{\partial v_z}$ have comparable magnitudes. Thus, if $\frac{\partial f}{\partial v_\perp} > 0$ for $v_\perp \lesssim v_{\perp max}$ then growth occurs. This situation corresponds to the Wu and Lee instability.

On the other hand when $k_z^2c^2 >> \omega^2$ (i.e. when the nonrelativistic resonance condition is valid), the resonance curve is approximately a straight line parallel to the $v_\perp$ axis and lies both in regions where $\frac{\partial f}{\partial v_\perp} < 0$ and where $\frac{\partial f}{\partial v_\perp} > 0$. Since the resonance condition is independent of $v_\perp$, the total contribution to the growth rate from the $\frac{\partial f}{\partial v_\perp}$ term in $\hat{D}f$ can be evaluated by integrating (4.6) by parts. This contribution is always negative for the distributions mentioned above (Hewitt et al.,

1981). Thus, growth can only occur in this case if $k_z \frac{\partial f}{\partial v_z}$ along the resonance ellipse is positive and large enough to overcome the net negative contribution from $\frac{\Omega_e}{v_\perp} \frac{\partial f}{\partial v_\perp}$. This type of instability is sometimes called the nonrelativistic maser cyclotron instability (Hewitt et al., 1982). In general, rather large anisotropies are required before this instability can occur because $|k_z|$ is usually much smaller than $\Omega_e/\langle v_\perp \rangle$ (Melrose 1976; Melrose et al., 1982).

It is also seen from (4.6) that the maximum growth rate for the Wu and Lee instability is obtained when the resonance ellipse samples those regions in velocity space where $\frac{\partial f}{\partial v_\perp}$ is large and positive (Hewitt et al., 1981). Further, because the position of the resonance ellipse is a sensitive function of ω and $\underset{\sim}{k}$, the growth rate and hence the emission are also sensitive functions of ω and $\underset{\sim}{k}$.

4.2.3 Reactive-Medium Electron-Cyclotron Instabilities

The simplest example of this class of instability occurs for waves propagating parallel to the magnetic field in a plasma which only has an energetic electron component (cf. Chu and Hirshfield, 1978). In this case, the dispersion equation (2.3)) reduces to

$$(\varepsilon_{xx} + i\varepsilon_{xy} - n_z^2)(\varepsilon_{xx} - i\varepsilon_{xy} - n_z^2)(\varepsilon_{zz} - n_z^2) = 0 \qquad (4.8)$$

where $n_z^2 = k_z^2 c^2/\omega^2$ and $\underset{\approx}{\varepsilon}$ is given by (4.1).

The mode of interest is described by the factor

$$\varepsilon_{xx} + i\varepsilon_{xy} - k_z^2 c^2/\omega^2 = 0 \qquad (4.9)$$

i.e.

$$\omega^2 - k_z^2c^2 = -\pi\omega_p^2 \int_0^\infty v_\perp^2 dv_\perp \int_{-\infty}^\infty dv_z \frac{[(\omega - k_z v_z)\frac{\partial f}{\partial v_\perp} + k_z v_\perp \frac{\partial f}{\partial v_z}]}{\omega - k_z v_z - \Omega_e/\gamma} \tag{4.10a}$$

$$= 2\pi\omega_p^2 \int_0^\infty v_\perp dv_\perp \int_{-\infty}^\infty dv_z f \left[\frac{\omega - k_z v_z}{\omega - k_z v_z - \Omega_e/\gamma} - \frac{v_\perp^2}{2c^2}\frac{(\omega\Omega_e - k_z^2c^2)}{(\omega - k_z v_z - \Omega_e/\gamma)^2}\right] \tag{4.10b}$$

where ω_p is the plasma frequency. Since $\omega \simeq \Omega_e$ and $\langle v^2\rangle/c^2 << 1$, (4.10) is essentially the dispersion relation given by Chu and Hirshfield (1978; a slight difference arises because all γ's in (4.10), except in the resonant denominator, have been set equal to unity). This mode is right hand polarized i.e. the wave fields rotate in the same sense as an electron gyrates, and is therefore subject to electron-cyclotron bunching instabilities.

In applications involving the reactive-medium instability, the distribution function f is sharply peaked in velocity space. A distribution which is frequently used (e.g. Sprangle and Drobot, 1977; Chu and Hirshfield, 1978; Chu et al., 1979) is the delta function distribution

$$f = \delta(v_\perp - v_{\perp o})\,\delta(v_z)/2\pi v_\perp . \tag{4.11}$$

With this distribution, (4.10b) reduces to

$$\omega^2 - k_z^2c^2 = \omega_p^2\left[\frac{\omega}{\omega - \Omega_e/\gamma} - \frac{v_{\perp o}^2}{2c^2}\frac{(\omega\Omega_e - k_z^2c^2)}{(\omega - \Omega_e/\gamma)^2}\right] . \tag{4.12}$$

In this case, the anti-hermitian part of the dielectric tensor is identically zero because there are no resonant electrons. Less extremely peaked distributions can be approximated by (4.11) when the number of resonant electrons is negligible.

It is seen from (4.12) if $|k_z^2c^2 - \omega^2| \lesssim \omega|\omega - \Omega_e/\gamma|$ then the last term on the right hand side of (4.12) is negligible compared to the first term on the right hand side. In this case the plasma is stable.

On the other hand, instabilities can occur when $|k_z^2c^2 - \omega^2| >> \omega|\omega - \Omega_e/\gamma|$ and $\omega \simeq \Omega_e$. In this case, the solutions to (4.12) are

$$\omega - \Omega_e/\gamma \simeq \frac{1}{2}\,\omega_p \left\{\frac{\omega_p}{\Omega_e} \pm \left(\frac{\omega_p^2}{\Omega_e^2} - \frac{2v_{\perp o}^2}{c^2}\right)^{1/2}\right\} \tag{4.13}$$

for $k_z^2c^2/\omega^2 << 1$ and

$$\omega - \Omega_e/\gamma \simeq -\frac{1}{2}\,\omega_p \left\{\frac{\omega_p \Omega_e}{k_z^2c^2} \pm \left[\left(\frac{\omega_p \Omega_e}{k_z^2c^2}\right)^2 - \frac{2v_{\perp o}^2}{c^2}\right]^{1/2}\right\} \tag{4.14}$$

for $k_z^2c^2/\omega^2 >> 1$. The azimuthal bunching instability is described by (4.13) and occurs when

$$k_z^2c^2 << \omega^2 \tag{4.15a}$$

$$\omega_p^2/\Omega_e^2 < 2v_{\perp o}^2/c^2 \tag{4.15b}$$

while the axial bunching instability as given by (4.14) occurs when

$$k_z^2 c^2 \quad >> \quad \omega^2 \tag{4.16a}$$

$$(\omega_p \Omega_e / k_z^2 c^2)^2 \quad < \quad 2 v_{\perp o}^2 / c^2 . \tag{4.16b}$$

The terms azimuthal and axial are used because the electrons bunch in these directions to produce the corresponding instability (Chu and Hirshfield, 1978).

Note that the condition (4.15a) for the azimuthal bunching instability is the same as that for the Wu and Lee instability while condition (4.16a) for the axial bunch instability is the same as that for the nonrelativistic maser cyclotron instability. Further, the azimuthal bunching instability like the Wu and Lee instability is only present if relativistic effects are included in the evaluation of the resonant denominator $\omega - k_z v_z - \Omega_e/\gamma$. In fact if γ is set equal to unity in (4.10a), the dispersion relation obtained for the delta function distribution is

$$\omega^2 - k_z^2 c^2 \quad = \quad \omega_p^2 \left\{ \frac{\omega}{\omega - \Omega_e} + \frac{v_{\perp o}^2}{2c^2} \frac{k_z^2 c^2}{(\omega - \Omega_e)^2} \right\} . \tag{4.17}$$

The main difference between this equation and (4.12) is that $- k_z^2 c^2$ replaces the factor $\omega\Omega_e - k_z^2 c^2$ in the second term on the right hand side. This correction is not important when $k_z^2 c^2 >> \omega^2$. However, for $k_z^2 c^2 << \omega^2$, (4.17) predicts that the plasma is stable i.e. the azimuthal bunching instability is not present (Chu and Hirshfield, 1978).

For an arbitrary angle of propagation the relevant dispersion relation is essentially the same as (4.12) except that $k_z^2 c^2$ on the left hand side of (4.12) is replaced by $k^2 c^2$ (e.g. Sprangle and Drobot, 1977).

For $k^2c^2 << \omega^2$, the growth rate of the azimuthal bunching instability is still given approximately by (4.13). The azimuthal bunching instability can also occur for $\omega^2 \simeq k^2c^2 \simeq \Omega_e$ if $(\omega_p/\Omega_e)^{1/2} \lesssim k_\perp v_{\perp o}/\Omega_e$; when $(\omega_p/\Omega_e)^{1/2} << k_\perp v_{\perp o}/\Omega_e$, the growth rate is approximately given by $\mathrm{Im}(\omega) = (\sqrt{3}/2)(\omega_p^2 k_\perp^2 v_{\perp o}^2/2kc)^{1/3}$ (Sprangle and Drobot, 1977).

It follows from the above that if condition (4.15b) is satisfied then the azimuthal bunching instability occurs over a large range of $\underset{\sim}{k}$ with its growth rate being an insensitive function of k when $k^2c^2 << \omega^2$. This property is used in later sections to distinguish it from the Wu and Lee instability which occurs only over a narrow range of $\underset{\sim}{k}$.

4.3 EVALUATION OF THE DIELECTRIC TENSOR FOR $\omega \simeq \Omega_e$

To determine the interrelation between the Wu and Lee and azimuthal bunching instabilities, both the hermitian and antihermitian parts of the dielectric tensor (4.1) are now evaluated using the approximation $\gamma \simeq (1 - v^2/2c^2)^{-1}$. In the calculations, it is assumed that the electrons have a cold component and an energetic component with a finite velocity spread.

The energetic component is described by a Dory, Guest and Harris (DGH) distribution of the form (Dory et al., 1965)

$$f = f_\perp(v_\perp)\, f_z(v_z) \tag{4.18}$$

$$f_\perp = (2\pi v_T^2 j!)^{-1} (v_\perp/\sqrt{2}v_T)^{2j} \exp(-v_\perp^2/2v_T^2) \tag{4.19}$$

$$f_z = ((2\pi)^{1/2} v_T)^{-1} \exp(-v_z^2/2v_T^2) \tag{4.20}$$

where j is a positive integer. Related types of distributions have been

used in discussion of the Wu and Lee instability (e.g. Wu and Lee, 1979; Lee et al., 1980; Hewitt et al., 1981). Note that for this distribution

$$\langle v_\perp \rangle := \int d^3\underset{\sim}{v}\, v_\perp f = \sqrt{2} v_T \Gamma(j + 3/2)/\Gamma(j + 1) \tag{4.21a}$$

$$\langle v_\perp^2 \rangle = 2(j + 1)\, v_T^2 \tag{4.21b}$$

$$\langle (v_\perp - \langle v_\perp \rangle)^2 \rangle = 2v_T^2 \left[j + 1 - \left(\Gamma(j + 3/2)/\Gamma(j + 1) \right)^2 \right]. \tag{4.21c}$$

When $j = 0$, (4.19) reduces to a Maxwellian distribution. For $j \neq 0$, the DGH distribution is peaked about $v_z = 0$ and $v_\perp \simeq \langle v_\perp \rangle$. The peak is evident in the contour plot of (4.18) for $j = 5$ as shown in Fig. 4.1. Further, if $j \to \infty$ and $v_T \to 0$ in such a way that $\sqrt{j} v_T$ remains constant then (4.18) reduces to the delta function distribution (4.12) with

$$v_{\perp o} = \langle v_\perp \rangle \tag{4.22}$$

since $\Gamma(j + 3/2)/\Gamma(j + 1) \to \sqrt{j}$ as $j \to \infty$ (Davis, 1970). Thus, the DGH distribution also allows the effect of a non-zero velocity spread on the azimuthal bunching instability to be determined.

Previously it was noted, both experimentally (e.g. Zaytsev et al., 1974) and theoretically (Sprangle and Drobot, 1977; Uhm and Davidson, 1979a,b) that a small but finite energy spread and/or axial momentum spread can have a large stabilizing influence on the azimuthal bunching instability. However, the initial electron distributions considered by Sprangle and Drobot (1977) and Uhm and Davidson (1979a,b) were restricted to a delta function distribution and to a Heaviside step-function distribution respectively, neither of which allow the presence of the Wu and Lee instability nor of cyclotron damping.

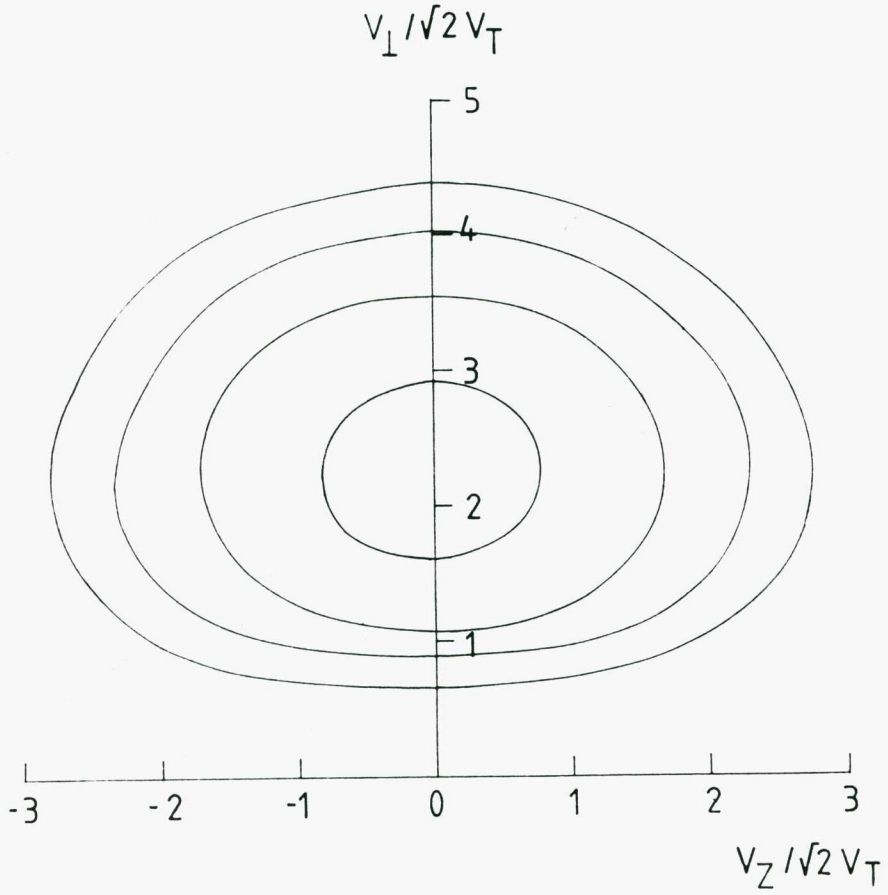

Fig. 4.1 Contour plot of a DGH distribution for j = 5. The distribution is peaked about $v_z = 0$ and $v_\perp \simeq 2.25 \sqrt{2} v_T \simeq \langle v_\perp \rangle$. Successive contour lines indicate decreases by factors of 10.

Tsai et al. (1981) have also determined the dielectric tensor for a plasma with a weakly relativistic energetic electron component. Wu et al. (1981) and Wong et al. (1982) used Tsai et al.'s (1981) results to determine the growth rate of the extraordinary mode for various densities of cold and suprathermal electron components. However, the azimuthal bunching instability was not considered in these studies.

For a plasma consisting of cold and energetic electron components, the general form of the dielectric tensor as given by (4.1) can be decomposed into the following form

$$\underset{\approx}{\varepsilon} = \underset{\approx}{I} + \underset{\approx}{Q}^{c} + \underset{\approx}{Q}^{E} \tag{4.23}$$

where the terms $\underset{\approx}{Q}^{c}$ and $\underset{\approx}{Q}^{E}$ represent the contributions to the dielectric tensor from the cold and suprathermal components respectively. The contribution from the cold electrons is given by (Stix, 1962, p. 10)

$$\underset{\approx}{Q}^{c} = \begin{pmatrix} Q_{\perp}^{c} & Q_{xy}^{c} & 0 \\ -Q_{xy}^{c} & Q_{\perp}^{c} & 0 \\ 0 & 0 & Q_{z}^{c} \end{pmatrix} \tag{4.24}$$

where

$$Q_{\perp}^{c} = -\frac{1}{2}\left(\frac{\omega_{pc}}{\omega}\right)^{2}\left(\frac{\omega}{\omega - \Omega_{e}} + \frac{\omega}{\omega + \Omega_{e}}\right) \tag{4.25}$$

$$Q_{xy}^{c} = i\,\frac{1}{2}\left(\frac{\omega_{pc}}{\omega}\right)^{2}\left(\frac{\omega}{\omega - \Omega_{e}} - \frac{\omega}{\omega + \Omega_{e}}\right) \tag{4.26}$$

$$Q_{z}^{c} = -\left(\frac{\omega_{pc}}{\omega}\right)^{2} \tag{4.27}$$

and $\omega_{pc} = (4\pi e^{2} n_{c}/m_{e})^{1/2}$ is the "cold" plasma frequency.

The contribution from the energetic electron component is more complicated as it contains integrals of the form (via (4.1) and Table 4.1)

$$I_{m,n} = \pi \int_{-\infty}^{\infty} dv_z \int_0^{\infty} dv_\perp \frac{v_\perp^2}{\Delta_n} \left(\frac{k_\perp v_z}{\Omega_e}\right)^m \left[(\omega - k_z v_z) \frac{\partial}{\partial v_\perp} + k_z v_\perp \frac{\partial}{\partial v_z}\right] f \tag{4.28}$$

where m = 0, 1 or 2 and Δ_n is as defined at the foot of Table 4.1. The integrals with n = 0, -1 can be calculated using the nonrelativistic theory of Stix (1962, Ch. 8). The integrals with n = 1 are calculated in Appendix B and the resultant form for $\underset{\approx}{Q}^E$ is given in Table 4.2. In this Table, ω_{pe} is the plasma frequency of the energetic electron component,

$$B_{m,j} = (i\sqrt{2}\, k_z v_T)^{-1} (k_\perp/\Omega_e)^m (\omega F_{m,-1} + jk_z F_{m+1,-1}) \tag{4.29}$$

$$I_{m,1} = \frac{c^2}{v_T^2} \left(\frac{k_\perp}{\Omega_e}\right)^m \left\{\frac{\omega}{\Omega_e} \left((j+1)\, Je_{j+2,m} - j\, Je_{j+1,m}\right) + \frac{k_z}{\Omega_e} j\, Je_{j+1,m+1}\right\} \tag{4.30}$$

$$F_{p,s} = F_p(\alpha_s) = -\frac{i(\sqrt{2}v_T)^p}{\pi^{1/2}} \int_{-\infty}^{\infty} \frac{z^p\, e^{-z^2}}{z - \alpha_s} dz \tag{4.31}$$

and $\alpha_s = \dfrac{\omega - s\Omega_e}{\sqrt{2}k_z v_T}$. The properties of F_p are given by Stix (1962, p. 179). The function $Je_{n,m}$ is described in Appendix B and is related to F_0 through the functions

$$F_{0\pm} = P \int_{-\infty}^{\infty} \frac{e^{-z^2}}{z - \alpha_\pm} dz \mp \pi^{1/2} \exp(-\alpha_\pm^2) \tag{4.32}$$

where

Table 4.2 Elements of $\underset{\approx}{Q}^E$

Element	Expression
Q^E_{xx}	$-\frac{1}{2}(\omega_{pE}/\omega)^2\ (I_{0,1} + B_{0,j})$
Q^E_{yy}	$Q^E_{xx} + (\omega_{pE} k_\perp v_T/\omega\Omega_e)^2\ (j+1)[i(j+2)(\omega/\sqrt{2}k_z v_T)\ F_{0,0} + j]$
Q^E_{zz}	$(\omega_{pE}/k_z v_T)^2(1 + i(\omega/\sqrt{2}k_z v_T)\ F_{0,0}) - \frac{1}{2}(\omega_{pE}/\omega)^2(I_{2,1} + B_{2,j})$
Q^E_{xy}, $-Q^E_{yx}$	$i\ \frac{1}{2}(\omega_{pE}/\omega)^2\ (I_{0,1} - B_{0,j})$
Q^E_{xz}, Q^E_{zx}	$-\frac{1}{2}(\omega_{pE}/\omega)^2\ (I_{1,1} - B_{1,j})$
Q^E_{yz}, $-Q^E_{zy}$	$-i(\omega_{pE}/\omega)^2[(j+1)(k_\perp\omega/k_z\Omega_e)(1 + i(\omega/\sqrt{2}k_z v_T)\ F_{0,0}) + \frac{1}{2}\ (I_{1,1} + B_{1,j})]$

$$\alpha_{\pm} = (k_z c^2/\Omega_e \pm u_e)/(\sqrt{2}v_T) \tag{4.33}$$

$$u_e = c((k_z c/\Omega_e)^2 - 2(\omega - \Omega_e)/\Omega_e)^{1/2}. \tag{4.34}$$

The functions $F_{0\pm}$ have been defined according to the Landau prescription i.e. the contour for F_{0-} has been taken below the pole α_- while for F_{0+} it has been taken above the pole α_+.

Numerical solutions to the dispersion equation ((2.3)) using the above dielectric tensor are presented in the following two Sections (Winglee, 1983b). The numerical solutions were obtained using a complex root finding subroutine developed by Botten et al. (1981). Emphasis is placed on the dispersion and growth rate of the extraordinary mode in a plasma in which $\omega_p^2 = \omega_{pc}^2 + \omega_{pE}^2 << \Omega_e^2$ because, for these parameters, the extraordinary mode, being right hand elliptically polarized, is subject to both relativistic instabilities (Section 4.2).

4.4 GROWTH RATES FOR $\omega_{pc} = 0$

The effect of a velocity spread in the electron distribution on the growth rate and dispersion of the extraordinary mode (hereafter called x mode) is examined in this Section for the case where there is no cold electron component i.e. $\omega_{pc} = 0$. The modification to the growth rate and dispersion due to a cold electron component is discussed in Section 4.5.

Consider first the case in which the x mode propagates parallel to the magnetic field and the electrons have the delta-function distribution given by (4.11). In this case, the dispersion relation for the x mode is given by (4.12).

Solutions to (4.12) are shown in Fig. 4.2. It is seen that the x mode has three branches; an upper, a middle and a lower branch with the upper and lower branches being separated by a stop band in frequency. For $\omega \simeq \Omega_e$, the branches are as described by (4.13) and (4.14) with the upper and lower branches given by the plus solutions in (4.13) and (4.14) and the middle branch by the minus solutions. For $\omega_p/\Omega_e >> v_{\perp o}/c$ (Fig. 4.2a) the three branches are stable with the upper and lower branches well approximated by "cold" plasma theory (i.e. $v_{\perp o} = 0$). The middle branch is due to a finite $v_{\perp o}$ and represents an approximately non-propagating "wave" arising from the cyclotron motion of the electrons.

However, for $\sqrt{2}v_{\perp o}/c \gtrsim \omega_p/\Omega_e$, the azimuthal and axial bunching instabilities can occur; an example is shown in Fig. 4.2b. The azimuthal bunching instability occurs for $\mathrm{Re}(\omega) = \omega_r > |k_z|c$ with the upper and middle branches corresponding to complex conjugate solutions; the axial bunching instability occurs for $\omega_r < |k_z|c$ with the lower and middle branches corresponding to complex conjuguate solutions. Note that these instabilities are characterized by an almost constant growth rate over a large range of k_z.

Suppose instead that the electrons have a DGH distribution with a small value of j (see (4.18)) rather than a delta function distribution ($j \to \infty$). In this case the solutions of the dispersion relation are always complex because the velocity spread and hence the antihermitian part of the dielectric tensor are non-zero. The real parts of the solutions to the dispersion equation are shown in Fig. 4.3 for a distribution with similar mean electron energy (i.e. $\langle v^2 \rangle$) and similar ω_p/Ω_e to those in Fig. 4.2. The upper and lower branches in

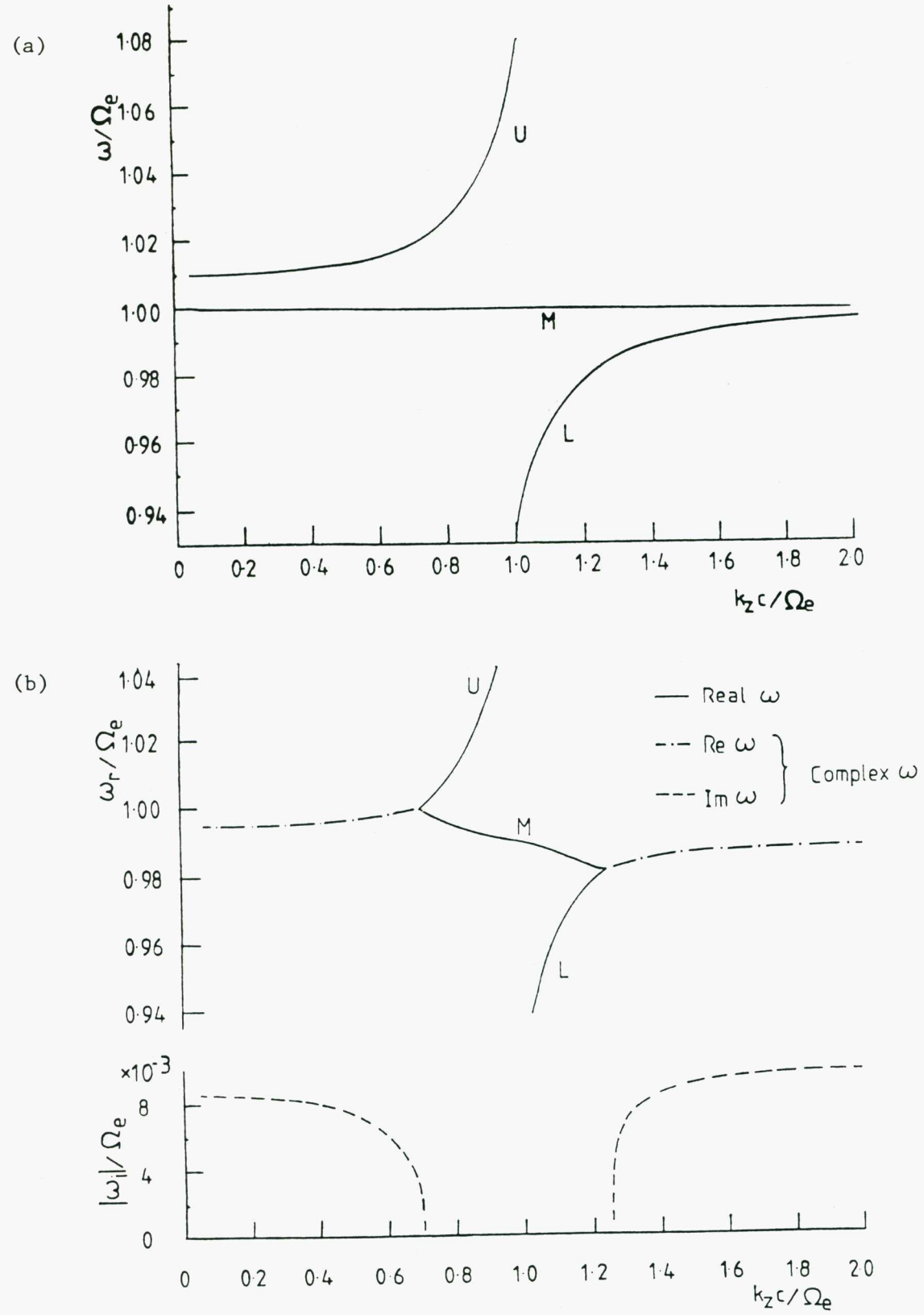

Fig. 4.2 Dispersion relation of the x mode for $\underset{\sim}{k} \parallel \underset{\sim}{B}$, $\omega_p/\Omega_e = 0.1$ and for a delta function distribution with (a) $v_{\perp o}/c = 0.\tilde{0}141$ and (b) $v_{\perp o}/c = 0.141$. In (a) the three branches, the upper (U), the middle (M) and the lower (L) branches, are distinct. In (b) the upper and middle branches are complex conjugates for $k_z c/\Omega_e \lesssim 0.7$ with the growing solution representing the azimuthal bunching instability; for $k_z c/\Omega_e \gtrsim 1.25$ the lower and middle branches are complex conjugates with growth due to the axial bunching instability.

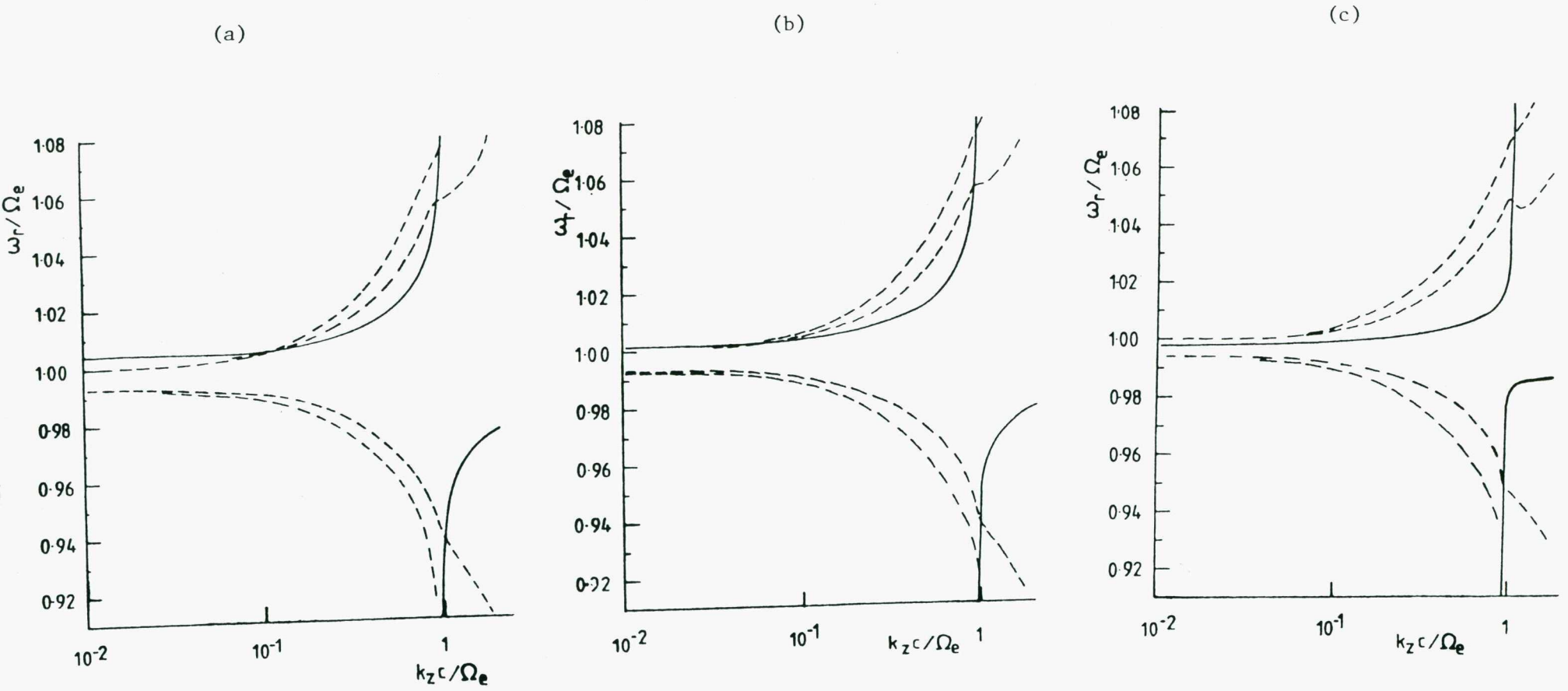

Fig. 4.3. Dispersion relation of the x mode for $\underset{\sim}{k} \| \underset{\sim}{B}$ and for a DGH distribution with j = 5, $v_T/c = 0.02$ and ω_p/Ω_e equal to (a) 0.1, (b) 0.09 and (c) 0.025. The upper and lower branches (solid lines) are topologically the same as in Fig. 4.2. The middle branch of Fig. 4.2 is now replaced by a series of Landau modes (dashed lines); the damping of these modes increases with $|\omega - \Omega_e|$. Only the least damped branches are shown.

Fig. 4.3 have the same form as those in Fig. 4.2 with the width of the stopband decreasing with ω_p/Ω_e. However, the middle branch is replaced by a series of Landau modes (Derfler and Simonen, 1969) of which only the least damped modes are shown. The Landau modes are always damped with their damping rates being faster than that of either the upper or lower branches.

Fig. 4.4a shows the damping of the upper branch for the same distribution as in Fig. 4.3 and for a range of values of ω_p/Ω_e. For some values of $k_z c/\Omega_e$ growth occurs rather than damping; in this case, the imaginary part of the solution is shown in Fig. 4.4b. For $\omega_p/\Omega_e = 0.1$, the upper mode is damped for $k_z c/\Omega_e \gtrsim 0.25$ and for $k_z c/\Omega_e \lesssim 0.1$ and growing for $0.1 \lesssim k_z c/\Omega_e \lesssim 0.25$. The rapid variation with k_z indicates that growth is due to the Wu and Lee instability. For the smaller values of ω_p/Ω_e shown, growth occurs for $k_z c/\Omega_e$ less than certain critical values. Except for $\omega_p/\Omega_e = 0.09$ and $\omega_p/\Omega_e = 0.022$ the growth rates rise rapidly and then remain essentially constant as $k_z c/\Omega_e$ decreases; in these cases growth is due to the azimuthal bunching instability. The case $\omega_p/\Omega_e = 0.09$ is an example of a transition between the Wu and Lee and azimuthal bunching instabilities.

When $\omega_p/\Omega_e \simeq v_T/c$, the azimuthal bunching instability is suppressed at low values of $k_z c/\Omega_e$, by the spread in velocities. This occurs for example when $\omega_p/\Omega_e = 0.022$ in Fig. 4.4b. This suppression is due to a reduction of the phase synchronism between the gyrating electrons and the wave when the average of the frequency mismatch is of the order of its variation over the distribution i.e. when $\langle\Delta\rangle^2 \simeq \langle(\Delta - \langle\Delta\rangle)^2\rangle$ where for ease of notation $\Delta = \Delta_1 = \Omega_e/\gamma + k_z v_z - \omega$.

(a)

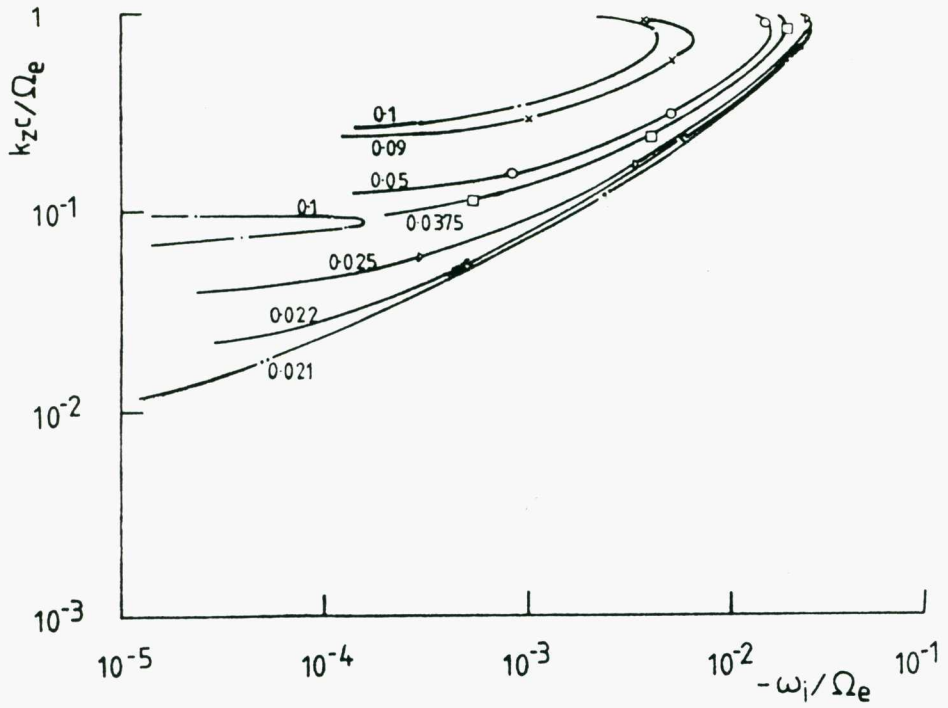

(b)

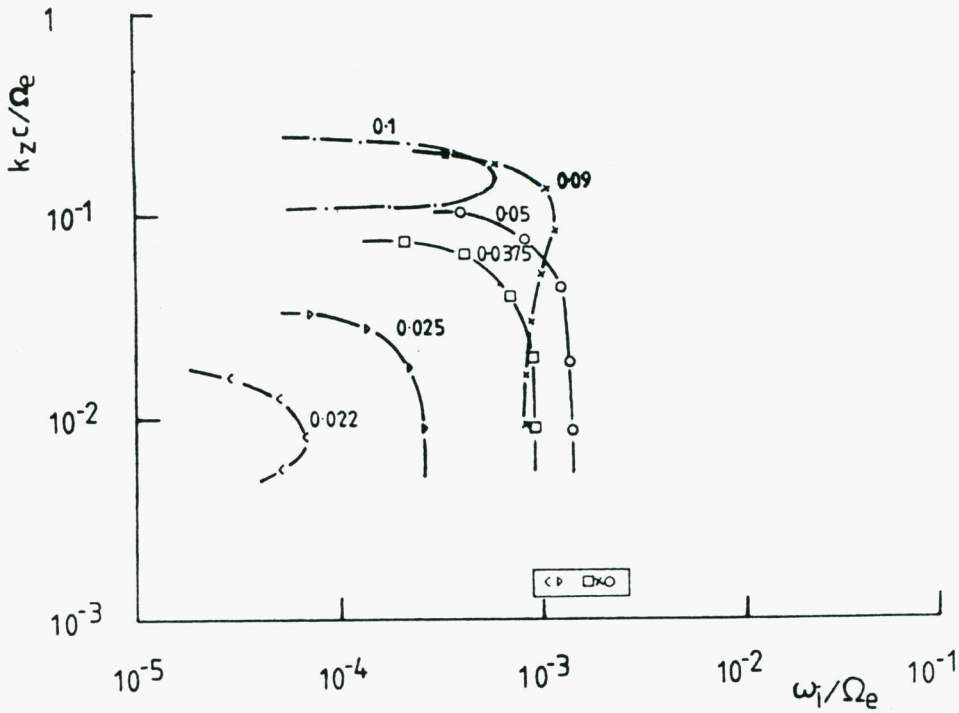

Fig. 4.4 Wave-number vs Im (frequency) diagram for the upper branch of the x mode for $\underset{\sim}{k} \| \underset{\sim}{B}$ and for a DGH distribution with j = 5, $v_T/c = 0.02$ with the given values of ω_p/Ω_e. (a) shows the damping rates $\omega_i < 0$ and (b) shows the growth rates $\omega_i > 0$. The Wu and Lee instability occurs in (b) when $0.1 < k_z c/\Omega_e \lesssim 0.3$ and the azimuthal bunching instability occurs when $k_z c/\Omega_e < 0.1$.

The axial bunching instability does not occur (i.e. the lower branch is stable) for the parameters considered in Figs. 4.3 and 4.4 because the velocity spread acting through the Doppler shift produces large variations in Δ when $k_z^2c^2 >> \omega_r^2$ and thereby prevents net phase bunching.

Fig. 4.5 shows the variation of the growth rate for the azimuthal bunching instability as a function of j when ω_p/Ω_e and $\langle v_\perp^2 \rangle$ are held constant at values 0.025 and 0.0048 respectively. As j increases and the velocity spread decreases, the growth rate approaches the result for a delta function distribution with the same $\langle v_\perp^2 \rangle$ indicated by the dashed line; the plasma is stable to the azimuthal bunching instability for $0 \leq j \leq 3$. Also evident in Fig. 4.5 is the suppression of the instability at the larger values of $k_z^2c^2/\Omega_e^2$ due to the velocity spread.

As ω_p/Ω_e is reduced below v_T/c, the difference between the electron cyclotron frequency and the wave frequency becomes much smaller than the variation of the frequency mismatch over the distribution when $n^2 \simeq 1$. In this case, the phase synchronism between the wave and the electrons is destroyed and the upper and lower branches reconnect so that the stopband vanishes. This is shown in Fig. 4.6 for two values of j, i.e. j = 0 (Fig. 4.6a) and j = 5 (Fig. 4.6b). In each case the reconnection of the upper and lower branches occurs when $\omega_p/\Omega_e \lesssim 0.01$.

Fig. 4.7 shows the damping and growth rates for the upper branch of the x mode for j = 5, $\omega_p/\Omega_e = 0.025$, $v_T/c = 0.02$ and for various angles of propagation with respect to the magnetic field. The growth rates are essentially independent of $k_\perp$, i.e. there is no strongly favoured direction of emission for the azimuthal bunching instability. This is because, for $\omega \simeq \Omega_e$ and $k^2c^2/\Omega_e^2 << 1$, the growth rate is

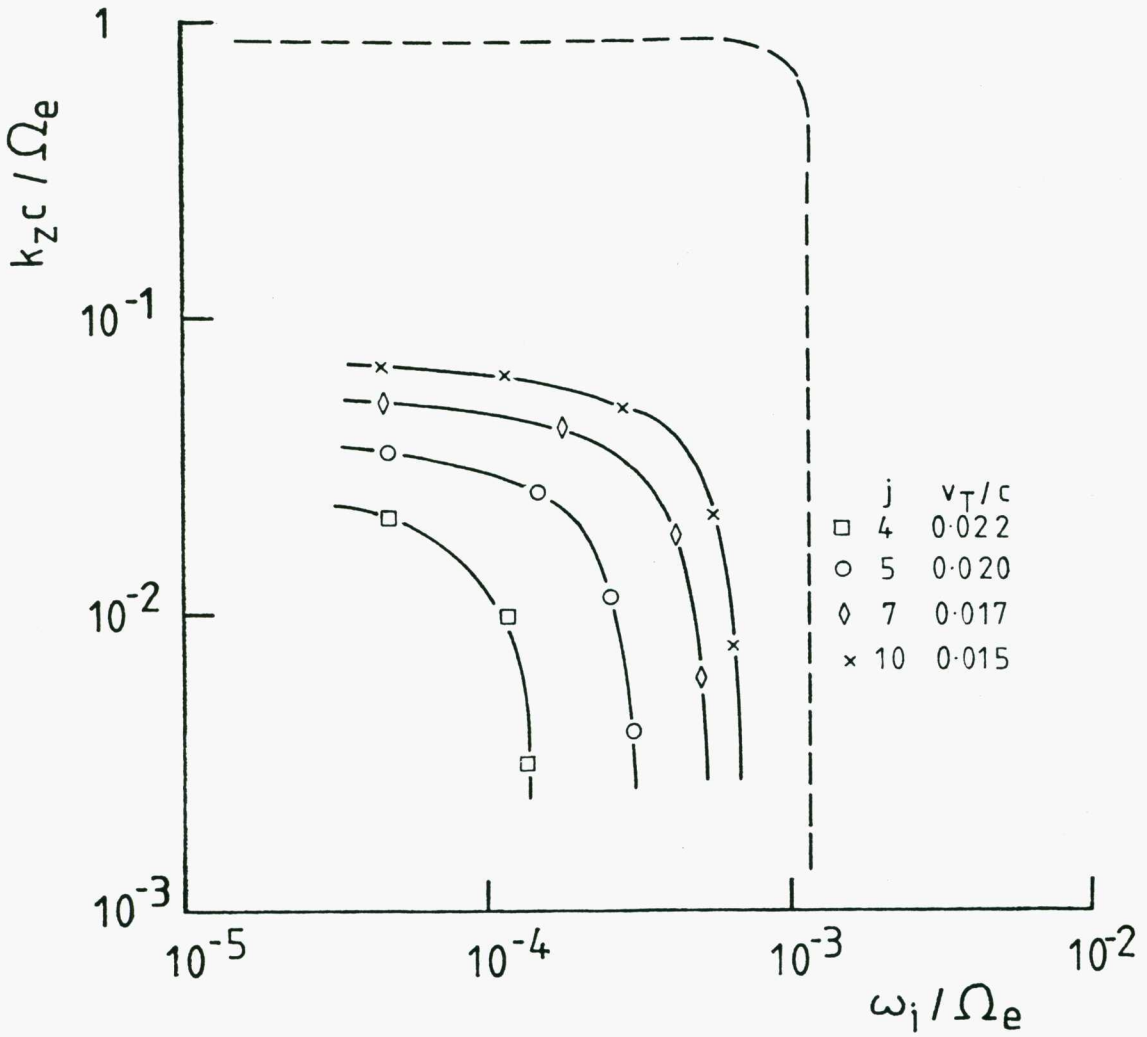

Fig. 4.5 Wave-number vs Im (frequency) diagram for the upper branch of the x mode, $\underset{\approx}{k} \| B$, $\omega_i > 0$, $\omega_p/\Omega_e = 0.025$ and for the values of j and v_T shown. The parameters j and v_T have been chosen so that the value of $\langle v_\perp^2 \rangle$ remains constant at 0.0048. The dashed line gives the result for a delta function distribution with the same ω_p/Ω_e and $\langle v_\perp^2 \rangle$. The growth rate for the DGH distribution approaches that for the delta function distribution as v_T decreases and j increases.

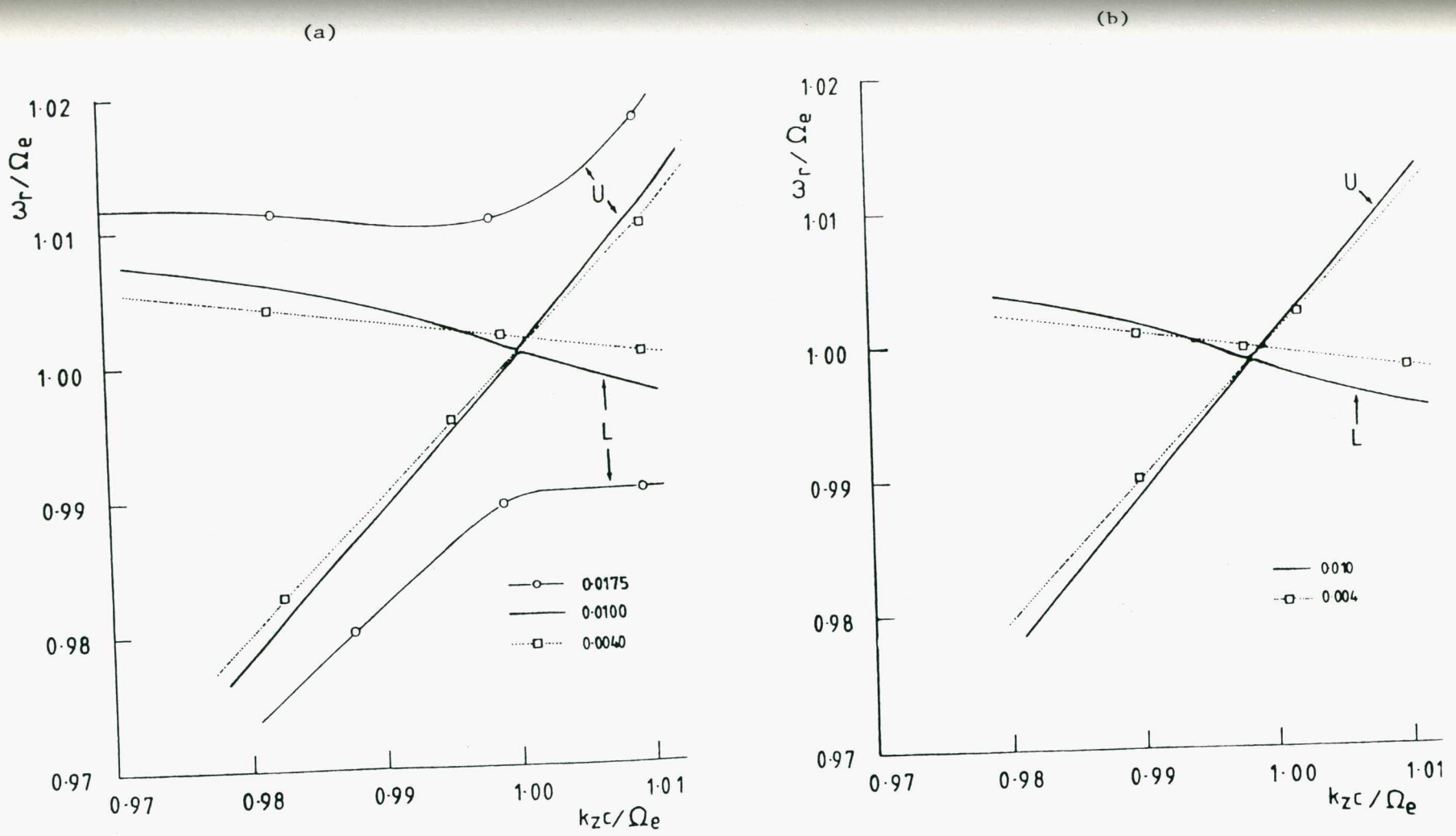

Fig. 4.6 The dispersion relation of the x mode for $\underset{\sim}{k} \| \underset{\sim}{B}$, $v_T/c = 0.02$ and (a) j = 0, (b) j = 5 and for the given values of ω_p/Ω_e. The upper (U) and lower (L) reconnect at $\omega_p/\Omega_e \simeq 0.01$ for both values of j.

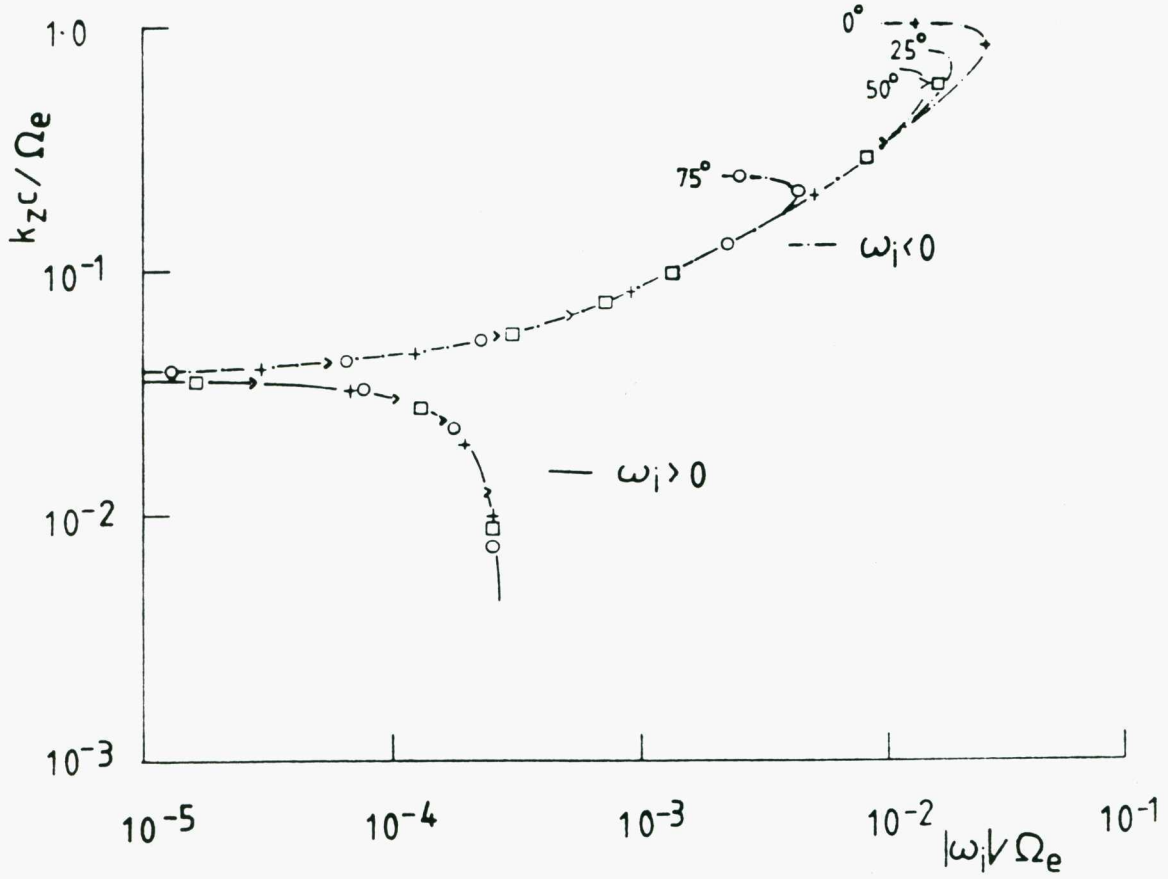

Fig. 4.7 Wave number vs Im (frequency) diagram for the upper branch of the x mode for j = 5, $\omega_p/\Omega_e = 0.025$, $v_T/c = 0.02$ and for an angle of propagation with respect to the magnetic field of i) 0^o (+), ii) 25^o (□), iii) 50^o (>) and iv) 75^o (o). The growth rate of the azimuthal bunching instability, i.e. $k_z c/\Omega_e < 0.04$, is an insensitive function of the angle of propagation.

independent of k^2 (cf. Section 4.2.2) except through its dependence on the spread of Δ over the distribution which is a function of k_z and not $k_\perp$.

The Wu and Lee instability also occurs for the plasma of Fig. 4.7 when $kc/\Omega_e \simeq 1$ and $k_z c/\Omega_e << 1$. However, its bandwidth is too small to be shown in Fig. 4.7 and a discussion of its features is left to the following Section.

4.5 GROWTH RATES FOR A NON-ZERO ω_{pc}

The properties of the x mode in a plasma with cold and energetic electron components are now examined. The situation considered here is similar to that studied by Wu and Lee (1979), Lee et al. (1980) and Hewitt et al. (1982) except that the results are not restricted to the case where $\omega_{pE}/\omega_{pc} << 1$.

The effect of the cold electron component on the dispersion relation of the x mode is shown in Fig. 4.8 for six values of ω_{pc}/Ω_e and for the same energetic component used in Fig. 4.3c. To avoid confusion only the four least damped branches appear. The upper (U) and lower (L) branches, indicated by solid lines, are separated by a stopband as in the case $\omega_{pc}/\Omega_e = 0$ (see Figs. 4.2a, 4.3c). The lower middle (LM) branch, indicated by dashed lines, is also present in Fig. 4.3c as a Landau mode. The upper middle (UM) branch, also indicated by dashed lines, is the analogue of the middle branch of Fig. 4.2a (i.e. when the electrons have an energetic delta function distribution).

In the regime $kc/\Omega_e \lesssim 0.9$, the dispersive properties of the portions of the branches with $\omega_r > \Omega_e$ are determined by the cold electron

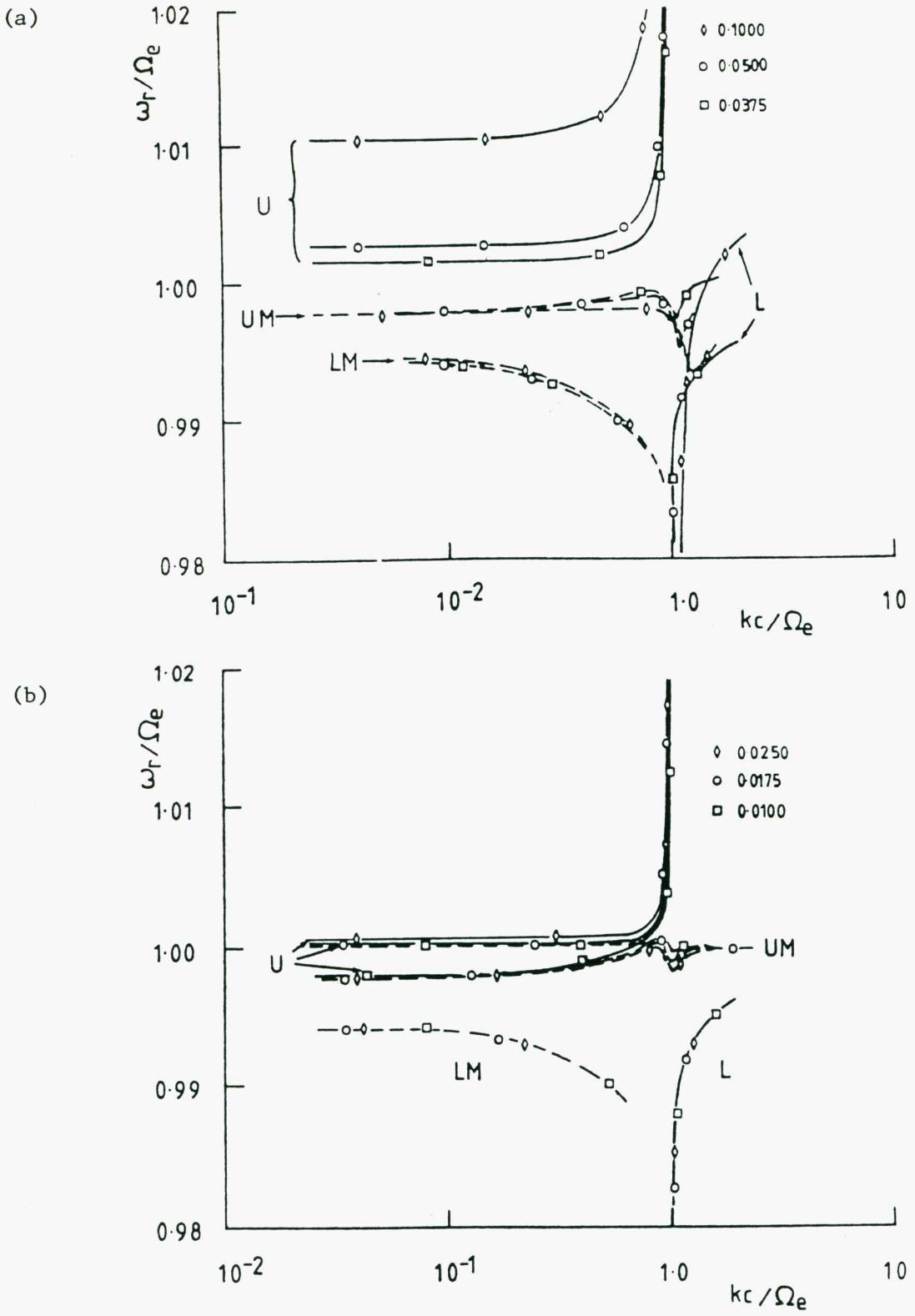

Fig. 4.8 The dispersion relation of the x mode for an angle of propagation of 75°, j = 5, ω_{pE}/Ω_e = 0.025, v_T/c = 0.02 and for the given values of ω_{pc}/Ω_e. The upper (U, solid curve), upper middle (UM, dashed curve) and lower (L, solid curve) are respectively topologically similar to the upper, middle and lower branches of Fig. 4.2a. The lower middle branch (LM) corresponds to the Landau branch of Fig. 4.3c. For $kc/\Omega_e \lesssim 0.9$, the dispersive properties of the portions of the branches $\omega_r > \Omega_e$ are determined by the cold electron component while those portions with $\omega_r < \Omega_e$ are determined by the energetic component. The upper and upper middle branches reconnect at $\omega_{pc}/\Omega_e \simeq 0.0175$.

component while those portions with $\omega_r < \Omega_e$ are determined by the energetic component. Note that for the lowest value of ω_{pc}/Ω_e, i.e. 0.01, the upper branch lies below the upper middle branch when $kc/\Omega_e \lesssim 0.9$. For the higher values of ω_{pc}/Ω_e shown, the converse is true with the two branches reconnecting when $kc/\Omega_e \simeq 1$ and $\omega_{pc}/\Omega_e \simeq 0.0175$. This reconnection is important because in some astrophysical and laboratory applications where the plasma density gradient is small, radiation can escape only if it is generated above its cutoff i.e. on the upper branch.

For the distributions considered here, instabilities occur only in the upper and upper-middle branches. The growth rates for these instabilities are shown in Figs. 4.9 and 4.10 for the same energetic component as in Fig. 4.8 and for the indicated values of ω_{pc}/Ω_e. The Wu and Lee instability (again indicated by a sharply peaked growth rate) occurs on both the upper and upper-middle branches in two regions, $0.1 < kc/\Omega_e \lesssim 0.8$ (Fig. 4.9) and $kc/\Omega_e \simeq 1$ (Fig. 4.10). The latter is shown separately as its bandwidth is too narrow to be included in Fig. 4.9. The bandwidth for $kc/\Omega_e \simeq 1$ is very narrow because ω_r and hence the position of the resonance ellipse depend sensitively on $\underset{\sim}{k}$. For the given values of ω_{pc}/Ω_e, the Wu and Lee instability is always present on the upper branch in at least one of these regions of k space.

On the other hand, the azimuthal bunching instability occurs on the upper branch only if $\omega_{pc}/\Omega_e \lesssim 0.01$ and on the upper middle branch if $0.0175 \lesssim \omega_{pc}/\Omega_e \lesssim 0.025$. Note also that its growth rate decreases with increasing overall plasma electron density in a similar fashion to that described by (4.14) and (4.16).

(a)

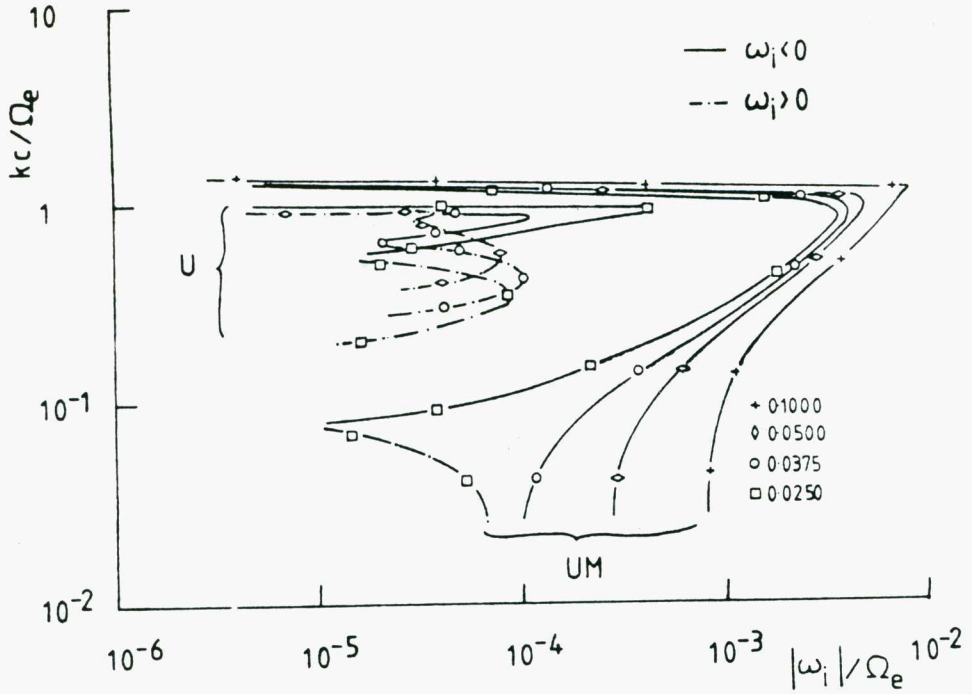

(b)

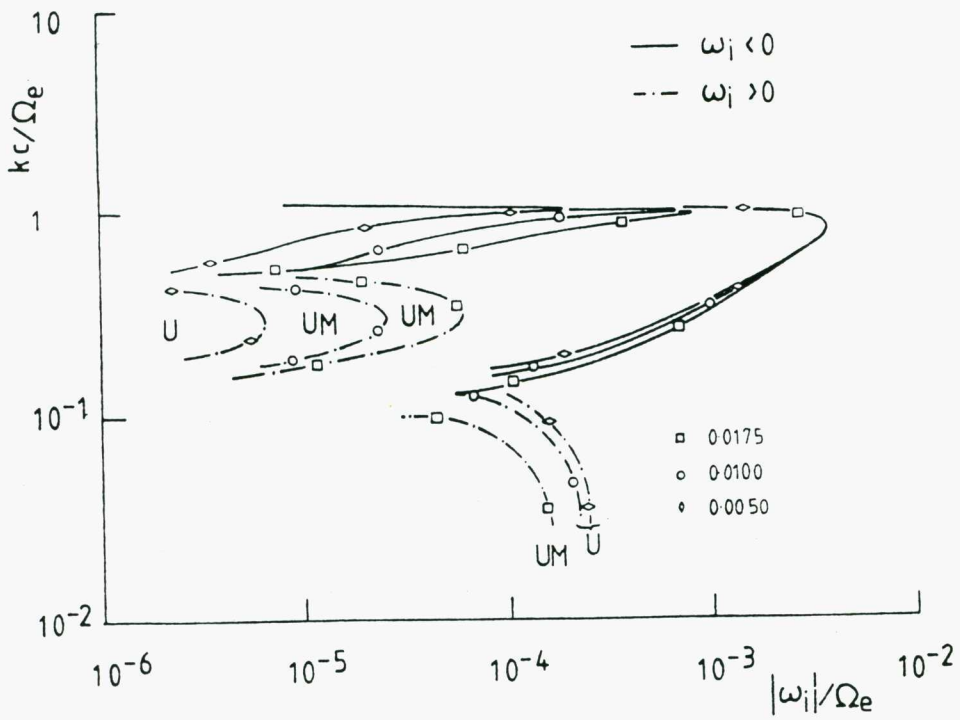

Fig. 4.9 Wavenumber vs Im (frequency) for the upper (U) and upper middle (UM) branches of the x mode for an angle of propagation of 75° to the magnetic field, j = 5, v_T/c = 0.02, ω_{pE}/Ω_e = 0.025 and for the given values of ω_{pc}/Ω_e. The azimuthal bunching instability occurs only on the upper branch for $\omega_{pc}/\Omega_e \lesssim 0.01$ and for $kc/\Omega_e \lesssim 0.1$. The Wu and Lee instability occurs between $0.1 \lesssim kc/\Omega_e \lesssim 1$ and for a small bandwidth about $kc/\Omega_e = 1$ (for clarity this latter region is shown in Fig. 4.10). In at least one of these regions, the Wu and Le instability occurs on the upper branch.

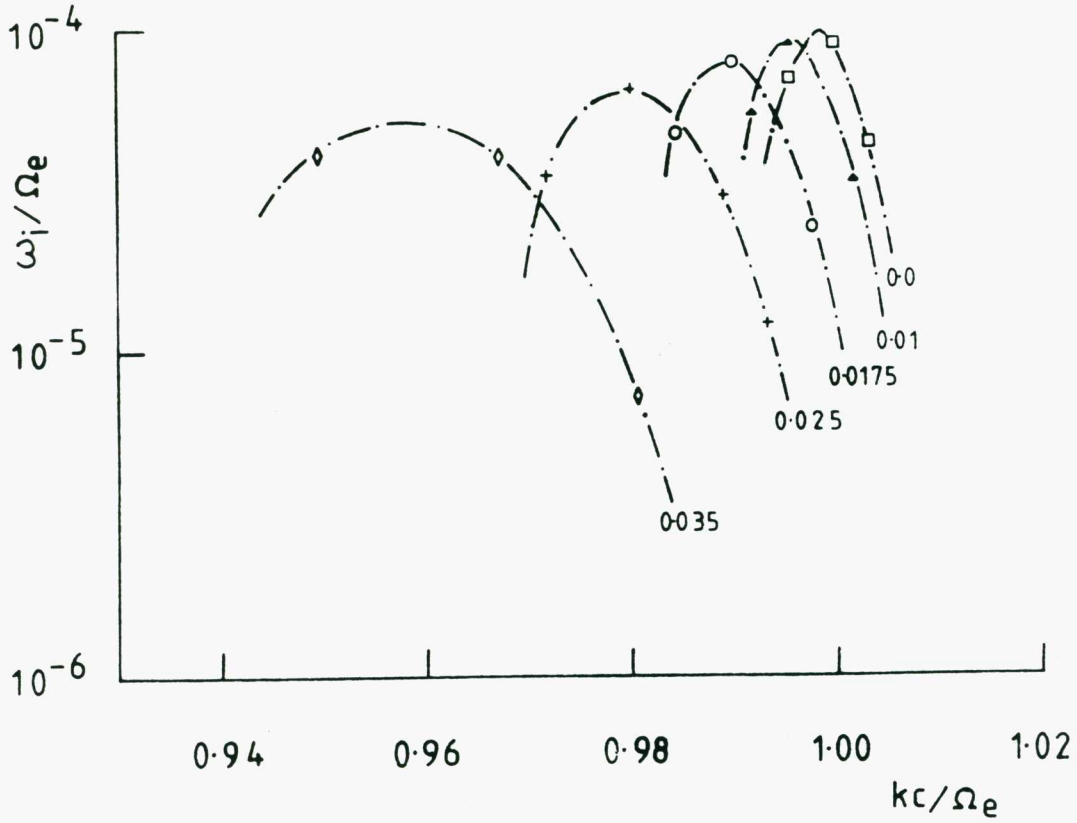

Fig. 4.10 Im (frequency) vs wavenumber diagram for the upper branch of the x mode for an angle of propagation of 75^{o} to the magnetic field, j = 5, $v_T/c = 0.02$, $\omega_{pE}/\Omega_e = 0.025$ and for the given values of ω_{pc}/Ω_e.

In Fig. 4.11, the solid curves show the growth rate of the Wu and Lee instability as a function of frequency for various propagation angles. The points near these curves were calculated by Hewitt (1981) using the method described in Hewitt et al. (1982). In their calculations, the hermitian part of the dielectric tensor was determined by the cold electron component and the antihermitian part (which was evaluated numerically in the fully relativistic limit) by the energetic component. Agreement between the two calculations is good except for very small growth rates where discrepancies arise from errors associated with the numerical techniques used in the non-analytic code and the use of the approximation $\gamma \simeq (1 - v^2/2c^2)^{-1}$ in the present work. Both these calculations confirm the result that the radiation with the largest growth rate from the Wu and Lee instability is emitted almost perpendicularly to the magnetic field.

4.6 THE PHYSICAL MECHANISM

To clarify the nature of the physical mechanisms driving these instabilities, the dispersion equation is rederived here using the equation of motion of an electron in the presence of the wave fields. In this way, the growth rates and the electron trajectories can then be determined self-consistently.

4.6.1 Electron Trajectories

For simplicity, the cold electron component is neglected and the wave is assumed to be in the x mode propagating parallel to the ambient magnetic field B_0 which is again assumed to be in the z direction.

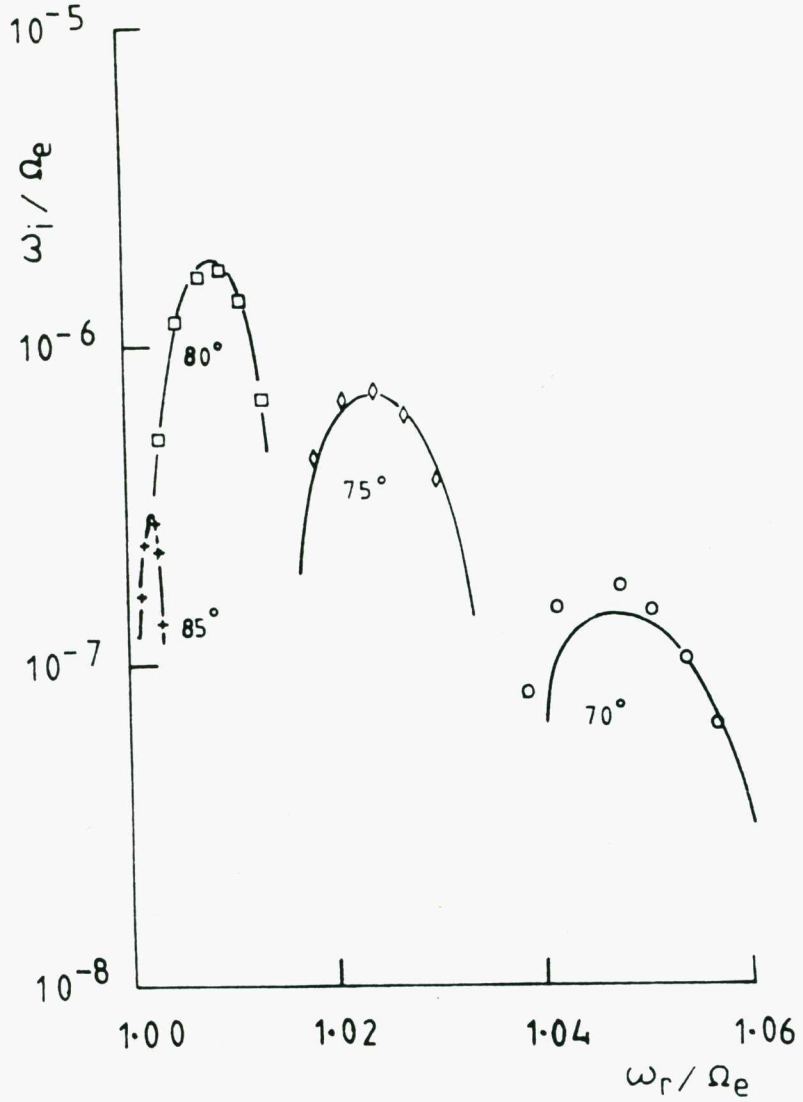

Fig. 4.11 Im (frequency) vs Real (frequency) for the upper branch of the x mode for j = 1, v_T/c = 0.1, ω_{pE}/Ω_e = 0.001, ω_{pc}/Ω_e = 0.01 and for the given angles of propagation relative to the magnetic field. The single points were obtained by Hewitt (1981) and the solid curves from the solution of the dispersion equation using (4.24). The largest growth rate occurs for an angle of propagation of about 80^o.

In this case, the wave is right hand circularly polarized with an electric field (in a Cartesian frame) of the form

$$\begin{aligned} \underset{\sim}{E} &= (E\cos\Psi, -E\sin\Psi, 0) \\ E &= E^0 \exp \int_0^t \omega_i dt \\ \Psi &= k_z z - \int_0^t \omega_r dt, \qquad t > 0. \end{aligned} \tag{4.35}$$

In this and subsequent equations, the initial values of quantities (i.e. those at t = 0) are denoted by a superscript zero. Note that the real and imaginary parts of ω (i.e. ω_r and ω_i) are each allowed to have a "slow" time dependence so that the evolution of the wave fields and the electron distribution can be determined self-consistently.

The equation of motion for an electron interacting with the wave can be written in terms of the polar coordinates v_z, $v_\perp$ and θ where θ, the angle between $-\underset{\sim}{E}$ and $\underset{\sim}{v}_\perp$, is given by

$$\theta = \Psi + \Phi \tag{4.36}$$

and

$$\Phi = \tan^{-1}(v_y/v_x). \tag{4.37}$$

In the limit where $\gamma = (1 - v^2/2c^2)^{-1}$ and $\omega_i^2 << \omega_r^2$, the equation of motion is

$$\frac{dv_z}{dt} = -\mu\Omega_e v_\perp n_r \cos\theta \tag{4.38}$$

$$\frac{dv_\perp}{dt} = -\mu\Omega_e c(1 - n_r v_z/c)\cos\theta \tag{4.39}$$

$$\frac{d\theta}{dt} = \Omega_e(1 - v^2/2c^2) + k_z v_z - \omega_r + \mu\Omega_e(c/v_\perp)(1 - n_r v_z/c)\sin\theta \tag{4.40}$$

where $n_r = k_z c/\omega_r$ and $\mu = E/B_0$. The rate of change of kinetic energy of the electron is

$$\frac{1}{2} m_e \frac{dv^2}{dt^2} = m_e\left\{v_z \frac{dv_z}{dt} + v_\perp \frac{dv_\perp}{dt}\right\} \tag{4.41}$$

$$= - m_e\mu\Omega_e v_\perp c \cos\theta.$$

In the following, it is assumed that the electrons first encounter the wave at time t = 0. Thus, if $|\frac{d\omega_r}{dt}|$, $|\frac{d\omega_i}{dt}| \ll \omega_i^2 + \Delta_r^2$ then linearized solutions to (4.38) - (4.40) are

$$v_{\perp 1,z1} = - G_{\perp,z}\left\{AD(\omega_i\cos\theta_0 + \Delta_r\sin\theta_0) - D^0(\omega_i^0\cos\theta^0 + \Delta_r^0\sin\theta^0)\right\} \tag{4.42}$$

$$\theta_0 = \theta^0 + \int_0^t \Delta_r dt := \theta^0 + \Pi_r t \tag{4.43}$$

$$\theta_1 = \mu^0\Omega_e(c/v_{\perp 0})(1 - n_r v_{z0}/c)\left\{AD(\omega_i\sin\theta_0 - \Delta_r\cos\theta_0) - D^0(\omega_i^0\sin\theta^0 - \Delta_r^0\cos\theta^0)\right\}$$

$$+ \mu^0\Omega_e(v_{\perp 0}/c)(\Omega_e - k_z c n_r) \times$$

$$\times \left\{AD^2((\omega_i^2 - \Delta_r^2)\cos\theta_0 + 2\Delta_r\omega_i\sin\theta_0) - D^{02}((\omega_i^{02} - \Delta_r^{02})\cos\theta^0 + 2\Delta_r^0\omega_i^0\sin\theta^0) - tD^0(\omega_i^0\cos\theta^0 + \Delta_r^0\sin\theta^0)\right\} \tag{4.44}$$

where

$$\Delta_r = \Omega_e(1 - v_0^2/2c^2) + k_z v_{z0} - \omega_r \tag{4.45}$$

and $G_z = \mu^0 v_{\perp 0} n_r \Omega_e$, $G_\perp = \mu^0 c(1 - n_r v_{z0}/c)\ \Omega_e$, $A = \exp(\Pi_i t)$, $\Pi_i t = \int_0^t \omega_i dt$ and $D = (\omega_i^2 + \Delta_r^2)^{-1}$. Here the subscripts zero and unity respectively indicate unperturbed and perturbed values. This linearization is only valid if $|\frac{d\theta_0}{dt}| >> |\frac{d\theta_1}{dt}|$ i.e. if $\mu << 1$ and if Δ_r is not identically equal to zero.

Now consider the trajectories of a group of electrons with the same values of $v_{\perp 0}$ and v_{z0} which are initially uniformly distributed in phase angle θ. Equation (4.43) indicates that $\frac{d\theta_0}{dt} = \Delta_r$ is the same for all electrons in the group since the frequency mismatch Δ_r is the same for each electron. On the other hand, (4.44) indicates that $\frac{d\theta_1}{dt}$ depends on the phase angle θ_0. Hence the relative phase of the electrons changes as they interact with the wave. This phenomenon is known as phase bunching and is shown for a group of 8 electrons in Fig. 4.12.

Phase bunching is most efficient when the electrons are resonant or near resonant i.e. when $\Delta_r^2 \lesssim \omega_i^2$. If these electrons also have energies such that

$$0 < (1 - n_r v_{z0}/c) < (v_{\perp 0}/c)^2 |(\Omega_e - k_z c n_r)/\Delta| \tag{4.46}$$

then

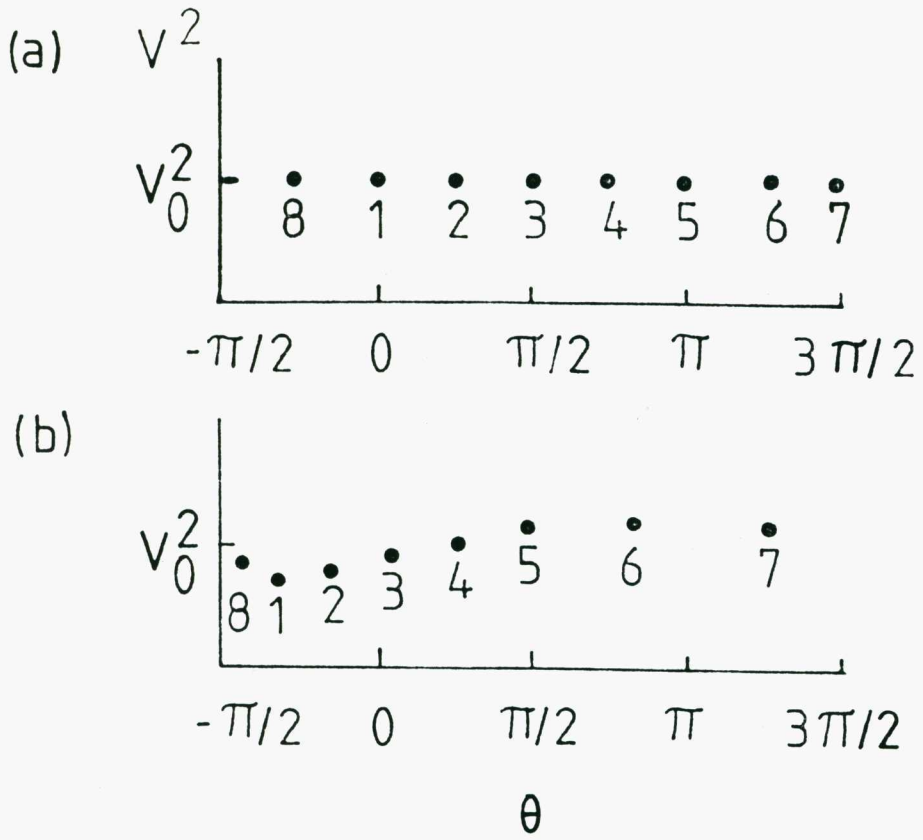

Fig. 4.12 Schematic diagram of a group of electrons with the same values of $v_{\perp 0}$ and v_{z0} and which are initially uniformly distributed in phase angle, θ. The initial distribution is shown in (a) as a function of θ. Electrons 8, 1 and 2 tend to lose energy while electrons 4, 5 and 6 tend to gain energy. If $|d\theta/dt|$ is also smaller for electrons 8, 1 and 2 than for electrons 4, 5 and 6 the electrons tend to bunch in the regions $-\pi/2 < \theta < \pi/2$ and the wave grows. This bunching is shown in (b).

$$\frac{d\theta_1}{dt} \simeq -(v_{\perp 0}v_{\perp 1}/c^2 + v_{z0}v_{z1}/c^2)\,\Omega_e + k_z v_{z1} \tag{4.47a}$$

$$\simeq \mu^0\Omega_e^2\,\frac{v_{\perp 0}}{c}\left(1 - \frac{k_z c n_r}{\Omega_e}\right)$$

$$\times \{AD(\omega_i\cos\theta_0 + \Delta_r\sin\theta_0) - D^0(\omega_i^0\cos\theta^0 + \Delta_r^0\sin\theta^0)\}\,. \tag{4.47b}$$

It can be seen from (4.47b) that if $\Delta_r^2 < \omega_i^2$ and $\omega_i > 0$ then $\frac{d\theta_1}{dt}$ is positive for electrons with $-\frac{\pi}{2} < \theta_0 < \frac{\pi}{2}$ (e.g. electrons 8, 1 and 2 in Fig. 4.12a) and negative for electrons with $\frac{\pi}{2} < \theta_0 < \frac{3\pi}{2}$ (e.g. electrons 4, 5 and 6) when $k_z^2c^2 << \omega_r^2$. The reverse signs for $\frac{d\theta_1}{dt}$ apply when $k_z^2c^2 >> \omega_r^2$.

In (4.47a), the terms proportional to Ω_e arise from a perturbation in the relativistic cyclotron frequency while the term $k_z v_{z1}$ arises from a perturbation in the Doppler shift in (4.40). For $k_z^2c^2 << \omega_{r1}^2$ the perturbation in the Doppler shift (which is represented by the term $k_z c n_r/\Omega_e$ in (4.47b)) is negligible. In this case, the electrons stream along the magnetic field at approximately the same axial velocity but rotate about the magnetic field at different rates so that the electrons become azimuthally bunched. On the other hand for $k_z^2c^2 >> \omega_r^2$, the perturbation in the cyclotron frequency is negligible and the perturbation in v_z results in axial bunching. The change in the direction of the electric field along the axis is responsible for a non-zero $\frac{d\theta_1}{dt}$ in this case.

Although the electrons become bunched in θ, they become dispersed in $v_\perp$ and v_z because the accelerations experienced by electrons of the group are different (as given by (4.42)). This spreading increases

as the wave grows; an example of this phenomenon is given in the computer simulations of Sprangle and Drobot (1977).

During the interaction, the kinetic energy lost by the electrons is transferred to the wave. To second order in μ, (4.41) for the rate of change of kinetic energy of any one electron of the group is

$$\frac{1}{2} m_e \frac{dv^2}{dt} = - m_e \Omega_e A \mu^0 c[v_{\perp 0}(\cos\theta_0 - \theta_1 \sin\theta_0) + v_{\perp 1}\cos\theta_0] . \qquad (4.48)$$

In the case where $\Delta_r^2 < \omega_i^2$, $\omega_i > 0$ and (4.46) is satisfied, $|v_{\perp 1}/v_{\perp 0}|$ is much less than θ_1 and hence the rate of change of kinetic energy is proportional to $- (\cos\theta_0 - \theta_1 \sin\theta_0) = - \cos(\theta_0 + \theta_1) = - \cos\theta$. Over time scales such that $|\Pi_r t| \gtrsim 2\pi$, the electron passes through all phase angles θ from 0 to 2π. During one traversal from $\theta = 0$ to $\theta = 2\pi$ the electron on average loses energy if it remains longer in the region $- \frac{\pi}{2} < \theta < \frac{\pi}{2}$ than in the region $\frac{\pi}{2} < \theta < \frac{3\pi}{2}$ i.e. if $|\frac{d\theta}{dt}|$ $(= |\Delta_r + \frac{d\theta_1}{dt}|)$ for $- \frac{\pi}{2} < \theta < \frac{\pi}{2}$ is less than $|\frac{d\theta}{dt}|$ for $\frac{\pi}{2} < \theta < \frac{3\pi}{2}$. Conversely, the electron gains energy if the reverse inequality for $|\frac{d\theta}{dt}|$ applies.

As discussed earlier for $k_z^2 c^2 << \omega_r^2$, $\frac{d\theta_1}{dt}$ is positive for $- \frac{\pi}{2} < \theta_0 < \frac{\pi}{2}$ and negative for $\frac{\pi}{2} < \theta_0 < \frac{3\pi}{2}$ when (4.46) is satisfied and $\Delta_r^2 < \omega_i^2$, $\omega_i > 0$. Thus, electrons on average lose energy if $\Delta_r < 0$ and gain energy if $\Delta_r > 0$. In the opposite limit when $k_z^2 c^2 >> \omega_r^2$, $\frac{d\theta_1}{dt}$ has the opposite sign and hence the electrons lose energy if $\Delta_r > 0$ and gain energy if $\Delta_r < 0$.

These conditions for phase bunching and net loss of energy to the wave are restricted to cases where $\Delta_r^2 < \omega_i^2$ and where condition (4.46) is satisfied. However, they can be derived without these restrictions by considering the total response of a group of electrons with the delta function distribution of (4.11) and with number density n_e.

For this group of electrons, conservation of total wave and particle energy requires that

$$\frac{\omega_i}{4\pi}\left(1 + \frac{k_z^2 c^2}{\omega_r^2}\right) E^2 = - n_e m_e \int d^3v \, \frac{f}{2} \, \frac{dv^2}{dt} \tag{4.49}$$

when $\omega_i^2 << \omega_r^2$. By using (4.42)-(4.44), (4.48) and considering a time t such that $\Pi_i t >> 1$, (4.49) can be written as

$$\omega_i \left(1 + \frac{k_z^2 c^2}{\omega_r^2}\right) = - \omega_p^2 \left\{\frac{\omega_i}{\omega_i^2 + \bar{\Delta}_r^2} + \frac{v_{\perp 0}^2}{c^2} \frac{(\Omega_e - k_z c n_r)\, \bar{\Delta}_r \omega_i}{(\omega_i^2 + \bar{\Delta}_r^2)^2}\right\} \tag{4.50}$$

where $\bar{\Delta}_r = \int d^3\underset{\sim}{v} \, f\Delta_r$. The dependence of the right hand side of (4.50) on ω_i may be attributed to the energy exchange between the electrons and the wave modifying the electron trajectories. On solving for ω_i the growth rate is found to have the form

$$\begin{aligned} 2\omega_i^2 \simeq & - (2\bar{\Delta}_r^2 + \omega_p^2 w_n) \\ & + \Bigg[(2\bar{\Delta}_r^2 + \omega_p^2 w_n)^2 \\ & \quad - 4\left(\bar{\Delta}_r^4 + \bar{\Delta}_r^2 \omega_p^2 w_n + \frac{v_{\perp 0}^2}{c^2} \bar{\Delta}_r \omega_p^2 (\Omega_e - k_z c n_r)\, w_n\right)\Bigg]^{1/2} \end{aligned} \tag{4.51}$$

where $w_n = (1 + k_z^2 c^2/\omega_r^2)^{-1}$.

For $\Delta_r^2 = (\Omega_e/\gamma - \omega)^2 << \omega_p^2 w_n$ (which is valid for the bunching instabilities; see (4.13) and (4.14)), (4.51) reduces to

$$\omega_i^2 \simeq - \left(\bar{\Delta}_r^2 + \frac{v_{\perp 0}^2}{c^2} \bar{\Delta}_r (\Omega_e - k_z c n_r)\right) . \tag{4.52}$$

Equation (4.52) implies that growth can occur for $k_z^2 c^2 << \omega_r^2 \simeq \Omega_e^2$ only if

$$-\frac{v_{\perp 0}^2}{c^2}\Omega_e < \bar{\Delta}_r < 0 \tag{4.53}$$

while for $k_z^2c^2 >> \omega_r^2$ growth can occur only if

$$0 < \bar{\Delta}_r < \frac{v_{\perp 0}^2}{c^2}\frac{k_z^2c^2}{\Omega_e^2} . \tag{4.54}$$

The conditions for growth derived from the qualitative examination of the electron trajectories are consistent with the criteria (4.53) and (4.54).

The growth rates for the azimuthal and axial bunching instabilities for a delta function distribution (i.e. (4.13) and (4.14)) can also be derived from (4.52) if $\bar{\Delta}_r$ is assumed to have the value given by the solution to the dispersion relation. In particular for $k_z^2c^2 << \omega_r^2$ and $\bar{\Delta}_r = -\omega_p^2/2\Omega_e$, (4.52) reduces to

$$\omega_i = \frac{1}{2}\omega_p\left(\frac{2v_{\perp 0}^2}{c^2} - \frac{\omega_p^2}{\Omega_e^2}\right)^{1/2} \tag{4.55}$$

while for $k_z^2c^2 >> \omega_r^2$ and $\bar{\Delta}_r = \omega_p^2\Omega_e/2k_z^2c^2$ (4.52) reduces to

$$\omega_i = \frac{1}{2}\omega_p\left(\frac{2v_{\perp 0}^2}{c^2} - \left(\frac{\omega_p\Omega_e}{k_z^2c^2}\right)^2\right)^{1/2} . \tag{4.56}$$

4.6.2 The Dispersion Relation with Phase Information

For wave fields described by (4.35), Maxwell's equations take the form

$$E(m_+\omega_i\cos\psi + m_-\omega_r\sin\psi) = -4\pi J_x \tag{4.57a}$$

$$E(m_+\omega_i\sin\psi - m_-\omega_r\cos\psi) = 4\pi J_y \tag{4.57b}$$

where $m_{\pm} = 1 \pm k_z^2c^2/(\omega_r^2 + \omega_i^2)$. The current density, $\underset{\sim}{J}(\underset{\sim}{x},t)$ is proportional to the sum of the velocities of all electrons arriving at $\underset{\sim}{x}$ at time t i.e.

$$J_{x,y} = -en_e \int d^3\underset{\sim}{v}_0 \int d^3\underset{\sim}{x}^0 \, f(v_{\perp 0}, v_{z0}, \theta^0) \, v_{x,y}(\underset{\sim}{x}^0, \underset{\sim}{v}_0, t) \, \delta(\underset{\sim}{x} - \underset{\sim}{x}(\underset{\sim}{x}^0, \underset{\sim}{v}_0, t)). \tag{4.58}$$

The initial distribution, $f(v_{\perp 0}, v_{z0}, \theta^0)$ is chosen to have an unperturbed component which is independent of azimuthal angle and a perturbed component i.e.

$$f(v_{\perp 0}, v_{z0}, \theta^0) = f_0(v_{\perp 0}, v_{z0}) + f_1(v_{\perp 0}, v_{z0}, \theta^0) \, . \tag{4.59}$$

The term f_1 is necessary to make the electron distribution and the wave fields self-consistent at t = 0.

The dispersion relation is obtained by integrating $\sin\psi$ times (4.57) and $\cos\psi$ times (4.57) over all positions $\underset{\sim}{x}$ and has the form

$$E(\omega - k_z^2c^2/\omega) = -4\pi\left\{\langle J_x\sin\psi + J_y\cos\psi\rangle_{\underset{\sim}{x}} + i\langle J_x\cos\psi - J_y\sin\psi\rangle_{\underset{\sim}{x}}\right\} . \tag{4.60}$$

Here $\omega = \omega_r + i\omega_i$ and $\langle(\ldots)\rangle_{\underset{\sim}{x}}$ denotes a spatial average, i.e. $\langle(\ldots)\rangle_{\underset{\sim}{x}} = (\text{volume})^{-1} \times \int d^3\underset{\sim}{x}(\ldots)$. Substitution of (4.36), (4.37), (4.58) and (4.59) into (4.60) yields

$$E(\omega - k_z^2c^2/\omega) = 4\pi e\, n_e \int d^3\underset{\sim}{v} \langle(\cos\theta_0 - i\sin\theta_0)\, I\rangle_{\underset{\sim}{x}} \tag{4.61}$$

where

$$I = iv_{\perp 0}f_0 + i(v_{\perp 0}f_1 + v_{\perp 1}f_0) + v_{\perp 0}\theta_1 f_0 \tag{4.62}$$

On substitution of (4.42) - (4.44) into (4.61), the dispersion relation is found to be

$$\omega^2 - k_z^2c^2 = -\omega_p^2 \int d^3\underset{\sim}{v}\, f_0\left\{\frac{(\omega - k_z v_z)(1 - X)}{\Delta}\right.$$

$$\left. + \frac{v_\perp^2}{2c^2}(\omega\Omega_e - k_z^2c^2)\left[\frac{(1-X)}{\Delta^2} - \frac{it\bar{X}}{\Delta}\right]\right\}$$

$$+ \frac{i\omega\, 4\pi e n_e}{E_0 \exp(\Pi_i t)} \int d^3\underset{\sim}{v}\, v_\perp \langle(\cos\theta_0 - i\sin\theta_0)\, f_1\rangle_{\underset{\sim}{x}} \tag{4.63}$$

where $\Delta = \Delta_r - i\omega_i = \Omega_e(1 - v^2/2c^2) + k_z v_z - \omega$, $X = \exp(-i\Pi t)$, $\Pi t = \Pi_r t - i\Pi_i t$. The subscript zero on $\underset{\sim}{v}$ has been dropped to simplify the notation. Note that the terms involving f_0 are identically zero for $t = 0$. If f_1 is also zero then $\omega^2 = k_z^2c^2$ at $t = 0$. This situation corresponds to the unphysical case where the plasma appears suddenly in the wave fields at $t = 0$. In the present application f_1 is assumed to be finite and such that the usual x-mode dispersion relation is approximately satisfied at $t = 0$. In this case, Δ_r and ω_i can be assumed to be approximately constant since the wave remains predominantly in the x mode. The actual form of f_1 is unimportant here because for growing modes the contribution from f_1 decreases exponentially in time and the contribution from f_0 dominates. Thus, the contribution to the growth rate from f_1 is neglected here.

An alternative form of the dispersion relation (4.63) is

$$\omega^2 - k_z^2 c^2 = \frac{1}{2}\omega_p^2 \int d^3\underset{\sim}{v}(1 - X)/\Delta)\ \bar{D}f \qquad (4.64)$$

where

$$\bar{D}f = (\omega - k_z v_z)\ v_\perp \frac{\partial f}{\partial v_\perp} + k_z v_\perp^2 \frac{\partial f}{\partial v_\perp}$$

and the contribution from f_1 has been neglected.(Equation (4.63) can be obtained from (4.64) by integration by parts.) The reactive behaviour of the plasma is most conveniently described using the form (4.63) and the resistive behaviour using the form (4.64).

4.6.3 Physical Interpretation

Consider first the limit where the variation of Δ_r over the distribution (hereafter denoted by $\partial\Delta_r$) is much smaller than $|\omega_i|$. In this case, the electron distribution can be considered as a single group of electrons with the same values of $v_\perp$ and v_z i.e. f_0 can be approximated by a delta function distribution. The electrons of the group become phase bunched. The bunch rotates with respect to the wave fields with a slow time period $t_p = 2\pi/|\bar{\Delta}_r|$ if the wave is not growing (see Section 4.6.1). The corresponding current gives rise to the trigonometric terms in (4.63). In this case the solution to the dispersion relation (4.63) is oscillatory with the slow time period t_p.

In an unstable plasma (i.e. $\omega_i > 0$) these oscillations decay in time since the electrons become bunched in a fixed region of the wave fields (i.e. in the region where they lose energy to the wave). This result is supported by the computer simulations of Sprangle and Smith (1980) in their linear regime. For $\Pi_i t \gg 1$, $|X|$ is much less

than unity and the dispersion relation (4.63) becomes

$$\omega^2 - k_z^2 c^2 = \omega_p^2 \, P \int d^3v \, f_0 \left\{ \frac{\omega - k_z v_z}{\omega - \Omega_e/\gamma - k_z v_z} - \frac{v_\perp^2}{2c^2} \frac{\omega\Omega_e - k_z^2 c^2}{(\omega - \Omega_e/\gamma - k_z v_z)^2} \right\} . \tag{4.65}$$

The solution to (4.65) is the same as that derived using the Vlasov theory (i.e. (4.10b)) assuming that the resistive properties of the plasma are negligible.

On the other hand in the limit $\partial\Delta_r >> |\omega_i|$ the electron component consists of a series of groups of electrons with a spread in Δ_r rather than a single group of electrons. Each individual group phase bunches but, because of the spread in Δ_r, these bunches rotate at different rates with respect to the wave fields and there is no overall macroscopic phase bunching. Further, the groups can have either sign for Δ_r so that some groups lose energy while others gain energy (Section 4.6.1). Whether the wave grows or damps depends on the net contribution from the various groups.

This net contribution can be evaluated by integrating the trigonometric functions (4.6.4) over the distribution. Since $\partial\Delta_r >> |\omega_i|$, there exists a time such that $\Pi_i t << 1$ and $\partial\Delta_r t >> 1$. In this limit, these integrals approach the asymptotic values (Stix, 1962, p. 134; Zucker, 1970)

$$\int d^3\underset{\sim}{v} \, g(\underset{\sim}{v})(1 - \mathrm{Re}(X))/\Delta \simeq P \int d^3\underset{\sim}{v} \, g(\underset{\sim}{v})/\Delta \tag{4.66}$$

$$\int d^3\underset{\sim}{v} \, g(\underset{\sim}{v}) \, \mathrm{Im}(X)/\Delta \simeq -\pi \int d^3\underset{\sim}{v} \, g(\underset{\sim}{v}) \, \delta(\Delta) \tag{4.67}$$

Equations (4.66) and (4.67) lead to the usual Landau prescription (4.2). Thus, (4.64) reduces to the dispersion equation (4.10a) which incorporates the resistive properties of the plasma. The condition for the resistive behaviour of the plasma to dominate i.e. $\partial\Delta_r >> |\omega_i|$ is equivalent to the condition that the random phase approximation (Melrose, 1973) is valid.

Both the resistive- and reactive-medium instabilities can occur in the same plasma because $\partial\Delta_r$ is a function of k_z with the resistive-medium instability passing over into the reactive medium instability when $\partial\Delta_r \simeq \omega_i$. In particular, for a DGH distribution with $\langle v_\perp^2 \rangle >> \langle v_z^2 \rangle$

$$\frac{\partial\Delta_r}{\Omega_e} \simeq \sqrt{2}\,\frac{v_T}{c}\left(\frac{\langle v_\perp^2\rangle^{1/2}}{c} + \left|\frac{k_z c}{\Omega_e}\right|\right) . \tag{4.68}$$

If (4.55) is used as an estimate for ω_i and if $k_z^2 c^2/\Omega_e^2 \lesssim \langle v_\perp^2\rangle/c^2 << 1$ then $\partial\Delta_r \simeq \omega_i$ when

$$\begin{aligned} \omega_p^2/\Omega_e^2 &\simeq 2\langle v_\perp^2\rangle/c^2 \\ 2\langle v_\perp^2\rangle/c^2 - \omega_p^2/\Omega_e^2 &\simeq v_T^2/c^2. \end{aligned} \tag{4.69}$$

When criteria (4.69) are satisfied, the Wu and Lee instability passes over into the azimuthal bunching instability as occurs for example in Fig. 4.3b at $\omega_p/\Omega_e = 0.09$ ($\langle v_\perp^2\rangle/c^2 = 0.0048$ and $v_T/c = 0.02$).

4.7 SUMMARY

In this Chapter, a theory which interrelates the Wu and Lee and azimuthal bunching instabilities has been presented. The theory shows that these instabilities are different limiting cases of the same instability, both instabilities being driven by azimuthal bunching produced by the relativistic dependence of the electron cyclotron frequency on the velocity of the electron. The free energy for these instabilities is provided by an anisotropy in the electron distribution.

The Wu and Lee instability unlike the azimuthal bunching instability tends to occur when the variation of the frequency mismatch over the electron distribution (i.e. $\partial\Delta_r$) is much greater than the growth rate i.e. when the spread in electron velocities is large. In this case, the total contribution from the phase bunching tends to cancel so that there is no macroscopic bunching. Whether or not growth occurs depends on the details of the distribution function in the neighbourhood of the resonance ellipse as in the standard treatment of this instability.

On the other hand, the azimuthal bunching instability tends to occur when $\partial\Delta_r \ll \omega_i$ i.e. when the spread in electron velocities is small. In this case, the electrons become macroscopically phase bunched with wave growth occurring if Δ_r is negative. A finite velocity spread partially destroys the phase bunching and hence reduces the growth rate of the azimuthal bunching instability.

Because $\partial\Delta_r$ depends on both the wave parameters and the velocity spread in the electron distribution, both the Wu and Lee and azimuthal bunching instabilities can occur simultaneously in the same plasma.

Further, the Wu and Lee instability can merge into the azimuthal bunching instability (and vice versa) when the wave and/or plasma parameters change so that $\partial\Delta_r \simeq \omega_i$ i.e. when criteria (4.69) are satisfied.

CHAPTER 5

AMPLIFICATION AND TRIGGERING OF DISCRETE VLF EMISSIONS

5.1 INTRODUCTION

Gyro-resonant interaction between electrons and waves is the basis of theories for discrete VLF emissions i.e. narrow band emissions in the very low frequency (VLF) band (from 200 Hz to 30 kHz) propagating in the whistler mode in the magnetosphere. These emissions tend to propagate in ducts which are field aligned regions of enhanced ionization acting as waveguides for the whistlers. VLF emissions can be excited or "triggered" by other naturally occurring whistlers or by manmade signals, such as Morse-code signals, propagating in the whistler mode (Helliwell et al., 1964; Helliwell, 1965). Amplification of the wave which triggers the emission can also occur (McNeill, 1968).

In Section 5.2, the main observations of the amplification and triggering are reviewed. One of the most striking features is the dash-dot anomaly i.e. the tendency of Morse-code dashes (duration 150 ms) rather than dots (50 ms) to trigger emissions (Helliwell et al., 1964; Helliwell, 1965). This feature implies the existence of a minimum duration for the signal before triggering can occur. Helliwell (1965) has also argued that this feature implies that the triggering wave (hereafter called TW) is organizing charged particles in the magnetosphere in such a way that they radiate coherently. Other observations such as the dependence of the amplification on the duration and phase of the TW (Helliwell and Katsufrakis, 1974; Koons et al., 1976; Chang and Helliwell, 1979) confirm that the TW is organizing particles with respect to the phase of the TW to produce the triggered emission (hereafter TE).

The idea of the TW organizing particles was incorporated in a phenomenological model developed by Helliwell (1967) to account for the various spectral forms of the triggered emission. In this model (which is reviewed in Section 5.3) the TW is assumed to phase bunch electrons through a gyro-resonant interaction. The current associated with the phase-bunched electrons then radiates to produce the TE.

More detailed theories for the phase bunching and/or amplification mechanisms are based on Helliwell's model for the interaction; these theories are reviewed in Section 5.3 (cf. also Matsumoto, 1979). Standard linear theory for the time asymptotic behaviour of whistlers cannot account for many of the features of the amplification and triggering (e.g. Ashour-Abdalla, 1970; Roux and Pellat, 1978) and hence nonlinear processes (with respect to the wave amplitude) were considered. Possibly relevant nonlinear processes include quasi-linear diffusion (Ashour-Abdalla, 1972) and trapping (Dysthe, 1971). It is argued in Section 5.3 that these "nonlinear" theories are not consistent with all the observed features of the amplification. In particular, they require that the TW amplitude exceed a threshold value before they become effective and waves with amplitudes well below this threshold have been observed to trigger emissions (Inan et al., 1977).

In this Chapter, an alternative theory for the dynamics of the phase bunching of electrons and the amplification of the TW is developed using the formalism of the previous Chapter. The features of the TE are derived from the details of the phase bunching mechanism and Helliwell's (1967) phenomenological model. The essential difference between this theory and existing theories is that the time asymptotic assumption is relaxed in evaluating the response of the plasma. Trapping is explicitly neglected

in the theory, i.e. the wave amplitude is assumed to be insufficient to trap electrons.

The mechanism by which the TW produces the phase bunching is discussed in Section 5.4. The phase-bunched electrons cause the TW to grow and excite the TE (as in Helliwell's (1967) phenomenological model). The growth rate for the amplification is derived in Section 5.5 and the features of the amplification and triggering are compared with observations in Section 5.6. A summary and discussion of the theory are given in Section 5.7.

5.2 EXPERIMENTAL OBSERVATIONS

In this Section, the main experimental observations of amplification and triggering are reviewed. Early observations (i.e. those from the mid 1960's to mid 1970's) were mainly concerned with the various spectral forms of the TE and with the dash-dot anomaly; they are reviewed in Section 5.2.1. More detailed information about the dependence of amplification and triggering on the properties of the TW was provided by special transmitters and detectors established in the mid 1970's (Helliwell and Katsufrakis, 1974; McPherson et al. 1974). Observations from these installations of triggering and amplification are reviewed in Sections 5.2.2 and 5.2.3 respectively.

5.2.1 Early Observations

5.2.1.1 *Spectral Forms*

Triggering of discrete VLF emissions was first detected by Helliwell et al. (1964) during Morse-code transmissions. An example is shown in Fig. 5.1. The spectrum of the detected subionospheric or

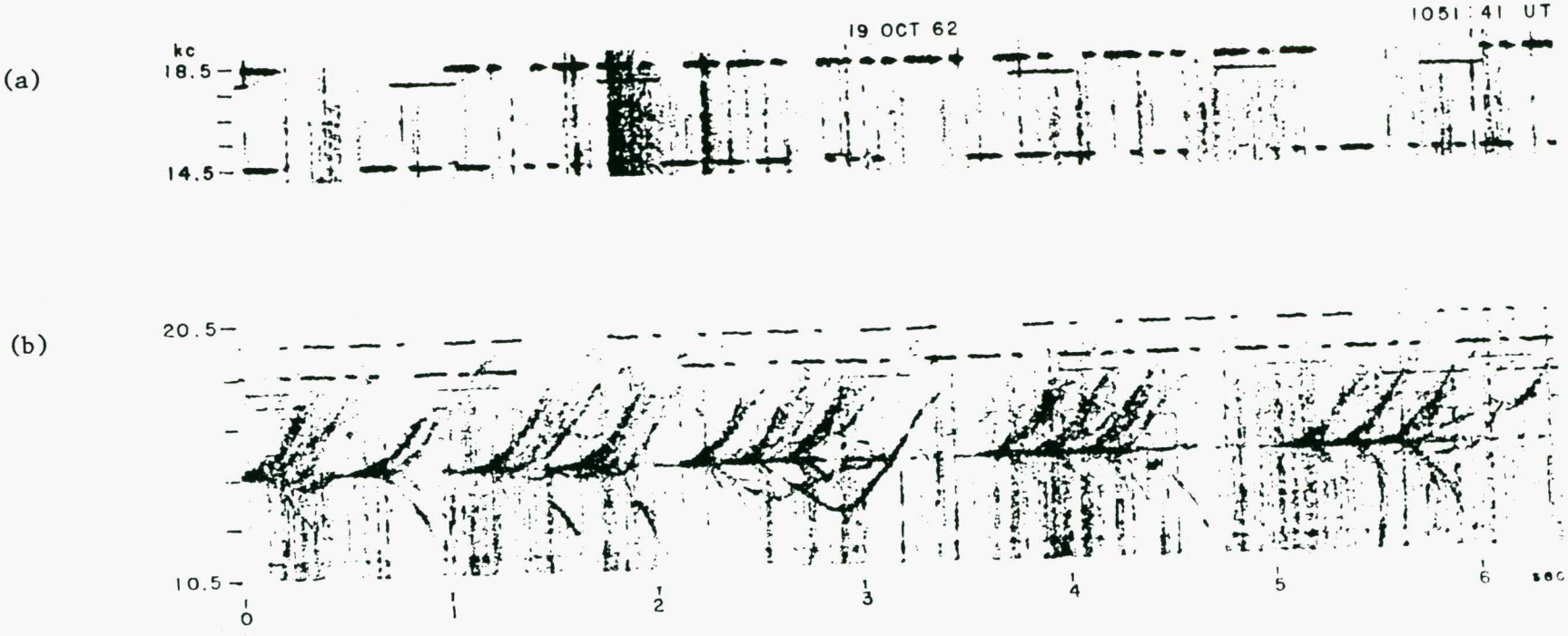

Fig. 5.1 Triggering of discrete VLF emissions by a Morse-code transmission at 14.7 kHz (after Helliwell, 1965). The spectrum of the detected subionospheric or direct signal is shown in (a). The spectrum of the signal which propagates through the magnetosphere is shown in (b). Emissions characterized by a sharply-defined centre frequency which is a function of time are triggered by the magnetospheric wave.

direct signal is shown in Fig. 5.1a. The spectrum of the magnetospheric signal is shown in Fig. 5.1b. The TE are characterized by a sharply-defined centre frequency which is a function of time and are excited only by the magnetospheric signal.

The frequency of the TE may decrease (known as a "faller"), increase (known as a "riser") with time or successively rise and fall to produce patterns in the spectrum like "hooks" or "inverted hooks". Triggering can occur at both the termination of the TW (which is called termination triggering) or prior to the termination of the TW (called pretermination triggering).

5.2.1.2 *The Dash-Dot Anomaly*

The dash-dot anomaly (Helliwell et al., 1964) is apparent in Fig. 5.1: dashes rather than dots trigger emissions. Further observations by Helliwell (1965) and Lasch (1969) showed that when dots do trigger an emission, the emission is usually in the form of a weak faller; dashes tend to trigger risers.

5.2.2 Triggering

5.2.2.1 *Triggering as a Function of the Frequency and Duration of the TW*

The dependence of triggering (as well as amplification) on the frequency and duration of the TW was investigated in detail by Helliwell and Katsufrakis (1974). Instead of using a Morse-code format as in previous experiments, they switched the transmitter frequency between 5.0 and 5.5 kHz periodically at intervals between 50 ms to 400 ms. An example of the spectrum of the detected signal is shown in Fig. 5.2. It can be seen that

(a) there is significant activity at 5.5 kHz and little activity at 5.0 kHz which implies that triggering is restricted to a narrow frequency bandwidth $\lesssim$ 0.5 kHz;

(b) triggering only occurs for pulses of duration greater than about 100 ms, consistent with the dash-dot anomaly;

(c) the longer duration pulses (duration $\gtrsim$ 300 ms) trigger risers while the shorter pulses (duration $\lesssim$ 300 ms) trigger fallers;

(d) triggering occurs in the absence of naturally occurring VLF emissions of similar intensity to the TE and in fact is often observed to occur when there are no other detectable magnetospheric signals in ground-based recordings (Helliwell et al., 1980).

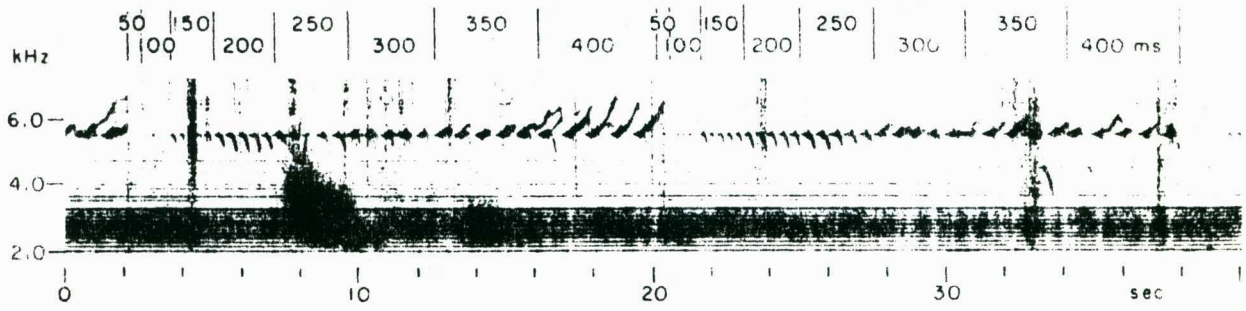

Fig. 5.2 Triggering by a variable pulse length sequence (after Helliwell and Katsufrakis, 1974). The pulsed output was produced by switching the frequency between 5.0 and 5.5 kHz at periods varying from 50 to 400 ms in 50 ms steps. No triggering occurs for pulses less than 100 ms duration. Fallers are triggered by pulses of duration between 100 ms and 300 ms and risers by pulses of duration greater than 300 ms.

Although the triggering in Fig. 5.2 occurs continuously over a period of tens of seconds, triggering is also observed to occur intermittently with gaps between triggering events of between a few seconds to a few tens of seconds (e.g. McPherson et al., 1974; Stiles and Helliwell, 1977; Dowden, 1981; Park, 1981). This feature implies that conditions of the medium along the propagation path of the TW are varying on this time scale (McPherson et al. 1974).

5.2.2.2 *Triggering as a Function of the Wave Amplitude*

Early observations indicated that triggering occurred for signals from both high power transmitters (1 MW, 14.7 kHz, Cutler, Maine; Helliwell et al., 1964) and low power transmitters (100 W, 10.2 kHz, Forest Port, New York; Kimura, 1967; 1968). However, the duration required to produce triggering for the low power transmission was about 1 s, i.e. considerably longer than the 150 ms dash which produced triggering in the high power signals. This feature implies that either the product of power and duration of the TW needs to be high before triggering occurs (Kimura, 1967) or the position and frequency of the transmitter rather than the wave amplitude are important in determining the triggering (Kimura, 1968).

Helliwell et al. (1980) examined the triggering as a function of the wave amplitude using the controlled VLF wave injection experiment of Siple Station, Antarctica, established by Helliwell and Katsufrakis (1974). They found that triggering (and amplification) can occur for radiated powers as low as 1 W. This threshold implies that either (i) the triggering mechanism is a function of the wave amplitude and that it vanishes below this threshold or (ii) that the triggering mechanism is

independent of the wave amplitude and that background noise suppresses triggering at small wave amplitudes (Helliwell et al., 1980).

Although there is as yet no compelling evidence in favour of either interpretation of the triggering threshold, there is some circumstantial evidence which favours the latter interpretation. In particular, Raghuram et al. (1977) observed that amplification and triggering can be suppressed by whistler mode echoes. They attributed this suppression to the reduction of the coherence of the total unamplified signal caused by the presence of the echoes. Chang et al. (1980) also observed suppression of the triggering when they modulated the frequency of the TW.

Inan et al. (1977) used a spacecraft to measure the wave magnetic amplitude in situ in the magnetosphere for a signal from the Siple Station transmitter which produced triggering. They found that for the transmitter operating at several hundred watts the unamplified amplitude was about 0.2 mγ (1 mγ = 10^{-12} T). The 1 W triggering threshold observed by Helliwell et al. (1980) implies that the in situ TW amplitude can be as small as 0.02 mγ and still trigger emissions.

5.2.3 Amplification

5.2.3.1 *Quasi-Exponential Growth and Pulsation Phenomenon*

McNeill (1968) reported that waves which trigger emissions can also be amplified. This was examined in greater detail by Helliwell and Katsufrakis (1974). They found that amplification, like triggering, is restricted to a narrow frequency range and that it is a function of the duration of the TW.

A specific example of the dependence of the growth rate on the duration of the TW is illustrated in Fig. 5.3 where the average amplitude of the 150-, 200-, 250- and 400- ms pulses (5.5 kHz) of Fig. 5.2 is shown as a function of time from the start of the pulse. It can be seen that during the first 80 ms of each pulse there is little amplification. Between 80 and 200 ms, the growth is exponential, and after 200 ms, the amplitude reaches a saturation level. Such temporal behaviour of the amplitude is hereafter called quasi-exponential growth.

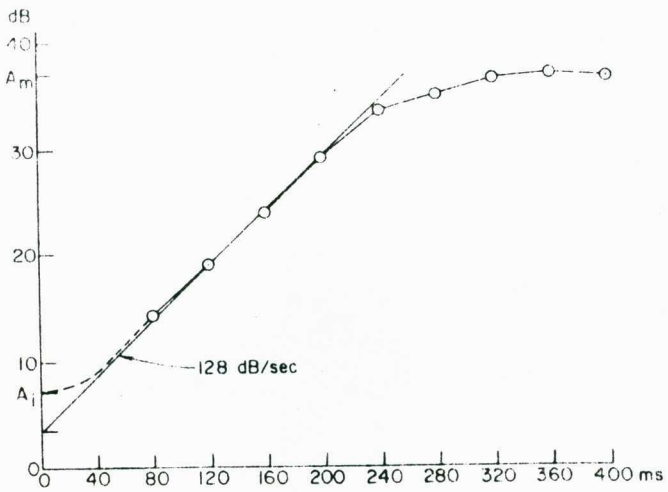

Fig. 5.3 Average amplitude of the 150-, 200-, 250- and 400 ms pulses (5.5 kHz) of Fig. 5.2 as a function of time from the start of the pulse (after Helliwell and Katsufrakis, 1974). A_i is the initial wave amplitude. Total growth is $A_m - A_i = 30$ dB. For the first 80 ms there is little amplification; exponential growth occurs between 80 ms and 200 ms. After this period saturation occurs.

Other observations indicate that the amplification need not necessarily be quasi-exponential. Specifically, Bell and Helliwell (1971) and Likhter et al.(1971) observed periodic oscillations in the amplitude as shown in Fig. 5.4. This "pulsation phenomenon" was also observed by Dowden et al. (1978) who found that the oscillations in the wave amplitude occurred after a period of quasi-exponential growth.

(a)

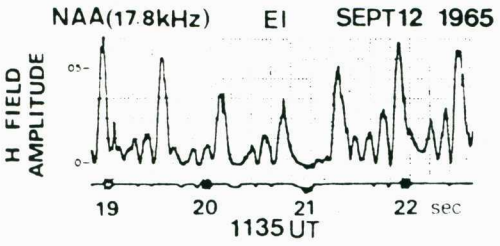

(b)

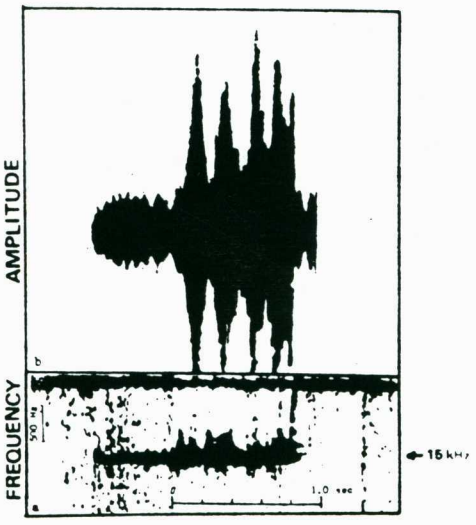

Fig. 5.4 Pulsation phenomena. (a) Relative amplitude of a key-down whistler-mode signal at 17.8 kHz (after Bell and Helliwell, 1971). (b) Pulsation in amplitude and corresponding spectral broadening of 800- ms whistler mode pulse (after Likhter et al., 1971).

5.2.3.2 *The Dependence of the Growth Rate on the Phase of the Wave*

The amplification of the TW is also a function of the phase of the TW. This was shown explicitly by Koons et al. (1976) who modified the phase of the TW by using a direct phase change in the driving voltage of the transmitter and by Chang and Helliwell (1979) who inserted a very short pulse with a frequency offset into the TW. After the phase change, the amplitude of the TW was observed to decrease and then recover to an amplitude comparable to that prior to the phase change.

5.3 THEORIES FOR AMPLIFICATION AND TRIGGERING

5.3.1 Outline of the Various Theories

In early theoretical work on VLF emissions, instabilities involving whistlers were examined (e.g. Dungey, 1963; Nakada et al., 1965; Kennel and Petschek, 1966; Roberts, 1966; Kimura, 1967). These theories used standard linear theory to determine the growth rate for the time asymptotic behaviour of the normal modes of oscillation of the plasma (cf. Section 4.2).

The growth rate implied by these theories is independent of both the length and phase of the TW which is inconsistent with observations (see Section 5.2.2). These theories are also inconsistent with the observation that amplification and triggering can occur in the absence of naturally occurring emissions in ground-based recordings (Section 5.2.2.1). Specifically, these theories imply that the growth rates for background noise and the TW are equal. However, the observed absence of naturally occurring VLF emissions in ground-based recordings implies that the growth rate for background noise is smaller than the loss rate

(e.g. due to leakage from the duct and/or attenuation in the ionosphere) while the observed amplification of the TW implies that the growth rate for the TW must be larger than this loss rate.

As discussed in Section 5.1, the idea that the TW organizes particles (specifically electrons) to produce the TE was introduced in a phenomenological model developed by Helliwell (1967). This model is able to account for the various spectral forms of the TE (Section 5.2.1.1) and is reviewed in Section 5.3.2.

Helliwell's (1967) phenomenological model did not specify how the TW actually organizes electrons to produce amplification and triggering. This point was addressed in later theories (reviewed in Subsection 5.3.3) which involve non-linear effects.

One of the major shortcomings of these later theories is that amplitudes greater than a certain threshold value (of a few milligamma) are required to produce the observed amplification while TW's with amplitudes well below this threshold have been observed to be amplified and trigger emissions (Section 5.2.2.2).

5.3.2 Triggering: Helliwell's Phenomenological Model

In Helliwell's (1967) phenomenological model the TW is assumed to phase bunch gyro-resonant electrons producing an oscillating current. This oscillating current then excites the TE. The frequency and wave-number of the TE are assumed to be determined by the region where the phase bunching and energy delivered to the TW by the electrons are at a maximum i.e. where the electrons are able to gyro-resonate with the TW for a long time.

Due to the inhomogeneity of the geomagnetic field, both the cyclotron frequency and the Doppler shifted wave frequency vary spatially and an electron can gyro-resonate with the TW for only a finite time. Long lasting resonance in this case requires that

$$\Delta_r \simeq \Omega_e + k_z v_z - \omega_r \simeq 0 \tag{5.1a}$$

$$\frac{d\Delta_r}{dz} \simeq 0. \tag{5.1b}$$

In (5.1) the z axis is along the magnetic field and the Lorentz factor γ is set to unity (since $k_z^2 c^2 >> \Omega_e^2$ for whistlers). Equations (5.1a) and (5.1b) are called the "consistent-wave condition" (Helliwell, 1967).

A schematic diagram of the interaction between the electrons and the TW is shown in Fig. 5.5. The region in the magnetosphere in which the consistent wave condition is satisfied is called the "interaction region". It lies near the magnetic equator where the spatial gradient of the magnetic field is smallest and (5.1) is most easily satisfied. Since $\omega_r < \Omega_e$ for whistlers, the gyro-resonant electrons travel in the opposite direction to the TW (i.e. $k_z v_z < 0$).

The various spectral forms of the TE are attributed to motion of the interaction region to maintain a balance between the input power from the electrons and the output wave power (Helliwell, 1967). A faller is triggered if the interaction region moves towards the equator, i.e. in the direction of decreasing gyrofrequency, and a riser is triggered if it moves away from the equator. A hook is triggered if the interaction region first moves towards the equator and then away from the equator; an inverted hook is triggered if the interaction region first moves away from the equator and then towards the equator.

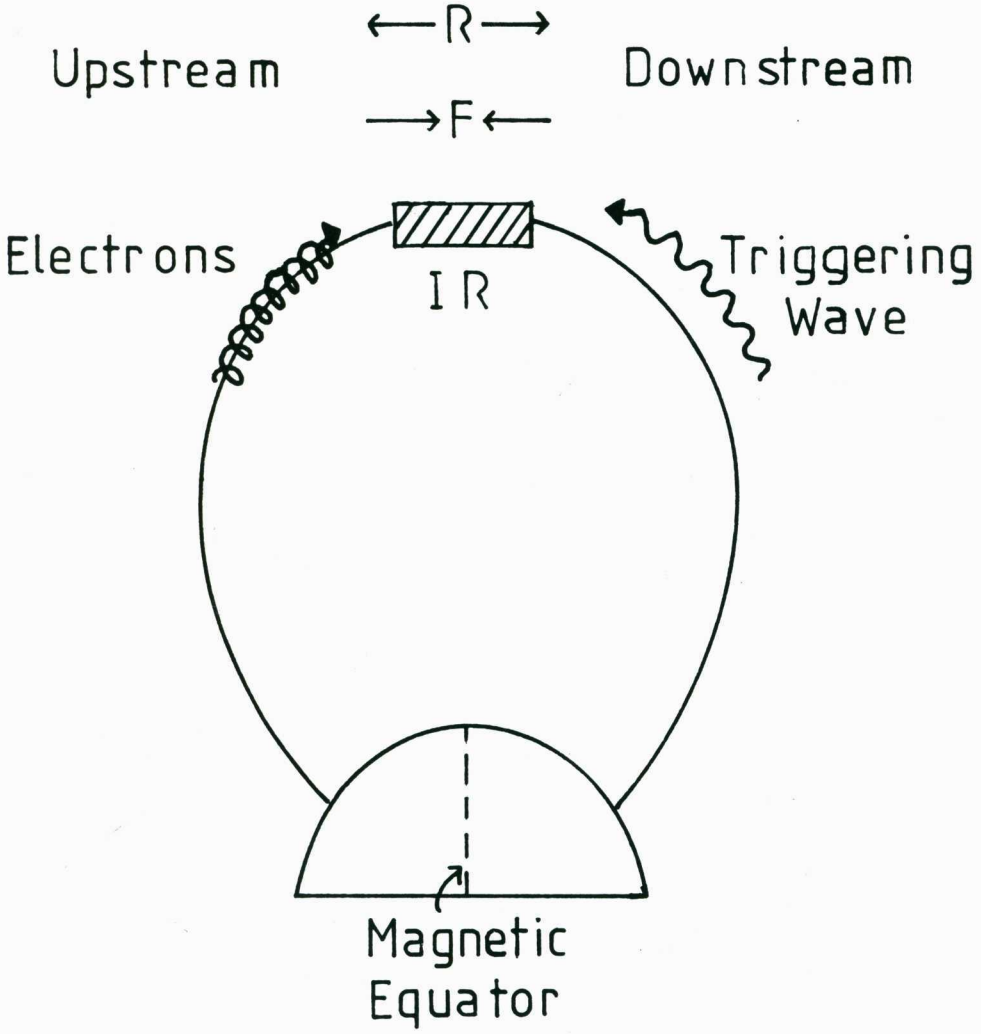

Fig. 5.5 Schematic diagram of the interaction between the whistler and gyro-resonant electrons. If the interaction region (IR) moves away from the equator, risers (R) are triggered while if it moves towards the equator fallers (F) are triggered.

Helliwell (1967) also argued that when the input electron flux and/or the length of the TW exceeds the value required for the wave to reach saturation the interaction region moves in the direction of the streaming electrons; when the particle flux and/or the length of the TW is less than this value, the interaction region drifts in the opposite direction i.e. in the direction of the TW. This implies that if the interaction region is downstream (upstream) of the magnetic equator and saturation occurs then risers (fallers) are triggered; if saturation does not occur then fallers (risers) are triggered. Since long duration TW's are more likely to reach saturation than short duration TW's, this model implies that long duration TW's tend to trigger risers and short duration TW's fallers (consistent with observations; Sections 5.2.1.2, 5.2.2.1) only when the interaction region is downstream of the magnetic equator.

5.3.3 Existing Theories for Phase Bunching and Amplification

Another class of theories concerns how the fields of the TW affects the electron trajectories to produce phase bunching and/or amplification. Specifically the wave fields, depending on their amplitude, may produce small perturbations in the trajectories (in which case the electrons are called untrapped) or they may cause the phase of an electron with respect to the wave to become bounded about some fixed phase angle (in which case the electron is called trapped; Dysthe, 1971). Theories which do not involve trapping are reviewed in Section 5.3.3.1 and theories involving trapped electrons are reviewed in (Section 5.3.3.2).

5.3.3.1 *Theories which invoke Quasi-Linear Diffusion*

Das (1968), Ashour-Abdalla (1972), Brinca (1972), Denavit and Sudan (1972) and Welti et al. (1973) examined the interaction between the TW and untrapped resonant and near-resonant electrons using quasi-linear theory. They found that the interaction causes these electrons to diffuse in both pitch angle and energy. Due to the diffusion, a slot develops in the distribution about the resonant velocity $v_R = (\omega - \Omega_e)/k_z$ with the gradients in the distribution at v_R being reduced and the gradient at the edge being enhanced (Ashour-Abdalla, 1972). The increase in the gradients at the edge of the slot enhances the growth rate near the TW frequency and triggers the emission.

A major shortcoming of this mechanism is that to produce the slot on a time scale of the order of several tens of seconds (e.g. Ashour-Abdalla, 1972) an initial wave amplitude of about 10 mγ is required whereas TW's with much smaller amplitudes and duration are observed to trigger emissions (Section 5.2.2). This mechanism is also unable to account for the observed dependence of the growth rate on the phase of the TW (Section 5.2.3.2).

5.3.3.2 *Theories which Invoke Trapping*

Two possible mechanisms for amplification and triggering involving trapped electrons have been considered. The first utilizes a distortion in the electron distribution produced by trapping. The second utilizes a nonlinear current produced by the phase bunching of trapped electrons.

Distortion of the Electron Distribution by Trapping

Asseo et al. (1972), Karpman et al. (1974a,b), Roux and Pellat (1976,1978), Cornilleau-Wehrlin and Gendrin (1979) and Melrose et al. (1983) considered the distortion of the electron distribution produced by the difference in the trajectories of trapped and untrapped electrons arising from the inhomogeneity of the geomagnetic field. They showed from constants of motion obtained by averaging over time that the motions of trapped electrons are governed by $v_z = v_R(z)$ and v = constant and those of untrapped electrons by $v_\perp^2 \propto B_0(z)$ and v = constant. Due to the inhomogeneity these trajectories are different. This difference causes a distortion in the velocity distribution which in turn modifies the growth rate.

This mechanism like quasi-linear diffusion modifies the growth rate of a wave with an initial amplitude of a few milligamma only after several seconds (e.g. Cornilleau-Wehrlin and Gendrin, 1979). As such this mechanism can be effective only for continuous transmissions and not for pulsed transmissions.

Phase Bunching of Trapped Electrons

Other theories are based on the nonlinear current produced by the phase bunching of trapped electrons. Specifically, Knox (1969), Ashour-Abdalla (1970), Istomin and Karpman (1972,1973a,b), Gendrin (1974) and Newman (1977) examined the phase bunching in a homogeneous magnetic field. They found that the phase bunching produced oscillations in the wave amplitude. These theories were, however, unable to identify a mechanism for producing quasi-exponential growth (Matsumoto, 1979).

To obtain quasi-exponential growth, Helliwell and Crystal (1973) considered a feedback system between the stimulated emission and

incoming resonant electrons which were simulated by discrete current sheets (rather than a continuous current). A phenomenological model of this feedback system was developed by Helliwell and Inan (1982) to explain pretermination triggering.

There is, however, some controversy over the validity of the simulation in Helliwell and Crystal's (1973) theory (e.g. Nunn, 1975; Helliwell and Crystal, 1975; Roux and Pellat, 1976; Newman, 1977; Matsumoto, 1979). In particular, Roux and Pellat (1976) suggested that the amplification in Helliwell and Crystal's (1973) theory is due to a beam-plasma instability which is inconsistent with the absence of naturally occurring VLF emissions in ground based recordings (Subsection 5.3.1).

Dysthe (1971) first pointed out that, if the phase bunching of trapped electrons is to produce amplification,an inhomogeneous magnetic field is required. This is because the force acting on a trapped electron causes the phase of the electron to vary sinusoidally and there is no net energy exchange averaged over time; an inhomogeneous magnetic field introduces an extra non-sinusoidal force which results in net energy exchange. This effect was examined in detail in numerical studies by Nunn (1971,1973,1974), Vomvoridis and Denavit (1979,1980), Matsumoto et al. (1980), Matsumoto and Omura (1981) and Omura and Matsumoto (1982).

Although wave amplification is possible in these theories, trapping by the TW in the inhomogenity of the geomagnetic field is only possible for wave amplitudes greater than a few milligamma (e.g. Dysthe, 1971; Nunn, 1975). This is inconsistent with observations which indicate that wave amplitudes less than about 0.2 mγ can be amplified and trigger emissions (Section 5.2.2.2).

5.4 PHASE BUNCHING OF UNTRAPPED ELECTRONS

5.4.1 Introduction

An alternative theory for the amplification and triggering of discrete VLF emissions which incorporates Helliwell's (1967) phenomenological model is developed here. It is shown in Section 5.4.2 that untrapped electrons can be phase bunched by the front of the TW without significant energy exchange between the electrons and the wave; this occurs in a region where the magnitude of the mismatch between the electron cyclotron frequency and the Doppler shifted wave frequency is greater than about the magnitude of the growth rate arising from the bunching i.e. where $|\Delta_r| \gtrsim |\omega_i|$. As these electrons move through the magnetosphere Δ_r changes due to the inhomogeneity in the magnetic field. The phase bunched electrons can then interact with a later portion of the TW in a region where $\Delta_r \simeq 0$ to produce the amplification and the TE.

The growth rate for the amplification arising from this process is derived in Section 5.5. This growth rate is independent of the initial wave amplitude, unlike those for the theories reviewed in the previous Section. The implied features of the amplification and triggering are compared with observational data in Section 5.6.

A similar mechanism was proposed by Sprangle and Smith (1980) and Chu et al. (1980b) to improve the efficiency of gyrotrons. In these theories the bunching is azimuthal; here however $k_z^2 c^2 > \Omega_e^2$ which implies that axial bunching is relevant (cf. Section 4.2).

In common with other theories of VLF emissions (e.g. Helliwell, 1967; Dysthe, 1971; Matsumoto, 1979) the TW is assumed to be a whistler

wave propagating parallel to the magnetic field (in the z direction) and amplification and triggering are assumed to occur near the magnetic equator. The variation of the velocity of an electron due to conservation of the adiabatic invariant is neglected since the change in the magnetic field near the magnetic equator is small. The variation in Ω_e is, however, retained in $\Delta_r \simeq \Omega_e + k_z v_z - \omega_r$ where small variations in Ω_e are important for $\Delta_r \simeq 0$. Further, the spatially varying ambient magnetic field as seen by an electron is simulated by a temporally varying magnetic field i.e. $\Omega_e(z) \rightarrow \Omega_e(v_z t)$ and terms of order $\frac{d\Omega_e}{dt}$ are neglected (cf. Sprangle and Smith, 1980). In effect it is assumed that the variation of the magnetic field is sufficiently slow that $|\frac{d\Delta_r}{dt}|$, $|\frac{d\omega_i}{dt}| \ll \Delta_r^2 + \omega_i^2$.

When the above inequalities are satisfied, the trajectories of the untrapped electrons are as described in Section 4.6. These trajectories are used to determine the phase bunching and the growth rate in the following Sections. (The notation used in this Chapter is the same as in Section 4.6.)

The neglect of the variation of the velocity due to the conservation of the adiabatic invariant and the assumption of a temporally varying magnetic field are valid only when the interacting electrons have small average pitch angles. This is the case for the parameters considered here which are thought to be appropriate for the relevant region of the magnetosphere (Section 5.6.1). In Appendix C, the growth rate is derived for the case where the magnetic field along the TW varies spatially. It is shown that the growth rate is essentially the same as derived in the following Sections except that instead of

the variation of Δ_r depending solely on Ω_e it also depends on the variation of the electron velocity due to the conservation of the adiabatic invariant.

5.4.2 Physical Picture of the Bunching and Amplification

A schematic diagram of the interaction between the TW and resonant and near-resonant electrons as envisaged here is shown in Fig. 5.6. In the following the interaction is referred to as resonant if $\Delta_r \simeq 0$, specifically if $|\Delta_r| < |\omega_i|$, and off-resonant if $|\Delta_r| \geq |\omega_i|$. Due to the variation of the geomagnetic field, the interaction can change from off-resonant to resonant. The region in which $\Delta_r \simeq 0$ corresponds to Helliwell's (1967) "interaction region" but is called here the "resonant interaction region" or RIR to distinguish it from the region prior to the RIR where the electrons interact off-resonantly with the TW. This latter region is called the "off-resonant interaction region" or OIR.

The resonant interaction between a right hand polarized electromagnetic wave and a group of electrons initially uniformly distributed in phase was examined in Section 4.6.1. It was shown there that, due to the energy exchange between the wave and the electrons, the electrons become bunched in phase but become dispersed in $v_\perp$ and v_z, and that this bunching could give rise to reactive- and resistive-medium instabilities. This phase bunching mechanism is hereafter called the "resonant bunching mechanism" or RBM and is relevant in the RIR.

The size of the RIR is, however, limited by the inhomogeneity of the geomagnetic field. A group of electrons which are not bunched

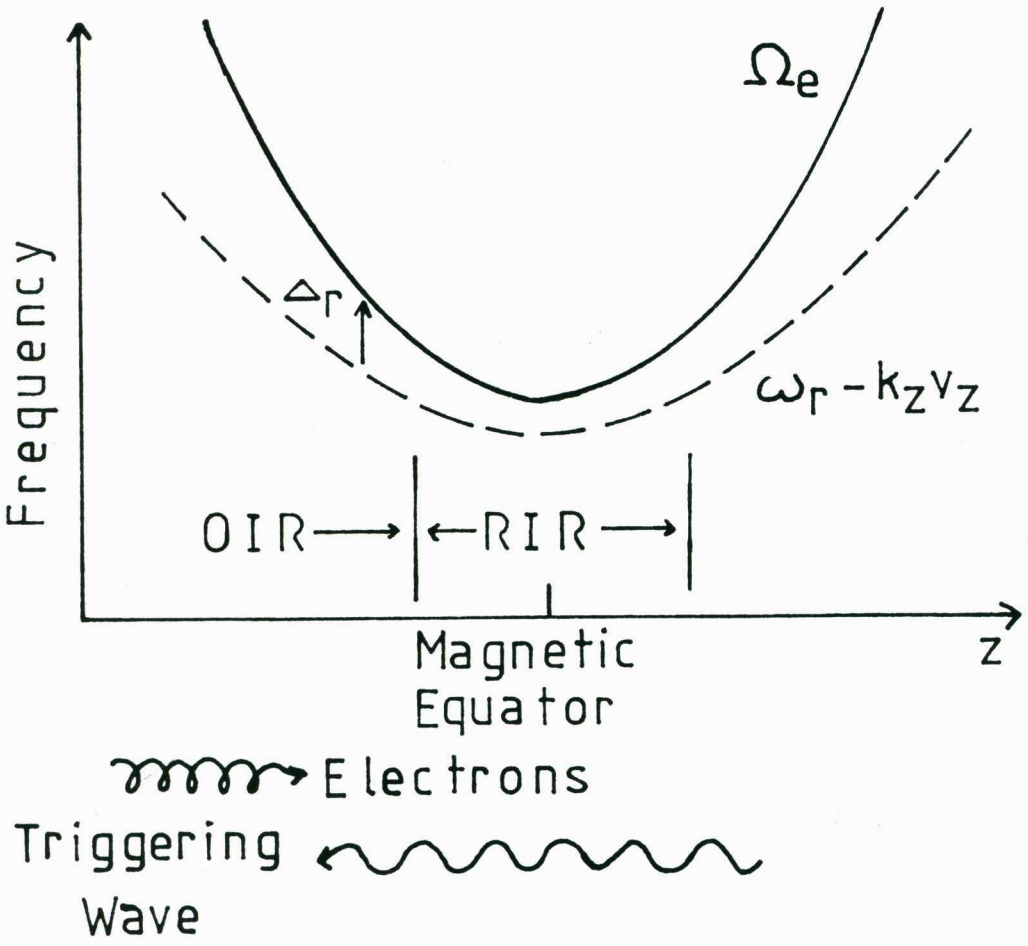

Fig. 5.6 Schematic diagram of the variation of the frequency mismatch between the electron cyclotron frequency (solid curve) and the Doppler shifted frequency of the TW. The Doppler shifted frequency is determined by the whistler dispersion relation and may always be less than the cyclotron frequency (dashed curve) or may exceed the cyclotron frequency at some point depending on the velocity of the streaming electrons. Electrons can exchange energy in the region (called the resonant interaction region on RIR) where Δ_r is small. A larger growth rate can be obtained if, on entering the RIR, the electrons are bunched by the front of the TW in the off-resonant interaction region or OIR.

when they enter the RIR cause little amplification if the corresponding growth rate is smaller than the reciprocal of the traversal time across the RIR. When the growth rate is sufficiently small for this to happen, the amplification is said to be "ineffective".

Naturally occurring VLF noise usually has no phase coherence and hence does not bunch electrons before they enter the RIR. Observations indicate that such noise does not cause amplification and triggering (Section 5.2.2.1). Thus, it is assumed in the following that amplification due to unbunched electrons entering the RIR is ineffective.

Amplification of the TW can occur nevertheless if the TW is sufficiently long to bunch the electrons in the OIR before they enter the RIR (Fig. 5.6). Without phase bunching half the electrons lose energy and half gain energy in the RIR (this may be seen from (4.41) which implies that the rate of change of kinetic energy of an electron is proportional to $\cos\theta$). Net energy exchange between the group of electrons and the TW arises only from perturbations in the electron trajectories. If instead the electrons are phase bunched on entering the RIR, they all lose or gain energy depending on the phase at which they are bunched. Thus, the energy transfer and the corresponding growth rate can be enhanced considerably.

The mechanism by which the front of the TW bunches electrons (hereafter called the "off-resonant bunching mechanism" or OBM) can be understood as follows. Consider the trajectories (i.e. (4.38)-(4.44)) of a group of electrons with the same value of $v_{\perp 0}$ and v_{z0} which are initially uniformly distributed in phase angle θ (Fig. 4.12a).

In the OIR, $\Delta_r^2 \geq \omega_i^2$ but for simplicity let it be assumed that $\Delta_r^2 >> \omega_i^2$. Then the time average (defined by $\langle \ldots \rangle_t := \frac{1}{t} \int_0^t dt(\ldots)$) of the rate of change of phase angle θ (cf. (4.40)) of an electron in the group after time t such that $|\Pi_r t = \int_0^t \Delta_r dt| >> 1$ and $|\Pi_i t = \int_0^t \omega_i dt| << 1$ is given by

$$\left\langle \frac{d\theta}{dt} \right\rangle_t \simeq \langle \Delta_r - (v_{\perp 0} v_{\perp 1}/c^2 + v_{z0} v_{z1}/c^2)\, \Omega_e + k_z v_{z1} + \mu \Omega_e (c/v_{\perp 0})(1 - n_r v_{z0}/c) \sin\theta \rangle_t \tag{5.2}$$

$$\simeq \langle \Delta_r \rangle_t - \mu^0 \Omega_e^2 (v_{\perp 0}/c)(1 - n_r k_z c/\Omega_e)\, D^0 \Delta_r^0 \sin\theta^0 \, . \tag{5.3}$$

In the derivation of (5.3) it is assumed that Δ_r is approximately constant. It follows that for $n_r k_z c/\Omega_e > 1$ the rate of change in θ is on average larger for electrons with $0 < \theta^0 < \pi$ (i.e. electrons 2,3 and 4 of Fig. 4.12a) than for electrons with $\pi < \theta^0 < 2\pi$ (i.e. electrons 6, 7 and 8 of Fig. 4.12a). Hence, the electrons become phase bunched. This phase bunching occurs because the average axial velocity of an electron is dependent on its initial phase with respect to the wave fields. There is little net energy exchanged between the electrons and the wave because of the rapid rotation (at a frequency Δ_r) of the electrons with respect to the wave fields.

When the electrons enter the RIR i.e. when Δ_r becomes small, the bunch is able to resonate with the wave to produce amplification. During the amplification the electrons continue to become bunched via the RBM but become dispersed in $v_\perp$ and v_z. According to Helliwell's

(1967) phenomenological model, these phase-bunched electrons on emerging from the end of the TW radiate at their own natural frequency to produce the TE.

5.5 THE WHISTLER DISPERSION RELATION

The effects of the OBM are now included in the dispersion relation for a whistler. As stated previously the whistler is assumed to be propagating parallel to the magnetic field whose spatial variation is simulated by a temporal variation. In Section 5.5.2, this dispersion relation is evaluated for the specific case where the plasma has cold and energetic components, as assumed by Nunn (1971,1974), Karpman (1974) and Omura and Matsumoto (1982).

5.5.1 Generalized Dispersion Relation

Since a whistler propagating parallel to the magnetic field is right hand circularly polarized, the derivation of the dispersion relation is similar to that in Section 4.6 except that (i) the magnetic field is assumed to be slowly varying in time, and (ii) the electron distribution is allowed to have more than one component. The initial magnitude of Δ_r, $|\Delta_r^0|$, is assumed to be much greater than the initial growth rate i.e. $|\Delta_r^0| >> |\omega_i^0|$ (cf. Section 5.4.2). Because the TW is not necessarily growing, the contribution to the dispersion relation from the perturbed distribution, f_1, need not be exponentially small (as in Section 4.6) and must be retained if the evolution of the TW is to be determined self-consistently.

In order for ω and k_z to satisfy the usual dispersion relation (i.e. (4.11)) at t = 0, f_1 is assumed to have the form

$$f_1 = \sum_j 2\mu^0 (c/v_{\perp 0})\, \Omega_e^0 f_{0j} \cos\theta^0 \times [(1 - n_r v_{z0}/c) + (v_{\perp 0}^2/2c^2)(\Omega_e^0 - n_r k_z c)/\Delta_r^0]/\Delta_r^0 \qquad (5.4)$$

where f_{0j} is the unperturbed distribution of the jth electron component. On substitution of (4.62) and (5.4) into (4.61), the dispersion relation is found to be

$$\omega^2 - k_z^2 c^2 + \sum_j \omega_{pj}^2 \int d^3 v\, f_{0j} \left[\frac{(\omega - k_z v_z)}{\Delta} + \frac{v_\perp^2}{2c^2} \frac{(\omega\Omega_e - k_z^2 c^2)}{\Delta^2}\right]$$
$$= it \sum_j \omega_{pj}^2 \int d^3 v\, \frac{v_\perp^2}{2c^2} \frac{(\omega\Omega_e^0 - k_z^2 c^2)}{\Delta^0} X f_{0j} \qquad (5.5)$$

where $X = \exp(-i \int_0^t \Delta\, dt)$

The left hand side of (5.5) when equated to zero gives the usual time asymptotic dispersion relation. The right hand side of (5.5) arises from the secular term in $\langle(\cos\theta_0 - i\sin\theta_0)\, v_{\perp 0}\theta_1 f_0\rangle_{\underset{\sim}{x}}$ in (4.61) and represents the modification to the dispersion relation by the phase bunching via the OBM of the unperturbed distribution f_0. For a given t, the magnitude of this term increases with increasing $|v_\perp^2/\Delta_r^0|$. However, because X is oscillatory, this term phase mixes in a time inversely proportional to the variation of Δ_r over the distribution. Hence, enhanced growth via the OBM is possible only for distributions with a narrow velocity spread and with mean energy such that $\langle v_\perp\rangle \neq 0$ and

$\langle \Delta^0 \rangle_r$ is small, i.e. for a sufficiently anisotropic electron distribution.

The dependence of the growth rate on the anisotropy can be determined explicitly by writing (5.5) in the form

$$\omega^2 - k_z^2 c^2 + \pi \sum_j \omega_{pj}^2 \int dv_z \int v_\perp dv_\perp \left[(\omega - k_z v_z)\, v_\perp \frac{\partial f_{0j}}{\partial v_\perp} + k_z v_\perp^2 \frac{\partial f_{0j}}{\partial v_z} \right] / \Delta$$

$$= - \pi \sum_j \omega_{pj}^2 \int dv_z \int dv_\perp \left[(\omega - k_z v_z) \frac{\partial}{\partial v_\perp} \left(\frac{v_\perp^2 f_{0j}}{\Delta^0} \right) + k_z v_\perp \frac{\partial}{\partial v_z} \left(\frac{v_\perp^2 f_{0j}}{\Delta^0} \right) \right] X . \qquad (5.5')$$

(Equation (5.5) can be obtained from (5.5') by integration by parts.) The semirelativistic and nonrelativistic resistive-medium instabilities (cf. Section 4.2) are driven by the $\frac{\partial f_{0j}}{\partial v_\perp}$ and $\frac{\partial f_{0j}}{\partial v_z}$ terms respectively on the left hand side of (5.5'). Amplification due to the OBM is driven by the term $\frac{\partial}{\partial v_\perp} \left(\frac{v_\perp^2 f_{0j}}{\Delta^0} \right)$ for $\omega_r^2 >> k_z^2 c^2$ and by the term $\frac{\partial}{\partial v_z} \left(\frac{v_\perp^2 f_{0j}}{\Delta^0} \right)$ for $\omega^2 << k_z^2 c^2$.

Thus, in the case of whistlers the dominant contribution to amplification via the OBM comes from regions of the distribution where $\frac{\partial}{\partial v_z} \left(\frac{v_\perp^2 f_{0j}}{\Delta^0} \right)$ is large. This derivative can be large if the distribution has a beam-like component or if the distribution has a "knee" i.e. if the distribution has a step-like feature with respect to v_z.

5.5.2 Whistlers in a Plasma with Cold and Energetic Electron Components

The time-dependent whistler dispersion relation is now evaluated for a plasma with a cold component and a beam-like energetic component. If amplification by phase-random electron entering the RIR is effective then the growth rate for the amplification is given by time asymptotic theory. Amplification in this case is due to either a reactive - or

resistive - medium instability (cf. Sections 4.2 and 4.6). Conditions and growth rates for these instabilities are derived in Section 5.5.2.2. The growth rate for the amplification produced by the bunching of electrons by the OBM before their entry into the RIR is derived in Section 5.5.2.3. It is shown that under certain conditions the amplification due to the OBM can exceed that from the reactive - and resistive - medium instabilities.

5.5.2.1 *Evaluation of the Dispersion Relation*

The unperturbed cold and energetic components are assumed to be described respectively by

$$f_{0c}(v_\perp, v_z) = (2\pi v_\perp)^{-1}\, \delta(v_\perp)\, \delta(v_z) \tag{5.6}$$

and

$$f_{0E}(v_\perp, v_z) = f_\perp(v_\perp)\, f_z(v_z)$$

$$f_\perp = (2\pi v_{T\perp}^2 j!)^{-1}\, (v_\perp/\sqrt{2}\, v_{T\perp})^{2j} \exp(-v_\perp^2/2v_{T\perp}^2) \tag{5.7}$$

$$f_z = ((2\pi)^{1/2} v_T)^{-1} \exp(-(v_z - V_{z0})^2/2v_T^2)$$

where j is a positive integer. In the following, $V_\perp^2 := \int d^3\underset{\sim}{v}\, v_\perp^2 f_{0E} = 2(j+1)\, v_{T\perp}^2$. The energetic component reduces to a beam distribution with $\langle v_\perp \rangle \neq 0$ when $v_T,\ v_{T\perp} \to 0$, $j \to \infty$ and $\sqrt{j} v_{T\perp}$ remains constant.

For a whistler it can be assumed that $\omega < \Omega_e$ and $k_z^2 c^2 >> \omega^2$. In this case substitution of (5.6) and (5.7) into (5.5) yields the whistler dispersion relation

$$k_z^2 c^2 + \omega_{pc}^2 \omega/(\omega - \Omega_e) + \omega_{pc}^2 \frac{\delta n U}{n} = - \omega_{pc}^2 \frac{\delta n W}{n} \tag{5.8}$$

where

$$U = (1 - (j + 1) v_{T\perp}^2/v_T^2) + \left[\Omega_e - (j + 1) \frac{v_{T\perp}^2}{v_T^2} \bar{\Delta}\right] \frac{F_0(\bar{y}(t))}{i \sqrt{2} k_z v_T} , \tag{5.9}$$

$$W = \frac{1}{2} t k_z^2 V_\perp^2 \exp(- i \int_0^t \bar{\Delta} dt) \exp(- \beta_T^2) \frac{F_0(\bar{y}(0) + i\beta_T)}{\sqrt{2} k_z v_T} , \tag{5.10}$$

and where $\bar{\Delta}(t) = \Omega_e(t) = k_z V_{z0} - \omega(t)$, $\bar{y} = \bar{\Delta}/\sqrt{2} k_z v_T$, $\beta_T = k_z v_T t/\sqrt{2}$, $\delta n/n$ is the ratio of the densities of the energetic and cold electron components, ω_{pc} is the plasma frequency of the cold electron component and F_0 is the plasma dispersion function in the notation of Stix (1962, p. 179). Appropriate parameters in the region of the magnetosphere where the interaction is thought to occur (i.e. near the magnetic equator at four earth radii) are $\delta n/n << 1$, $\omega_{pc} \simeq 10 \Omega_{0E}$ and $\omega \simeq \frac{1}{2} \Omega_{0E}$ where $\Omega_{0E} = 2\pi \times 14$ kHz is the equatorial electron cyclotron frequency (e.g. Vomvoridis and Denavit, 1979; Omura and Matsumoto, 1982; Helliwell and Inan, 1982).

For $\delta n/n = 0$, (5.8) reduces to the cold plasma dispersion relation for whistlers (e.g. Dysthe, 1971)

$$\omega = \omega_0 := \Omega_e k_z^2 c^2/(k_z^2 c^2 + \omega_{pc}^2) . \tag{5.11}$$

For $\omega \simeq \frac{1}{2} \Omega_{0E}$, (5.11) implies that $k_z^2 c^2 \simeq \omega_{pc}^2$.

The low density energetic component causes a small shift in the frequency given by (5.11) and more importantly can lead to amplification of the wave via resistive - and reactive - medium instabilities (described by the term U) or via the OBM (described by the term W).

5.5.2.2 *Amplification due to Resistive - and Reactive - Medium Instabilities*

Consider first the case where the right hand side of (5.8) is negligible so that amplification is due to either a resistive - or reactive - medium instability. The reactive-medium instability applies when the axial velocity spread is sufficiently small. Specifically when

$$\left|\frac{k_z v_T}{\Omega_e}\right| \lesssim \left(\frac{\delta n}{8n}\ \frac{k_z^2 V_\perp^2}{\Omega_e^2}\right)^{1/3}, \tag{5.12}$$

the solutions to (5.8) for $\omega \simeq \frac{1}{2}\Omega_e$ and $\omega_{pc}^2 \simeq k_z^2 c^2$ (Section 5.5.2.1) correspond to $|\bar{y}| \gtrsim 1$; the imaginary part of U is then exponentially small and hence any growth due to a resistive-medium instability is negligible. The reactive-medium instability can occur when the frequency of the whistler, ω also satisfies the resonance condition $\bar{\Delta} \simeq 0$ i.e. when

$$\omega \simeq \omega_0 + \delta\omega$$

and

$$\omega_0 = \Omega_e k_z^2 c^2/(k_z^2 c^2 + \omega_{pc}^2) \simeq k_z V_{z0} - \Omega_e. \tag{5.13}$$

In this case, (5.8) reduces to

$$\frac{(k_z^2 c^2 + \omega_{pc}^2)(\delta\omega)^3}{\omega_0 - \Omega_e} + \omega_{pc}^2 \frac{\delta n}{n}\left(\Omega_e \delta\omega + \frac{1}{2} k_z^2 V_\perp^2\right) = 0. \tag{5.14}$$

On solving for $\delta\omega$, growth is found to occur only over a bandwidth of the order of $k_z^2 V_\perp^2/2\Omega_e^2$ and for

$$\frac{\delta n}{n} < \left(\frac{\delta n}{n}\right)_{crit} = 27\left(\frac{k_z^2 V_\perp^2}{2\Omega_e^2}\right)^2. \tag{5.15}$$

When $\delta n/n$ is much smaller than this critical value

$$\begin{aligned} \delta\omega &\simeq \left(-0.5 + i\frac{\sqrt{3}}{2}\right)\left(\frac{\delta n}{2n}\,\frac{\omega_{pc}^2 k_z^2 v_\perp^2 (\Omega_e - \omega_0)}{k_z^2 c^2 + \omega_{pc}^2}\right)^{1/3} \\ &\simeq \left(-0.5 + i\frac{\sqrt{3}}{2}\right)\left(\frac{\delta n}{8n}\, k_z^2 v_\perp^2 \Omega_e\right)^{1/3} \end{aligned} \tag{5.16}$$

for $\omega_{pc}^2 = k_z^2 c^2$ and $\omega \simeq \frac{1}{2}\Omega_e$.

When the inequality in (5.12) is reversed, the reactive-medium instability passes over into the resistive-medium instability (cf. Section 4.6.3). The growth rate in this case is given by

$$\omega_i \simeq \frac{\omega_{pc}^2}{k_z^2 c^2}\,\frac{\delta n}{n}\,\frac{(\Omega_e - \omega)}{\sqrt{2}k_z v_T}\left[\bar{\Delta}\,\frac{v_{T\perp}^2}{2v_T^2} - \Omega_e\right]\exp(-\bar{y}^2). \tag{5.17}$$

Growth occurs if

$$\bar{\Delta}\,\frac{v_{T\perp}^2}{2v_T^2} > \Omega_e \tag{5.18}$$

and damping occurs if the inequality is reversed.

It follows from the above that the plasma is stable to the reactive-medium instability if

$$\frac{\delta n}{n} \gtrsim \left(\frac{k_z^2 v_\perp^2}{2\Omega_e^2}\right)^2 \tag{5.19}$$

and stable to the resistive-medium instability if

$$|k_z v_T| \ll \frac{k_z^2 v_\perp^2}{2\Omega_e^2}\,. \tag{5.20}$$

5.5.2.3 *Amplification due to the OBM*

The modification to the dispersion relation (5.8) arising from the OBM, represented by the term W, can be considered as a transient response of the plasma. This is because on a time scale $t >> 1/\sqrt{2}|k_z|v_T$ the bunching arising from the OBM phase mixes to zero and the term W is negligible. Amplification due to the OBM can occur even when the plasma is stable to reactive - and resistive - medium instabilities, i.e. when conditions (5.19) and (5.20) are satisfied. In particular, suppose the term U in (5.8) is negligible, as is the case when $\sqrt{2}|k_z|v_T t \lesssim 1$ and conditions (5.19) and (5.20) are satisfied. On solving (5.8), the frequency of the TW and the growth rate due to the OBM are found to be given by

$$\omega_r = [\omega_{pc}^2 \frac{\delta n}{n} \mathrm{Im}(W)\ \omega_i + \Omega_e(k_z^2c^2 + \omega_{pc}^2 \frac{\delta n}{n} \mathrm{Re}(W))]/R \tag{5.21}$$

$$\omega_i = \frac{\omega_{pc}^2 \frac{\delta n}{n} \mathrm{Im}(W)\ \Omega_e[1 - (k_z^2c^2 + \omega_{pc}^2 \frac{\delta n}{n} \mathrm{Re}(W))/R]}{R + (\omega_{pc}^2 \frac{\delta n}{n} \mathrm{Im}(W))^2/R} \tag{5.22}$$

$$\mathrm{Im}(W) = -\frac{1}{2}\frac{V_\perp^2}{c^2}\frac{tk_z^2c^2}{\bar{\Delta}_r^0} \exp(-[\tfrac{1}{2}(k_z v_T t)^2 + \Pi_i t]) \cos(\bar{\Pi}_r t) \tag{5.23}$$

$$\mathrm{Re}(W) = -\frac{1}{2}\frac{V_\perp^2}{c^2}\frac{tk_z^2c^2}{\bar{\Delta}_r^0} \exp(-[\tfrac{1}{2}(k_z v_T t)^2 + \Pi_i t]) \sin(\bar{\Pi}_r t) \tag{5.24}$$

where $R = k_z^2c^2 + \omega_{pc}^2(1 + (\delta n/n)\ \mathrm{Re}(W))$, $\bar{\Pi}_r t = \int_0^t \bar{\Delta}_r\, dt$ and $\bar{\Delta}_r = \Omega_e + k_z V_{z0} - \omega_r$. If

$$|(\delta n/n)\ \mathrm{Re}(W)| \ll (k_z^2c^2 + \omega_{pc}^2)/\omega_{pc}^2 \tag{5.25}$$

then (5.21) and (5.22) reduce to

$$\omega_r = \omega_0 + \omega_{r1} \tag{5.21'}$$

$$\omega_{r1} = \frac{\delta n}{n} \frac{\omega_{pc}^2}{k_z^2 c^2 + \omega_{pc}^2} (\Omega_e - \omega)\, \mathrm{Re}(W)$$

$$\omega_i = \frac{\delta n}{n} \frac{\omega_{pc}^2}{k_z^2 c^2 + \omega_{pc}^2} (\Omega_e - \omega)\, \mathrm{Im}(W) \tag{5.22'}$$

where ω_0 is given by (5.11). When the amplitude of the TW is very much less than its initial amplitude (i.e. if $\Pi_i t << -1$), $|\mathrm{Re}(W)|$ can be very much larger than unity and the condition $\delta n/n << 1$ is not sufficient to ensure that the inequality (5.25) is satisfied.

The magnitude of the growth rate given by (5.22) or (5.22') increases in time but the sign of the growth rate is oscillatory (through its dependence on the term W). In terms of the physical model presented in Section 5.4.2, this corresponds to the electrons becoming increasingly phase bunched and rotating with respect to the wave fields. When $|\bar{\Delta}_r|$ becomes small i.e. when $|\bar{\Delta}_r| \lesssim |\omega_i|$ the bunch resonates with the wave and amplification occurs.

The magnitude of the growth rate also increases with increasing $(\delta n/n)(V_\perp^2/\Delta_r^0)$. This corresponds to the growth rate being an increasing function of the number of electrons being bunched (i.e. on $\delta n/n$) and on the rate at which they become bunched (i.e. on the magnitude of the perturbation in $\frac{d\theta}{dt}$ which, as given by (5.3), is proportional to $v_\perp^2/\Delta_r^0$ for $\omega_i^0 \simeq 0$).

5.6 FEATURES OF THE AMPLIFICATION AND TRIGGERING DUE TO THE OBM

A numerical example of the phase bunching and amplification due to the OBM using parameters thought to apply in the relevant region of the magnetosphere is presented in Section 5.6.1. In Section 5.6.2, general conditions are derived for the amplification of the TW due to the OBM. Conditions for triggering are also derived using Helliwell's (1967) phenomenological model and the results are compared with experimental observations.

5.6.1 A Specific Example

In the example of phase bunching and amplification due to the OBM, the following assumptions are made. The TW propagates in the negative z direction and the energetic electrons stream in the positive z direction. The plasma parameters are $V_{z0}/c = 5 \times 10^{-2}$, $\omega_{pc}^2/\Omega_{0E}^2 = 10^2$, Ω_{0E} (the equatorial cyclotron frequency) = $2\pi \times 14$ kHz (cf. Helliwell and Inan, 1982), $\delta n/n = 10^{-4}$, $v_T/c = 10^{-6}$ and $V_\perp^2/c^2 = 2 \times 10^{-5}$. The last three values have been chosen so that the energetic component has a similar number density and average perpendicular energy to the anisotropic component of the distribution about $v_z = V_{z0}$ reported by Edgar and Koons (1982).

The magnetic field as seen by the energetic electrons is assumed to have the form

$$B_0 = B_{0E}(1 + a(V_{z0}/c)^2 (\tau - \tau_s)^2) \qquad (5.26)$$

where $a = 8 \times 10^{-8}$, τ is the normalized time $\Omega_{0E}t$ and $\tau_s = 1.2 \times 10^4$ (cf. Omura and Matsumoto, 1982). The time τ_s/Ω_{0E} is that taken by an

electron with $v_z = V_{z0}$ and initially at the front of the wave to reach the magnetic equator. The initial wave amplitude is assumed to be 10^{-6} of the equatorial magnetic field, consistent with the observations of Inan et al. (1977).

The wave number k_z of the TW is assumed to be - 9.98 Ω_{0E}/c so that $\omega \simeq \frac{1}{2} \Omega_{0E}$. For these parameters, $\bar{\Delta}_r$ is initially 1.6×10^{-2} Ω_{0E} and decreases to a minimum of approximately 2×10^{-3} Ω_{0E} at $\tau = \tau_s$ i.e. at the magnetic equator. A non-zero value of $\bar{\Delta}_r(\tau_s)$ has been chosen to illustrate that effective amplification can occur for $\bar{\Delta}_r(\tau_s)$ small but not necessarily zero. Also, for these parameters, the plasma is stable to reactive - and resistive - medium instabilities (i.e. conditions (5.19) and (5.20) are satisfied and the term U in (5.8) is negligible).

Fig. 5.7 shows the temporal evolution of the normalized wave amplitude, $A = \exp(\Pi_i t)$. It can be seen that the normalized amplitude oscillates about a mean value of unity for $\tau \lesssim 6 \times 10^3$. As discussed in Sections 5.4.2 and 5.5.2.3, these oscillations represent the bunching and rotation of the bunched electrons with respect to the wave fields in the OIR. The magnitude of these oscillations increases as the electrons become increasingly phase bunched.

As τ increases and $\bar{\Delta}_r(\tau)$ decreases, the electrons enter the RIR where they resonate with the TW to produce net amplification. The average growth rate for the amplification in Fig. 5.7 is about 150 dB/s. This growth rate is comparable to that inferred from the observations of Helliwell and Katsufrakis (1974, Fig. 5.3).

Fig. 5.8 shows the temporal evolution of a group of 20 electrons with $v_{\perp 0} = V_\perp$, $v_{z0} = V_{z0}$ and initially uniformly distributed in θ,

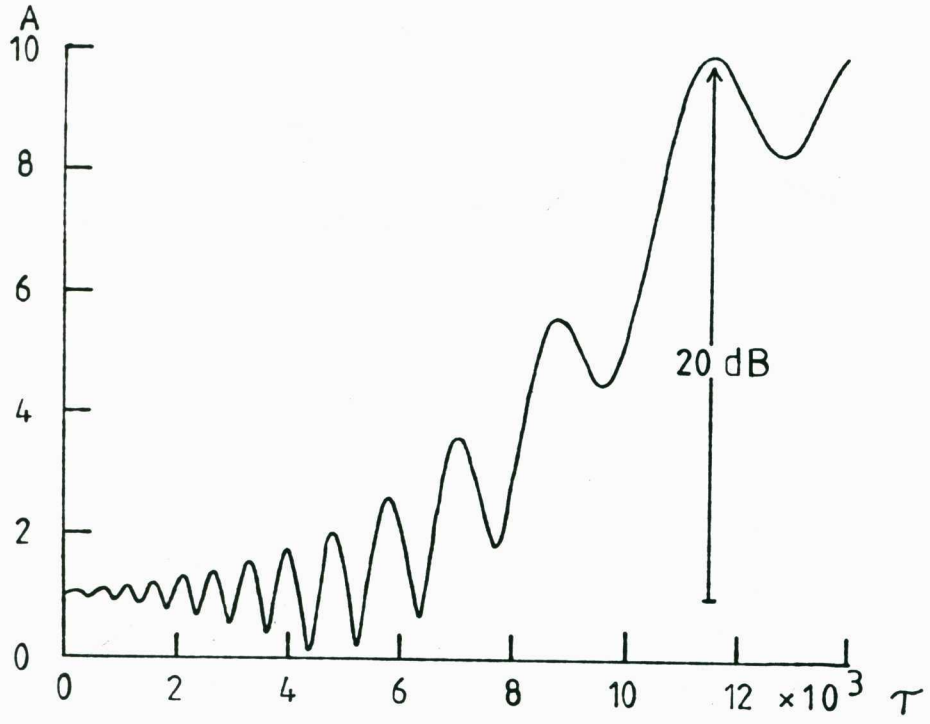

Fig. 5.7 The temporal evolution of the normalized wave amplitude, $A = \exp(\Pi_i t)$. For $\tau \lesssim 6 \times 10^3$, there is little net amplification of the wave. During this period the electrons are becoming increasingly bunched. This is represented by the increasing magnitude of the oscillations of the amplitude. For $\tau \gtrsim 6 \times 10^3$, $|\bar{\Delta}_r|$ is sufficiently small to allow the bunched electrons to resonate and amplify the wave.

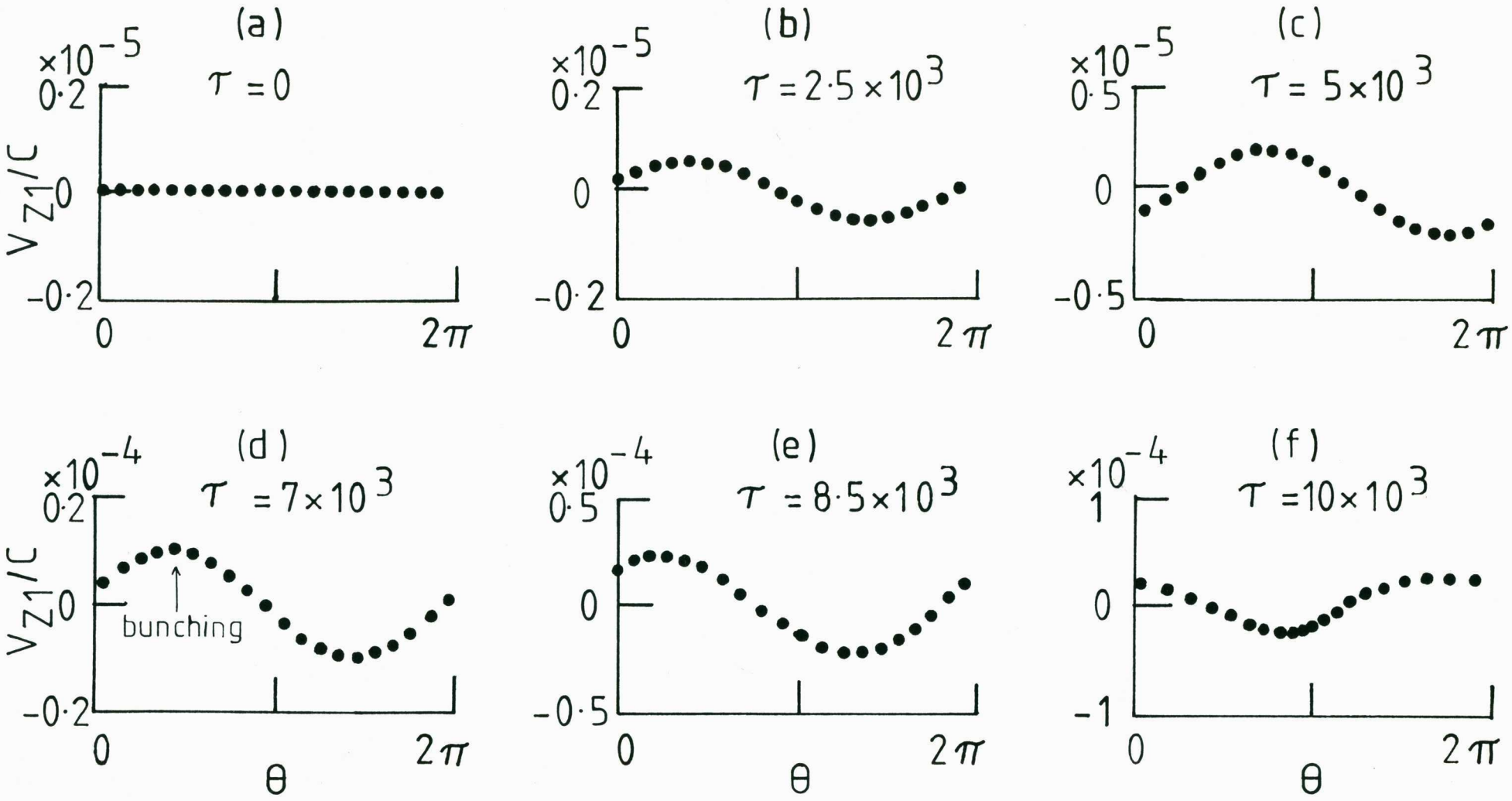

Fig. 5.8 (continued)

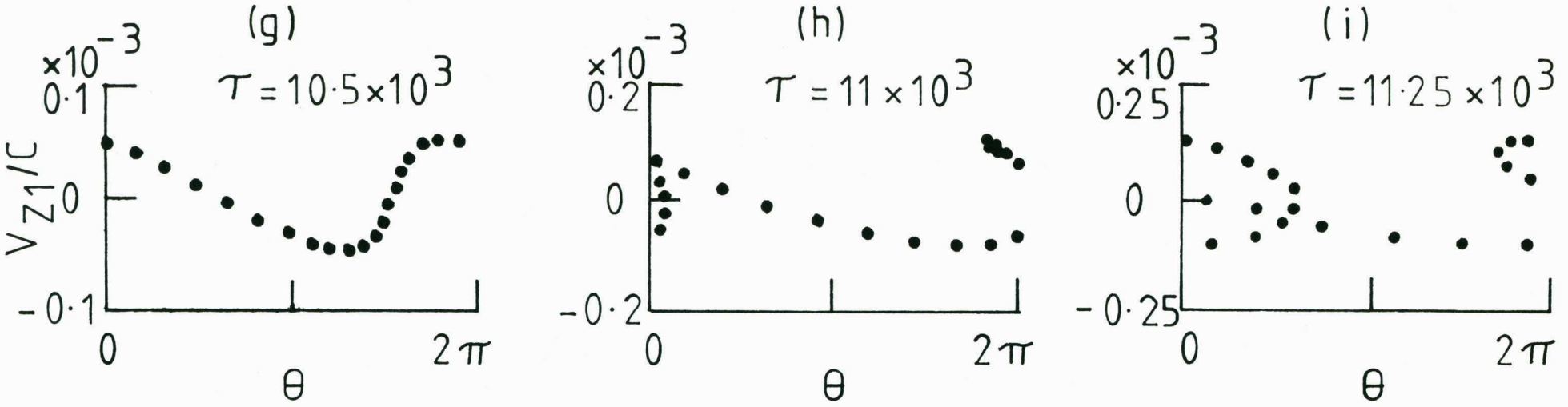

Fig. 5.8 (continued) The temporal evolution of a group of 20 electrons with $v_{\perp 0} = V_\perp$, $v_{z0} = V_{z0}$ and initially uniformly distributed in θ during their interaction with the wave fields given in Fig. 5.7. Fig. (a) shows the initial distribution. The bunching first becomes evident for $\tau \simeq 7 \times 10^3$ (Fig. d). Bunching is also present for smaller τ but cannot be seen due to the coarseness of the scale. As the electrons amplify the TW, they continue to bunch in θ but become spread in v_z (Figs. e-h) and $v_\perp$ (which is not shown). In Fig. (i) the perturbation in θ due to the wave fields is of order unity and linear theory is no longer valid.

during their interaction with the wave fields given in Fig. 5.7. (The electron trajectories were determined self-consistently from (4.42)-(4.44), (5.21) and (5.22).) Bunching is present at all times but is not evident until $\tau = 7 \times 10^3$ (Fig. 5.8d) because of the smallness of the initial wave amplitude and the coarseness of the scale. During the amplification of the TW, the electrons continue to bunch in θ via the RBM but become spread in v_z and $v_\perp$ (Figs. 5.8e-h).

In Fig. 5.8i, $|\theta_1|$ is of order unity for some of the electrons so that linear theory is no longer valid and nonlinear effects must be included. The actual time at which these nonlinear effects become important depends on the initial wave amplitude.

Similar phase distributions (and oscillations in the wave amplitude) were also obtained by Sprangle and Drobot (1977) and Sprangle and Smith (1980) in their studies of the azimuthal bunching instability. They found that amplification saturates when nonlinear effects become important.

Fig. 5.9 shows the temporal evolution of the real part of the frequency for the wave fields shown in Fig. 5.7. The frequency has two components. The first component is non-oscillatory and is due to the variation of the magnetic field. This component is represented by the dashed line which shows ω_0 (i.e. (5.11)) as a function of time. The second component is oscillatory and, like the oscillations in the amplitude, is due to the bunching and rotation of the bunched electrons with respect to the wave fields. The period of these oscillations increases as the magnitude of the frequency mismatch $|\bar{\Delta}_r|$ decreases.

The magnitude of the frequency shift due to the bunched electrons (i.e. $\omega - \omega_0$) becomes large when the wave amplitude becomes very

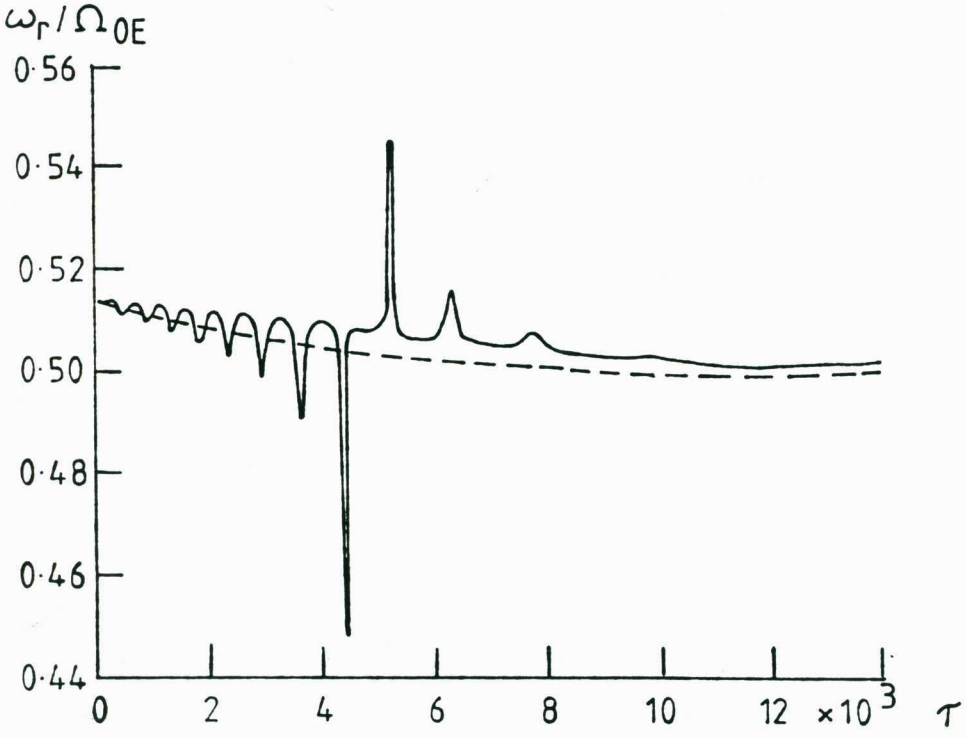

Fig. 5.9 The temporal evolution of the real part of the frequency for the wave fields shown in Fig. 5.7. The dashed line shows the real part of the frequency when there is no energetic component. The phase bunching of the energetic component gives the frequency an oscillatory component with large frequency shifts occurring when the wave amplitude becomes very small i.e. at $\tau = 4.4 \times 10^3$ and 5.3×10^3.

small or "null". This occurs in Figs. 5.7 and 5.9 at $\tau = 4.4 \times 10^3$ and 5.3×10^3. (Although the frequency is sharply peaked during these periods, the assumption of a slowly varying frequency is still valid since $|\frac{d\omega_r}{dt}|, |\frac{d\omega_i}{dt}| \lesssim |\omega_i^2 + \Delta_r^2|$.) These nulls arise when phase-bunched electrons enter a region of the wave fields where they gain sufficient energy from the wave to cause the wave amplitude to become small. The wave amplitude does not remain small because the electrons, being bunched, reradiate the energy.

Helliwell and Inan (1982) also observed nulls in their feedback oscillator model. They attributed pretermination triggering to nulls on the basis that a null resembles the end of the TW which is known to cause triggering.

5.6.2 Conditions for Amplification and Triggering

Amplification due to the OBM must occur within a time period less than about $t_d (= \sqrt{2}/|k_z| v_T)$ otherwise the current arising from the bunching phase mixes to zero due to the variation of Δ_r over the distribution. Further, net amplification occurs only in a region where $|\bar{\Delta}_r| \lesssim |\omega_i|$ (Section 5.5.2.3).

Thus, a criterion for net wave amplification is that

$$T = |\frac{\omega_i(t_B)}{\bar{\Delta}_r(t_B)}| \simeq |\frac{\omega_{pc}^2}{\omega_{pc}^2 + k_z^2 c^2} \frac{\delta n}{n} \frac{\omega_r(t_B) - \Omega_e(t_B)}{\bar{y}^0 \bar{\Delta}_r(t_B)} \frac{V_\perp^2}{2v_T^2} \frac{t_B}{t_d}| \gtrsim 1 \qquad (5.27)$$

where $t_B (\lesssim t_d)$ is the time the electrons are in the OIR and $\bar{y}^0 = \bar{\Delta}_r^0 / \sqrt{2} k_z v_T$. Equation (5.27) is valid only when $|\bar{y}^0| \gtrsim 1$. This inequality applies when the conditions (5.19) and (5.20) for the plasma to be stable to reactive - and resistive - medium instabilities are

satisfied. If $|\bar{y}^0| << 1$ then the term $\bar{y}^0$ in (5.27) must be replaced by $(2\bar{y}^0)^{-1}$ so that T is at a maximum when $|\bar{y}^0| \simeq 1$. Criterion (5.27) must be satisfied for a period greater than about $1/|\omega_i|$ if amplification of several dB is to occur.

Conditions for amplification are most favourable when both the phase bunching in the OIR and the time the electrons are in the RIR are at a maximum i.e. when $t_B/|\bar{\Delta}_r^0|$ is large and $\bar{\Delta}_r$ and $|\frac{d\bar{\Delta}_r}{dt}|$ for $t \gtrsim t_B$ are small. These conditions are analogous to Helliwell's (1967) "consistent-wave condition" (Section 5.3.2).

From (5.22') and (5.27), the following properties of the amplification and triggering of discrete VLF emissions can be deduced.

(a) If the energetic component has a Maxwellian distribution the whistler is stable; this is because $\delta n/n << 1$, $\omega_p^2 \simeq k_z^2 c^2$, $V_\perp^2 = 2v_T^2$ and $\bar{y}^0 \gtrsim 1$ imply $T << 1$.

(b) Amplification is favoured when the energetic component has a small velocity spread and a streaming velocity such that $\bar{\Delta}_r \simeq 0$ near the equator.

(c) For given plasma parameters, T increases with increasing t_B so that triggering is more likely for dashes than dots. This is consistent with the dash-dot anomaly (Helliwell et al., 1964).

(d) The growth rate is independent of the initial wave amplitude so that triggering can be induced by both high power and low power transmissions. The threshold effect observed by Helliwell et al. (1980) is attributed here to the presence of background noise of similar amplitude to the TW. This noise

reduces the coherence of the total signal and thereby prevents phase bunching.

(e) Amplification and triggering occur only for those frequencies and in those regions where $|\bar{\Delta}_r^0|$ and $|\frac{d\bar{\Delta}_r}{dt}|$ are small. These conditions imply that maximum amplification occurs when $|\bar{\Delta}_r|$ is at a minimum near the magnetic equator (i.e. $|\bar{\Delta}_r^0| > |\Delta_r(t_B)|$, $\frac{d\bar{\Delta}_r}{dt}|_{t_B} \simeq 0$) and the front and back ends of the TW are on opposite sides of the magnetic equator. In this case, Helliwell's (1967) phenomenological model implies that long TW's are more likely to trigger risers and short TW's fallers. Further, the bandwidth in which $\bar{\Delta}_r^0$ and $|\frac{d\bar{\Delta}_r}{dt}|$ are small is narrow. These features are consistent with the observations of Helliwell and Katsufrakis (1974).

(f) A change of only a few per cent in either V_{z0} or Ω_e (arising possibly from changes in the position of the duct guiding the TW) is required to change T from above threshold to below threshold (and vice-versa). This can produce the intermittent amplification and triggering observed by McPherson et al. (1974), Stiles and Helliwell (1977), Dowden (1981) and Park (1981).

(g) The bandwidth in which criterion (5.27) is satisfied increases with increasing $(\delta n/n)(V_\perp^2/c^2)$ i.e. with increasing density and perpendicular energy of the energetic component. The growth rate also increases with $(\delta n/n)(V_\perp^2/c^2)$.

(h) The amplification saturates if (i) $\bar{\Delta}_r^2$ exceeds ω_i^2, (ii) the time of interaction exceeds $1/|k_z|\ v_T$ or (iii) the number density of the interacting electrons decreases (e.g. due to particle precipitation) to below the threshold given by (5.27). Saturation

is also expected to occur when the amplitude becomes sufficiently large so that the nonlinear effects become important (e.g. Sprangle and Smith, 1980).

5.7 SUMMARY AND DISCUSSION

In the theory for discrete VLF emissions presented here, amplification and triggering is attributed to resonant interactions between the TW and phase bunched electrons. The interaction is envisaged to occur in two stages and for convenience these two stages are regarded as occurring in two spatially adjoint regions called the OIR and the RIR. In the OIR where $|\Delta_r| \gtrsim |\omega_i|$, the front of the TW phase bunches electrons without significant energy exchange between the TW and the electrons. As the electrons move through the magnetosphere Δ_r changes due to the inhomogeneity of the geomagnetic field. The bunched electrons then resonantly interact with a later portion of the TW (in the RIR) to produce amplification. On emerging from the end of the TW, the bunched electrons radiate to produce the TE as in Helliwell's (1967) phenomenological model.

An important new idea in the theory is the relaxation of the time asymptotic assumption in evaluating the plasma response. The bunching in the OIR phases mixes to zero on a time scale inversely proportional to the variation of Δ_r over the interacting electrons and its effects would therefore be excluded if time asymptotic theory were used. Put another way, the phase bunching is a transient effect. The amplification, however, occurs on a timescale shorter than that over which phase mixing would cause the initial phase bunching to be destroyed. Being a transient, this effect is not described by time asymptotic theory.

This theory supplies the unspecified phase-bunching mechanism assumed in Helliwell's (1967) phenomenological model for the various spectral forms of TE. The theory also overcomes fundamental objections to existing theories. Theories which appeal to growth in the usual time-asymptotic limit imply that background noise should be amplified and that this growth should be independent of the phase of the wave. Observations are not consistent with this and seem to require that amplification occur only in a narrow frequency range about the frequency of the TW (Sections 5.2.2 and 5.3.1). Theories which appeal to nonlinear effects, notably quasi-linear diffusion and trapping, require the amplitude of the TW to exceed some threshold before the nonlinear effects become significant (Section 5.3.3). Observations indicate that amplification and triggering can occur when the TW has an amplitude well below this threshold (Section 5.2.2.2). In the theory presented here, enhanced growth about the frequency of the TW is attributed to the phase bunching of untrapped electrons by the TW. This theory is linear in the wave amplitude. A condition for it to produce amplification is that the amplitude be well above the noise level otherwise the noise affects the coherence of the signal and prevents phase bunching.

Both the inhomogeneity of the geomagnetic field and the bunching of electrons are important in the theory. The inhomogeneity limits the width of the RIR. Amplification by a phase random group of electrons entering the RIR is ineffective if the corresponding growth rate is much less than the reciprocal of the time to traverse the RIR. If instead the electrons are phase bunched on entering the RIR they all lose or gain energy (depending on their phase). The corresponding growth

rate can be much larger than for a phase random group where approximately half the electrons lose energy and half gain energy.

Effective amplification of the TW by bunching of electrons in the OIR prior to their entry into the RIR requires (a) an electron distribution with a component which has a narrow axial velocity spread and a mean energy such that $\langle v_\perp \rangle \neq 0$ and $\langle \Delta_r^0 \rangle$ is small (i.e. a component where $\frac{\partial}{\partial v_z} (\frac{v_\perp^2 f}{\Delta_r^0})$ is large) and (b) that the frequency and duration of the TW satisfy criterion (5.27). Amplification can occur in a plasma which is stable to both time independent reactive - and resistive - medium instabilities (Section 5.5.2.2). This may explain the observation that amplification and triggering can occur in the absence of other detectable VLF emissions in ground-based recordings (Section 5.4.2).

A weakness in the existing form of the theory is that the magnetic field as seen by an electron interacting with the TW is simulated by a temporally varying magnetic field. In a more realistic theory, the magnetic field should be spatially inhomogeneous and the electrons and the TW should move through the spatial inhomogeneity. The details of the evolution of the wave packet may not be treated adequately by the present theory since it describes the amplification arising from interactions in only one region of the magnetosphere. Further work is required to include contributions to the amplification from all points along the propagation path of the TW.

The model is also limited by the neglect of nonlinear effects such as electron trapping and electron diffusion in velocity space. The view adopted here is that these processes are unimportant in the actual phase bunching and amplification mechanisms and they become important only as saturation mechanisms.

In conclusion, the theory presented here complements Helliwell's (1967) phenomenological model for triggering of discrete VLF emissions by providing a mechanism which allows enhanced narrow-band wave growth due to phase bunching of electrons by the TW. Existing theories do not describe this bunching and nonlinear theories require a threshold which is inconsistent with observational data. The essentially new feature is the relaxation of the time asymptotic assumption in evaluating the linear response of the plasma. This introduces a new phenomenon, off-resonant bunching of electrons, which in the theory presented here, eventually gives rise to amplification and triggering. Although several aspects of the theory need to be examined in greater detail, this bunching seems likely as the basic mechanism for the amplification and triggering of discrete VLF emissions.

APPENDICES

APPENDIX A

DERIVATION OF THE AMPLITUDE REFLECTION COEFFICIENT FOR $M^2 \gtrsim 1$

In this Appendix, the amplitude reflection coefficient for the magnetosonic wave is evaluated using the method of matched asymptotic solutions (Nayfeh, 1973) to analytically continue the solutions to the wave equation (Section 3.3.2) through the density gradient.

The asymptotic expansions of the confluent hypergeometric function, ${}_1F_1$, the logarithmic hypergeometric function and the Airy functions are, respectively (Budden, 1961; Luke, 1969)

$$ {}_1F_1(a;c;z) \simeq \frac{\Gamma(c)}{\Gamma(c-a)} \left(z^{-1} e^{i\epsilon\pi}\right)^a + \frac{\Gamma(c)}{\Gamma(a)} e^z z^{a-c} \tag{A.1} $$

$$ g(a;c;z) \simeq (-)^{m+1} m!\, \Gamma(a-m) z^{-a} \qquad |\arg(z)| < \frac{\pi}{2} \tag{A.2} $$

$$ \simeq e^z g(c-a;c;-z) - \frac{\pi e^{-i\pi\epsilon a}}{\sin(\pi a)} {}_1F_1(a;c;z) \qquad \frac{\pi}{2} \lesssim |\arg(z)| < \pi $$

$$ \mathrm{Ai}(z) \simeq \frac{1}{2}\pi^{-1/2} z^{-1/4} \exp\left(-\frac{2}{3}z^{3/2}\right) \qquad -\frac{2}{3}\pi \lesssim \arg(z) \lesssim \frac{2}{3}\pi \tag{A.3} $$

$$ \simeq \frac{1}{2}\pi^{-1/2} z^{-1/4} \left\{\exp\left(-\frac{2}{3}z^{3/2}\right) + i\exp\left(\frac{2}{3}z^{3/2}\right)\right\} $$

$$ \frac{2}{3}\pi \lesssim \arg(z) \lesssim \frac{4}{3}\pi $$

$$\mathrm{Bi}(z) \simeq \frac{1}{2}\pi^{-1/2}z^{-1/4}\{i\exp(-\frac{2}{3}z^{3/2}) + 2\exp(\frac{2}{3}z^{3/2})\} \qquad 0 \leq \arg(z) \leq \frac{2}{3}\pi \tag{A.4}$$

$$\simeq \frac{1}{2}\pi^{-1/2}z^{-1/4}\{-i\exp(-\frac{2}{3}z^{3/2}) + \exp(\frac{2}{3}z^{3/2})\} \qquad \frac{2}{3}\pi \leq \arg(z) \leq \frac{4}{3}\pi$$

where Γ is the gamma function, $|z| >> 1$, $m = c - 1$, $\epsilon = 1$ if $\mathrm{Im}(z) > 0$ and $\epsilon = -1$ if $\mathrm{Im}(z) < 0$ and $|a| < 1$.

Using (A.1) - (A.4), the asymptotic expansions of (3.37) - (3.39) are

$$E_{Y1}^{(0)} \simeq \frac{\eta^{1/2}e^{-\nu\eta}}{\Gamma(1-a_R)}(2\nu\eta e^{-i\pi})^{-a_R} + \frac{\eta^{1/2}e^{\nu\eta}(2\nu\eta)^{a_R-1}}{\Gamma(a_R)} \qquad 2\nu\eta << -1 \tag{A.5}$$

$$\simeq \frac{\eta^{1/2}e^{-\nu\eta}}{\Gamma(1-a_R)}(2\nu\eta e^{i\pi})^{-a_R} + \frac{\eta^{1/2}e^{\nu\eta}(2\nu\eta)^{a_R-1}}{\Gamma(a_R)} \qquad 2\nu\eta >> 1$$

$$E_{Y2}^{(0)} \simeq -\eta^{1/2}e^{-\nu\eta}\Gamma(a_R)(2\nu\eta)^{-a_R} \qquad |2\nu\eta| >> 1 \tag{A.6}$$

$$E_{Y1}^{(1)} \simeq \xi^{-1/2}\exp(\xi) \qquad |\xi| >> 1 \tag{A.7}$$

$$E_{Y2}^{(1)} \simeq \frac{1}{2}\xi^{-1/2}\exp(\xi) - \xi^{1/2}\exp(-\xi) \qquad |\xi| >> 1 \tag{A.8}$$

$$E_{Y1}^{(T)} \simeq \frac{1}{2}\pi^{-1/2}(-\lambda_M)^{-1/6}(\rho(\eta))^{-1/4}\exp(-\frac{2}{3}\lambda_M(-\phi)^{3/2}) \qquad \eta < \eta_T \tag{A.9}$$

$$\simeq \frac{1}{2}\pi^{-1/2}(-\lambda_M)^{-1/6}(\rho(\eta))^{-1/4}\{\exp(-\frac{2}{3}\lambda_M(-\phi)^{3/2}) + i\exp(\frac{2}{3}\lambda_M(-\phi)^{3/2})\} \qquad \eta > \eta_T. \tag{A.10}$$

The WKB solutions in the region $\delta^0 < \eta < 1 - \delta^1$ have the form

$$E_{Y-}^{(0)} = (-\lambda_M^2\rho(\eta))^{-1/4} \exp(-\lambda_M \int_{\delta^0}^{\eta} \sqrt{-\rho(\eta)}d\eta) \tag{A.11}$$

$$E_{Y+}^{(0)} = (-\lambda_M^2\rho(\eta))^{-1/4} \exp(\lambda_M \int_{\delta^0}^{\eta} \sqrt{-\rho(\eta)}d\eta). \tag{A.12}$$

These WKB solutions reduce to

$$E_{Y-}^{(0)} = (\nu)^{-1/2}\eta^{1/2-a_R} \exp(-\nu\eta) \tag{A.13}$$

$$E_{Y+}^{(0)} = (\nu)^{-1/2}\eta^{a_R-1/2} \exp(\nu\eta) \tag{A.14}$$

for $\eta \simeq \delta^0$ and to

$$E_{Y-}^{(0)} \simeq \sigma_M^{-1/2}|\eta-1|^{1/2} \exp(-\lambda_M \int_{\delta^0}^{1-\delta^1} \sqrt{-\rho(\eta)}d\eta) \exp(-\xi) \tag{A.15}$$

$$E_{Y+}^{(0)} \simeq \sigma_M^{-1/2}|\eta-1|^{-1/2} \exp(\lambda_M \int_{\delta^0}^{1-\delta^1} \sqrt{-\rho(\eta)}d\eta) \exp(\xi) \tag{A.16}$$

for $\eta \simeq 1 - \delta^1$.

The WKB solutions in the region $1 + \delta^1 < \eta < \eta_T$ have the form

$$E_{Y-}^{(1)} = (-\lambda_M^2\rho(\eta))^{-1/4} \exp(-\lambda_M \int_{1+\delta^1}^{\eta} \sqrt{-\rho(\eta)}d\eta) \tag{A.17}$$

$$\simeq \sigma_M^{-1/2}(\eta-1)^{1/2} \exp(-\xi) \qquad |\eta - (1+\delta^1)| \lesssim \delta^1$$

$$E_{Y+}^{(1)} = (-\lambda_M^2\rho(\eta))^{-1/4} \exp(\lambda_M \int_{1+\delta^1}^{\eta} \sqrt{-\rho(\eta)}d\eta) \qquad (A.18)$$

$$\simeq \sigma_M^{-1/2}(\eta-1)^{-1/2} \exp(\xi) \qquad |\eta - (1+\delta^1)| \lesssim \delta^1.$$

By matching the asymptotic forms (A.5) - (A.18), the WKB solution which is finite for $\lambda_M\eta << -1$ is found to have the form

$$E_Y = E_{Y2}^{(0)} + \frac{\pi\exp(-i\pi a_R)}{\sin(\pi a_R)} E_{Y1}^{(0)} \qquad \eta \simeq 0$$

$$= a_1 E_{Y-}^{(0)} + a_2 E_{Y+}^{(0)} \qquad \delta^0 < \eta < 1 - \delta^1$$

$$= -ia_1 \exp(-\lambda_M \int_{\delta^0}^{1-\delta^1}) E_{Y-}^{(1)} \qquad 1 + \delta^1 < \eta < \eta_T$$

$$+ ia_2 \exp(\lambda_M \int_{\delta^0}^{1-\delta^1}) E_{Y+}^{(1)}$$

$$= b_1 E_{Y1}^{(T)} + b_2 E_{Y2}^{(T)} \qquad \eta \gtrsim \eta_T \qquad (A.19)$$

where

$$a_1 = \nu^{1/2}(2\nu)^{a_R} \Gamma(a_R)[-1 + \exp(-2\pi a_R i)]$$

$$a_2 = \nu^{1/2}(2\nu)^{a_R-1} \Gamma(1-a_R) \exp(-i\pi a_R)$$

$$b_2 = -i\pi(-\lambda_M)^{-1/3} a_1 \exp(-\chi)$$

$$b_1 = i\pi(-\lambda_M)^{-1/3} a_2 \exp(\chi) - ib_2$$

$$\int_{\delta 0}^{1-\delta^1} = \int_{\delta 0}^{1-\delta^1} \sqrt{-\rho(\eta)}\, d\eta$$

$$\chi = \lambda_M \left(\int_{\delta 0}^{1-\delta^1} + \int_{1+\delta^1}^{\eta_T} \right).$$

From (A.19) the amplitude reflection coefficient is found to have the form

$$R = \left| \frac{b_1 + ib_2}{b_1 - ib_2} \right| = \left| 1 + i\theta_M \exp(-2\chi) \right|^{-1} \qquad \text{(A.20)}$$

where

$$\theta_M = (2\nu)^{-\alpha/\nu} (\Gamma(a_R)/\Gamma(1-a_R)) \exp(i\pi a_R) \, [-1 + \exp(-i2\pi a_R)].$$

APPENDIX B

EVALUATION OF THE INTEGRAL $I_{m,1}$

The purpose of this Appendix is to evaluate the integral $I_{m,1}$ which appears in the dielectric tensor (Section 4.3). The distribution is assumed to have the form given by (4.19) except that it is generalized to include a streaming velocity parallel to the magnetic field i.e. f_z in (4.20) is replaced by

$$f_z = \left((2\pi)^{1/2} v_T\right)^{-1} \exp\left(-(v_z - V_{z0})^2/2v_T^2\right) . \tag{B.1}$$

In this case, $I_{m,1}$ reduces to

$$I_{m,1} = -\pi \int_0^\infty v_\perp dv_\perp \int_{-\infty}^\infty dv_z \frac{\{2j(\omega - k_z v_z) - (v_\perp^2/v_T^2)(\omega - k_z V_{z0})\} f (k_\perp v_z/\Omega_e)^m}{\omega - \Omega_e(1 - v^2/2c^2) - k_z v_z}$$

$$= \frac{c^2}{v_T^2} \left(\frac{k_\perp}{\Omega_e}\right)^m \left\{\frac{\omega - k_z V_{z0}}{\Omega_e} (j + 1)\, Je_{j+2,m} - \frac{\omega}{\Omega_e} j\, Je_{m+1,m} \right.$$

$$\left. + j(k_z/\Omega_e)\, Je_{m+1,m+1}\right\} \tag{B.2}$$

where

$$Je_{n,m} = \int_{-\infty}^\infty dv_z\, v_z^m\, f_z \exp(\Gamma_e)\, E_n(\Gamma_e)$$

$$= a_J\left((2\pi)^{1/2} v_T\right)^{-1} \int_{-\infty}^\infty dv_z\, v_z^m\, E_n \exp(-\sigma_v v_z) \tag{B.3}$$

$$\Gamma_e = c^2\{(\omega - \Omega_e - k_z v_z)/\Omega_e + v_z^2/2c^2\}/v_T^2$$

$$a_j = \exp\{c^2(\omega - \Omega_e)/(v_T^2\Omega_e) - V_{z0}^2/2v_T^2\}$$

$$\sigma_v = c(k_z c/\Omega_e - V_{z0}/c)/v_T^2$$

and E_n is the nth exponential integral (Gautschi and Cahill, 1970).

It can be shown using integration by parts that the Je functions are related as follows

$$Je_{n,0} = Je_n \tag{B.4}$$

$$Je_{n,1} = w(Je_n - Je_{n+1}) + V_{z0}Je_{n+1} \tag{B.5}$$

$$Je_{n,2} = v_T^2 Je_{n+1} + w^2(Je_n - 2Je_{n+1} + Je_{n+2}) + 2V_{z0}\, w(Je_{n+1} - Je_{n+2}) + V_{z0}^2 Je_{n+2} \tag{B.6}$$

$$Je_{n,3} = w^3(Je_n - 3Je_{n+1} + 3Je_{n+2} - Je_{n+3}) + (V_{z0}/c)\, w^2(2Je_{n+1} - 6Je_{n+2} + 3Je_{n+3}) + 3V_{z0}^2 c\, w(Je_{n+2} - Je_{n+3}) + V_{z0}^3\, Je_{n+3} + v_T^2(2w(Je_{n+1} - Je_{n+2}) + 2V_{z0}\, Je_{n+2}) \tag{B.7}$$

where

$$Je_n = \sum_{i=0}^{n-1} (-)^i\, C_{i,n} A_{n-i} \left(\frac{v_T}{c}\,\frac{\Omega_e}{k_z c}\right)^{2i} \Big/ \left(1 - \frac{\Omega_e}{k_z c}\,\frac{V_{z0}}{c}\right)^{n+i} \tag{B.8}$$

$$A_n = \left((2\pi)^{1/2}\, v_T\right)^{-1} \int_{-\infty}^{\infty} dv_z \left(1 - \frac{v_z}{c}\,\frac{\Omega_e}{k_z c}\right)^n \Gamma_e^{-1} \exp\left(-(v_z - V_{z0})^2/2v_T^2\right) \tag{B.9}$$

$$C_{0,n} = 1$$

$$C_{i,n} = (n - i)\, C_{i-1,n} + C_{i,n-1}$$

$$w = k_z c^2/\Omega_e .$$

The function, A_n, has the recursion relation

$$A_n = \left(\frac{\Omega_e}{k_z c}\right)^2 \frac{u_e^2}{c^2} A_{n-2} + \left(\frac{v_T}{c}\frac{\Omega_e}{k_z c}\right)^2 \int_{-\infty}^{\infty} dv_z\, f_z\, 2\left(1 - \frac{\Omega_e}{k_z c}\frac{v_z}{c}\right)^{n-2}$$

$$A_0 = \frac{i}{\sqrt{2}}\frac{v_T}{u_e}\,(F_{0+} - F_{0-})$$

$$A_1 = -\frac{i}{\sqrt{2}}\frac{v_T}{c}\frac{\Omega_e}{k_z c}\,(F_{0+} + F_{0-}) \qquad \text{(B.10)}$$

where $F_{0\pm}$ are described by (4.32) except that $\alpha_\pm$ must now be replaced by

$$\alpha'_\pm = (w - V_{z0} \pm u_e)/\sqrt{2}\, v_T . \qquad \text{(B.11)}$$

APPENDIX C

THE WHISTLER DISPERSION RELATION FOR A SPATIALLY INHOMOGENEOUS MAGNETIC FIELD

In this Appendix, the dispersion relation is derived for a whistler propagating parallel to a magnetic field directed along the z axis. It is assumed that the magnetic field is a function of z and that the plasma has cold and energetic components. The energetic component is assumed to be streaming in the positive z direction and in the opposite direction to the whistler.

The derivation is similar to that in Sections 4.6 and 5.5 except that the whistler wave fields in the spatial inhomogenity are assumed to be described by

$$\begin{aligned} \underset{\sim}{E} &= (E\cos\psi, -E\sin\psi, 0) \\ E &= E^0 \exp\left(-\int_0^z k_{zi}\,dz\right) \\ \psi &= \int_0^z k_{zr}\,dz - \omega t, \qquad z > 0 \end{aligned} \tag{C.1}$$

rather than by (4.35). In this and subsequent equations, the initial values of quantities (i.e. those at z = 0) are denoted by superscript zero.

The equation of motion of an electron in the presence of a wave described by (C.1) in the limit $v^2/c^2 \ll 1$ is

$$\frac{dv_\perp}{dt} = \frac{v_z v_\perp}{2\Omega_e}\frac{\partial \Omega_e}{\partial z} - \Omega_e^0 c\left(1 - n_r \frac{v_z}{c}\right)\frac{E(z)}{B^0}\cos\theta \tag{C.2}$$

$$\frac{dv_z}{dt} = -\frac{v_\perp^2}{2\Omega_e}\frac{\partial \Omega_e}{\partial z} - \Omega_e^0 v_\perp n_r \frac{E(z)}{B^0}\cos\theta \tag{C.3}$$

$$\frac{d\theta}{dt} = \Omega_e(1 - v^2/2c^2) + k_z v_z - \omega + \Omega_e^0 \frac{c}{v_\perp}\left(1 - n_r \frac{v_z}{c}\right)\frac{E(z)}{B^0}\sin\theta. \tag{C.4}$$

The unperturbed velocity is

$$v_{\perp 0}^2 = \frac{B(z)}{B^0} v_\perp^{02} \tag{C.5}$$

$$v_{z0}^2 = v_z^{02} + v_\perp^{02} - v_{\perp 0}^2 = v_z^{02} + v_\perp^{02}(1 - B(z)/B^0) \tag{C.6}$$

$$\theta_0 = \theta^0 - \int_{t^0}^{t} \Delta_r(z_0)dt \tag{C.7a}$$

$$= \theta^0 - \int_0^{z_0} \frac{\Delta_r(z_0)}{v_{z0}} dz_0 \tag{C.7b}$$

where t^0 is the time the electron passes the point $z = 0$. The perturbed velocity is given by (4.42)-(4.44) except that ω_i is replaced by $-k_{zi}v_{z0}$, t by $t' = z/v_{z0} = t - t^0$ and $v_{\perp 0}$ and v_{z0} appearing in coefficients of $\cos\theta^0$ and $\sin\theta^0$ by $v_\perp^0$ and v_z^0 respectively.

The dispersion relation is obtained by averaging Maxwell's equations over a wave period (rather than a wavelength as in Sections 4.6 and 5.5). In this case the dispersion relation is given by

$$E^0 \exp\left(-\int_0^z k_{zi}\,dz\right)(\omega - k_z^2c^2/\omega)$$

$$= \sum_j 4\pi e n_j \frac{\omega}{2\pi} \int v_\perp^0 dv_\perp^0 \int dv_z^0 \int d\theta^0 \int dz^0 \int_t^{t+2\pi/\omega} dt\; v_\perp f_j$$

$$\times (\sin\theta + i\cos\theta)\; \delta(z - z(z^0, \underset{\sim}{v}^0, t)) \; . \qquad (C.8)$$

If the distribution is assumed to have the form

$$f_j = f_{0j} + f_{1j} \qquad (C.9)$$

where
$$f_{1j} = 2\mu^0 (c/v_\perp^0)\; \Omega_e^0 f_{0j} \cos\theta^0 \left[\frac{(1 - n_r v_z^0/c)}{\Delta_r^0} + \frac{v_\perp^{02}}{2c^2} \frac{(\Omega_e^0 - n_r k_z c)}{\Delta_r^{02}}\right] \qquad (C.10)$$

(cf. Section 5.4.3) then on substitution of the perturbed and unperturbed velocities into (C.8) the dispersion equation is found to have the form

$$\omega^2 - k_z^2c^2 + \sum_j \omega_{pj}^2 \int d^3\underset{\sim}{v}^0 f_{0j} \left[\frac{\omega - k_z v_{z0}}{\Delta(z)} + \frac{v_{\perp 0}^2}{2c^2} \frac{(\omega\Omega_e - k_z^2c^2)}{\Delta^2(z)}\right]$$

$$= i \sum_j \omega_{pj}^2 \int d^3\underset{\sim}{v}^0 \frac{v_\perp^{02}}{2c^2} \frac{z}{v_z^0} \frac{\omega\Omega_e - k_z^2c^2}{\Delta_r^0} \exp\left(-i \int_0^z \frac{\Delta(z)}{v_{z0}}\, dz\right) . \qquad (C.11)$$

The right hand side of (C.11) represents the modification to the dispersion relation by the OBM. The magnitude of this term increases with increasing $|v_\perp^{02}/\Delta_r^0|$ and phase mixes to zero in a distance inversely proportional to the variation of $\Delta(z)/v_{z0}$ over the distribution (cf. Section 5.5.1). Hence, enhanced growth via the OBM is possible only

for distributions with a narrow axial velocity spread and with mean energy such that $\langle v_\perp \rangle \neq 0$ and $\langle \Delta_r^0 \rangle \simeq 0$. Further, if the distribution also has a small average pitch angle and if the magnetic field changes by only a few percent, then the variation of $v_{\perp 0}$ and v_{z0} arising from gradients in the magnetic field can be neglected and (C.11) reduces to (5.15) with $z = v_{z0}t$ and $\omega_i = - k_{zi} v_{z0}$.

REFERENCES

AKHIEZER A.I., AKHIEZER I.A., POLOVIN R.V., SITENKO A.G. and STEPANOV K.N. (1967) *Collective Oscillations in a Plasma*, M.I.T. Press, Cambridge, Mass.

ALIKAEV V.V., BOBROVSKII G.A., POZNYAK V.I., RAZUMOVA K.A., SANNIKOV V.V., SOKOLOV Yu. A. and SHMARIN A.A. (1976) Sov. J. Plasma Phys. 2, 212.

ANTOSIEWICZ H.A. (1970) In *Handbook of Mathematical Functions*, p.435, Edited by Abramowitz M. and Stegun I.A., Dover Publications, N.Y.

APPERT K., BALET B., GRUBER R., TROYEN F., SUNEMATSU T. and VACLAVIK J. (1982) Nucl. Fusion 22,903.

APPERT K., GRUBER R. and VACLAVIK J. (1974) Phys. Fluids 17,1471.

APPERT K. and VACLAVIK J. (1982) Ecol. Polytechnique Federale de Lausanne LRP 207/82.

ASHOUR - ABDALLA M. (1970) Planet. Space Sci. 18,1799.

ASHOUR - ABDALLA M. (1972) Planet. Space Sci. 20,639.

ASSEO E., LAVAL G., PELLAT R., WELTI R. and ROUX A. (1972) J. Plasma Phys. 8,341.

BALDWIN D.E., BERNSTEIN I.B. and WEENINK M.P.H. (1969) Advances in Plasma Physics 3,1.

BEKEFI G. (1966) *Radiation Processes in Plasma*, John Wiley & Sons, N.Y.

BEKEFI G., HIRSHFIELD J.L. and BROWN S.D. (1961) Phys. Rev. 122,1037.

BELL T.F. and HELLIWELL R.A. (1971) J. Geophys. Res. 76,8414.

BENGSTON R.D., BENESCH J.F., CHEN G. - L., EVANS T.E., LI Y.M., LIN S. -H., MAHAJAN S.M., MICHIE R.B., OAKES M.E., ROSS D.W., SURKO C.M. and VALNAJU P. (1982) *Proceedings of the 3rd. Joint Varenna - Grenoble International Symposium on Heating in Toroidal Plasmas*, p.151, Como, Italy.

BOTTEN L.C., CRAIG M.S. and MCPHEDRAN R.C. (1981) Optica Acta 28,1103.

BRAND G.F., DOUGLAS N.G., GROSS M., MA J.Y.L., ROBINSON L.C. and ZHIYI C. (1982) Int. J. Infrared and Millimeter Waves 3,725.

BRIGGS R.J. (1964) *Electron - Stream Interaction with Plasmas*,M.I.T. Press, Cambridge, Mass.

BRINCA A.L. (1972) J. Geophys. Res. 77,3508.

BUDDEN K.G. (1961) *Radio Waves in the Ionosphere*, Cambridge University Press, Cambridge.

CARPENTER D.L. (1968) J. Geophys. Res. 73,2919.

CHANG D.C.D. and HELLIWELL R.A. (1979) J. Geophys. Res. 84,7170.

CHANG D.C.D., HELLIWELL R.A. and BELL T.F. (1980) J. Geophys. Res. 85,1703.

CHEN F.F. (1974) *An Introduction to Plasma Physics*,Plenum Press, N.Y.

CHEN L. and HASEGAWA A. (1974) Phys. Fluids 17,1399.

CHIU S.C.,CHAN V.S., HSU J.Y. and SWANSON D.G. (1982) J.Plasma Phys. 27,327.

CHU K.R. (1978) Phys. Fluids 21,2354.

CHU K.R., DROBOT A., GRANATSTEIN V.L. and SEFTOR J.L. (1979) IEEE Trans. Microwave Theory Tech. MTT-27,128.

CHU K.R., DROBOT A., SZU H.H. and SPRANGLE P. (1980a) IEEE Trans. Microwave Theory Tech. MTT-28,313.

CHU K.R. and HIRSHFIELD J.L. (1978) Phys. Fluids 21,461.

CHU K.R., READ M.E. and GRANGULY A.K. (1980b) IEEE Trans. Microwave Theory Tech. MTT-28,318.

COLESTOCK P.L., DAVIS S.L., HOSEA J.G., HWANG D.Q. and THOMPSON H.R. (1980) *Proceedings of the 2nd. Joint Grenoble - Varenna International Symposium on Heating in Toroidal Plasmas*, p.471, Como, Italy.

CORNILLEAU - WEHRLIN N. and GENDRIN R. (1979) J. Geophys. Res. 84,883.

CRAMER N.F. and DONNELLY I.J. (1983) Plasma Phys. 25,703.

CROSS R.C., BLACKWELL B.D., BRENNAN M.H., BORG G. and LEHAME J.A. (1982) *Proceedings of the 3rd. Joint Varenna - Grenoble International Symposium on Heating in Toroidal Plasmas*,p.173, Como, Italy.

DAS A.C. (1968) J. Geophys. Res. 73,7457.

DAVIS J. (1970) In *Handbook of Mathematical Functions*,p.253, Edited by Abramowitz M. and Stegun I.A., Dover Publications, N.Y.

DE CHAMBRIER A., CHEETHAM A.D., HEYM A., HOFMANN F., JOYE B., KELLER R., LIETTIC A., LISTER J.B., POCHELON A., SIMM W., TORINATO J.L. and TUSZEL A. (1982a) *Proceedings of the 3rd. Joint Varenna - Grenoble International Symposium on Heating in Toroidal Plasmas*,p.161, Como, Italy.

DE CHAMBRIER A., HEYM A., HOFMANN F., JOYE B., KELLER R., LIETTI A., LISTER J.B., MORGAN P.D., PEACOCK N.J., POCHELON A. and STAMP M.J. (1982b) Association Euratom, LRP 216/82.

DENAVIT J. and SUDAN R.M. (1972) Phys. Rev. Lett. 28,404.

DERFLER H. and SIMONEN T.C. (1969) Phys. Fluids 12,269.

DONNELLY I.J. (1982) TP82-2, Dept. Thearetical Physics, Uni. of Sydney.

DONNELLY I.J. and CRAMER N.F. (1983) Plasma Phys. (in press)

DORY R.A., GUEST G.E. and HARRIS E.G. (1965) Phys. Rev. Lett. 14,131.

DOWDEN R.L. (1981) J. Geophys. Res. 86,4815.

DOWDEN R.L., McKAY A.D., AMON L.E.S., KOONS H.C. and DAZEY M.H. (1978) J. Geophys. Res. 83,169.

DUNGEY J.W. (1963) Planet. Space Sci. 11,591.

DYSTHE K.B. (1971) J. Geophys. Res. 76,6915.

EDGAR B.C. and KOONS H.C. (1982) J. Geophys. Res. 87,271.

EQUIPPE TFR (1982) Plasma Phys. 24,615.

FEJER J.A. and KAN J.R. (1969) J. Plasma Phys. 3,331.

FLYAGIN V.A., GAPONOV A.V., PETELIN M.I. and YULPATOV V.K. (1977) IEEE Trans. Microwave Theory Tech. MTT-25,514.

GAPONOV A.V. (1959) Izv. Vyssh. Uchebn. Zaved. Radio Fizi. 2,450 and 836.

GAUTSCHI W. and CAHILL W.F. (1970) In *Handbook of Mathematical Functions*, p.227, Edited by Abramowitz M. and Stegun I.A., Dover Publications, N.Y.

GENDRIN R. (1974) Astrophys. Space Sci. 28,245.

HASEGAWA A. and CHEN L. (1975) Phys. Rev. Lett. 35,370.

HASEGAWA A. and CHEN L. (1976) Phys. Fluids 19,1924.

HELLIWELL R.A. (1965) *Whistlers and Related Ionospheric Phenomena*, Stanford University Press Stanford, California.

HELLIWELL R.A. (1967) J. Geophys. Res. 72,4773.

HELLIWELL R.A., CARPENTER D.L. and MILLER T.R. (1980) J. Geophys. Res. 85,3360.

HELLIWELL R.A. and CRYSTAL T.L. (1973) J. Geophys. Res. 78,7357.

HELLIWELL R.A. and CRYSTAL T.L. (1975) J. Geophys. Res. 80,4399.

HELLIWELL R.A. and INAN U.S. (1982) J. Geophys. Res. 87,3537.

HELLIWELL R.A. and KATSUFRAKIS J.P. (1974) J. Geophys. Res. 79,2511.

HELLIWELL R.A., KATSUFRAKIS J.P., TRIMPI M. and BRICE N. (1964) J. Geophys. Res. 69,2391.

HEWITT R.G. (1981) Private Communication.

HEWITT R.G., MELROSE D.B. and RÖNNMARK K.G. (1981) Proc. Astron. Soc. Aust. J. Phys. 35,447.

HEWITT R.G., MELROSE D.B. and RÖNNMARK K.G. (1982) Aust

HIRSHFIELD J.L. and GRANATSTEIN V.L. (1977) IEEE Trans. Microwave Theory Tech. MTT-25,522.

HOLMAN G.D., EICHLER D. and KUNDU M.R. (1980) In *IAU Symposium 86, Radio Physics of the Sun,* p.457, Edited by Kundu M. and Gergeley T., D. Reidel Pub. Co., Dordrecht, Holland.

HOOKE W.M. and BERNABEI S. (1972) Phys. Rev. Lett. 29,1218.

HUNG R.G. and BARNES A. (1973) Ap. J. 180,253.

INAN U.S., BELL T.F., CARPENTER D.L. and ANDERSON R.R. (1977) J. Geophys. Res. 82,1177.

INCE E.L. (1956) *Ordinary Differential Equations*,Dover Publications, N.Y.

IONSON J.A. (1978) Ap. J. 226,650.

ISTOMIN Ya. N. and KARPMAN V.I. (1972) Planet. Space Sci. 20,1790.

ISTOMIN Ya. N. and KARPMAN V.I. (1973a) Soviet Phys. JETP 36,69.

ISTOMIN Ya. N. and KARPMAN V.I. (1973b) Soviet Phys. JETP 39,897.

JACQUINOT J., McVEY B.D. and SCHARER J.E. (1977) Phys. Rev. Lett. 39, 88.

JFT-2 GROUP (1982) *Proceedings of 3rd. Joint Varenna - Grenoble International Symposium on Heating in Toroidal Plasmas*,p.259, Como, Italy.

KARNEY C.F.F., PERKINS F.W. and SUN Y. - C. (1979) Phys. Rev. Lett. 42,1621.

KARPMAN V.I. (1974) Space Sci. Rev. 16,361.

KARPMAN V.I., ISTOMIN Ya. N. and SHKLYAR D.R. (1974a) Plasma Phys. 16,685.

KARPMAN V.I., ISTOMIN Ya. N. and SHKLYAR D.R. (1974b) Planet Space Sci. 22,859.

KENNEL C.F. and PETSCHEK H.E. (1966) J. Geophys. Res. 71,1.

KIMURA I. (1967) Planet. Space Sci. 15,1427.

KIMURA I. (1968) J. Geophys. Res. 73,445.

KNOX I.B. (1969) Planet. Space Sci. 17,13.

KOONS H.C., DAZEY M.H., DOWDEN R.L. and AMON L.E.S. (1976) J. Geophys. Res. 81,5536.

KRALL N.A. and TRIVELPIECE A.W. (1973) *Principles of Plasma Physics*, McGraw - Hill, N.Y.

LASCH S. (1969) J. Geophys. Res. 74,1856.

LASHMORE - DAVIES C.N. and MAY R.M. (1972) Phys. Fluids 15,1616.

LEE L.C., KAN J.R. and WU C.S. (1980) Planet. Space Sci. 28,703.

LIKHTER Ya. I., MOLCHANOV O.A. and CHMYREV V.M. (1971) Soviet Phys. JETP Lett. 14,325.

LORRAIN P. and CORSON D.R. (1970) *Electromagnetic Fields And Waves*, W.H. Freeman and Co., San Francisco.

LUKE Y.L. (1969) *The Special Functions and Their Approximations*, Academic Press, N.Y.

MATHEWS J. and WALKER R.L. (1970) *Mathematical Methods of Physics*, W.A. Benjamin Inc., Menlo Park.

MATSUMOTO H. (1979) In *Wave Instabilities in Space Plasmas*, p.163, Edited by Palmadesso P.J. and Papadopoulos K., D. Reidel Pub. Co., Dordrecht, Holland.

MATSUMOTO H., HASHIMOTO K. and KIMURA I. (1980) J. Geophys. Res. 85,644.

MATSUMOTO H. and OMURA Y. (1981) J. Geophys. Res. 86,779.

McKENZIE J.I. (1979) J. Plasma Phys. 22,361.

McNEILL F.A.(1968) J. Geophys. Res. 73,6860.

McPHERSON D.A., KOONS A.C., DAZEY M.H., DOWDEN R.L., AMON L.E.S. and THOMPSON N.R. (1974) J. Geophys. Res. 79,1555.

MELROSE D.B. (1973) Aust. J. Phys. 26,229.

MELROSE D.B. (1976) Astrophys. J. 207,651.

MELROSE D.B. (1980a) *Plasma Astrophysics: Nonthermal Processes in Diffuse Magnetized Plasmas*, Vol. I, Gordon and Breach, N.Y.

MELROSE D.B. (1980b) *Plasma Astrophysics: Nonthermal Processes in Diffuse Magnetized Plasmas*, Vol. II, Gordon and Breach, N.Y.

MELROSE D.B. and DULK G.A. (1982) Astrophys. J. 259,844.

MELROSE D.B., RÖNNMARK K.G. and HEWITT R.G. (1982) J. Geophys.Res. 87,5140.

MELROSE D.B., WINGLEE R.M. and CAIRNS I.H. (1983) Presented at Chapman Conference on Waves in Magnetospheric Plasmas, Hawaii 1983.

MILEY G.H. (1976) *Fusion Energy Conversion*, American Nuclear Society, Illinois.

MURPHY G.M. (1960) *Ordinary Differential Equations and Their Solutions*, Van Nostrand, Princeton, N.J.

MUTOH T., KINOSHITA S., SATO M., OBIKI T., VO K. and IIYOSHI A. (1979) J. Phys. Soc. Japan 47,642.

NAKADA N.P., DUNGEY J.W. and HESS W.N. (1965) J. Geophys. Res. 70,3529.

NAYFEH A.H. (1973) *Pertubation Methods*, John Wiley & Sons, N.Y.

NEWMAN C.E. (1977) J. Geophys. Res. 82,105.

NUNN D. (1971) Planet. Space Sci. 19,1141.

NUNN D. (1973) Planet. Space Sci. 21,67.

NUNN D. (1974) Planet. Space Sci. 22,349.

NUNN D. (1975) J. Goephys. Res. 80,4397.

OBERHETTINGER F. (1970) In *Handbook of Mathematical Functions*, p.555, Edited by Abramowitz M. and Stegun I.A., Dover Publications, N.Y.

OBIKI T., MUTOH T., ADACHI S., SASAKI A., IIYOSHI A. and VO K. (1977) Phys. Rev. Lett. 39,812.

OLVER T.W. (1970) In *Handbook of Mathematical Functions*, p.435, Edited by Abramowitz M. and Stegun I.A., Dover Publications, N.Y.

OMIDI N. and GURNETT D.A. (1982) J. Geophys. Res. 87,2377.

OMURA Y. and MATSUMOTO H. (1982) J. Geophys. Res. 87,4435.

OTT E., WERSINGER J.- M. and BONOLI P.T. (1978) Phys. Fluids 21,2306.

PARK C.G. (1981) J.Geophys. Res. 86,2286.

PERKINS F.W. (1977) Nucl. Fusion 17,1197.

PURI S. (1979) Max - Planck Institut. Für Plasma Physik Report Ipp 4/183.

PURI S. and TARTONIS J.A. (1978) Max - Planck Institut. Für Plasma Physik Report Ipp 4/173.

PURI S. and TUTLER M. (1973) Nucl. Fusion 13,55.

RABENSTEIN A.L. (1958) Arch. Ratl. Mech. Anal. 1,418.

RAGHURAM R., BELL T.F., HELLIWELL R.A. and KATSUFRAKIS J.P. (1977) J. Geophys. Res. 82,2787.

ROBERTS C.S. (1966) *Radiation in the Earth's Magnetic Field*, p.403, Edited by McCormac B.M., D. Reidel Pub. Co., Dordrecht, Holland.

ROSE D.J. and CLARK M. (1961) *Plasmas and Controlled Fusion*, M.I.T. Press, Mass.

ROSS D.W., CHEN G.L. and MAHAJEN S.W. (1982) Phys. Fluids 25,652.

ROUX A. and PELLAT R. (1976) *Magnetospheric Particles*, p.209, Edited by McCormac B.M., D. Reidel Pub. Co., Dordrecht, Holland.

ROUX A. and PELLAT R. (1978) J. Geophys. Res. 83,1433.

RUTHERFORD P. (1980) Nucl. Fusion 20,1086.

SCHARER J.E., McVEY B.D. and MAU T.K. (1977) Nucl. Fusion 17,297.

SCHNEIDER J. (1959) Phys. Rev. Lett. 2,504.

SHARMA R.R., VLAHOS L. and PAPADOPOULOS K. (1982) Astron. Astrophysics 112,377.

SITENKO A.G. (1967) *Electromagnetic Fluctuations in Plasma*, Academic Press, N.Y.

SLATER L.J. (1970) In *Handbook of Mathetical Functions*, p.503, Edited by Abramowitz M. and Stegun I.A., Dover Publications, N.Y.

SPRANGLE P. and DROBOT A.T. (1977) IEEE Trans. Microwave Theory Tech. MTT-25,528.

SPRANGLE P. and SMITH R.A. (1980) J. Appl. Phys. 51,3001.

STÉFANT R.G. (1970) Phys. Fluids 13,440.

STILES G.S. and HELLIWELL R.A. (1977) J. Geophys. Res. 82,523.

STIX T.H. (1962) *The Theory of Plasma Waves*, McGraw - Hill, N.Y.

STIX T.H. (1975) Nucl. Fusion 15,737.

STIX T.H. (1980) *Proceedings of 2nd. International Grenoble - Varenna Symposium On Heating in Toroidal Plasmas*, Como, Italy.

STIX T.H. and PALLADINO W.R. (1958) Phys. Fluids 1,113.

SWANSON D.G. (1974) Phys. Fluids 17,2241.

SWANSON D.G. (1975) Phys. Fluids 18,1269.

TATARONIS J.A. and GROSSMANN W. (1973) Z. Phys. 261,217.

TSAI S.T., WU C.S., WANG Y.D. and KANG S.W. (1981) Phys. Fluids 24,2186.

TWISS R.Q. (1958) Aust. J.Phys. 11,564.

UHM H.S. and DAVIDSON R.C. (1979a) Phys. Fluids 22,1804.

UHM H.S. and DAVIDSON R.C. (1979b) Phys. Fluids 22,1811.

VOMVORIDIS J.L. and DENAVIT J. (1979) Phys. Fluids 22,367.

VOMVORIDIS J.L. and DENAVIT J. (1980) Phys. Fluids 23,174.

WELTI R., PELLAT R. and ROUX A. (1973) Ann. Geophys. 29,263.

WENTZEL D.G. (1979a) Ap. J. 227,319.

WENTZEL D.G. (1979b) Ap. J. 233,756.

WINGLEE R.M. (1982) Plasma Phys. 24,1161.

WINGLEE R.M. (1983a) Plasma Phys. (in press).

WINGLEE R.M. (1983b) Plasma Phys. 25,217.

WONG H.K., WU C.S., KE F.J., SCHNEIDER R.S. and ZIEBELL L.F. (1982) J. Plasma Phys. 28,503.

WU C.S. and LEE L.C. (1979) Astrophys. J. 230,624.

WU C.S., LIN C.S., WONG H.K., TSAI S.T. and ZHAI R.L. (1981) Phys. Fluids 24, 2191.

WU C.S., WONG H.K., GORNEY D.J. and LEE L.C. (1982) J. Geophys. Res. 87,4476.

ZAYTSEV N.I., PANKRATOVA T.B., PETELIN M.I. and FLYAGIN V.A. (1974) Radiotekhnikai Electronica 19,1056.

ZUCKER R. (1970) In *Handbook of Mathematical Functions*, p.65, Edited by Abramowitz M. and Stegun I.A., Dover Publications, N.Y.